

REPORT NO.
UCB/EERC-85/07
JULY 1985

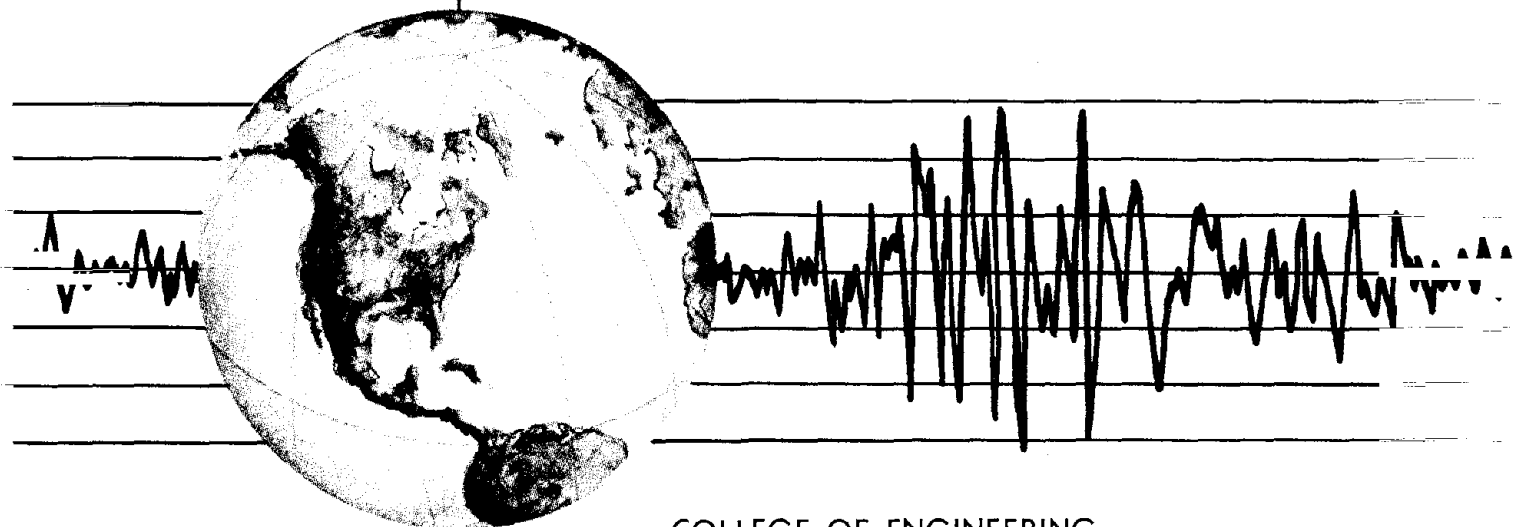
EARTHQUAKE ENGINEERING RESEARCH CENTER

EARTHQUAKE ANALYSIS AND RESPONSE OF CONCRETE ARCH DAMS

by

KA-LUN FOK
ANIL K. CHOPRA

A Report on Research Conducted Under
Grants CEE-8120308 and CEE-8401439
from the National Science Foundation



COLLEGE OF ENGINEERING

UNIVERSITY OF CALIFORNIA · Berkeley, California

REPRODUCED BY
NATIONAL TECHNICAL
INFORMATION SERVICE
U.S. DEPARTMENT OF COMMERCE
SPRINGFIELD, VA. 22161

For sale by the National Technical Information Service, U.S. Department of Commerce, Springfield, Virginia 22161.

See back of report for up to date listing of EERC reports.

DISCLAIMER

Any opinions, findings, and conclusions or recommendations expressed in this publication are those of the authors and do not necessarily reflect the views of the National Science Foundation

EARTHQUAKE ANALYSIS AND RESPONSE OF CONCRETE ARCH DAMS

by

Ka-lun Fok

Anil K. Chopra

A Report on Research Conducted Under
Grants CEE-8120308 and CEE-8401439
from the National Science Foundation

Report No. UCB/EERC-85/07
Earthquake Engineering Research Center
University of California
Berkeley, California

July 1985

file

ABSTRACT

Reliable analytical procedures to predict the earthquake response of arch dams are necessary to design earthquake resistant dams and to evaluate the earthquake safety of existing dams. The objectives of this investigation are to develop an effective and computationally efficient analytical procedure for computing the earthquake response of concrete arch dams, and to investigate how this response is affected by dam-water interaction, foundation-rock flexibility, and the alluvium and sediments usually present at the reservoir boundary.

An earlier analytical procedure for computing the response of arch dams to harmonic ground motion including dam-water interaction and reservoir boundary absorption effects has been extended to consider the flexibility of the foundation rock and to include Fourier synthesis of harmonic responses to obtain earthquake responses. The computational efficiency of the extended analytical procedure has been improved by an order of magnitude by developing more efficient analytical formulations and computational procedures for evaluating the hydrodynamic terms, and by developing procedures for interpolation of the frequency response functions.

Utilizing the resulting analytical procedure and computer program, the response of a selected arch dam to harmonic and earthquake ground motion has been computed and studied for a wide range of the important parameters characterizing the properties of the dam, foundation rock, impounded water and reservoir boundary materials. This investigation led to the following conclusions: (a) dam-water interaction generally increases the earthquake response of arch dams, especially the response to vertical ground motion; (b) reservoir boundary absorption generally reduces the dam response, most significantly that due to vertical ground motion; however, increasing wave absorption may in some cases increase the response to upstream or cross-stream ground motions; (c) foundation-rock flexibility increases the response of the dam and has little influence on dam-water interaction and reservoir boundary absorption effects; (d) an absorptive reservoir boundary gives a more realistic estimate of the earthquake response of arch dams, especially of the response to the vertical component of ground motion; and (e) water compressibility should be considered in the earthquake analysis of arch dams because the effects of dam-water interaction and reservoir boundary absorption are not properly represented by the assumption of incompressible water.

ACKNOWLEDGEMENTS

This research investigation was supported by the National Science Foundation under Grants CEE-8120308 and CEE-8401439. The authors are grateful for this support.

Except for editorial changes and the addition of a few sections, the report is the same as Ka-lun Fok's doctoral dissertation, which has been submitted to the University of California, Berkeley. The dissertation committee consisted of Professors A.K. Chopra (Chairman), R.W. Clough and B.A. Bolt. The authors are grateful to Professors Clough and Bolt for reviewing the manuscript and suggesting improvements.

Parts of this investigation are closely related to a companion work: "Earthquake Analysis and Response of Concrete Gravity Dams" by Gregory Fenves and Anil K. Chopra, published in August 1984. The superb organization of the figures and tables presenting the response results and of their discussion in this companion study served as an excellent model for this report.

TABLE OF CONTENTS

ABSTRACT	i
ACKNOWLEDGEMENTS	ii
TABLE OF CONTENTS	iii
1.INTRODUCTION	1
2. SYSTEM AND GROUND MOTION	4
2.1 Arch Dam	4
2.2 Foundation Rock	4
2.3 Impounded Water	7
2.4 Absorptive Reservoir Boundary	8
2.5 Ground Motion	10
2.6 Morrow Point Dam-Water-Foundation Rock System	11
2.6.1 Morrow Point Dam	11
2.6.2 Impounded Water	13
2.6.3 Shape of the Foundation-Rock Region	13
2.6.4 Size of the Foundation-Rock Region	20
3. RESPONSE ANALYSIS PROCEDURE	34
3.1 Outline of Analysis Procedure	34
3.2 Evaluation of Hydrodynamic Terms	40
3.3 Efficient Evaluation of Hydrodynamic Terms	44
3.3.1 Major Computational Steps	44
3.3.2 Number of Eigenvectors of the Infinite Channel	45
3.3.3 Interpolation of Eigenproperties of the Infinite Channel	49

3.4 Interpolation of Frequency Response Functions	61
3.4.1 Basic Concept	61
3.4.2 Two Mode Approximation	63
3.4.3 Selection of Frequencies for Exact Computation	65
3.4.4 Summary of Interpolation Procedure	69
3.5 Efficient Response Analysis Procedure	69
3.6 Computer Program	74
4. FREQUENCY RESPONSE FUNCTIONS	75
4.1 Introduction	75
4.2 System, Ground Motion, Cases Analyzed, and Response Quantities	75
4.2.1 Dam-Water-Foundation Rock System	75
4.2.2 Ground Motion	75
4.2.3 Cases Analyzed	76
4.2.4 Response Quantities	76
4.3 Hydrodynamic Forces on Rigid Dam	78
4.4 Dam-Water Interaction Effects	86
4.4.1 Hydrodynamic Effects	86
4.4.2 Effects of Reservoir Boundary Absorption	92
4.4.3 Influence of Young's Modulus E_s	94
4.4.4 Comparison of Responses to Three Ground Motion Components	99
4.5 Foundation Flexibility Effects	99
4.6 Dam-Water Interaction and Foundation Flexibility Effects	103
4.6.1 Hydrodynamic and Reservoir Boundary Absorption Effects	103
4.6.2 Influence of Moduli Ratio E_f/E_s	111

5. EARTHQUAKE RESPONSE OF MORROW POINT DAM	117
5.1 Introduction	117
5.2 System and Ground Motion	117
5.2.1 Dam-Water-Foundation Rock System	117
5.2.2 Ground Motion	117
5.3 Response Results	118
5.4 Dam-Water Interaction Effects	123
5.4.1 Hydrodynamic Effects	123
5.4.2 Effects of Reservoir Boundary Absorption	135
5.5 Foundation Flexibility Effects	138
5.6 Dam-Water Interaction Effects with Flexible Foundation Rock	140
5.6.1 Hydrodynamic Effects	140
5.6.2 Effects of Reservoir Boundary Absorption	142
5.7 Relative Significance of Response to Ground Motion Components	150
5.8 Practical Earthquake Analysis of Arch Dams	172
6. CONCLUSIONS	178
REFERENCES	183
APPENDIX A: NOTATION	186
APPENDIX B: FLUID EIGENVALUE PROBLEM	193
B.1 Fluid Eigenvalue Problem of a Rectangular Section Channel	193
B.2 Boundary Condition at the Absorptive Reservoir Boundary of the Fluid Eigenvalue Problem As the Excitation Frequency Tends to Infinity	196
APPENDIX C: TWO MODE FREQUENCY RESPONSE FUNCTION FOR THE DAM-FOUNDATION SYSTEM WITH INCOMPRESSIBLE WATER	198

1. INTRODUCTION

Reliable analytical procedures to evaluate the earthquake response of arch dams are necessary to design earthquake resistant dams and to evaluate the earthquake safety of existing dams. ADAP [1] was one of the earliest computer programs developed for analysis of arch dams by the finite element method. While foundation flexibility effects were included in this computer program, it was only recently that an added mass approximation of hydrodynamic effects was included [2]. In order to develop better representations of hydrodynamic effects in the earthquake response of dams, considerable work has been reported on analysis of hydrodynamic pressures on arch dams [3,4,5,6]. While the earthquake analysis of arch dams has been implemented in the time domain including the hydrodynamic effects of the impounded water discretized by the finite difference method [7], the most promising approach seems to be a substructure method implemented in the frequency domain. In this method, the finite element equations of motion for the dam are modified by hydrodynamic terms arising from dam-water interaction. These hydrodynamic terms, which are functions of the excitation frequency, are determined from solutions of the wave equation over the fluid domain for appropriate boundary conditions.

For a simple geometry of the arch dam and fluid domain -- the dam assumed to be a segment of a circular cylinder, bounded by vertical, radial banks of the river canyon enclosing a central angle of 90° -- mathematical solutions of the wave equation were obtained to determine the hydrodynamic terms [6]. For arch dam-reservoir systems of realistic geometry, the hydrodynamic terms were determined from analysis of finite element models of the fluid domain [5].

Utilizing these hydrodynamic solutions, the substructure method has been implemented to analyze the response of arch dams supported on rigid foundation rock to harmonic ground motion, including the dynamic effects of the impounded water and the wave absorptive effects of the alluvium and sediments that may be present at the boundary (bottom and sides) of actual reservoirs [5,8]. Although only limited response results obtained by these analytical procedures were presented, they were sufficient to indicate that the response of arch dams may be significantly influenced by dam-water interaction, water compressibility, and absorption of hydrodynamic waves at the reservoir

boundary [5,8].

In the above-mentioned analytical procedure [5], the hydrodynamic terms in the equations of motion for the dam were determined from analysis of finite element models of the impounded water. The finite element procedure was developed for fluid domains extending to infinity in the upstream direction, consisting of an irregular region of finite size connected to a region of uniform cross-section and infinite length in the upstream direction. For the latter region, a finite element discretization within the cross-section combined with a continuum representation in the infinite direction provides for the proper transmission of pressure waves. However, as originally developed [5,9], considerable computational effort is required in finite element analysis of reservoirs of complex geometry extending to large distances in the upstream direction, especially when effects of water compressibility and of sediments at the reservoir boundary are included.

The objectives of this investigation are: (a) to develop an effective and computationally efficient analytical procedure for computing the earthquake response of concrete arch dams; and (b) to study how dam-water interaction, reservoir boundary absorption, and foundation-rock flexibility affect the earthquake response of arch dams.

The earlier analytical procedure [9] is first summarized in Chapter 3, with an extension to include Fourier synthesis of responses to harmonic ground motions and thus obtain dam response to earthquakes. Furthermore, as a first step towards considering the effects of dam-foundation rock interaction, the analysis procedure is extended to include a massless finite element model for the foundation rock. Efficient analytical formulations and computational procedures are presented for evaluation of the hydrodynamic terms and computation of dam response. The resulting response analysis procedure and its implementation in a computer program are described.

Utilizing the analytical procedure presented in Chapter 3, the responses of Morrow Point Dam to harmonic ground motions in the upstream, vertical and cross-stream directions are determined and presented in Chapter 4. The response results are presented in the form of complex-valued frequency response functions, for a wide range of the important parameters characterizing the properties of the dam, foundation rock, impounded water and reservoir boundary materials. Based on the frequency

response results, the effects of dam-water interaction, reservoir boundary absorption, and foundation-rock flexibility on the response of the dam are investigated, and shown to influence significantly the response of arch dams in many cases.

Presented in Chapter 5 is the response of Morrow Point Dam to the three components of Taft ground motion, determined for a range of properties of the reservoir boundary materials and various assumptions for the impounded water and foundation rock. Based on these response results, the effects of dam-water interaction, reservoir boundary absorption, and foundation-rock flexibility on the earthquake induced displacements and stresses in the dam, and the relative significance of the response to the three components of ground motion, are investigated. The results of practical earthquake analyses of the arch dam are also presented to demonstrate the effectiveness and efficiency of the analytical procedure.

Chapter 6 presents the principal conclusions regarding the analytical procedure developed and the effects of dam-water interaction, reservoir boundary absorption, and foundation-rock flexibility on the earthquake response of arch dams.

2. SYSTEM AND GROUND MOTION

2.1 Arch Dam

The system considered consists of a concrete arch dam supported by flexible foundation rock in a canyon and impounding a reservoir of water (Figure 2.1). The system is analyzed under the assumption of linear behavior for the concrete dam, impounded water and foundation rock. Thus the possibility of water cavitation, concrete cracking, or the construction joints of the dam opening during vibration is not considered.

The dam is idealized as an assemblage of finite elements [Figure 2.2(a)], with a major part of the dam represented by thick shell finite elements [10], and the part of the dam near its junction with foundation rock represented by transition elements [1,10], designed to connect thick shell elements in the dam to three-dimensional solid elements employed in idealizing the foundation rock. The properties of each finite element are characterized by the Young's modulus E_s , Poisson's ratio ν_s , and unit weight w_s of the concrete. The vibrational energy dissipation properties of the dam are characterized by the constant hysteretic damping factor η_s .

2.2 Foundation Rock

Required in the substructure method for analysis of earthquake response of dams is the frequency-dependent stiffness (or impedance) matrix for the foundation rock, defined at the nodal points on the dam-foundation rock interface. This matrix for a viscoelastic half plane was determined for two-dimensional analysis of concrete gravity dams supported on the horizontal surface of foundation rock [11]. However, such a foundation model is inappropriate for analysis of arch dams because they are usually built in narrow canyons with the dam boundary in contact with the foundation rock extending over the height of the dam.

An alternative approach is to idealize a portion of the foundation rock as a finite element system and to determine the impedance matrix for this idealization. The principal decision required in defining this idealization is the three-dimensional extent and boundary conditions of the foundation

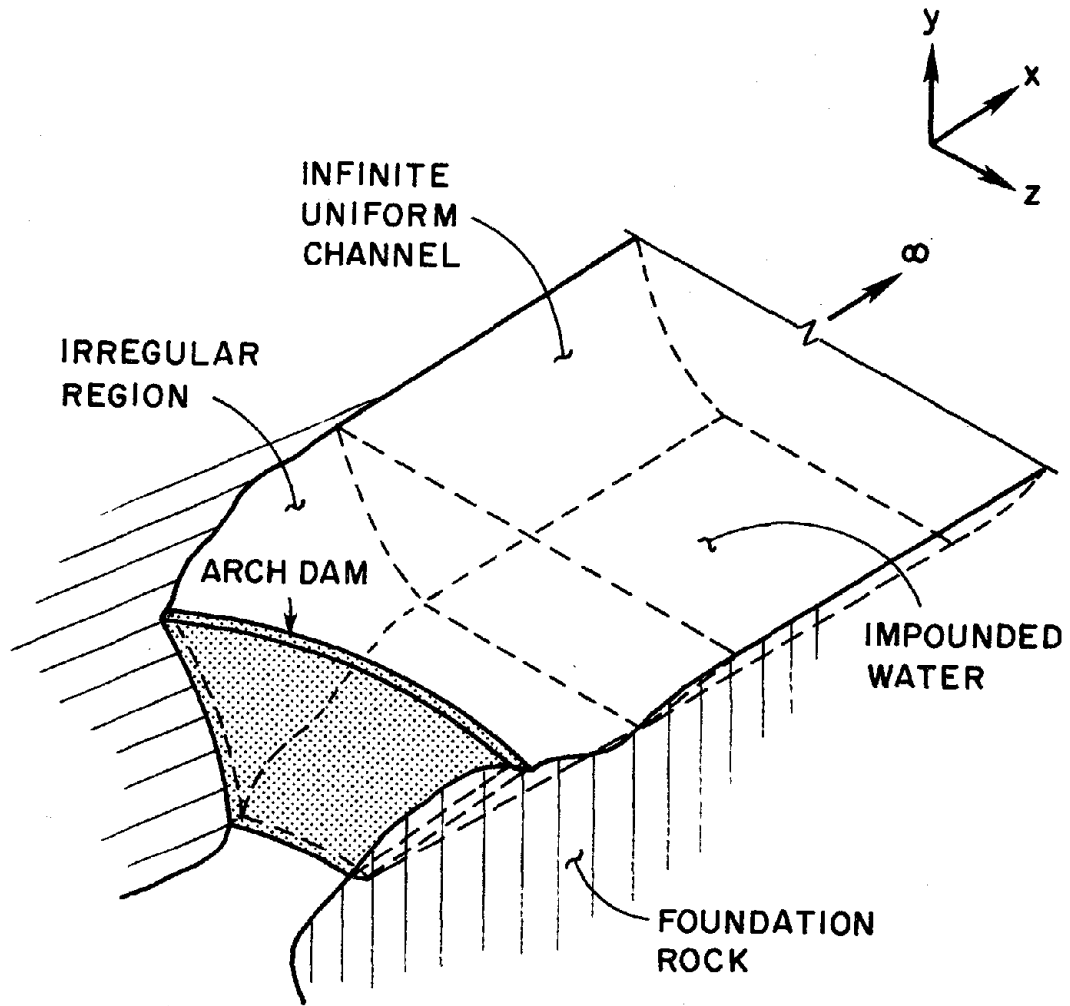


Figure 2.1 Arch dam-water-foundation rock system.

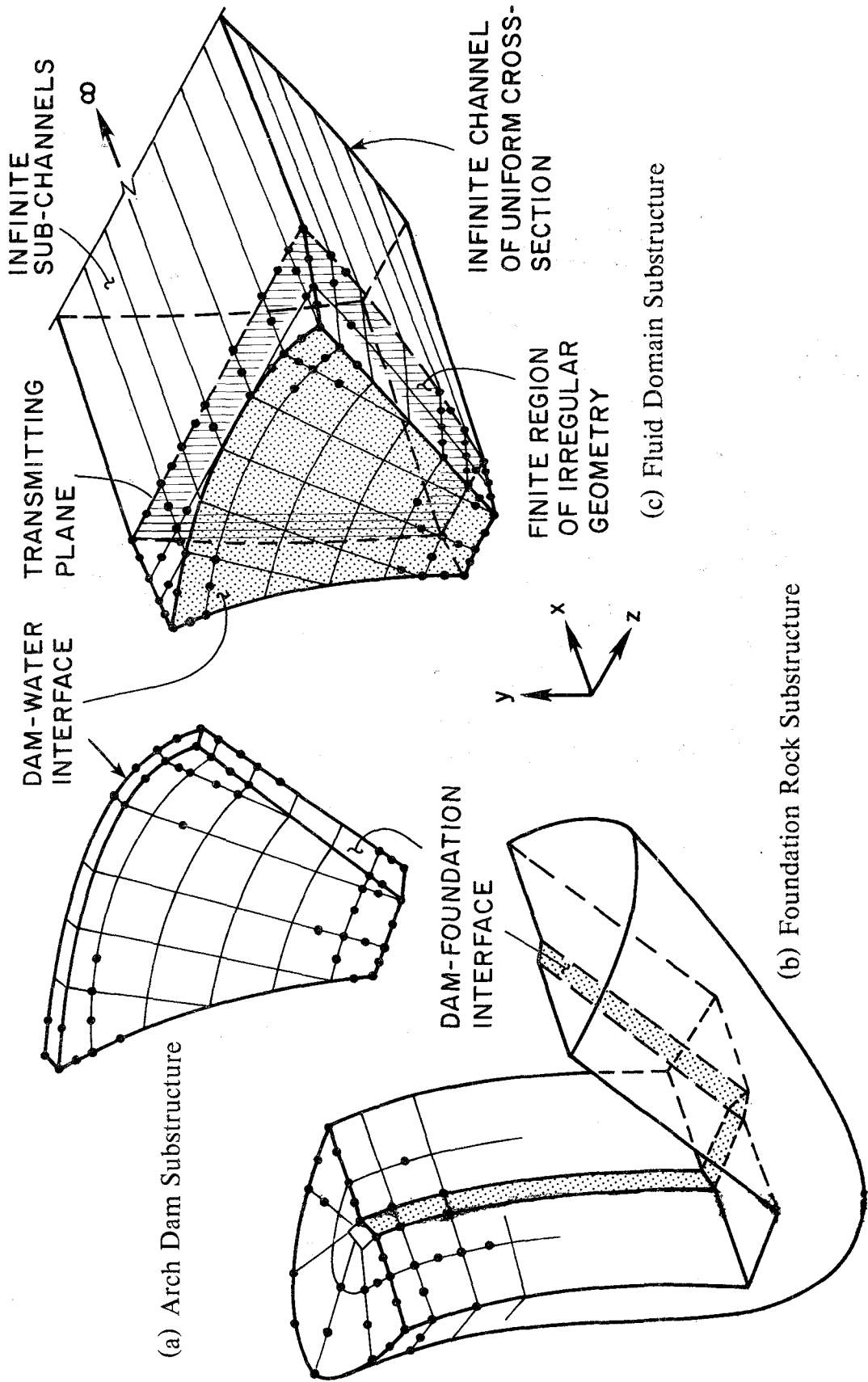


Figure 2.2 Finite element models of dam, foundation rock, and fluid domain substructures. (Parts (a) and (c) adapted from reference [9])

rock to be included in the analysis. For arch dam sites where typically similar rocks extend to considerable distances, wave-transmitting boundaries are necessary if the finite sized foundation-rock region is to represent the unbounded extent in the field. Such transmitting boundaries have been developed for two-dimensional analysis [12] with seemingly ad-hoc extensions proposed for three-dimensional analyses. The latter, if developed properly, would be computationally expensive perhaps to the point of being prohibitive for practical problems.

For these reasons and because it is virtually impossible to rationally specify the free-field earthquake motions at an arch dam-rock interface, an extremely simple idealization for the foundation rock is used here [13]. Only the foundation rock flexibility is considered in this investigation; i.e. the inertial and damping effects of the foundation rock are ignored in considering dam-foundation interaction effects. As shown in Figure 2.2(b), an appropriate portion of the foundation-rock region is idealized as an assemblage of three-dimensional solid finite elements, with the finite element meshes of the dam and foundation rock matching at their interface. The properties of each finite element are characterized by the Young's modulus E_f and Poisson's ratio ν_f .

2.3 Impounded Water

The reservoir behind a dam is of complicated shape, as dictated by the natural topography of the site. Typically the impounded water extends to great distances, up to a few tens of miles, in the upstream direction. Finite element idealizations are necessary to properly represent the complicated geometry of the impounded water. But such an idealization would be exorbitantly expensive, to the point of becoming impractical, if the standard finite element idealization was employed to large distances in the upstream direction.

An effective approach is to idealize the fluid domain as shown in Figure 2.1, with a finite region of irregular geometry adjacent to the dam connected to an infinite uniform channel -- a region that extends to infinity along the upstream direction (x axis) with uniform y-z cross-section. This restriction of a uniform cross-section for the fluid domain upstream of some cross-section is imposed because it permits uncoupling of the three-dimensional boundary value problem for the infinite

channel into two problems: a one-dimensional problem in the upstream direction and a two-dimensional problem over the cross-section. With this restriction, it is possible to efficiently recognize the infinite extent of the reservoir in the upstream direction.

The finite region of irregular geometry is idealized as an assemblage of three-dimensional finite elements as shown in Figure 2.2(c), with the finite element mesh compatible with that of the dam at its upstream face. For the infinite channel, a finite element discretization of the cross-section, compatible with the discretization of the irregular region over the common cross-section -- the transmitting plane in Figure 2.2(c) -- combined with a continuum representation in the infinite direction provides for the proper transmission of pressure waves. Physically this treatment can be interpreted as a discretization of the fluid domain into sub-channels of infinite length [Figure 2.2(c)]. The properties of the impounded water are characterized by the velocity of pressure waves C and the mass density ρ or unit weight w_w .

2.4 Absorptive Reservoir Boundary

The boundary of a reservoir upstream from a dam would typically consist of alluvium, silt, and other sedimentary material. This section on the modelling of these materials is taken from a recent work on concrete gravity dams [14].

Over a long period of time, the sediments may deposit to a significant depth in some reservoirs. The depth of sediments can be recognized in the analytical procedure presented in this paper by correspondingly reducing the depth of the fluid domain. However, the influence of the sediments on the static stresses in the dam or on the vibration properties of the dam are not considered in the analysis because it should be negligible as the sediments are very soft, highly saturated and exert lateral forces only on the lower part of the dam.

The effects of interaction between the impounded water and the foundation rock would be dominated by the overlying alluvium and sediments, possibly deposited to a significant depth. These reservoir boundary materials are highly saturated with a low shear modulus. A hydrodynamic pressure wave impinging on such materials will partially reflect back into the water and partially refract,

primarily as a dilatational wave, into the layer of reservoir boundary materials. Because of the considerable energy dissipation that results from hysteretic behavior and sediment particle turbulence, the refracted wave is likely to be absorbed in the layer of soft, saturated sediments and essentially dissipated before reaching the underlying foundation rock.

The absorption of hydrodynamic pressure waves at the reservoir boundary can be represented approximately by a one-dimensional model, normal to the boundary and independent of the location on the boundary, that does not explicitly consider the thickness of the sediment layer. For this model, the boundary condition at the reservoir boundary is developed in references [9,14,15]. The fundamental parameter characterizing the effects of absorption of hydrodynamic pressure waves at the reservoir boundary is the admittance or damping coefficient $q = \rho / \rho_r C_r$ in which $C_r = \sqrt{E_r / \rho_r}$ where E_r is the Young's modulus and ρ_r is the mass density of the materials at the reservoir boundary. The wave reflection coefficient α , which is the ratio of the amplitude of the reflected hydrodynamic pressure wave to the amplitude of a normally propagating pressure wave incident on the reservoir boundary, is related to the damping coefficient [5,15] by

$$\alpha = \frac{1 - qC}{1 + qC} \quad (2.1)$$

The wave reflection coefficient α is a more physically meaningful description than q of the behavior of the absorption of hydrodynamic pressure waves at the reservoir boundary. Although the wave reflection coefficient depends on the angle of incidence of the pressure wave at the reservoir boundary, the value α for normally incident waves, as given by equation (2.1) is used here for convenience. The wave reflection coefficient α may range within the limiting values of 1 and -1. For rigid reservoir boundary materials, $C_r = \infty$ and $q = 0$ resulting in $\alpha = 1$. For very soft reservoir boundary materials, C_r approaches zero and $q = \infty$, resulting in $\alpha = -1$. It is believed that α values from 1 to 0 would cover the wide range of materials encountered at the boundary of actual reservoirs.

2.5 Ground Motion

In earthquake response analysis of dams by the substructure method, the earthquake input is specified as the free-field ground motion at the dam-foundation rock interface [9]. This free-field ground motion was assumed to be uniform across the base in two-dimensional analyses of concrete gravity dams [14]. This approach of specifying the same motion over the entire dam-foundation rock interface is not appropriate for arch dams because the dam boundary in contact with the foundation rock extends through the height of the dam, and the free-field motion is expected to vary significantly over the height. Non-uniform boundary motions can be included in finite element analysis of structures [16]. The principal difficulty, however, is in rationally defining the variations in motions over height because no measurements have been obtained of actual ground motion variations in arch dam locations. Another possible approach is to define the earthquake input as a rigid-body translation of the basement rock on which the finite element model of the dam and foundation is supported. However, very little is known about earthquake motion at depth because most of the available strong motion records are from accelerographs located at the ground surface or in basements of buildings.

From the preceding discussion it is clear that it is difficult to define a suitable earthquake input mechanism for an arch dam. Neither of the two approaches can be justified rationally, thus a much simpler approximation is employed in this investigation. Specifically, a sufficient portion of the foundation rock is included to represent only the static foundation flexibility effects; the foundation rock is assumed to be massless for the dynamic analysis, and the earthquake input is specified as spatially-uniform motion of the basement rock [13]. Since there is no wave propagation mechanism in the massless foundation rock, the specified basement rock motion is transmitted without modification to the dam-foundation rock interface. In the context of the substructure method of analysis, the above mentioned approximation is equivalent to specifying the same free-field ground motion throughout the dam-foundation rock interface with the foundation rock assumed to be massless in computing the foundation impedance matrix. The ground acceleration is defined by its three components: $a_g^x(t)$ in the upstream direction, $a_g^z(t)$ in the cross-stream direction, and $a_g^y(t)$ in the vertical direction.

2.6 Morrow Point Dam-Water-Foundation Rock System

2.6.1 Morrow Point Dam

Numerical results are presented later to demonstrate the effectiveness of the various concepts and procedures developed in Chapter 3 for efficient earthquake response analysis of arch dams. In addition, results are presented later in Chapters 4 and 5 respectively for the harmonic response and earthquake response of an arch dam. These response results are all for Morrow Point Dam, located on the Gunnison River in Colorado. It is a 465 ft high, approximately symmetric, single centered arch dam. A detailed description of the geometry of the dam is available in references [5] and [17]. For the purpose of dynamic analysis, the dam is assumed to be symmetric about the x-y plane with the dimensions averaged from the two halves. The foundation and fluid domains are also assumed symmetric about the x-y plane, with the fluid domain extending to infinity in the upstream direction. Since the dam, fluid domain, and the foundation rock are assumed symmetric about the x-y plane, only one-half of the dam-fluid-foundation rock system will be analyzed. The response to upstream (x) or vertical (y) components of ground motion, which is symmetric about the x-y plane, is determined by analyzing one-half the system with symmetric boundary conditions on the x-y plane. The response to cross-stream (z) ground motion, which is antisymmetric about the x-y plane, is determined by analyzing one-half the system with antisymmetric boundary conditions on the x-y plane.

The finite element idealizations of one-half of the arch dam, foundation rock and the impounded water are shown in Figure 2.3. The finite element idealization of the dam, shown in Figure 2.3(a), consists of 8 thick shell finite elements in the main part of the dam and 8 transition elements in the part of the dam near its junction with foundation rock, with a total of 61 nodal points. When foundation-rock flexibility is considered, this idealization has 296 degrees of freedom for symmetric (x and y components) ground motion and 284 degrees of freedom for antisymmetric (z component) ground motion. The mass concrete in the dam is assumed to be homogeneous, isotropic and linearly elastic with the following properties: Young's modulus = 4.0 million psi, unit weight = 155 pcf and Poisson's ratio $\nu_s = 0.2$, except that the Young's modulus is varied as discussed in Section 4.2.1 for the frequency response functions presented in Chapter 4. A constant hysteretic damping

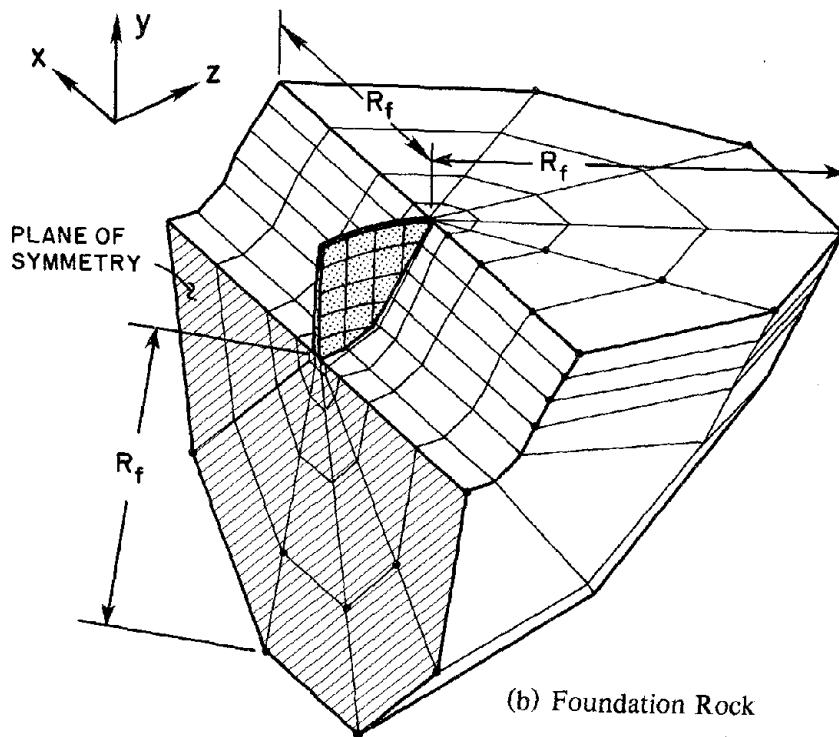
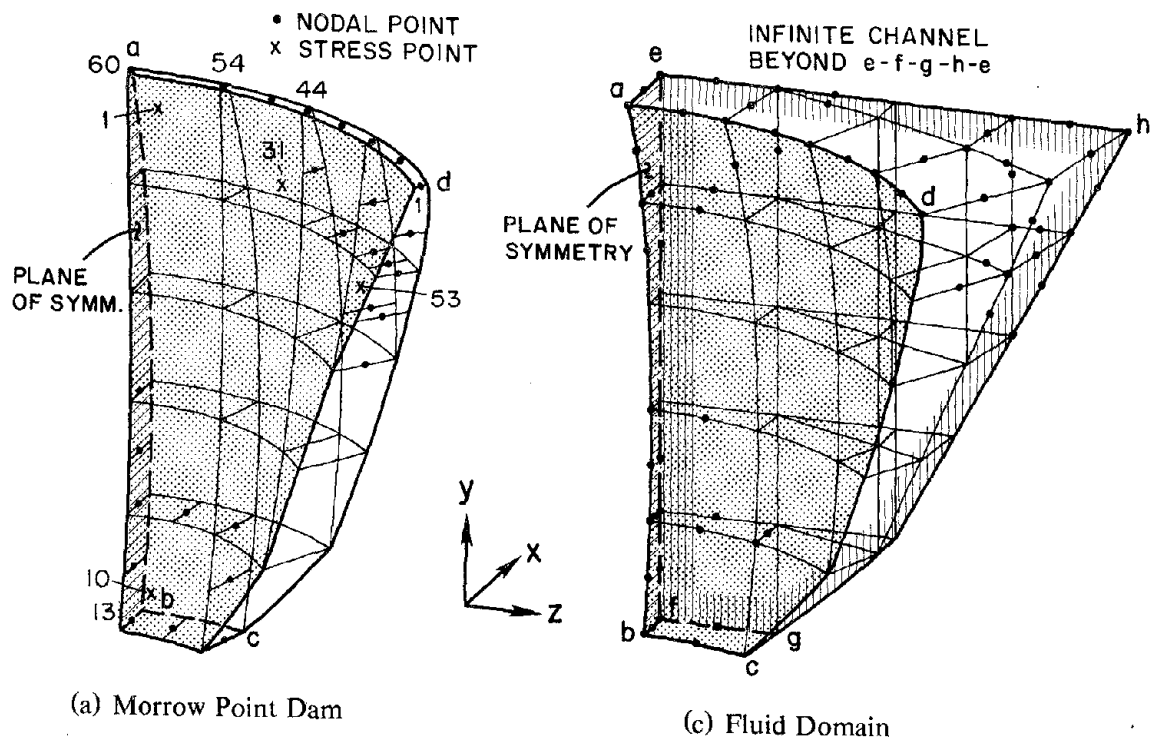


Figure 2.3 Finite element meshes of one-half of the Morrow Point Dam-water-foundation rock system. (Parts (a) and (c) adapted from reference [9])

factor $\eta_s = 0.10$, which corresponds to five percent damping in all natural vibration modes of the dam with empty reservoir on rigid foundation rock, is selected.

2.6.2 Impounded Water

The response analysis can handle any water level provided the finite element mesh for the dam is defined to include nodal points at the water level. However, for computational convenience, if the reservoir is not empty, the water level is assumed to be at the crest level in this investigation unless stated otherwise. The finite element idealization of the fluid region [Figure 2.3(c)] consists of 27 three-dimensional finite elements for the irregular fluid region with 189 nodal points; and has 157 pressure degrees of freedom for symmetric (x and y components) ground motion and 132 degrees of freedom for antisymmetric (z component) ground motion. Special equilibrium and compatibility conditions are imposed on the transmitting plane e-f-g-h-e [Figure 2.3(c)] connecting the irregular region with the infinite channel, to represent the upstream transmission of the hydrodynamic pressure waves. The following properties are assumed for the impounded water: velocity of pressure waves $C = 4720$ ft/sec and unit weight = 62.4 pcf.

There are no data available for the alluvium and sediments at the bottom and sides of the reservoir impounded by Morrow Point Dam, or for that matter at any other dam. The wave reflection coefficient α is varied between 0 and 1 in this investigation.

2.6.3 Shape of the Foundation-Rock Region

The flexibility effects of the foundation rock is included in the response analysis procedure to be described in Section 3.1 by including a certain volume of the foundation rock under the dam in modelling the complete dam-water-foundation rock system. Because the finite element method is used to discretize the foundation rock, there is no restriction to the geometry of the foundation model in the analysis procedure. In fact, the shape of the foundation can be selected to resemble, to a certain extent, the actual topography of the foundation rock at the dam site.

In analyzing Morrow Point Dam, the shape of the foundation rock is idealized using a procedure that has been adopted in the computer program ADAP [1]. Basically, this procedure assumes

that the dam canyon is prismatic in the upstream direction (x direction), as shown in Figure 2.4, and the volume of the foundation rock is described by a size parameter R_f . The shape of this foundation-rock region is further explained below.

First, let's assume that the thickness of the dam at the abutment is so small compared to the other dimensions that the dam-foundation rock interface can be represented by a line in space. The shape of the foundation rock can then be visualized as the volume in space described by moving a semicircular plane with its straight edge always parallel to the x axis (i.e. pointing in the upstream direction) and its center always lying on and moving along the dam-foundation line, as shown in Figure 2.5 for one-half of the dam-foundation rock system. As the semicircular plane is moved, it is also rotated simultaneously such that its plane is always perpendicular to the projection of the dam-foundation line on the y-z plane (Figure 2.5). The radius of the semicircular plane is the parameter R_f which controls the size of the plane and thus the volume covered by the moving plane.

Because the dam-foundation rock interface is not the single line shown in Figure 2.5, but a surface with finite width, the shape of the volume of foundation rock as described above is modified to recognize this finite width of the dam at the abutment. Since the dam-foundation rock interface usually intersects the straight edge of the semicircular plane at an oblique angle, a connection surface needs to be developed between the semicircular plane and the dam-foundation rock interface. The construction of such a connection surface is illustrated in Figures 2.6 and 2.7. The projection of the nodal points (in the finite element idealization of the dam) at its abutment on the y-z plane is shown in Figure 2.6, where A_1, B_1, \dots, M_1 represent the nodal points on the downstream face; A_2, B_2, \dots, M_2 represent the corresponding nodal points on the upstream face; and A, B, \dots, M represent the mid-surface nodal points (midway between the corresponding surface nodal points). The projection of the dam abutment on the y-z plane may be symmetric or non-symmetric about the y axis, depending on the geometry of the dam. The mid-surface points A, B, \dots, M have been joined together by the smooth curve shown as a dotted line, which can be regarded as the above-described dam-foundation line (Figure 2.5). Lines normal to this curve are extended from each of these mid-surface points with a length R_f . Denoted by AA^*, BB^*, \dots, MM^* in Figure 2.6, these

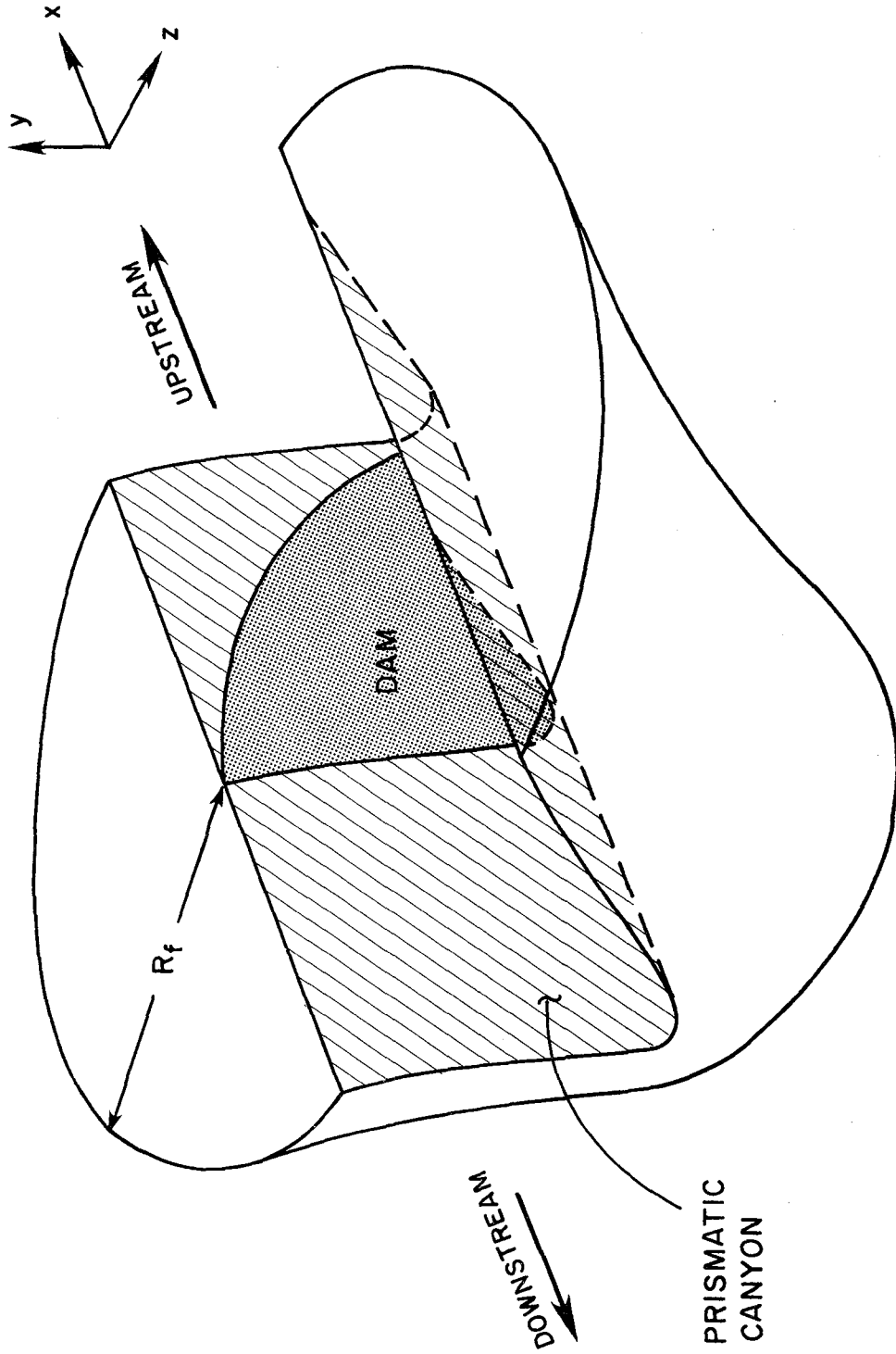


Figure 2.4 Idealized shape of foundation-rock region included in analysis.

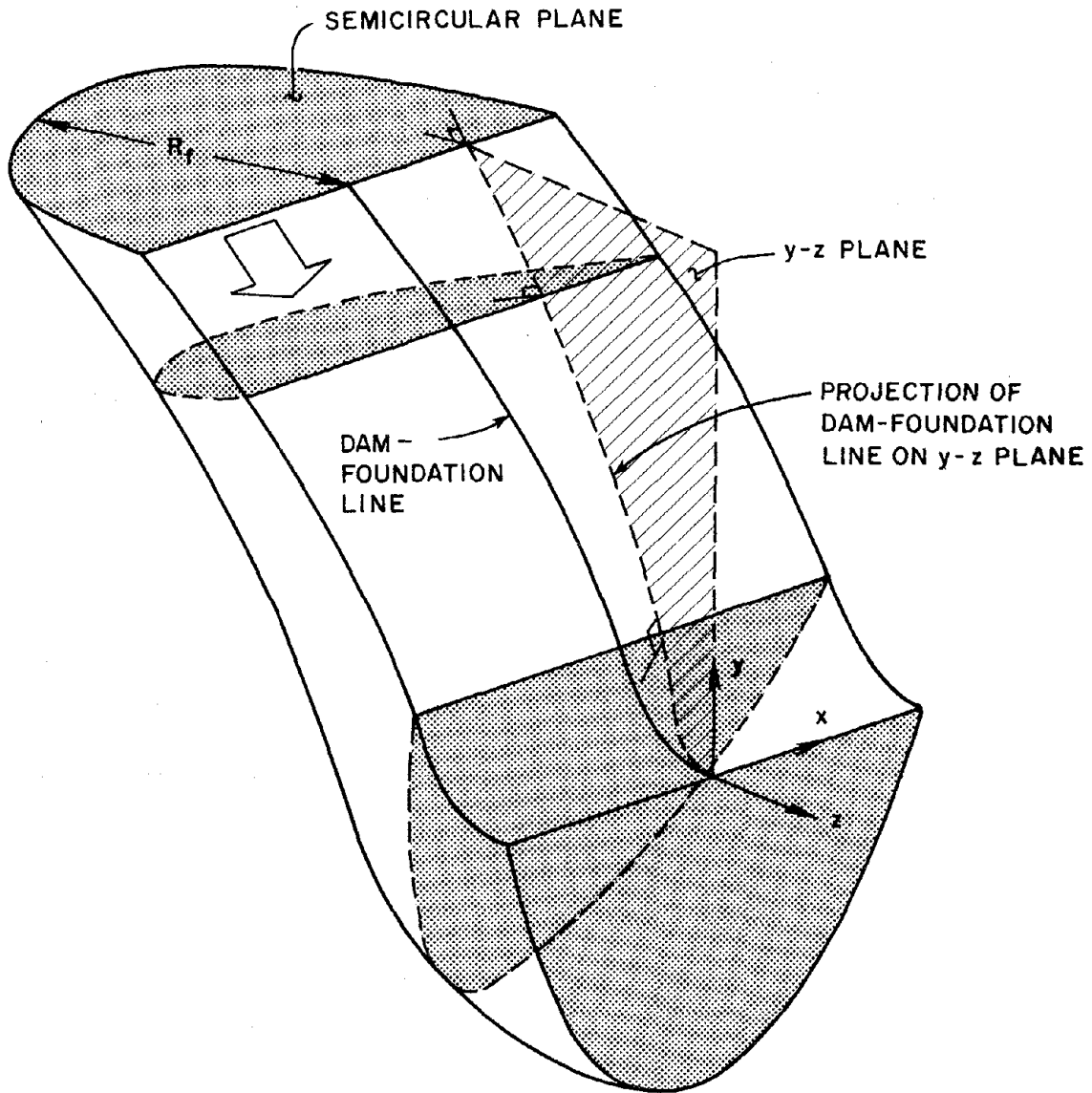


Figure 2.5 Illustrative sketch of the shape of the foundation-rock region. Only half of the region is shown.

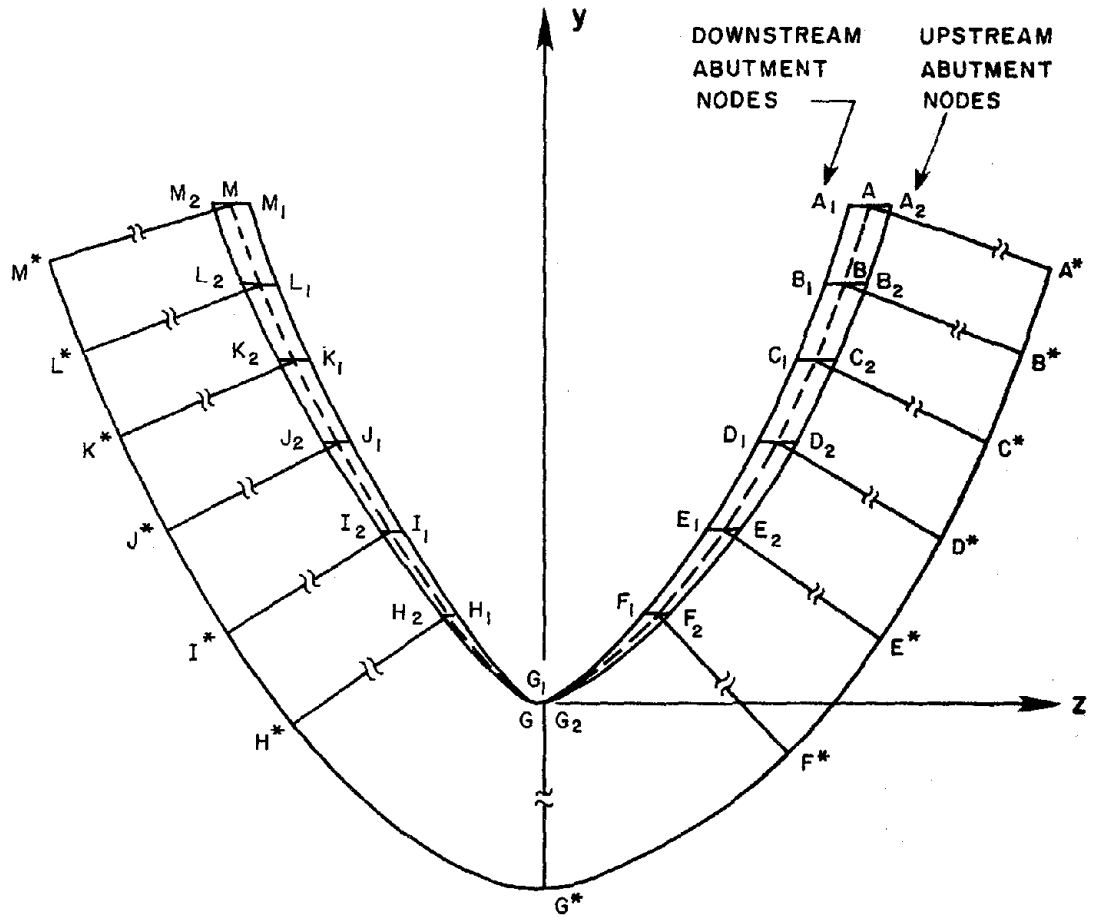
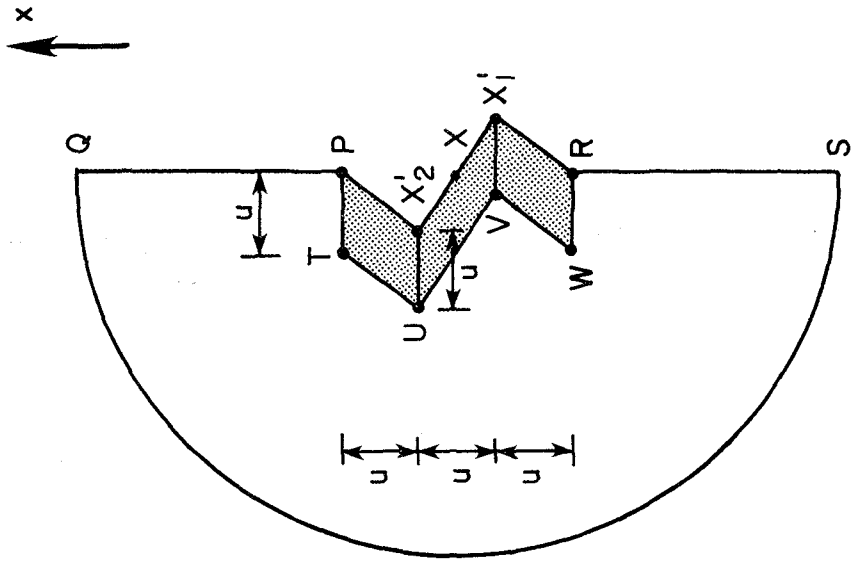
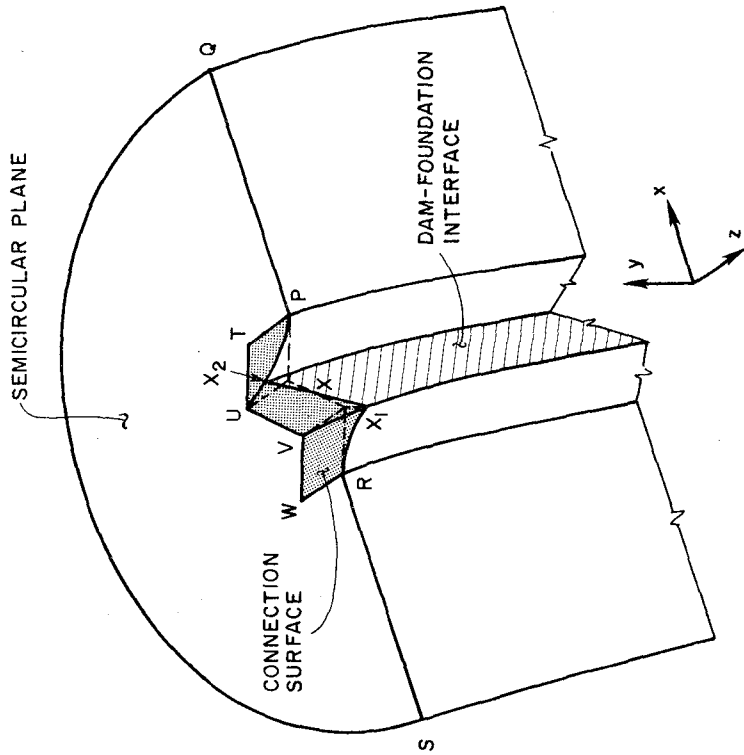


Figure 2.6 Projection of the shape of the foundation-rock region on y - z plane.



(b) Vertical (y) Projection on the Semicircular Plane



(a) Perspective View

Figure 2.7 Surface connecting the semicircular plane with the dam-foundation interface.

lines represent the projection on the y - z plane of the above-mentioned semicircular plane at the different positions along the dam-foundation line. Figure 2.7(a) shows the semicircular plane at one of the mid-surface nodes X and a connection surface connecting the plane to the dam-foundation interface. This connection surface, which is defined by points P, T, U, V, W, R, X_1 , and X_2 in Figure 2.7(a), is further illustrated in Figure 2.7(b) which shows the semicircular plane and the vertical (y) projection of the connection surface on the semicircular plane. This area of projection of the connection surface is defined by points $X'_1, X'_2, P, T, U, V, W$, and R [Figure 2.7(b)]. Points X'_1 and X'_2 are respectively the vertical projections of the downstream abutment nodal point X_1 and the upstream abutment nodal point X_2 . Points P and R on the straight edge of the semicircular plane are located such that the x coordinate difference of points R and X'_1 , X'_1 and X'_2 , and X'_2 and P are the same and equal to a distance denoted by u [Figure 2.7(b)]. Points T, U, V, W are located by extending lines perpendicular to the straight edge of the semicircle from points P, X'_2, X'_1 , and R , respectively, for a distance along the plane that is again equal to u [Figure 2.7(b)]. Thus the projection of the connection surface on the semicircular plane consists of three parallelograms [Figure 2.7(b), shown also in Figure 2.7(a)], whereas the connection surface itself consists of three separate surfaces joined together in space [Figure 2.7(a)].

With the above procedure to define the shape of the foundation-rock region, the size of the region depends entirely on R_f . This parameter should be chosen to be large enough to satisfactorily represent foundation flexibility effects in analysis of the dam.

Theoretically, the shape of the foundation-rock region should be compatible with the geometry of the dam and impounded water in the finite element system to be analyzed. However, this may sometimes be difficult to achieve with the shape of the foundation-rock region described earlier. Since foundation-rock flexibility is represented by the condensed stiffness matrix defined with reference to the degrees-of-freedom at the dam-foundation rock interface (see Chapter 3), compatibility must be satisfied at this interface but minor violations at the foundation-water interface may be acceptable.

2.6.4 Size of the Foundation-Rock Region

In order to represent the flexibility effects of the foundation rock on the earthquake response of the dam, an adequate volume of the foundation should be included in the dam-water-foundation rock system to be analyzed. However, the larger the foundation and the more finite elements needed to discretize the foundation, the greater is the required computational effort. Therefore, with the idealization of the shape of the foundation described in Section 2.6.3, the minimum value of R_f that can adequately represent the foundation-rock flexibility effects should be selected.

The natural frequencies and mode shapes of vibration play a central role in analyzing the earthquake response of the dam; in static analysis, the static displacements and stresses of the dam are the responses of concern. Therefore, the foundation-rock flexibility effects are adequately represented if, with the portion of the foundation rock included in the analysis, the static displacements and stresses, and natural vibration frequencies and mode shapes are accurately predicted. The minimum R_f beyond which increasing R_f has little influence on the computed results would be appropriate for practical analysis.

The variation of the natural frequencies of the first three symmetric vibration modes and of the first three antisymmetric vibration modes with the size parameter R_f are respectively shown in Figures 2.8 and 2.9. The natural frequencies are normalized with respect to their values for a rigid foundation (represented by $R_f = 0$); and three values of E_f/E_s are considered: 1, 1/2, and 1/4. The natural frequencies decrease as the size of the flexible foundation increases, but they are essentially independent of size beyond $R_f = H_s$, $1.5H_s$, and $2H_s$ approximately for $E_f/E_s = 1$, 1/2, and 1/4, respectively, where H_s is the maximum height of the dam. Although this observation is based on the first three natural frequencies, it is found to be true also for the higher natural frequencies. The first three symmetric mode shapes along the crest arch and the crown cantilever ($\theta = 0^\circ$) are plotted in Figures 2.10, 2.11, and 2.12 for $E_f/E_s = 1$, 1/2, and 1/4, respectively. The corresponding antisymmetric mode shapes along the crest arch and the $\theta = 13.25^\circ$ cantilever are plotted in Figures 2.13, 2.14, and 2.15. As shown in these figures, both the symmetric and antisymmetric mode shapes experience little or no changes as R_f increases from H_s to $3H_s$ for $E_f/E_s = 1$, from $1.5H_s$ to $3H_s$ for

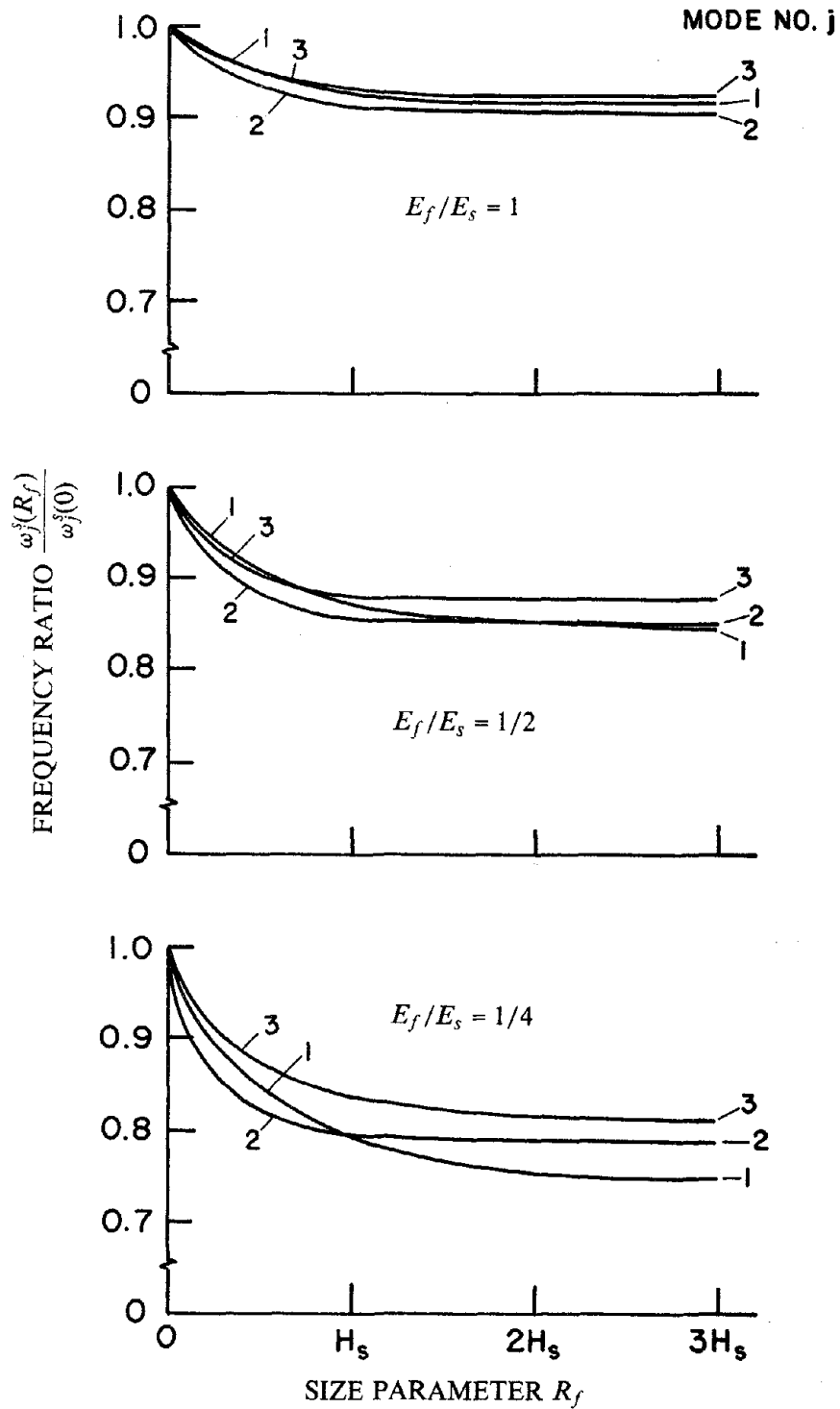


Figure 2.8 Variation of the natural frequencies of the first three symmetric vibration modes of the dam-foundation rock system with the size parameter R_f of the foundation-rock region.

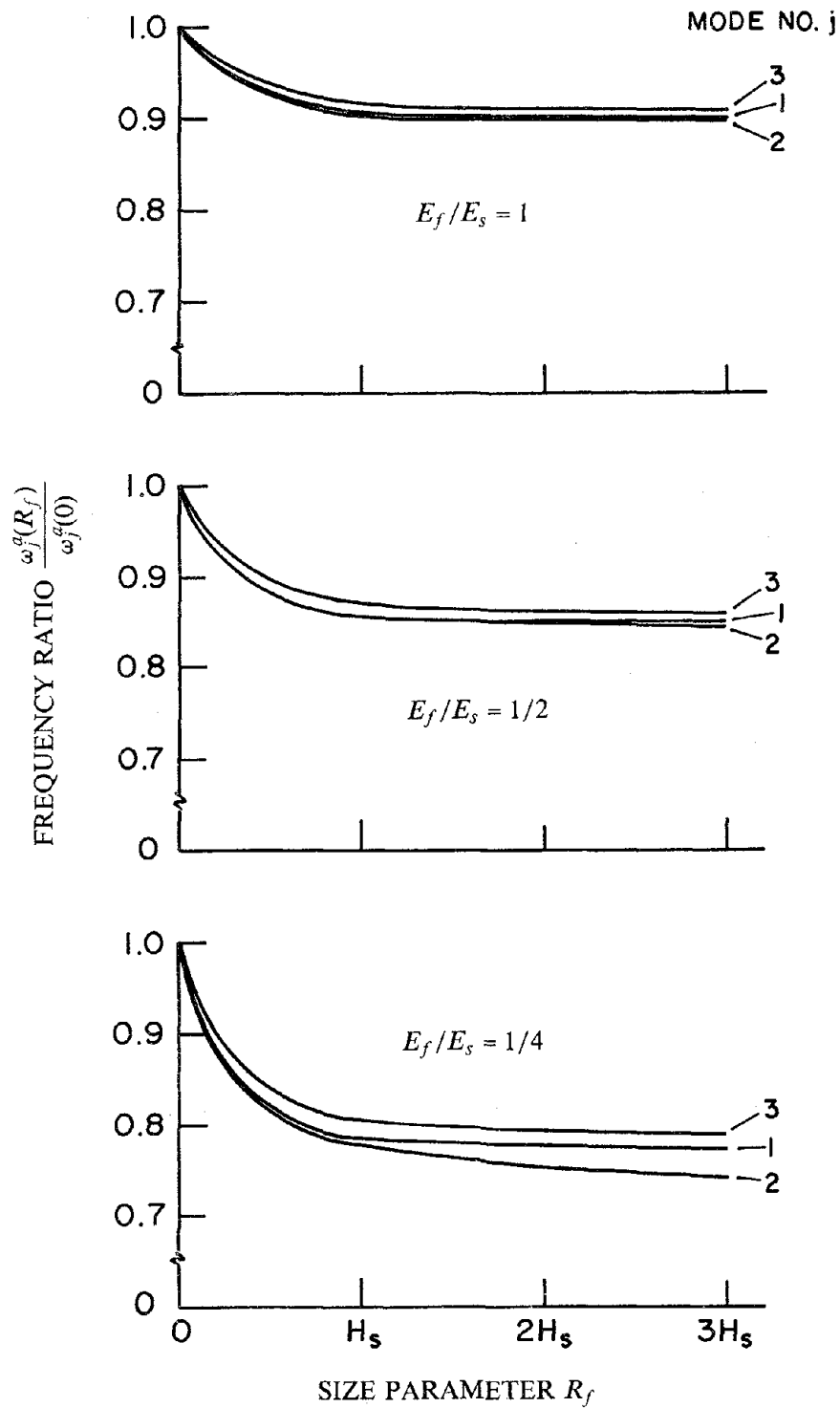


Figure 2.9 Variation of the natural frequencies of the first three antisymmetric vibration modes of the dam-foundation rock system with the size parameter R_f of the foundation-rock region.

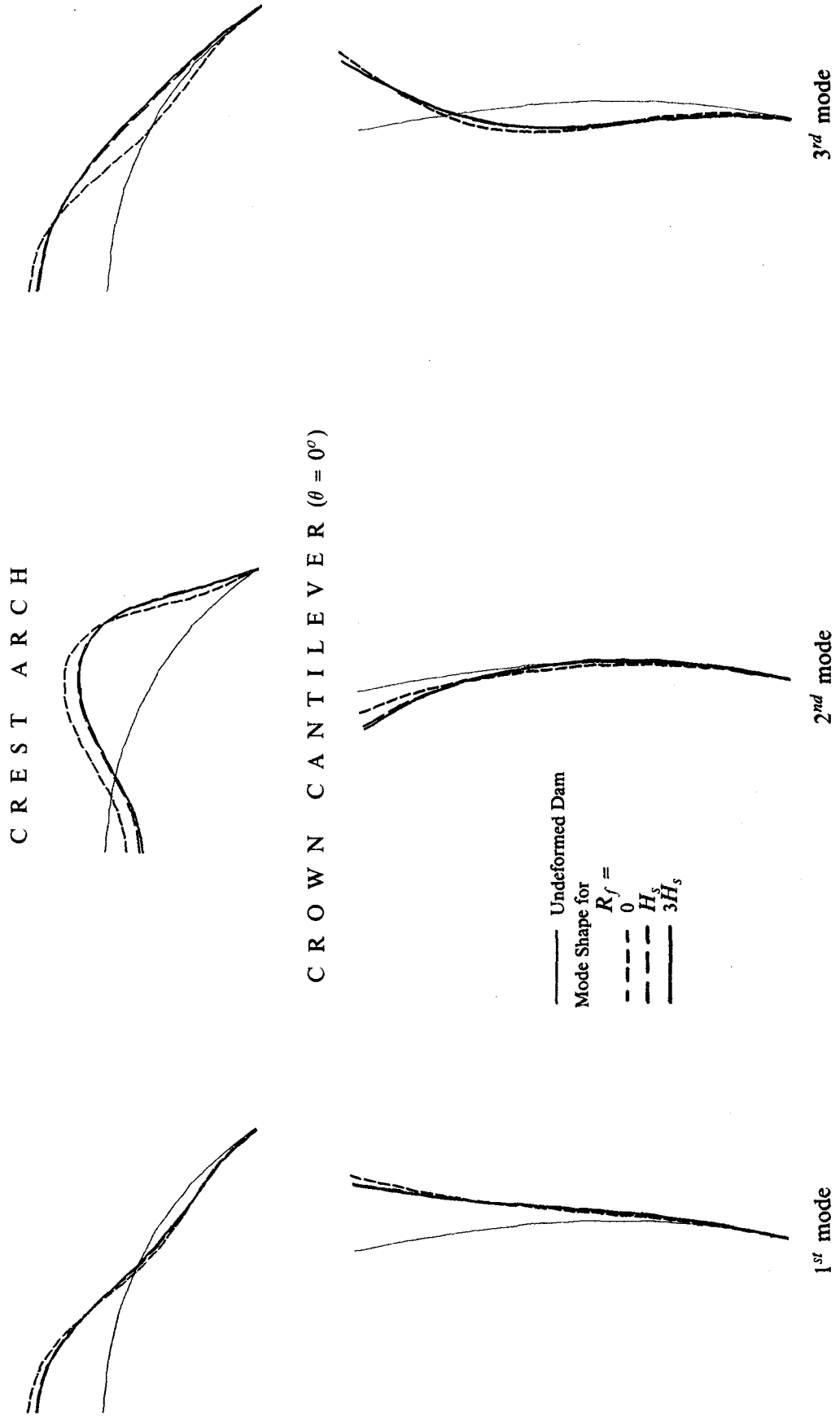


Figure 2.10 Variation of the shapes of the first three symmetric vibration modes with size parameter R_f of the foundation-rock region; $E_f/E_s = 1$.

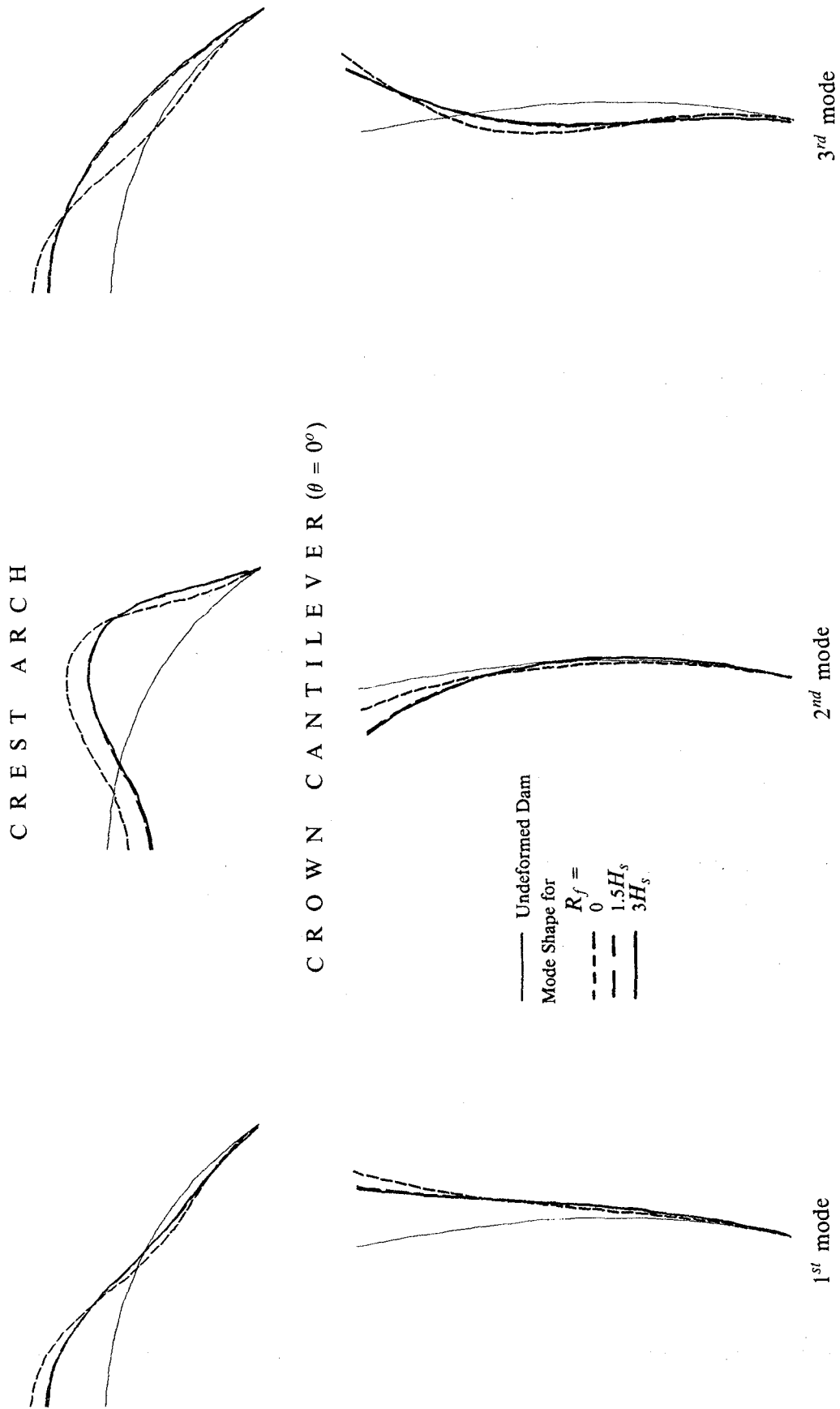


Figure 2.11 Variation of the shapes of the first three symmetric vibration modes with size parameter R_f of the foundation-rock region; $E_f/E_s = 1/2$.

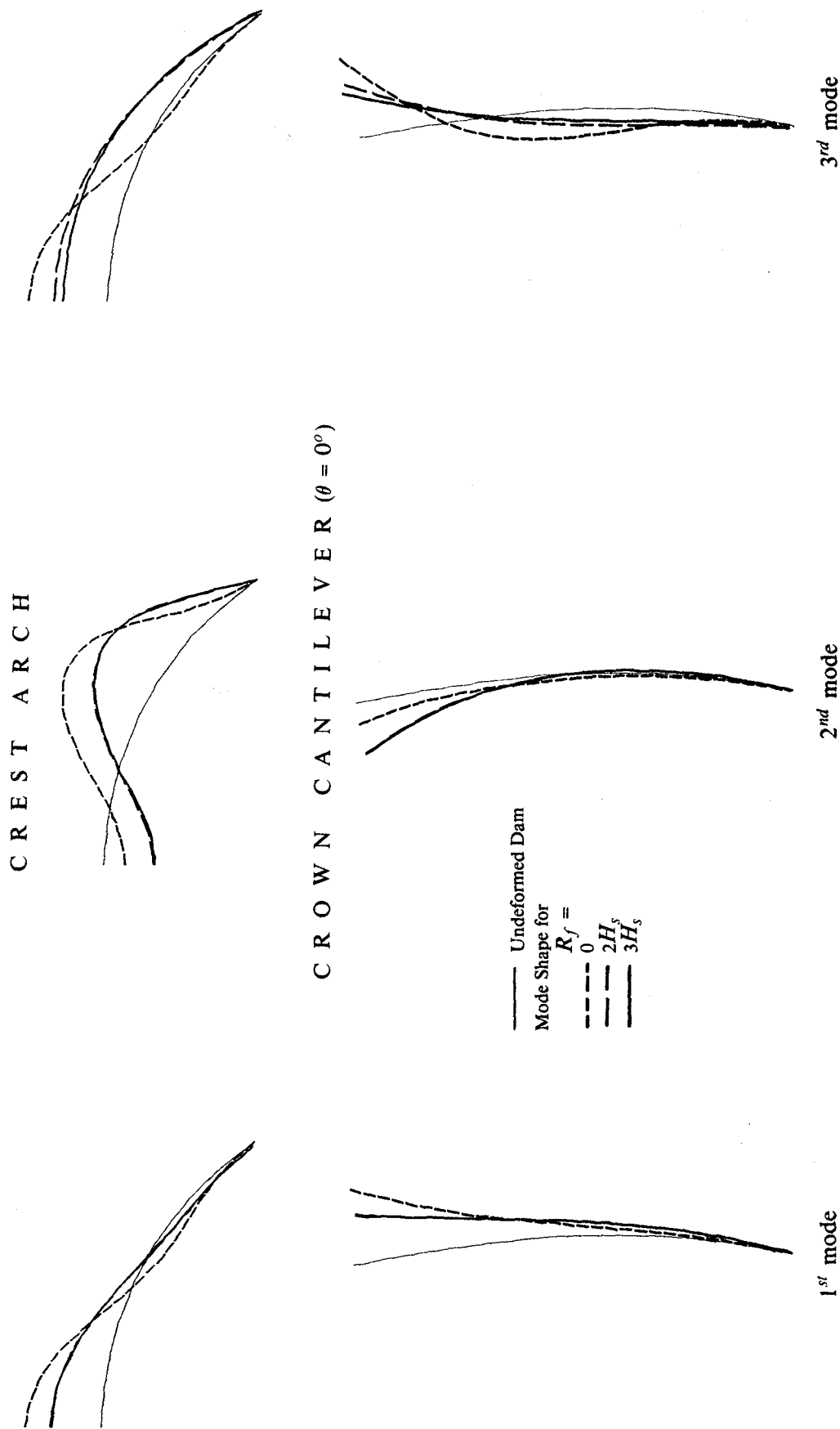
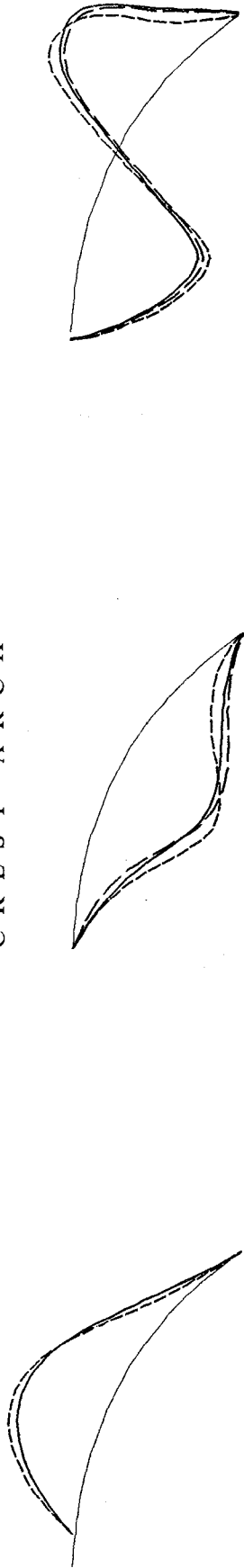
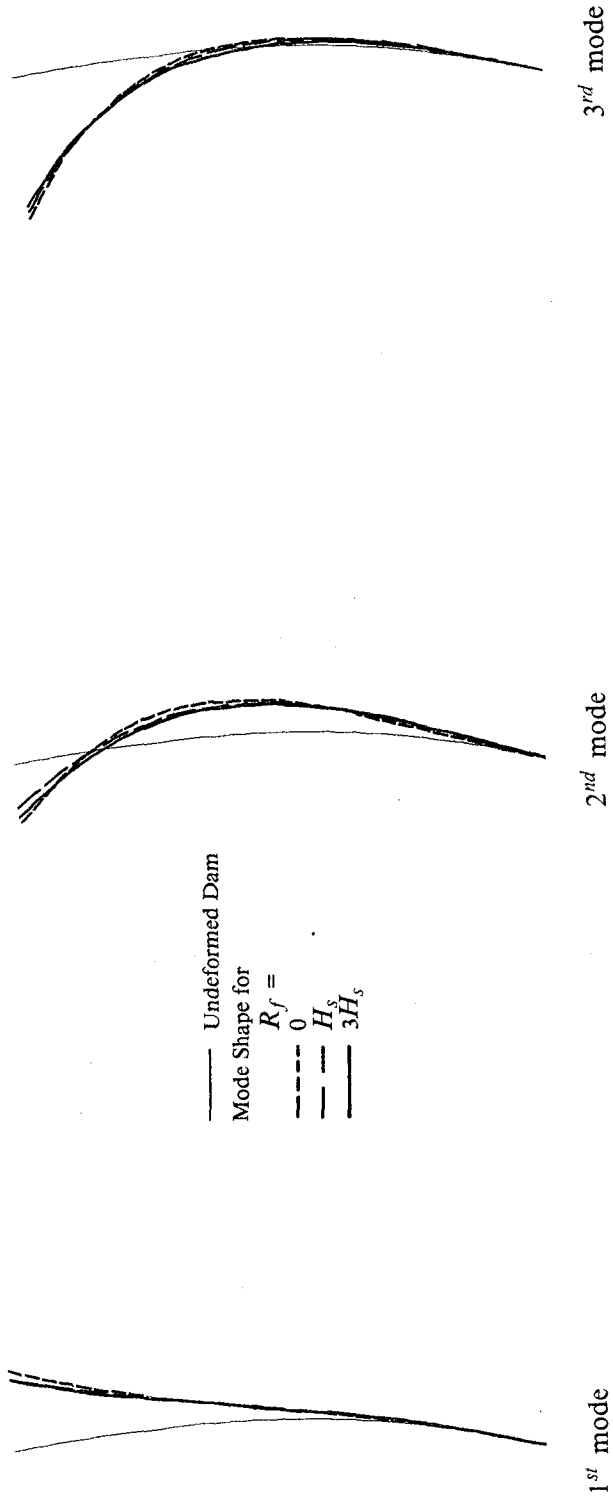


Figure 2.12 Variation of the shapes of the first three symmetric vibration modes with size parameter R_f of the foundation-rock region; $E_f/E_s = 1/4$.

CREST ARCH



CANTILEVER AT $\theta = 13.25^\circ$



— Undeformed Dam
 Mode Shape for
 $R_f =$
 0 — — — —
 H_s — · — · —
 $3H_s$ — — — —

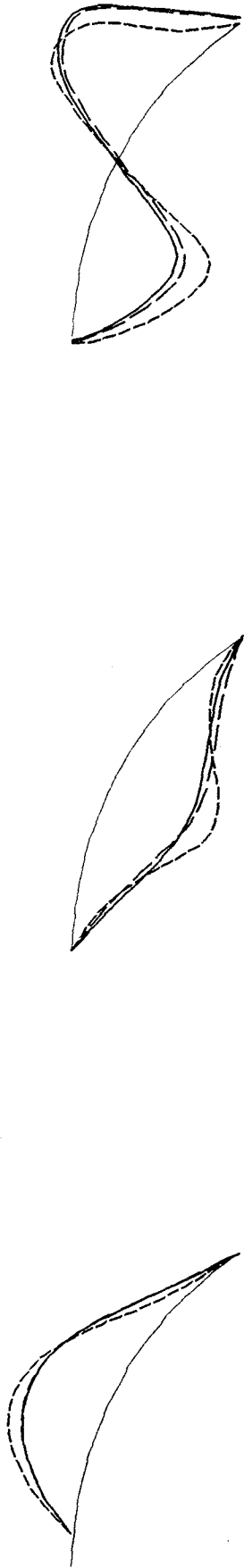
1st mode

2nd mode

3rd mode

Figure 2.13 Variation of the shapes of the first three antisymmetric vibration modes with size parameter R_f of the foundation-rock region; $E_f/E_s = 1$.

CREST ARCH



CANTILEVER AT $\theta = 13.25^\circ$

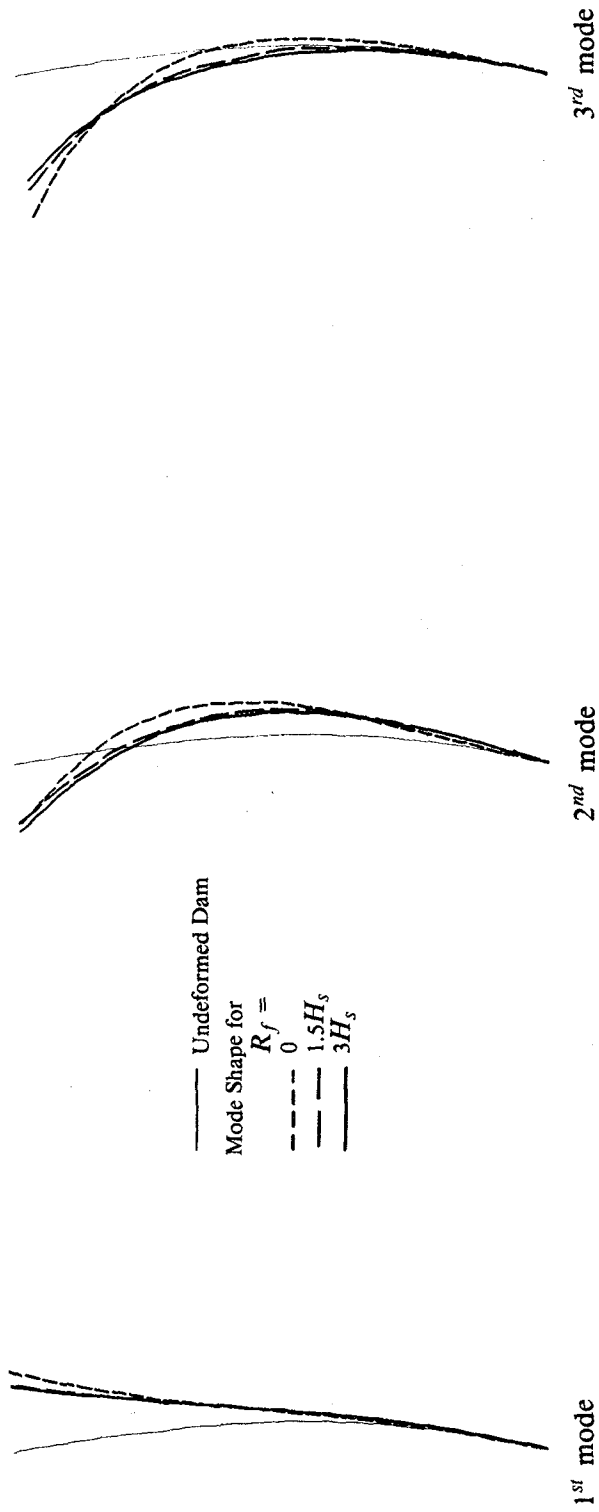
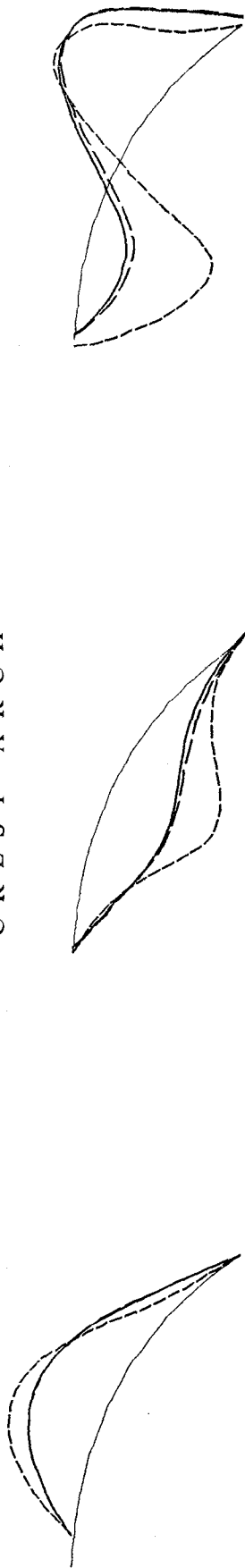
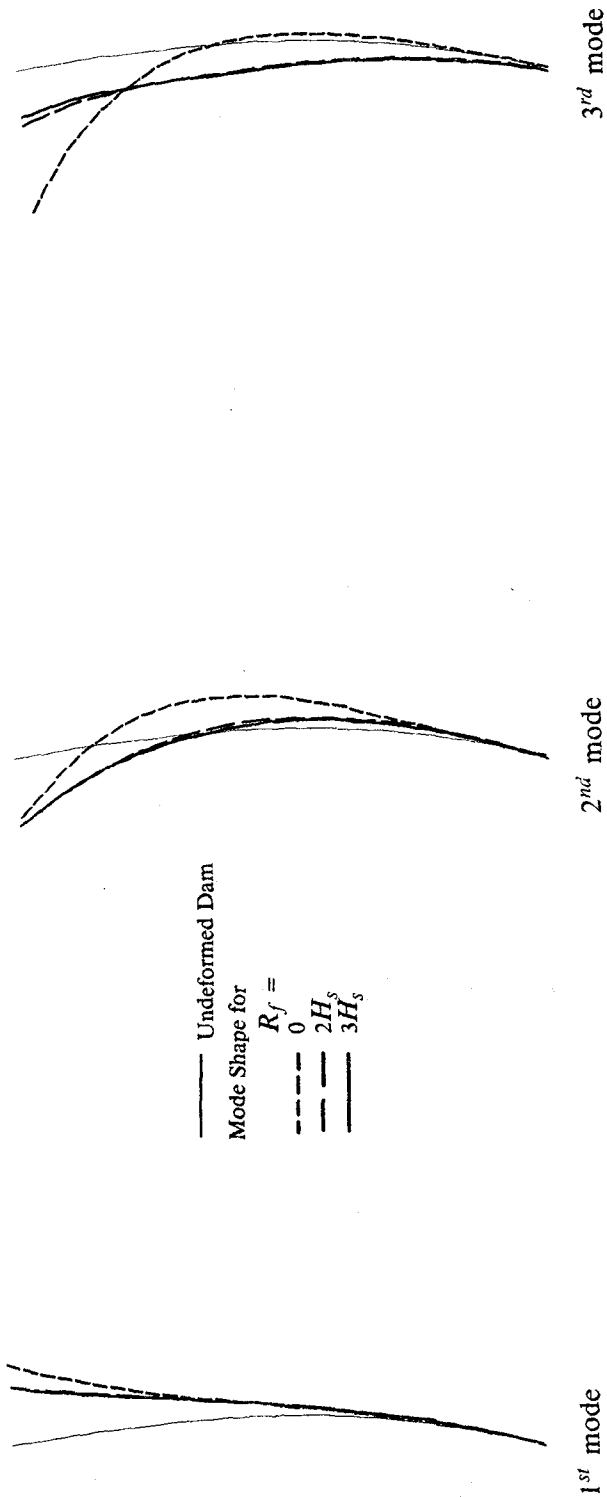


Figure 2.14 Variation of the shapes of the first three antisymmetric vibration modes with size parameter R_f of the foundation-rock region; $E_f/E_s = 1/2$.

C R E S T A R C H



C A N T I L E V E R A T $\theta = 13.25^\circ$



— Undeformed Dam
 Mode Shape for
 $R_f =$
 - - - 0
 - · - 2H_s
 - - - 3H_s

Figure 2.15 Variation of the shapes of the first three antisymmetric vibration modes with size parameter R_f of the foundation-rock region; $E_f/E_s = 1/4$.

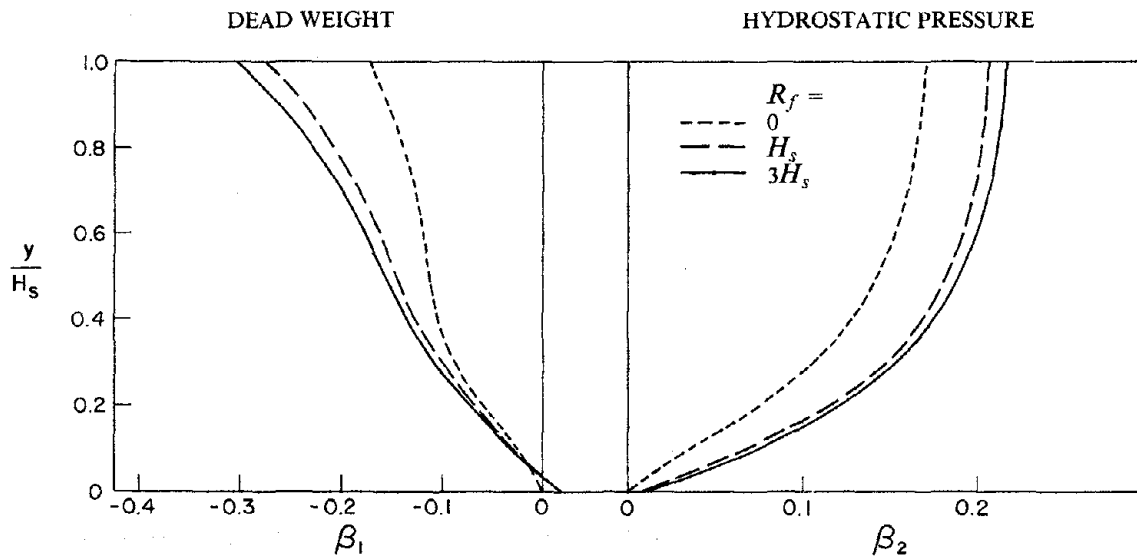
$E_f/E_s = 1/2$, and from $2H_s$ to $3H_s$ for $E_f/E_s = 1/4$.

The static displacements along the crown cantilever and the arch stresses adjacent to the crown cantilever section, both due to the dead weight of the dam, can be expressed as $\beta_1 w_s H_s^2/E_s$ and $\mu_1 w_s H_s$, respectively. Similarly, these response quantities due to the hydrostatic pressure with a full reservoir can be expressed as $\beta_2 w_w H_s^2/E_s$ and $\mu_2 w_w H_s$, respectively. The coefficients β_1 , β_2 , μ_1 , and μ_2 are presented in Figures 2.16, 2.17, and 2.18 for $E_f/E_s = 1$, $1/2$ and $1/4$, respectively. Tensile stresses and displacements in the downstream direction are defined as positive. It is apparent that the static displacements and stresses do not change much as R_f increases from H_s to $3H_s$ for $E_f/E_s = 1$, from $1.5H_s$ to $3H_s$ for $E_f/E_s = 1/2$, and from $2H_s$ to $3H_s$ for $E_f/E_s = 1/4$.

Since the natural frequencies, mode shapes, and the static responses remain essentially constant beyond $R_f = H_s$, $1.5H_s$, and $2H_s$ for $E_f/E_s = 1$, $1/2$, and $1/4$, respectively, the foundation-rock flexibility effects would be adequately represented if the above values of R_f are used for the corresponding E_f/E_s ratios. Thus, it is recommended that the shape of the foundation-rock region included in the analysis be selected as described above with its size defined by the following values of R_f , the size parameter: $R_f = H_s$ for $E_f/E_s = 1$; $R_f = 1.5H_s$ for $E_f/E_s = 1/2$; and $R_f = 2H_s$ for $E_f/E_s = 1/4$; with the value of R_f appropriately interpolated between H_s and $2H_s$ for E_f/E_s between 1 and $1/4$. For $E_f/E_s > 1$, it is recommended that a conservative choice of the size of the foundation with $R_f = H_s$ be used. While these recommendations are based on analysis of Morrow Point Dam, they should be useful in analysis of other arch dams.

Since the smallest value of E_f/E_s for which frequency response functions are presented in Chapter 4 is $1/4$, as suggested by the above guidelines, the foundation-rock region chosen to represent its flexibility effects should have the size parameter R_f equal to two times the height H_s of the dam. However, for additional conservatism in this research investigation, the size parameter R_f is selected as three times the height of the dam. The portion of the foundation rock included in the analysis to represent its static flexibility effects, with its shape defined in Section 2.6.3 and the size parameter $R_f = 3H_s$, is shown in Figure 2.3(b) with its external boundaries assumed fixed. The three-dimensional finite element idealization of the foundation rock region consists of 138 solid finite elements with 236

STATIC DISPLACEMENTS



ARCH STRESSES

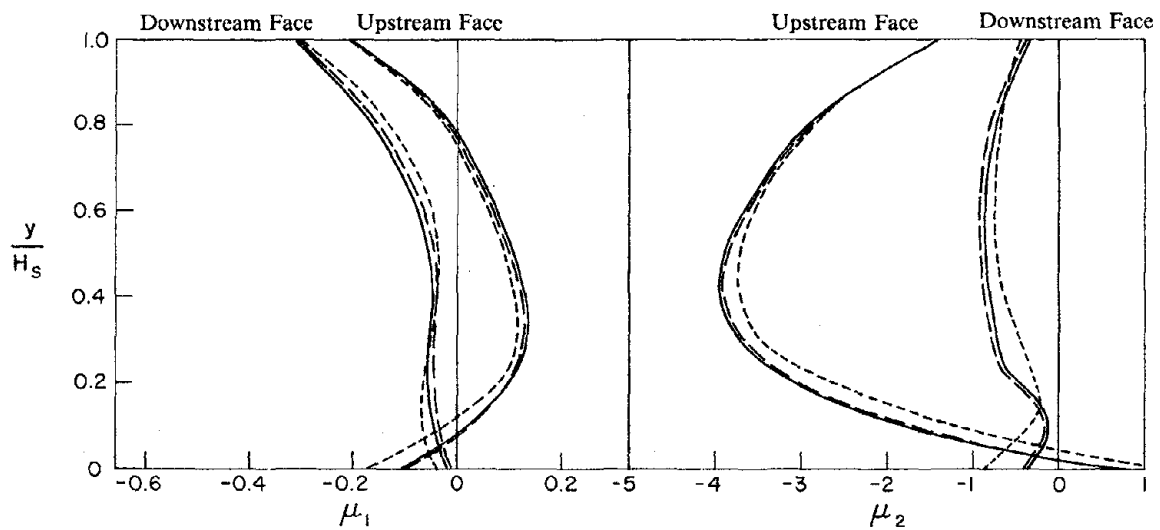
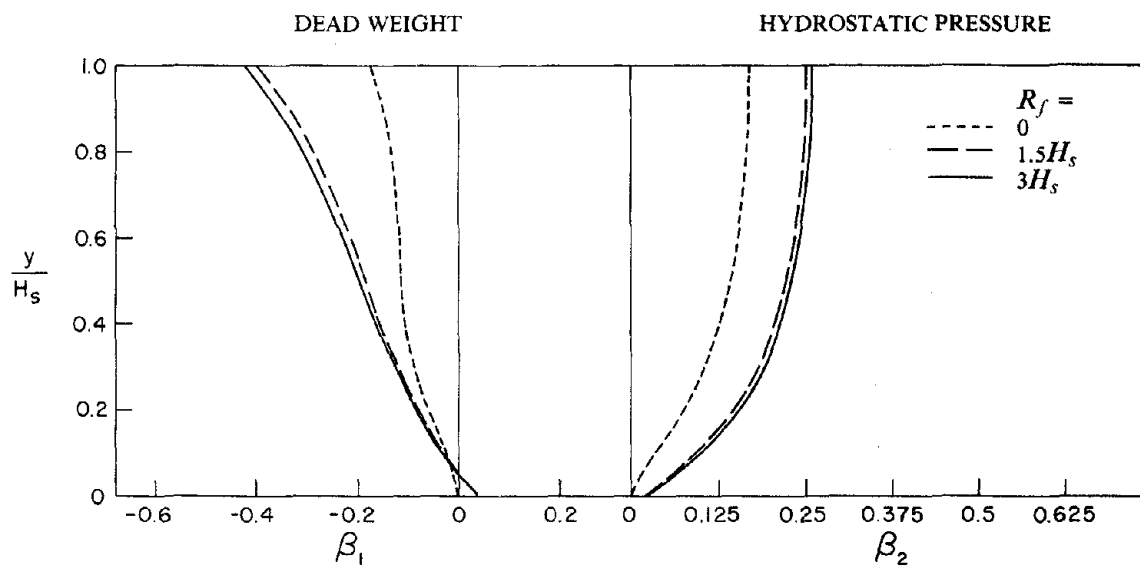


Figure 2.16 Variation of static responses due to dead weight and hydrostatic pressure, separately, with size parameter R_f of the foundation-rock region; $E_f/E_s = 1$. Results presented are for static displacements at crown cantilever and arch stresses near the crown cantilever ($\theta = 0^\circ$).

STATIC DISPLACEMENTS



ARCH STRESSES

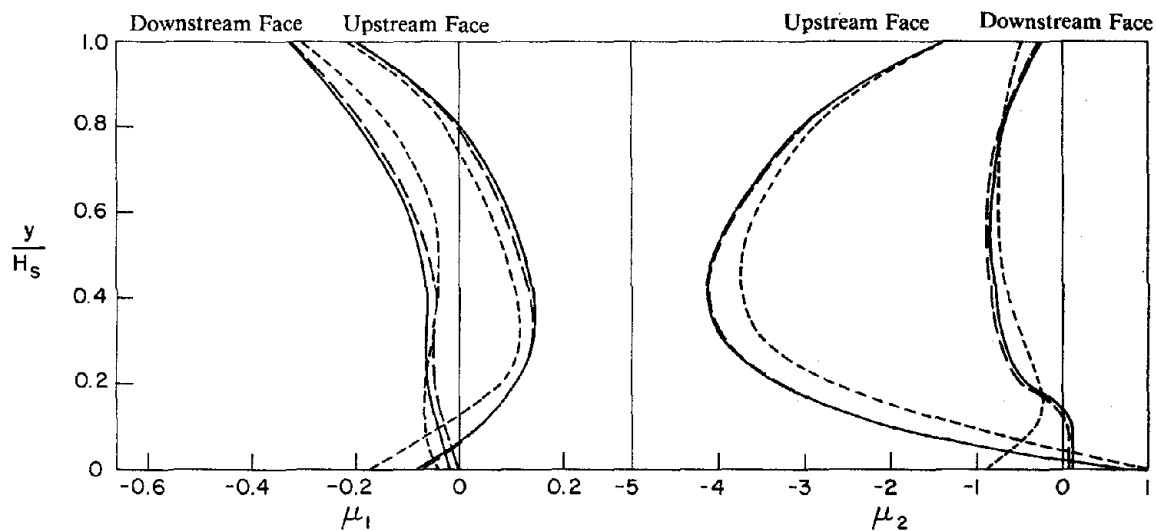


Figure 2.17 Variation of static responses due to dead weight and hydrostatic pressure, separately, with size parameter R_f of the foundation-rock region; $E_f/E_s = 1/2$. Results presented are for static displacements at crown cantilever and arch stresses near the crown cantilever ($\theta = 0^\circ$).

nodal points; and has 556 degrees of freedom for symmetric (x and y components) ground motion and 530 degrees of freedom for antisymmetric (z component) ground motion. The foundation rock is assumed to be homogeneous, isotropic, and linearly elastic with the following properties: Young's modulus = 4.0 million psi, and Poisson's ratio $\nu_f = 0.2$, except that the Young's modulus is varied as discussed in Section 4.2.1 for the frequency response functions presented in Chapter 4. As mentioned earlier, the inertial and damping effects of the foundation rock are neglected.

3. RESPONSE ANALYSIS PROCEDURE

3.1 Outline of Analysis Procedure

Based on the substructure method of analysis and frequency domain analysis concepts, a procedure is available [5,9] to evaluate the dynamic response of arch dams to harmonic ground motion, including hydrodynamic interaction effects. Developed earlier under the assumption of rigid foundation rock, this analysis procedure is extended in this investigation to include foundation rock flexibility; and to include Fourier synthesis of harmonic responses to obtain earthquake response. With this extension the procedure is summarized here, without derivation [9], as a sequence of analytical steps:

1. (a) Formulate \mathbf{m}_c and \mathbf{k}_c , the mass and stiffness matrices for the finite element idealization of the arch dam, with reference to the degrees of freedom (DOF) of all the nodal points in the idealization, including those on the dam-foundation rock interface.

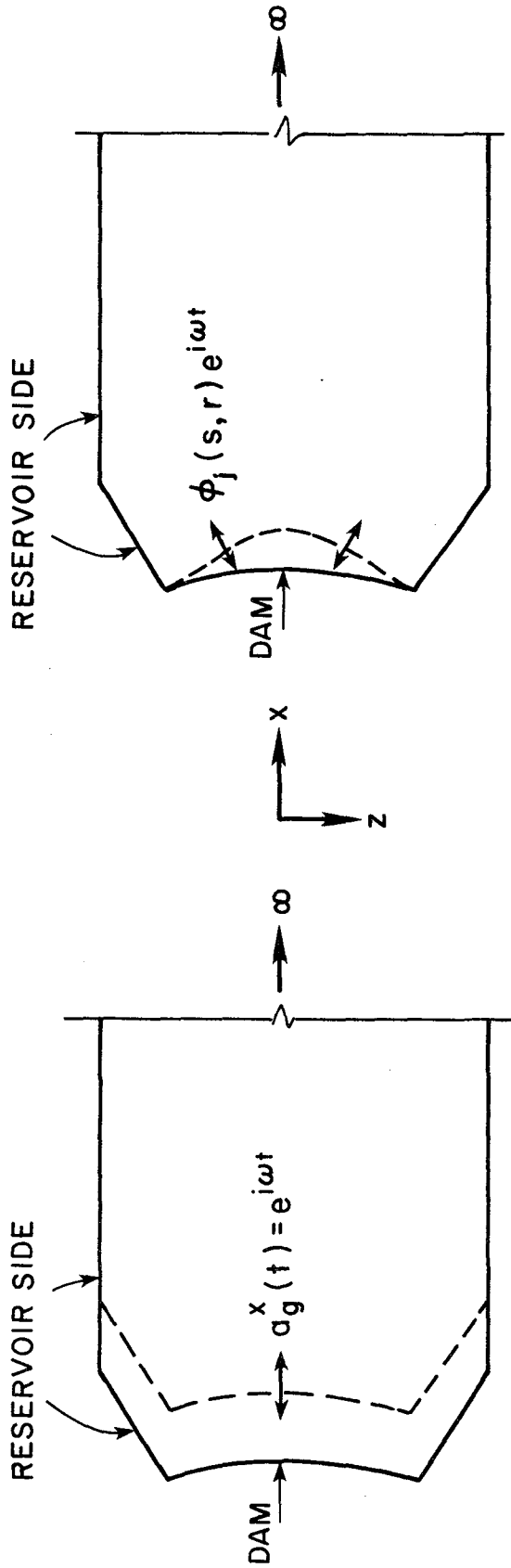
(b) Formulate \mathbf{k}_f , the stiffness matrix for the finite element idealization of the foundation rock region, with reference to the DOF of nodal points on the dam-foundation rock interface. The DOF not on this interface can be "condensed out" because the forces acting on the foundation rock arise only from dam-foundation rock interaction, thus existing only at the interface.

2. Solve the eigenproblem

$$\left[\mathbf{k}_c + \tilde{\mathbf{k}}_f \right] \boldsymbol{\phi}_j = \omega_j^2 \mathbf{m}_c \boldsymbol{\phi}_j \quad (3.1)$$

to obtain the first J natural vibration frequencies ω_j and corresponding mode shapes $\boldsymbol{\phi}_j$, of the dam supported on rigid or flexible foundation rock, consistent with the assumption made in the analysis; and normalize the mode shapes with respect to \mathbf{m}_c . In equation (3.1), $\tilde{\mathbf{k}}_f$ is the expanded version of \mathbf{k}_f described in step 1(b) with zero values corresponding to all DOF of the dam not on the dam-foundation rock interface.

3. Evaluate the frequency response function $\bar{p}_0^l(s,r,\omega)$ for hydrodynamic pressures on the upstream face of the dam due to the l -th component of ground (includes reservoir boundary) acceleration with a rigid dam [Figure 3.1(a)]. This function is obtained from the solution $\bar{p}(x,y,z,\omega)$



(a) Boundary Accelerations Causing $\bar{p}_0^x(s, r, \omega)$

(b) Boundary Accelerations Causing $\bar{p}_j(s, r, \omega)$

Figure 3.1 Reservoir boundary accelerations causing hydrodynamic pressures on the upstream face of the dam defined by frequency response functions $\bar{p}_0^x(s, r, \omega)$ and $\bar{p}_j(s, r, \omega)$. Only plan view is shown.

of the Helmholtz equation, governing the steady state harmonic motion of water:

$$\frac{\partial^2 \bar{p}}{\partial x^2} + \frac{\partial^2 \bar{p}}{\partial y^2} + \frac{\partial^2 \bar{p}}{\partial z^2} + \frac{\omega^2}{C^2} \bar{p} = 0 \quad (3.2)$$

subject to the radiation condition for $x = \infty$ and the following boundary conditions at the upstream face of the dam, the reservoir boundary, and the free surface of water, respectively:

$$\begin{aligned} \frac{\partial \bar{p}}{\partial n}(s, r, \omega) &= -\rho \epsilon^l(s, r) \\ \left[\frac{\partial}{\partial n} - i \omega q \right] \bar{p}(s', r', \omega) &= -\rho \epsilon^l(s', r') \end{aligned} \quad (3.3)$$

$$\bar{p}(x, H, z, \omega) = 0$$

In equations (3.2) and (3.3), H is the y - coordinate of the free surface of water measured from the base of the dam; s, r are the spacial coordinates on the upstream face of the dam; s', r' are the spacial coordinates on the reservoir boundary; n is the inward normal direction at the upstream dam face or reservoir boundary (Figure 3.2); and ρ is the mass density of water; $\epsilon^l(s, r)$ ($s, r = s, r$ or s', r') is a function defined along accelerating boundaries which gives the length of the component of a unit vector along l in the direction of the inward normal n (Figure 3.2). Procedures for solving this boundary value problem and evaluating $\bar{p}_0^l(s, r, \omega)$ are presented in Section 3.2.

4. Evaluate the frequency response function $\bar{p}_j(s, r, \omega)$ for hydrodynamic pressure due to normal acceleration $\phi_j(s, r)$ of the upstream face of the dam corresponding to the j th natural vibration mode shape, with no motion of the reservoir boundary [Figure 3.1(b)]. This function is obtained from the solution $\bar{p}(x, y, z, \omega)$ of the Helmholtz equation (3.2) subject to the radiation condition for $x = \infty$ and the following boundary conditions at the upstream face of the dam, the reservoir boundary, and the free surface of water, respectively:

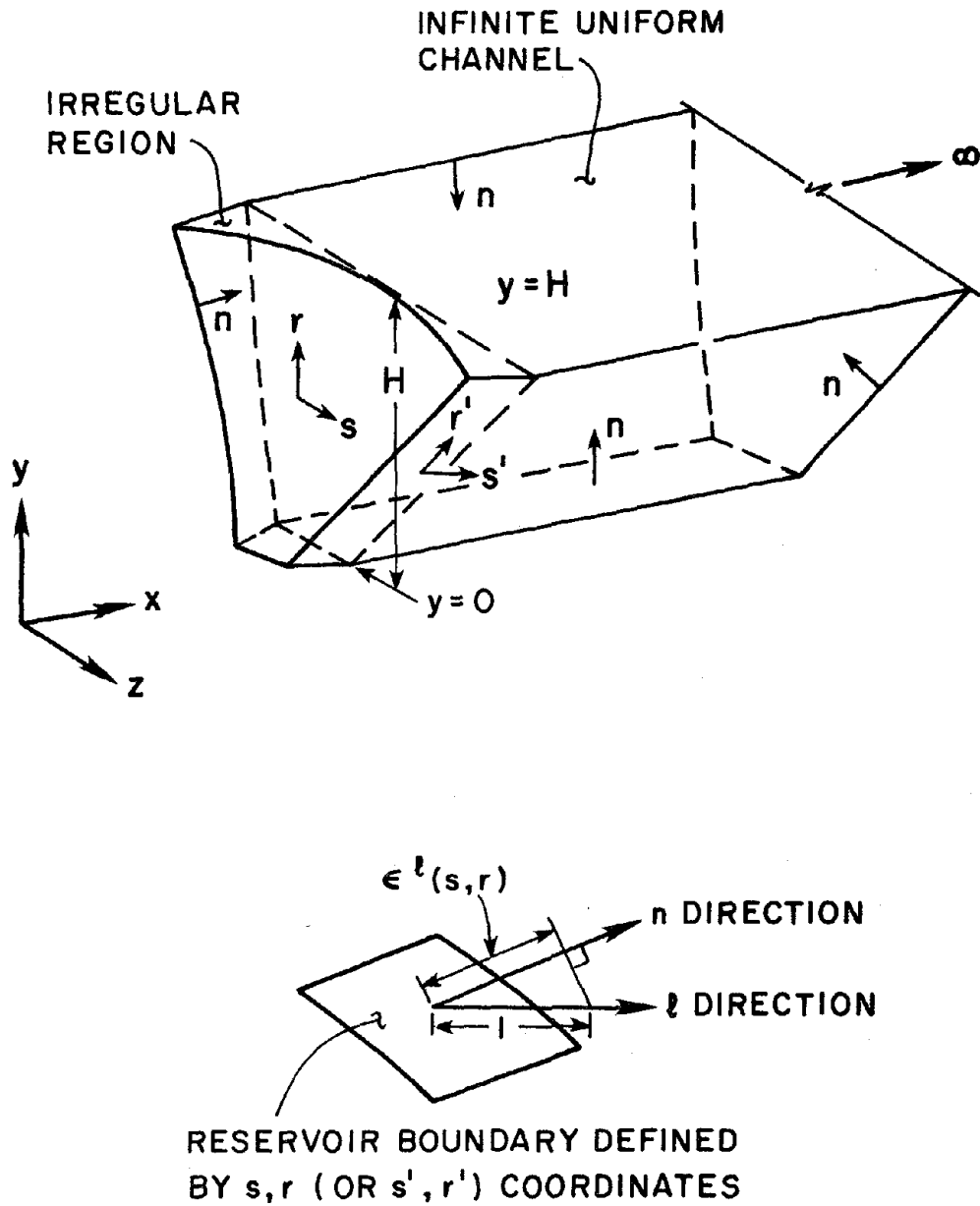


Figure 3.2 Definition of various terms associated with the fluid domain substructure. (Adapted from reference [9])

$$\begin{aligned} \frac{\partial \bar{p}}{\partial n}(s,r,\omega) &= -\rho \phi_j(s,r) \\ \left[\frac{\partial}{\partial n} - i\omega q \right] \bar{p}(s',r',\omega) &= 0 \\ \bar{p}(x,H,z,\omega) &= 0 \end{aligned} \quad (3.4)$$

Procedures for solving this boundary value problem and evaluating $\bar{p}_j(s,r,\omega)$ are presented in Section 3.2.

5. Evaluate the vectors of nodal forces $\bar{\mathbf{Q}}_0^l(\omega)$ and $\bar{\mathbf{Q}}_j^f(\omega)$ statically equivalent to the negatives of the corresponding pressure functions at the upstream face of the dam computed in steps 3 and 4: $\bar{p}_0^l(s,r,\omega)$ and $\bar{p}_j(s,r,\omega)$, respectively.

6. Formulate the J complex-valued equations in the unknown frequency response functions $\bar{\mathbf{Y}}_j^l(\omega)$, $j = 1, 2, \dots, J$, for the generalized coordinates corresponding to the vibration modes included in the analysis:

$$\mathbf{S}(\omega) \bar{\mathbf{Y}}^l(\omega) = \mathbf{L}^l(\omega) \quad l = x, y, z \quad (3.5)$$

where the elements of the matrix \mathbf{S} and the vector \mathbf{L} are

$$S_{nj}(\omega) = \left[-\omega^2 + (1 + i\eta_s) \omega_n^2 \right] \delta_{nj} - i\eta_s \{\phi_n^b\}^T \mathbf{k}_f \{\phi_j^b\} + \omega^2 \{\phi_n^f\}^T \bar{\mathbf{Q}}_j^f(\omega) \quad (3.6)$$

$$L_n^l(\omega) = -\phi_n^T \mathbf{m}_c \mathbf{1}_c^l + \{\phi_n^f\}^T \bar{\mathbf{Q}}_0^l(\omega)$$

where δ_{nj} is the Kronecker delta function; η_s is the constant hysteretic damping factor for the dam; ϕ_n^f is a subvector of ϕ_n containing only the elements corresponding to the nodal points at the dam-water interface; ϕ_n^b is a subvector of ϕ_n containing only the elements corresponding to the nodal points at the dam-foundation rock interface; and vectors $\mathbf{1}_c^x$, $\mathbf{1}_c^y$, and $\mathbf{1}_c^z$ contain ones in positions corresponding to the x, y, and z translational DOF, respectively, with zeros elsewhere. The matrix $\mathbf{S}(\omega)$ and vector $\mathbf{L}^l(\omega)$ are determined according to equation (3.6) for each excitation frequency ω of interest.

7. Determine the frequency response functions $\bar{Y}_j^l(\omega)$ for the generalized coordinates. Repeated solution of equation (3.5) for excitation frequencies covering the range over which the earthquake ground motion and structural response have significant components lead to the complete frequency response functions $\bar{Y}_j^l(\omega)$.

8. Determine the response of the dam to arbitrary ground motion. The generalized coordinates are given by the Fourier integral as a superposition of responses to individual harmonic components of the ground motion

$$Y_j^l(t) = \frac{1}{2\pi} \int_{-\infty}^{\infty} \bar{Y}_j^l(\omega) A_g^l(\omega) e^{i\omega t} d\omega \quad (3.7)$$

where $A_g^l(\omega)$ is the Fourier transform of the l -component of the specified free-field ground acceleration $a_g^l(t)$:

$$A_g^l(\omega) = \int_0^d a_g^l(t) e^{-i\omega t} dt \quad (3.8)$$

in which d is the duration of the ground motion. The Fourier integrals in equations (3.7) and (3.8) are computed in their discrete form using a recent version of the Fast Fourier Transform (FFT) algorithm [18].

9. Determine the relative displacement response to the upstream (x), cross-stream (z), and vertical (y) components of ground motion simultaneously by transforming the generalized coordinates to the nodal coordinates:

$$\mathbf{v}_c(t) = \sum_{j=1}^J \left[Y_j^x(t) + Y_j^y(t) + Y_j^z(t) \right] \boldsymbol{\phi}_j \quad (3.9)$$

10. Determine the stresses in the dam as a function of time from the nodal displacements. At any instant of time, the vector $\boldsymbol{\sigma}_p(t)$ of stress components in finite element p are related to the nodal displacement vector $\mathbf{v}_p(t)$ for that element by

$$\boldsymbol{\sigma}_p(t) = \mathbf{T}_p \mathbf{v}_p(t) \quad (3.10)$$

where \mathbf{T}_p is the stress-displacement transformation matrix for element p .

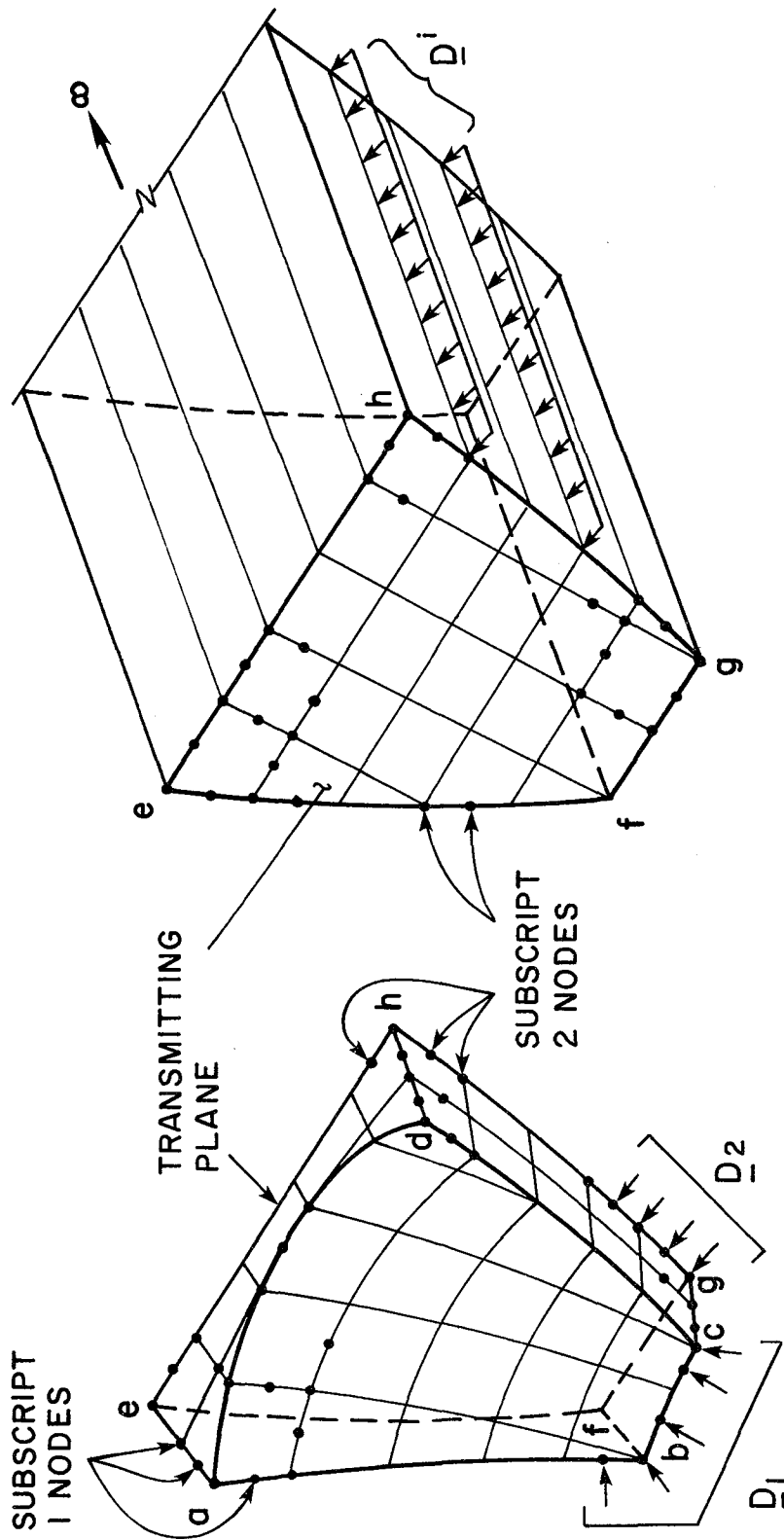
3.2 Evaluation of Hydrodynamic Terms

The frequency response functions $\bar{p}'_0(s,r,\omega)$ and $\bar{p}_j(s,r,\omega)$ for hydrodynamic pressures on the upstream face of the dam, required in step 5 of the analysis procedure summarized in Section 3.1, are solutions of the Helmholtz equation (3.2) subjected to the boundary conditions of equations (3.3) and (3.4), respectively. For practical problems these solutions are implemented by finite element procedures with the nodal pressures as the unknowns. As described earlier [9], the fluid domain of Figure 3.3 is idealized as an irregular region adjacent to the dam, discretized as an assemblage of three-dimensional finite elements, which is coupled at the plane e-f-g-h-e to a channel of uniform cross-section and infinite length in the upstream direction, discretized as an assemblage of infinitely long subchannels; with the two finite element meshes matched along e-f-g-h-e. Standard procedures are employed to formulate the finite element matrices of the irregular region. The restrictions of a uniform cross-section for the infinite region and boundary accelerations that are spatially uniform in the upstream direction permit a finite element treatment of the transmitting plane e-f-g-h-e combined with a continuum formulation in the upstream direction. This analysis procedure permits proper transmission of hydrodynamic pressure waves in the upstream direction; thus the boundary common to the two regions may be referred to as a transmitting plane. The procedure developed earlier [9] to determine \bar{p}'_0 and \bar{p}_j is summarized here, without derivation, as a sequence of analytical steps:

1. Formulate \mathbf{H}^i , \mathbf{B}^i and \mathbf{G}^i , the symmetric matrices for the finite element idealization of the infinitely long channel of constant cross-section [Figure 3.3(b)], with reference to the pressure degree of freedom (DOF) at each nodal point on the transmitting plane below the free surface of water. These matrices are analogous to the stiffness, damping, and mass matrices, respectively, that arise in dynamic finite element analysis of solid continua. The matrix \mathbf{B}^i , which arises from the wave absorptive effects of the reservoir boundary, contains non-zero terms associated only with the DOF of nodal points on the boundary e-f-g-h of the transmitting plane.

2. Solve the eigenproblem for the infinitely long channel:

$$\left[\mathbf{H}^i + i\omega q \mathbf{B}^i \right] \psi = \lambda^2 \mathbf{G}^i \psi \quad (3.11)$$



(a) Finite Element Discretization of Irregular Region (b) Finite Element Discretization of the Channel of Uniform Cross Section

Figure 3.3 Finite element discretization of fluid domain. (Adapted from reference [9])

to obtain the first N_ψ eigenvalues λ_n^2 and eigenvectors ψ_n . The eigenvectors are orthogonal with respect to the two square matrices, $[\mathbf{H}^i + i\omega q \mathbf{B}^i]$ and \mathbf{G}^i , and they are normalized with respect to \mathbf{G}^i .

If energy absorption through the reservoir boundary is considered, i.e. $q \neq 0$, equation (3.11) must be solved repeatedly for each value of ω because the complex-valued eigenvalues and eigenvectors depend on the excitation frequency ω ; otherwise they are real-valued and independent of excitation frequency and equation (3.11) need be solved only once.

3. Formulate the eigenvector matrix

$$\Psi = \begin{bmatrix} \psi_1 & \psi_2 & \cdots & \cdots & \cdots & \psi_{N_\psi} \end{bmatrix}$$

and $\boldsymbol{\kappa}$, an $N_\psi \times N_\psi$ diagonal matrix with n th diagonal term = κ_n which is complex-valued and computed from $\kappa_n = \sqrt{\lambda_n^2 - \frac{\omega^2}{C^2}}$, selecting the root for which both the real and imaginary parts are positive.

4. Formulate \mathbf{H} , \mathbf{B} and \mathbf{G} , the symmetric matrices for the finite element idealization of the three-dimensional irregular region of the fluid domain [Figure 3.3(a)], with reference to the pressure DOF at each nodal point below the free surface of water. These matrices are analogous to the stiffness, damping and mass matrices, respectively, that arise in dynamic finite element analysis of solid continua. The matrix \mathbf{B} , which arises from the wave absorptive effects of the reservoir boundary, contains non-zero terms associated only with the DOF of nodal points on the reservoir boundary.

5. (a) Formulate \mathbf{D}^i , the vector of normal accelerations at the nodal points on the transmitting plane e-f-g-h-e, from the prescribed accelerations along the boundary e-f-g-h in equations (3.3) and (3.4). The vector $\{\mathbf{D}^i\}_0^l$ computed from $\epsilon^l(s',r')$ in equation (3.3), which enters into the solution for \bar{p}_0^l , contains non-zero terms only for nodes along the boundary e-f-g-h. All terms in the vector $\{\mathbf{D}^i\}_j$, which enters into the solution for \bar{p}_j and is computed from the zero boundary accelerations of equation (3.4), are zero.

(b) Formulate \mathbf{D} , the vector of normal accelerations at the nodal points in the finite element idealization of irregular fluid region, from the prescribed boundary accelerations. The vector $\{\mathbf{D}\}'_0$, computed from prescribed accelerations $\epsilon^l(s,r)$ at the upstream face of the dam a-b-c-d-a and $\epsilon^l(s',r')$ at the reservoir boundary [equation (3.3)], which enters into the solution for \bar{p}'_0 , contains non-zero terms only for nodes along these boundaries. The vector $\{\mathbf{D}\}_j$ computed from prescribed accelerations $\phi_j(s,r)$ at the upstream face of the dam a-b-c-d-a [equation (3.4)], which enters into the solution for \bar{p}_j , contains non-zero terms only for nodes along this boundary.

6. Formulate the complex-valued equations in the unknown frequency response functions for the pressures at the nodal points

$$\begin{bmatrix} \left[\mathbf{H}_{11} + i\omega q \mathbf{B}_{11} - \frac{\omega^2}{C^2} \mathbf{G}_{11} \right] \\ \Psi^T \left[\mathbf{H}_{21} + i\omega q \mathbf{B}_{21} - \frac{\omega^2}{C^2} \mathbf{G}_{21} \right] \end{bmatrix} \Psi \begin{bmatrix} \left[\mathbf{H}_{12} + i\omega q \mathbf{B}_{12} - \frac{\omega^2}{C^2} \mathbf{G}_{12} \right] \Psi \\ \left[\mathbf{H}_{22} + i\omega q \mathbf{B}_{22} - \frac{\omega^2}{C^2} \mathbf{G}_{22} \right] \Psi + \boldsymbol{\kappa} \end{bmatrix} \begin{bmatrix} \bar{\mathbf{p}}_1(\omega) \\ \bar{\boldsymbol{\eta}}_2(\omega) \end{bmatrix} = \rho \begin{bmatrix} \mathbf{D}_1 \\ \Psi^T \mathbf{D}_2 + \boldsymbol{\kappa}^{-1} \Psi^T \mathbf{D}^i \end{bmatrix} \quad (3.12)$$

where the nodal points on the transmitting plane are identified by subscript 2 and the remaining nodes by subscript 1, and the matrices \mathbf{H} , \mathbf{B} and \mathbf{G} for the finite, irregular region (step 4) and the vector \mathbf{D} (step 5b) have been partitioned accordingly; $\bar{\mathbf{p}}_1(\omega)$ is the vector of hydrodynamic pressures at all subscript-1 nodal points, and $\bar{\boldsymbol{\eta}}_2(\omega)$ is related to $\bar{\mathbf{p}}_2(\omega)$ the vector of hydrodynamic pressures at all subscript-2 nodes by

$$\bar{\mathbf{p}}_2(\omega) = \Psi \bar{\boldsymbol{\eta}}_2(\omega) \quad (3.13)$$

7. Determine the frequency response functions $\bar{\mathbf{p}}_1(\omega)$ and $\bar{\boldsymbol{\eta}}_2(\omega)$:

(a) Solution of equation (3.12), with $\mathbf{D} = \{\mathbf{D}\}'_0$ from step 5b and $\mathbf{D}^i = \{\mathbf{D}^i\}'_0$ from step 5a, provides $\bar{\mathbf{p}}_1(\omega)$ and $\bar{\boldsymbol{\eta}}_2(\omega)$. This solution is repeated for each ground motion component, $l = x, y$ and z .

(b) Solution of equation (3.12), with $\mathbf{D} = \{\mathbf{D}\}_j$ from step 5b and $\mathbf{D}^i = \{\mathbf{D}^i\}_j$ from step 5a, provides $\bar{\mathbf{p}}_1(\omega)$ and $\bar{\boldsymbol{\eta}}_2(\omega)$. This solution is repeated for each vibration mode j to be included in the

analysis.

Repeated solution of equation (3.12) for excitation frequencies covering the range over which the earthquake ground motion and structural response have significant components leads to the complete frequency response functions $\bar{\mathbf{p}}_1(\omega)$ and $\bar{\boldsymbol{\eta}}_2(\omega)$.

8. Assemble the vector of frequency response functions for the hydrodynamic pressures at the nodal points on the upstream face of the dam: $\bar{\mathbf{p}}_0^l(\omega)$ from $\bar{\mathbf{p}}_1(\omega)$ determined in step 7a, $l = x, y$ and z ; and $\bar{\mathbf{p}}_j^f(\omega)$ from $\bar{\mathbf{p}}_1(\omega)$ determined in step 7b. The hydrodynamic force vectors $\bar{\mathbf{Q}}_0^l(\omega)$ and $\bar{\mathbf{Q}}_j^f(\omega)$, which are statically equivalent to the negatives of the pressure functions $\bar{p}_0^l(s, r, \omega)$ and $\bar{p}_j(s, r, \omega)$, respectively (step 5 of Section 3.1), are computed from the corresponding discrete versions $\bar{\mathbf{p}}_0^l(\omega)$ and $\bar{\mathbf{p}}_j^f(\omega)$.

3.3 Efficient Evaluation of Hydrodynamic Terms

3.3.1 Major Computational Steps

The complex-valued frequency response functions for the generalized coordinates of the dam are determined by solving equations (3.12) and (3.5) for each excitation frequency in the range of interest. The major computational effort in the solution process is the evaluation of the hydrodynamic terms in equations (3.5) and (3.6) involving the hydrodynamic force vectors $\bar{\mathbf{Q}}_0^l(\omega)$ and $\bar{\mathbf{Q}}_j^f(\omega)$, which are obtained from the frequency response functions $\bar{\mathbf{p}}_0^l(\omega)$ and $\bar{\mathbf{p}}_j^f(\omega)$ (steps 6-8 of Section 3.2) by using the principle of virtual displacements.

If compressibility of water is neglected, the hydrodynamic force vectors are independent of the excitation frequency ω , equal to the zero-frequency value; and their computation requires minimal effort.

The consideration of water compressibility, a factor that is known to significantly influence the earthquake response of concrete dams [9,19,20,21], leads to considerable increase in the computational effort. In particular the hydrodynamic force vectors are now frequency-dependent, requiring repeated formulation and solution of equation (3.12) for the range of frequencies over which the

ground motion and structural response have significant components. For each frequency, the number of complex-valued algebraic equations to be solved in equation (3.12) is equal to the number of subscript-1 nodal points in the finite element idealization of the irregular fluid region plus N_ψ , the number of eigenvectors ψ_j included to represent the pressures $\bar{p}_2(\omega)$ on the transmitting plane. Such solutions need to be repeated for each ground motion component $l = x, y$ and z and for each vibration mode of the dam $\phi_j, j = 1, 2, \dots, J$, included in the analysis.

The consideration of hydrodynamic wave absorption due to alluvium and sediments at the reservoir boundary, which is also known to significantly influence the earthquake response of dams [9,20] leads to further increase in computational effort. In this case, the eigenvalue problem for the infinitely long channel, equation (3.11), must be solved repeatedly for each value of ω (step 2 of Section 3.2), because the complex-valued eigenvalues and eigenvectors depend on the excitation frequency ω ; otherwise they are real-valued and independent of the excitation frequency requiring only one solution of equation (3.11). The computational effort required for repeated solution of the frequency-dependent, complex-valued eigenproblem is a very large portion, in some cases as much as half, of the total computational effort required to obtain the dam response. The computational effort required for one solution of equation (3.11) depends on the problem size, as determined by the number of nodal points in the finite element idealization of the transmitting plane plus N_ψ , the number of eigenvectors to be included.

Two aspects of computing the hydrodynamic force vectors $\bar{Q}_0^f(\omega)$ and $\bar{Q}_0^f(\omega)$ which contribute a major share of the computational effort are examined next with the objective of developing efficient computational procedures.

3.3.2 Number of Eigenvectors of the Infinite Channel

In computing the frequency response functions $\bar{Q}_0^f(\omega)$ and $\bar{Q}_0^f(\omega)$ for the hydrodynamic force vectors as described in Section 3.2, the pressures on the transmitting plane are sums of the contributions of an infinite number of natural vibration modes of the infinite channel, which must be truncated at a finite number N_ψ . Because the computational effort involved in several of the computational steps increases with N_ψ , only those eigenvectors that are necessary for accurate evaluation of

the dam response should be included in the analysis.

The summations should obviously include the contributions of all the eigenvectors of the infinite channel with eigenfrequencies ω_n^i less than the maximum excitation frequency ω_{\max} considered in the analysis. The eigenfrequencies of the infinite channel are functions of the wave reflection coefficient α , although their dependence on α is slight [20]. Consequently, the criterion for determining the number of eigenvectors to be included can be stated in terms of the eigenfrequencies of the infinite channel with rigid reservoir boundary -- as the largest n that satisfies

$$\omega_n^i < \omega_{\max} \quad (3.14)$$

where ω_n^i for a rigid reservoir boundary is given by $\omega_n^i = \lambda_n C$; and λ_n is the square root of the eigenvalue from equation (3.11). A few additional eigenvectors should be included in the summations to ensure convergence of the hydrodynamic terms for excitation frequencies close to ω_{\max} . Several numerical experiments indicated that three additional eigenvectors are sufficient. Thus from equation (3.14) the number N_ψ of included eigenvectors is given by

$$N_\psi = \text{max. } n \text{ satisfying eq. (3.14) } + 3 \quad (3.15)$$

N_ψ increases as the cross-sectional dimensions of the infinite channel increase and the maximum excitation frequency ω_{\max} to be considered in the analysis increases.

If the dam, foundation, as well as the entire fluid domain, including the irregular region and the infinite channel, are symmetric about the x-y plane, only one-half of the dam-fluid-foundation system need be analyzed to determine the dam response. The response to upstream or vertical components of ground motion is determined by analyzing one-half the system with symmetric boundary conditions on the x-y plane, and only the symmetric eigenvectors of the infinite channel need to be included. Similarly, the response to cross-stream ground motion is determined by analyzing one-half of the system with antisymmetric boundary conditions on the x-y plane, and only the antisymmetric eigenvectors of the infinite channel need to be included. In each case, the number N_ψ of symmetric or antisymmetric eigenvectors of the infinite channel included is determined from equation (3.15) with $\omega_n^i = \omega_n^{is}$ or ω_n^{ia} , which are respectively the eigenfrequencies of the symmetric and antisymmetric

eigenvectors of the infinite channel.

To demonstrate the adequacy of equation (3.15), the response of Morrow Point Dam with a full reservoir to harmonic ground motion was computed. The foundation rock was assumed rigid, wave absorption at reservoir boundary was neglected ($\alpha = 1$), and twelve ($J = 12$) vibration modes of the dam were included in the solution of equation (3.5) to analyze the dam response. Figure 3.4 shows the absolute value of the complex-valued frequency response functions for radial acceleration at the dam crest due to upstream, vertical, and cross-stream ground motion. The response functions are plotted against the excitation frequency ω normalized by the natural vibration frequencies ω_1^s or ω_1^a of the fundamental symmetric and antisymmetric modes of the dam on rigid foundation rock with an empty reservoir. For the dam-water system considered here: $\omega_{\max} = 18.3$ Hz; $\omega_n^{is} = 3.02, 7.63, 10.09, 11.98, 14.17, 16.02, 17.29, 18.91, \dots$ Hz; and $\omega_n^{ia} = 6.21, 9.78, 13.3, 14.08, 17.24, 18.05, 20.58, \dots$ Hz. According to equation (3.15), $N_\psi = 10$ and 9 for analysis of the symmetric and antisymmetric problems, respectively. The response functions obtained by solving equations (3.12) and (3.5), wherein the first N_ψ eigenvectors of the infinite channel were included in equation (3.12) to evaluate $\bar{\mathbf{p}}_1(\omega)$ and $\bar{\mathbf{r}}_2(\omega)$ and hence the hydrodynamic force vectors $\bar{\mathbf{Q}}_0^H(\omega)$ and $\bar{\mathbf{Q}}_j^f(\omega)$, are presented in Figure 3.4. Also included are the response functions obtained with $N_\psi = 15$ and 30. The number of eigenvectors of the infinite channel, $N_\psi = 10$ or 9, given by equation (3.15) provides accurate response results over the entire frequency range. In fact the response results are essentially independent of the three values used for $N_\psi = 10$ or 9, 15 and 30. Although Figure 3.4 shows the response for a rigid reservoir boundary ($\alpha = 1$), similar accuracy was obtained in the response of the dam with an absorptive reservoir boundary ($\alpha < 1$). Thus accurate dam responses can be obtained with the hydrodynamic terms in equation (3.6) evaluated from equation (3.12) using N_ψ vibration modes of the impounded water, where N_ψ is given by equation (3.15). The resulting computational savings are significant, e.g. the computational effort is reduced to slightly less than half compared to the effort required with $N_\psi = 30$ in the particular example considered here, and reduced even further if the reservoir boundary is absorptive.

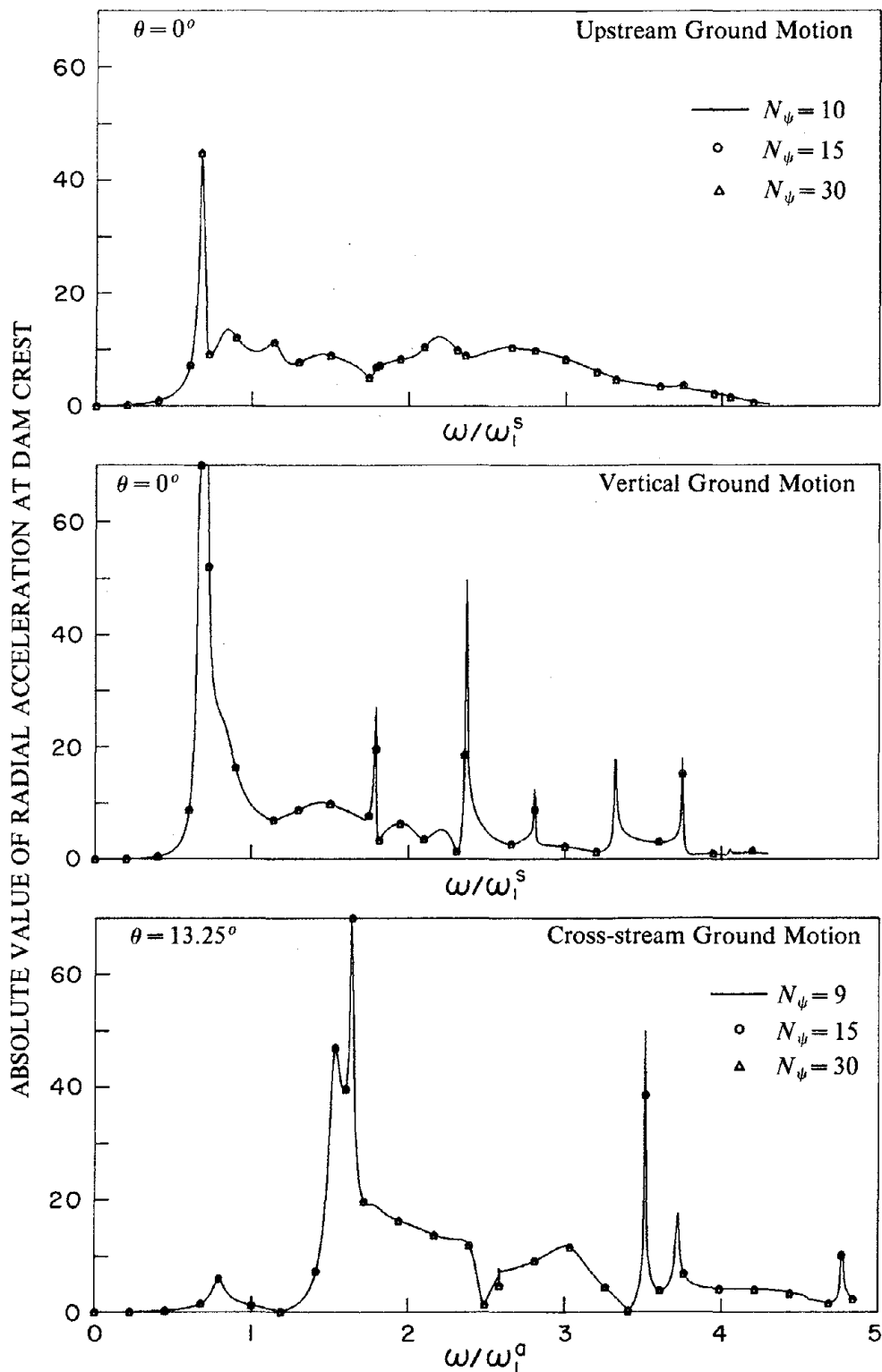


Figure 3.4 Influence of N_ψ , the number of eigenvectors of the infinite channel included in the analysis, on response of Morrow Point Dam, with full reservoir on rigid foundation rock, with rigid reservoir boundary ($\alpha = 1$), to harmonic ground motion. Dam crest locations are defined by θ measured from plane of symmetry.

3.3.3 Interpolation of Eigenproperties of the Infinite Channel

The hydrodynamic pressure functions $\bar{p}_0^f(\omega)$ and $\bar{p}_f^f(\omega)$, which enter into the hydrodynamic terms in equation (3.6), need to be evaluated at each excitation frequency by solving equation (3.12). Needed in this solution process are the eigenvalues $\lambda_n^2(\omega)$ and eigenvectors $\psi_n(\omega)$ of the infinitely long channel with uniform cross-section, governed by equation (3.11), which are frequency-dependent and complex-valued when reservoir boundary absorption is included in the analysis. It would be very expensive to solve equation (3.11) and compute the eigenproperties $\lambda_n^2(\omega)$ and $\psi_n(\omega)$ for each excitation frequency [5,9]. But fortunately it is not necessary to do so. Accurate response results can be efficiently obtained when the hydrodynamic pressures $\bar{p}_0^f(\omega)$ and $\bar{p}_f^f(\omega)$ are evaluated from equation (3.12) with the eigenproperties linearly interpolated from their exact values computed only at widely separated values of ω and the eigenvectors $\psi_n(\omega)$ renormalized with respect to \mathbf{G}^i after linear interpolation.

The largest permissible frequency interval ω^* over which the eigenproperties may be linearly interpolated can be determined by considering how the eigenvalues $\lambda_n^2(\omega)$ vary with the excitation frequency ω . This variation is first studied for a channel with rectangular cross-section and subsequently for an arbitrary cross-section. The objective is to determine the frequency ω^{**} at which the fundamental eigenvalue, which varies most rapidly, reaches close to its limiting value at infinite frequency; and then divide the frequency range 0 to ω^{**} into sufficiently fine subintervals to determine ω^* .

Rectangular Section. -- The two-dimensional, y-z, eigenvalue problem of equation (3.11) for an infinitely long channel with rectangular section of depth H and width $B=2D$ can be formulated in continuum form, without discretization, and uncoupled into two, y and z, one-dimensional eigenvalue problems (Appendix B). The eigenvalues $\lambda_{jk}^2(\omega)$ and the eigenfunctions $\psi_{jk}(y,z,\omega)$ of the channel are related to the eigenproperties of the two one-dimensional problems by:

$$\lambda_{jk}^2(\omega) = \gamma_j^2(\omega) + \delta_k^2(\omega) \quad (3.16a)$$

$$\psi_{jk}(y, z, \omega) = \chi_j(y, \omega) \zeta_k(z, \omega) \quad (3.16b)$$

Determined by solving the y -eigenvalue problem (Appendix B), the eigenvalues $\gamma_j^2(\omega)$, which are complex-valued and depend on the excitation frequency, satisfy equation (3.17) and the corresponding eigenfunctions $\chi_j(y, \omega)$ are defined by equation (3.18):

$$e^{2i\gamma_j(\omega)H} = -\frac{\gamma_j(\omega) - \omega q}{\gamma_j(\omega) + \omega q} \quad (3.17)$$

$$\chi_j(y, \omega) = \frac{1}{2\gamma_j(\omega)} \left\{ [\gamma_j(\omega) + \omega q] e^{i\gamma_j(\omega)y} + [\gamma_j(\omega) - \omega q] e^{-i\gamma_j(\omega)y} \right\} \quad (3.18)$$

The eigenfunctions of the z -eigenvalue problem are either symmetric or antisymmetric about $z = 0$ axis (Appendix B). The symmetric eigenfunctions $\zeta_k^s(z, \omega)$ are defined by equation (3.20), where the associated frequency-dependent, complex-valued eigenvalues $[\delta_k^s(\omega)]^2$ are solutions of equation (3.19):

$$e^{2i\delta_k^s(\omega)D} = \frac{\delta_k^s(\omega) - \omega q}{\delta_k^s(\omega) + \omega q} \quad (3.19)$$

$$\zeta_k^s(z, \omega) = \cos \delta_k^s z \quad (3.20)$$

The antisymmetric eigenfunctions $\zeta_k^a(z, \omega)$ are defined by equation (3.22), where the associated frequency-dependent, complex-valued eigenvalues $[\delta_k^a(\omega)]^2$ are solutions of equation (3.21):

$$e^{2i\delta_k^a(\omega)D} = -\frac{\delta_k^a(\omega) - \omega q}{\delta_k^a(\omega) + \omega q} \quad (3.21)$$

$$\zeta_k^a(z, \omega) = \sin \delta_k^a z \quad (3.22)$$

If the reservoir bottom is rigid ($q=0$ and $\alpha=1$), the eigenvalues $\gamma_j^2(\omega)$ and eigenfunctions $\chi_j(y, \omega)$ are real valued and independent of the excitation frequency and given by equations (3.23) and (3.24):

$$\gamma_j(\omega) = \omega_j^{py}/C \quad (3.23a)$$

where

$$\omega_j^{py} = \frac{2j-1}{2} \pi \frac{C}{H} \quad (3.23b)$$

$$\chi_j(y, \omega) = \cos \gamma_j y \quad (3.24)$$

ω_j^{py} are the natural frequencies associated with the uniform height H of water of a rectangular section channel with a free surface boundary condition at the top and a rigid boundary condition at the bottom.

Similarly if the reservoir sides are rigid ($q=0$ and $\alpha=1$), the eigenvalues $\delta_k^z(\omega)$ are real-valued and independent of the excitation frequency. The square roots of the eigenvalues associated with antisymmetric eigenfunctions are:

$$\delta_k^z(\omega) = \omega_k^{rz}/C \quad (3.25a)$$

where

$$\omega_k^{rz} = \frac{2k-1}{2} \pi \frac{C}{D} \quad (3.25b)$$

ω_k^{rz} are the natural frequencies associated with the uniform width D of water of a rectangular section channel with a free surface boundary condition at one end and a rigid boundary condition at the other. The square roots of the eigenvalues associated with the symmetric eigenfunctions are:

$$\delta_k^s(\omega) = (\omega_k^{rz} - \omega_1^{rz})/C = (k-1) \frac{\pi}{D} \quad (3.26)$$

Figure 3.5(a) shows the numerically-obtained real and imaginary components of $\gamma_j(\omega)$ normalized by the zero frequency value of equation (3.23a), which is also the frequency-independent value when the reservoir boundary is rigid ($q=0$, $\alpha=1$), and then squared. The normalized eigenvalues are plotted against the frequency parameter $qC(\omega/\omega_j^{py})$ so that the plots apply to any non-zero value of the admittance coefficient q for the absorptive reservoir boundary. The plots of Figure 3.5(a) also apply to the eigenvalues $\left[\delta_k^z(\omega) \right]^2$ associated with the antisymmetric eigenfunctions of the z-eigenvalue

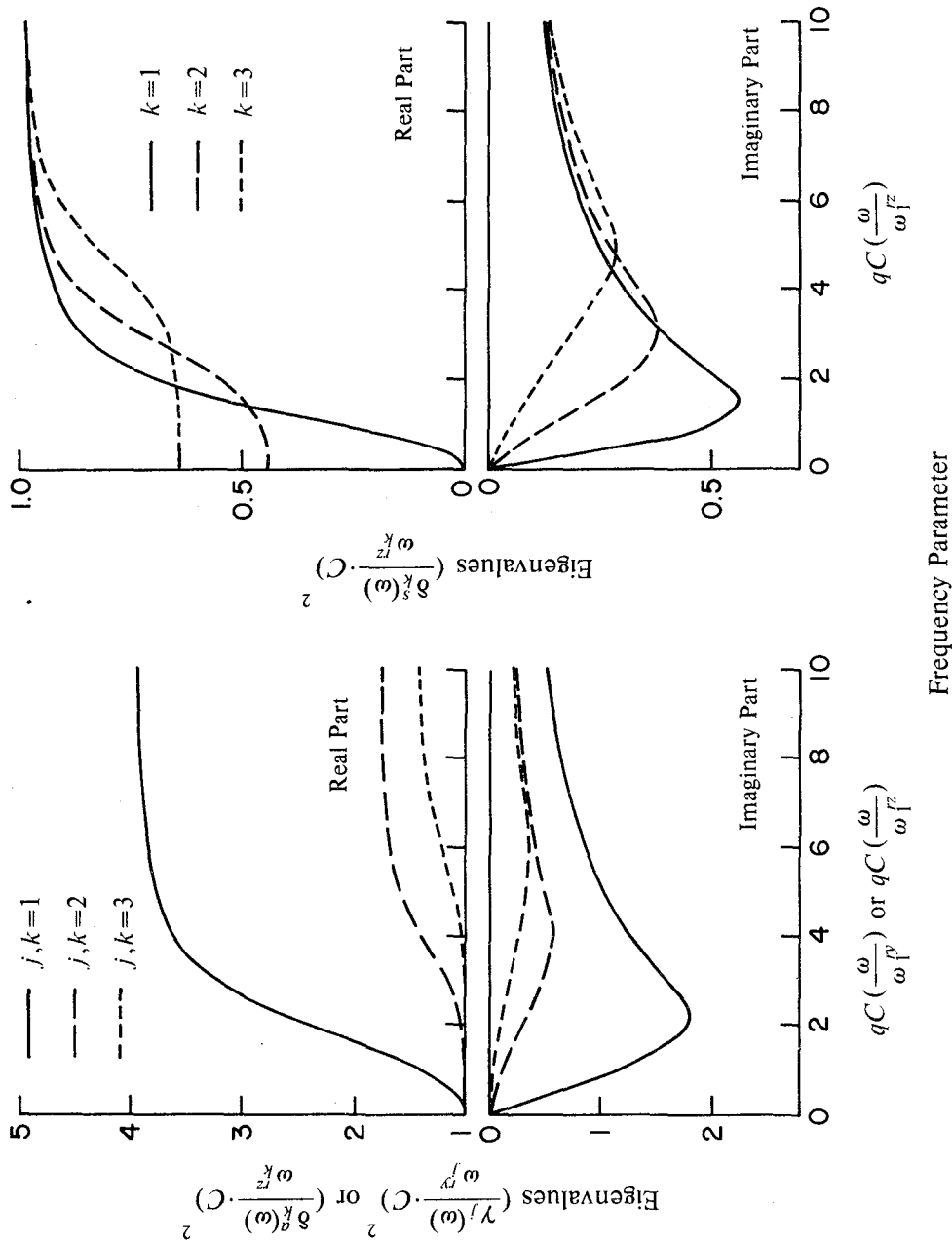


Figure 3.5 Variation of $\gamma_j^k(\omega)$, $[\delta_d^k(\omega)]^2$, and $[\delta_s^k(\omega)]^2$, the eigenvalues of the uncoupled y-, antisymmetric z- and symmetric z- eigenvalue problems for an infinite channel of rectangular section considering reservoir boundary absorption, with excitation frequency ω .

problem if $\omega_1^{j'}$ is replaced by $\omega_1^{k'}$ in the frequency parameter. Figure 3.5(b) shows the numerically-obtained real and imaginary components of $\delta_k^{\beta}(\omega)$ normalized by the infinite frequency value of equation (3.29), and then squared, plotted against the frequency parameter $qC(\omega/\omega_1^{k'})$.

It can be shown from equations (3.17), (3.19), and (3.21) that $\gamma_j(\omega)$, $\delta_k^{\beta}(\omega)$ and $\delta_k^{\delta}(\omega)$ approach real-valued limits as the excitation frequency becomes large:

$$\lim_{\omega \rightarrow \infty} \gamma_j(\omega) = j \frac{\pi}{H} \quad (3.27)$$

$$\lim_{\omega \rightarrow \infty} \delta_k^{\beta}(\omega) = k \frac{\pi}{D} \quad (3.28)$$

$$\lim_{\omega \rightarrow \infty} \delta_k^{\delta}(\omega) = \omega_k^{k'}/C = \frac{2k-1}{2} \frac{\pi}{D} \quad (3.29)$$

Multiplying equation (3.27) by $C/\omega_1^{j'}$, equation (3.28) by $C/\omega_k^{k'}$ and equation (3.29) by $C/(\omega_k^{k'} - \omega_1^{k'})$ gives:

$$\frac{C}{\omega_1^{j'}} \lim_{\omega \rightarrow \infty} \gamma_j(\omega) = \frac{2j}{2j-1} \quad (3.30)$$

$$\frac{C}{\omega_k^{k'}} \lim_{\omega \rightarrow \infty} \delta_k^{\beta}(\omega) = \frac{2k}{2k-1} \quad (3.31)$$

$$\frac{C}{\omega_k^{k'} - \omega_1^{k'}} \lim_{\omega \rightarrow \infty} \delta_k^{\delta}(\omega) = \frac{2k-1}{2k-2} \quad (3.32)$$

Equations (3.30) to (3.32) give the ratios of the real-valued limits of the eigenvalues at infinite frequency to the corresponding real-valued limits at zero frequency.

Figures 3.5 shows that the rate at which $\gamma_j(\omega)$, $\delta_k^{\beta}(\omega)$ and $\delta_k^{\delta}(\omega)$ approach their infinite-frequency limits given by equations (3.30) to (3.32), respectively, depends on the vibration mode j (or k) with a slower rate for larger values of j (or k). The lowest eigenvalues approach their limiting values most rapidly. In particular, $\gamma_1^2(\omega)$ has reached close to its limiting value when the frequency parameter $qC(\omega/\omega_1^{j'}) = 4$, i.e. $\omega^{**} = 4\omega_1^{j'}/qC$; $[\delta_1^{\beta}(\omega)]^2$ has reached close to its limiting value when the frequency parameter $qC(\omega/\omega_1^{k'}) = 4$, i.e. $\omega^{**} = 4\omega_1^{k'}/qC$; and $[\delta_1^{\delta}(\omega)]^2$ has reached close to its limiting value when the frequency parameter $qC(\omega/\omega_1^{k'}) = 3$, i.e. $\omega^{**} = 3\omega_1^{k'}/qC$. Therefore, from equation (3.16a), the

symmetric $\lambda_{11}^2(\omega)$ will reach close to its limiting value at a frequency

$$\omega^{**} = \max \left[\frac{4\omega_1^{ry}}{qC}, \frac{3\omega_1^{rz}}{qC} \right] \quad (3.33)$$

and the antisymmetric $\lambda_{11}^2(\omega)$ will reach close to its limiting value at a frequency

$$\omega^{**} = \max \left[\frac{4\omega_1^{ry}}{qC}, \frac{4\omega_1^{rz}}{qC} \right] \quad (3.34)$$

For a rectangular channel section with its half-width D equal to depth H , $\omega_1^{ry} = \omega_1^{rz}$ and from equations (3.33) and (3.34), $\omega^{**} = \frac{4\omega_1^{ry}}{qC} = \frac{4\omega_1^{rz}}{qC}$ for both the symmetric and antisymmetric $\lambda_{11}^2(\omega)$. At this value of ω^{**} , $\lambda_{11}^2(\omega)$ reaches close to its limiting value as shown in Figure 3.6.

Arbitrary Channel Section. -- As indicated earlier in this section, the frequency interval ω^* necessary to accurately interpolate the lowest eigenvalue $\lambda_1^2(\omega)$ will be satisfactory for the higher eigenvalues. It is necessary, therefore, to study how the eigenvalue $\lambda_1^2(\omega)$ varies with the excitation frequency, in order to appropriately select this frequency interval. Unlike a rectangular section, this frequency variation cannot be analytically determined for a channel of arbitrary section. However, it can be estimated from the frequency variation of eigenvalues for two rectangles such that the actual section is completely contained by the larger rectangle while it completely contains the smaller rectangle [Figure 3.7(a)].

This estimation is made possible, in part, by a result from the boundedness property of eigenvalues [22] that, under certain conditions, relates the eigenvalues of the actual section to those of the two rectangular sections. As the excitation frequency ω tends to infinity the absorptive reservoir boundary behaves like a free surface (Appendix B), i.e. $\bar{p} = 0$; a boundary condition that then applies to the entire boundary of the channel section [Figure 3.7(a)]. For this limiting frequency, the eigenvalues are real-valued and for this particular free-surface boundary condition on the entire boundary, the boundedness property of eigenvalues provides the following inequality:

$$\lambda_{jl}^2 \leq \lambda_j^2 \leq \lambda_{ju}^2 \quad \text{at } \omega = \infty, \quad j = 1, 2, \dots \quad (3.35)$$

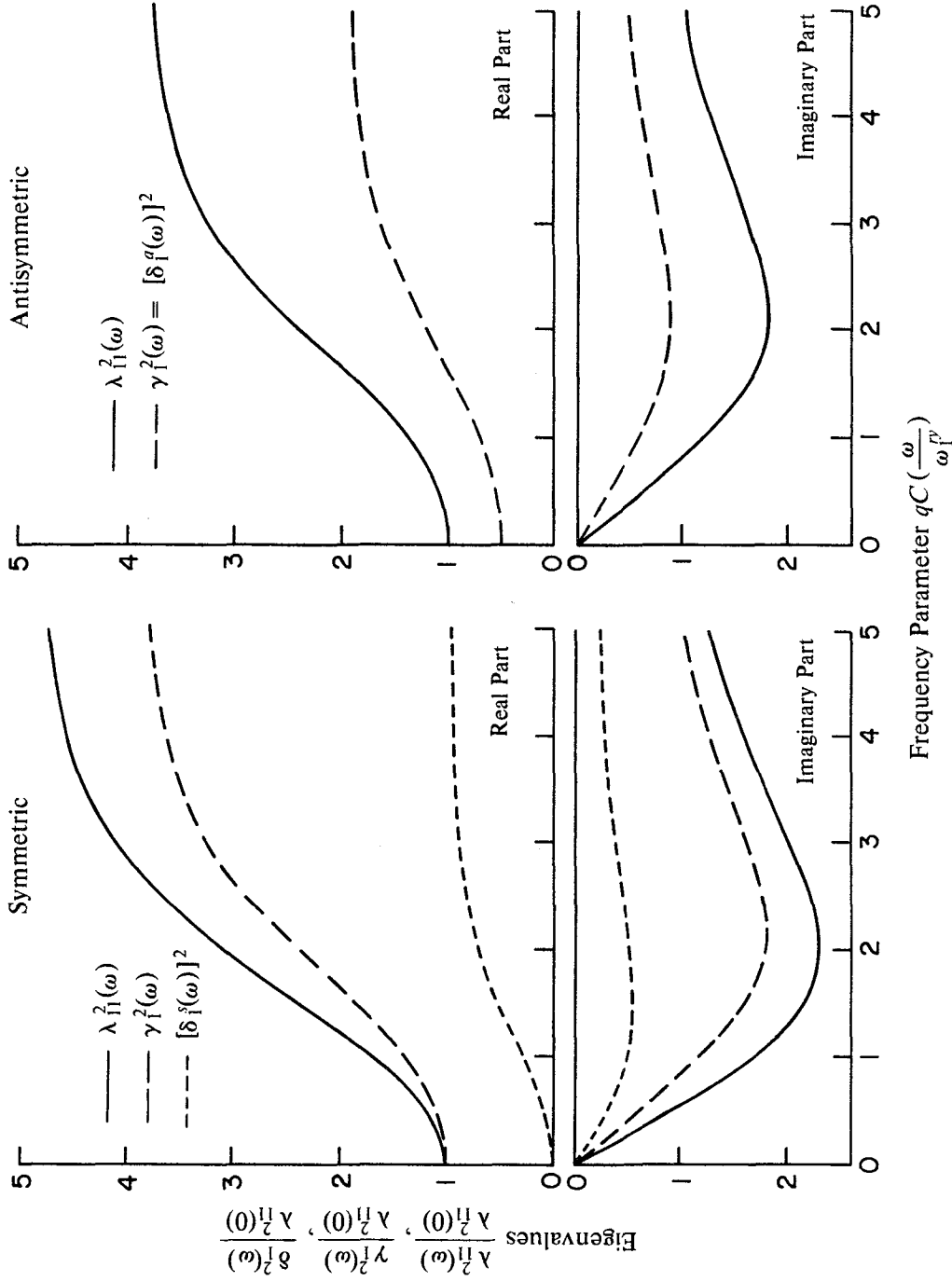
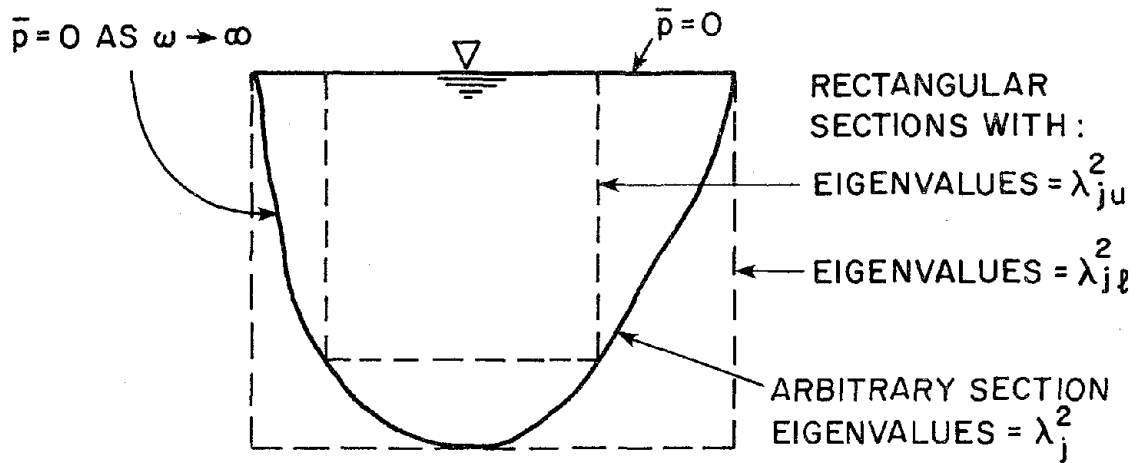
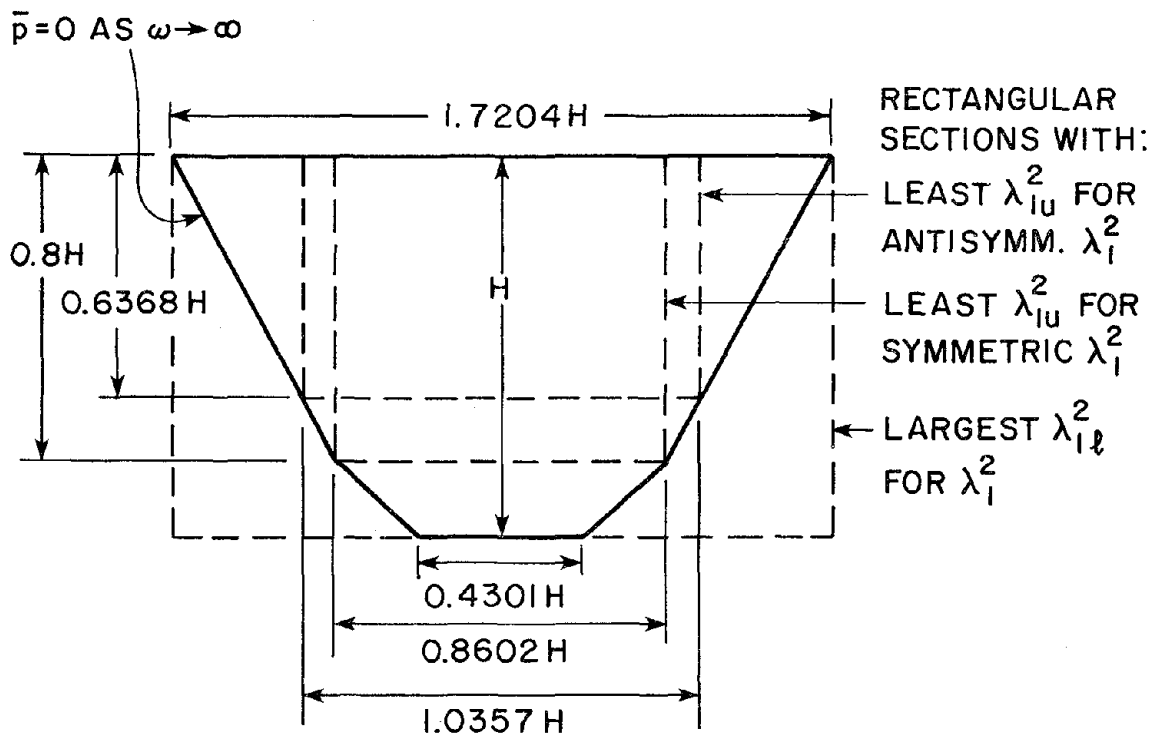


Figure 3.6 Variation of $\lambda_{11}^2(\omega)$, the first eigenvalue of a rectangular section with $H = D$ considering reservoir boundary absorption, with excitation frequency ω . Also shown are the variation of $\gamma_1^2(\omega)$ and $\delta_1^2(\omega)$, the first eigenvalue of the y- and z- eigenvalue problems.



(a) Arbitrary Channel Cross Section



(b) Morrow Point Dam Channel Cross Section

Figure 3.7 Rectangular sections to obtain upper and lower bounds for eigenvalues of infinite channel of uniform cross-section.

Thus λ_j^2 , the j th eigenvalue of the actual section, is bounded on the lower side by λ_{jl}^2 , the j th eigenvalue of the larger rectangular section, and on the upper side by λ_{ju}^2 , the j th eigenvalue of the smaller rectangular section.

Inequality (3.35) holds, in general, for a symmetric, real, positive-definite eigenvalue problem over certain domains with boundary conditions independent of the eigenvalue. The relative sizes of the two domains should be such that the smaller domain (with larger eigenvalues) is completely contained in the larger domain (with corresponding smaller eigenvalues) and the field variable (pressure \bar{p} in this case) must vanish at the portion of the boundary of the smaller domain which does not belong to the boundary of the larger domain. The eigenvalue problem of the infinite channel with the domains depicted in Figure 3.7(a) is a special case of the above condition.

As mentioned in Section 3.3.2, if the dam, foundation, as well as the entire fluid domain are symmetric about the x-y plane, only one-half of the dam-fluid-foundation system need be analyzed to determine the dam response. The response to upstream or vertical components of ground motion is determined by analyzing one-half the system with symmetric boundary conditions on the x-y plane, and only the symmetric eigenvectors (discretized representation of eigenfunctions) of the infinite channel need to be included. Similarly, the response to cross-stream ground motion is determined by analyzing one-half of the system with antisymmetric boundary conditions on the x-y plane, and only the antisymmetric eigenvectors of the infinite channel need to be included. In bounding the eigenvalues associated with the symmetric eigenvectors, the corresponding eigenvalues of the two rectangles should be used in equation (3.35). Similarly, in bounding the eigenvalues associated with the antisymmetric eigenvectors, the corresponding eigenvalues of the two rectangles should be used in equation (3.35).

The frequency variation of λ_{1l}^2 and λ_{1u}^2 , the first eigenvalues of the larger and smaller rectangular sections, can be determined by the procedures described earlier in this section. Although the inequality of equation (3.35) does not apply at excitation frequency values other than infinity, the functions $\lambda_{1l}^2(\omega)$ and $\lambda_{1u}^2(\omega)$ would provide some guidance to the variation of $\lambda_1^2(\omega)$, the first eigenvalue of the actual section, with excitation frequency.

These concepts are next applied to the idealized section of the infinite channel used in the analysis of Morrow Point Dam [Figure 3.7(b)]. As shown, the smallest possible rectangular section that can contain the actual section has been chosen to maximize the lower bound value λ_{1l}^2 . Each of the several rectangular sections that can be contained within the actual section provides a different value of λ_{1u}^2 . Obviously it would be desirable to choose the rectangular section that minimizes the upper bound value λ_{1u}^2 . The associated minimization problem can be solved analytically for actual cross-sections with boundaries defined by simple functions. It was on this basis that the smaller rectangular section was chosen. Because the same rectangle, in general, does not minimize the upper bound value λ_{1u}^2 for symmetric and antisymmetric eigenvectors, two rectangular sections contained within the actual section are chosen as shown in Figure 3.7(b).

The variation of λ_{1l}^2 and λ_{1u}^2 with the normalized excitation frequency, obtained by the procedures described earlier, is shown in Figures 3.8(a) and 3.8(b) for the symmetric and antisymmetric eigenvectors, respectively. Also shown are the eigenvalues $\lambda_1^2(\omega)$ for the actual section obtained numerically by solving the eigenvalue problem of equation (3.11). The high-frequency limiting values of the plotted functions are consistent with the inequality of equation (3.35). For this section, the real and imaginary components of $\lambda_1^2(\omega)$ are bounded by the corresponding components of $\lambda_{1l}^2(\omega)$ and $\lambda_{1u}^2(\omega)$ at all values of ω . Such may not be the case for every cross-section shape, but whether it is or not does not influence determination of the frequencies ω^{**} at which the first eigenvalues reach their limiting values. The fundamental, symmetric eigenvalues $\lambda_{1l}^2(\omega)$ and $\lambda_{1u}^2(\omega)$ of the larger and smaller rectangle sections reach close to their respective limiting values at frequencies given by equation (3.33): $\omega^{**} = 4\omega_1^y/qC$ and $6.98\omega_1^y/qC$ [Figure 3.8(a)]. The fundamental symmetric eigenvalue $\lambda_1^2(\omega)$ of the actual section is observed to reach close to its limiting value at an intermediate frequency of about $\omega^{**} = 5\omega_1^y/qC$, where ω_1^y is the value given by equation (3.23b) for the larger rectangular section. The fundamental antisymmetric eigenvalues $\lambda_{1l}^2(\omega)$ and $\lambda_{1u}^2(\omega)$ reach close to their respective limiting values at frequencies given by equation (3.34): $\omega^{**} = 4.65\omega_1^y/qC$ and $7.72\omega_1^y/qC$ [Figure 3.8(b)]. The fundamental antisymmetric eigenvalue $\lambda_1^2(\omega)$ of the actual section is observed to reach close to its limiting value at an intermediate frequency of about $\omega^{**} = 6\omega_1^y/qC$. Thus, a conservative

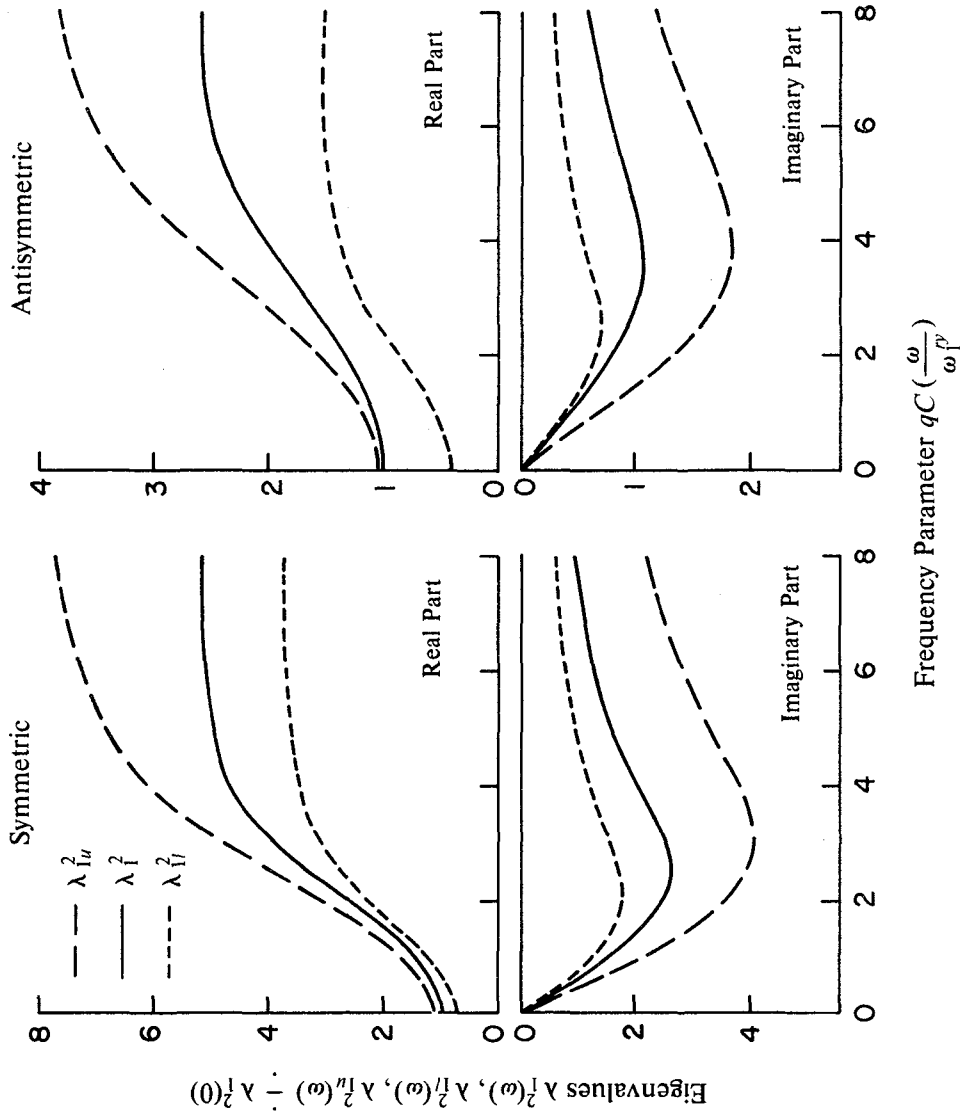


Figure 3.8 Variation of $\lambda_1^2(\omega)$, the fundamental eigenvalue, of the infinite channel cross section for Morrow Point Dam and of the corresponding lower and upper bounds $\lambda_{1r}^2(\omega)$, $\lambda_{1i}^2(\omega)$ with excitation frequency ω .

choice for ω^{**} would be to select the smaller of the two values corresponding to the two rectangles, which is always the value for the larger rectangle.

Interpolating Frequency Interval. -- As noted earlier, the frequency interval ω^* necessary to accurately interpolate the lowest eigenvalue $\lambda_1^2(\omega)$ will be satisfactory for the higher eigenvalues. In the preceding part in this section, we have presented a procedure to determine, for an infinite channel of arbitrary cross-section, the excitation frequency ω^{**} at which $\lambda_1^2(\omega)$ reaches close to its high-frequency limiting value. Several response computations have demonstrated that the response of an arch dam is computed to sufficient accuracy when the hydrodynamic terms are evaluated using eigenproperties linearly interpolated over an excitation frequency interval $\omega^* = \omega^{**}/8$. Using this criterion, ω^{**} based on the larger rectangle, and equations (2.1), (3.33) and (3.34), the excitation frequency interval is given by:

$$\frac{\omega^*}{\max(\omega_1^{ry}, \omega_1^{rz})} = \frac{1}{2} \frac{1 + \alpha}{1 - \alpha} \quad (3.36a)$$

for symmetric dam-fluid-foundation systems subjected to z ground motion; and

$$\frac{\omega^*}{\max(\omega_1^{ry}, 0.75\omega_1^{rz})} = \frac{1}{2} \frac{1 + \alpha}{1 - \alpha} \quad (3.36b)$$

for all other cases, where ω_1^{ry} and ω_1^{rz} refer to the larger rectangular section. Equation (3.36a) is derived from equation (3.34) for the antisymmetric λ_{1l}^2 which should be used for the lower bound of the fundamental eigenvalue for z ground motion of a symmetric dam-fluid-foundation system. Equation (3.36b) is derived from equation (3.33) for the symmetric λ_{1l}^2 which should be used for the lower bound of the fundamental eigenvalue for all other cases, because : (1) it should be used for x and y ground motions of a symmetric dam-fluid-foundation system, (2) the symmetric λ_{1l}^2 is always smaller than the antisymmetric λ_{1l}^2 , thus it should be used to bound the fundamental eigenvalue for x, y, and z ground motion of a non-symmetric dam-fluid-foundation system. Equation (3.36) shows that the frequency interval ω^* decreases as α decreases, i.e. as the reservoir boundary becomes more absorptive.

The effectiveness of linearly interpolating the frequency-dependent eigenproperties of the infinite channel over the excitation frequency interval ω^* , given by equation (3.36), is demonstrated in Figure 3.9. The absolute values of the frequency response functions for radial acceleration at the crest of Morrow Point Dam with full reservoir to harmonic ground motion are plotted against the normalized excitation frequency ω/ω_1^s or ω/ω_1^z , as appropriate. Reservoir boundary absorption is included with a wave reflection coefficient $\alpha = 0$ to provide the most severe test for the interpolation procedure. The response functions are computed for two cases: $\lambda_n^2(\omega)$ and $\psi_n(\omega)$ in equations (3.11) and (3.12) evaluated for every excitation frequency; or by linear interpolation over the frequency interval $\omega^*/\omega_1^{xy} = 0.5$ for x and y ground motion and $\omega^*/\omega_1^z = 0.5$ for z ground motion as given by equation (3.36). There is no observable difference between the response functions computed for the two cases. However, the total computational effort required in the second case using linear interpolation of the eigenproperties of the infinite channel, requires only 60 - 65 % of the computational effort in the first case. Thus the hydrodynamic terms in equation (3.6) may be efficiently evaluated by linearly interpolating the eigenproperties of the infinite channel over the frequency interval ω^* given by equation (3.36).

3.4 Interpolation of Frequency Response Functions

3.4.1 Basic Concept

At the heart of the earthquake response analysis procedure for dams is the formulation and solution of equation (3.5) governing the frequency response functions $\bar{Y}_j^l(\omega)$ for the generalized coordinates. Efficient methods were presented in Section 3.3 to minimize the major computational effort required in evaluating the hydrodynamic terms that enter into these equations. In this section, a procedure for efficient interpolation of the frequency response functions $\bar{Y}_j^l(\omega)$ is developed to further reduce the computational effort [23]. Then the frequency response functions need to be obtained exactly by solving equation (3.5) at fewer selected frequencies; and their values at other frequencies are obtained by interpolation.

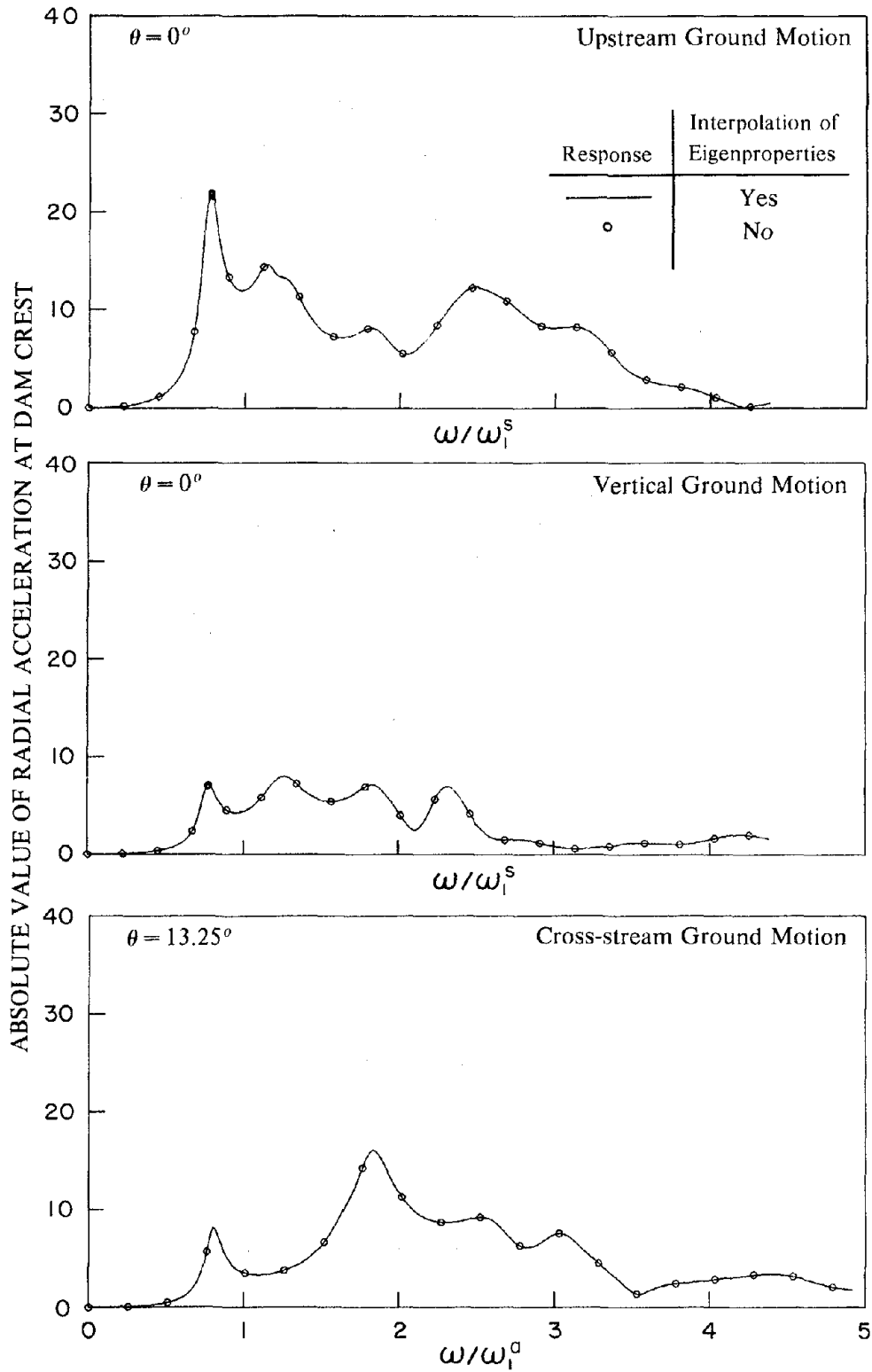


Figure 3.9 Influence of linear interpolation of eigenproperties of the infinite channel on response of Morrow Point Dam to harmonic ground motion. Results presented for full reservoir, rigid foundation rock and wave reflection coefficient, $\alpha = 0$; were obtained with $J = 12$ and $N_\psi = 10$ or 9.

The frequency response function for acceleration at the crest of the dam due to each of the three components of ground motion is presented in Figure 3.10 along with the contributions of the various modes of vibration. Within certain ranges of frequencies (such as between a and b in Figure 3.10), no more than two peaks exist, only two modes contribute significantly, and the contributions of other modes are negligible. Thus it may be possible to approximate the response by subdividing the frequency range into subranges where the above conditions are met, and by using the response function for two modes within each range.

3.4.2 Two Mode Approximation

Including only two modes in equation (3.5) and neglecting water compressibility, which leads to hydrodynamic terms independent of excitation frequency, the frequency response functions for the generalized coordinates $\bar{Y}_j^l(\omega)$ can be expressed (Appendix C) as:

$$\bar{Y}_j(\omega) = \frac{C_{1j} \omega^2 + C_{2j}}{\omega^4 + C_{3j} \omega^2 + C_{4j}} \quad (3.37)$$

where the constant C_{1j} is real-valued, and the constants C_{2j}, C_{3j} and C_{4j} are complex-valued because of hysteretic damping in the dam. Just like $\bar{Y}_j^l(\omega)$, these constants would also depend on the ground motion component, $l = x, y$ or z , but this superscript is dropped for convenience.

Four frequencies $\Omega_i, i = 1, 2, 3, \text{ and } 4$, are selected within each frequency range n , and the j th generalized coordinate response $\bar{Y}_{ji} = \bar{Y}_j(\Omega_i)$ is determined at these frequencies by solving the set of equations (3.5) including all the vibration modes having significant contributions. The four constants in equation (3.37) can be evaluated by solving the system of linear equations:

$$\begin{bmatrix} \Omega_1^2 & 1 & -\bar{Y}_{j1}\Omega_1^2 & -\bar{Y}_{j1} \\ \Omega_2^2 & 1 & -\bar{Y}_{j2}\Omega_2^2 & -\bar{Y}_{j2} \\ \Omega_3^2 & 1 & -\bar{Y}_{j3}\Omega_3^2 & -\bar{Y}_{j3} \\ \Omega_4^2 & 1 & -\bar{Y}_{j4}\Omega_4^2 & -\bar{Y}_{j4} \end{bmatrix} \begin{bmatrix} C_{1j} \\ C_{2j} \\ C_{3j} \\ C_{4j} \end{bmatrix} = \begin{bmatrix} \bar{Y}_{j1}\Omega_1^4 \\ \bar{Y}_{j2}\Omega_2^4 \\ \bar{Y}_{j3}\Omega_3^4 \\ \bar{Y}_{j4}\Omega_4^4 \end{bmatrix} \quad (3.38)$$

Once the constants C_{1j}, C_{2j}, C_{3j} and C_{4j} have been determined for the frequency range n , the

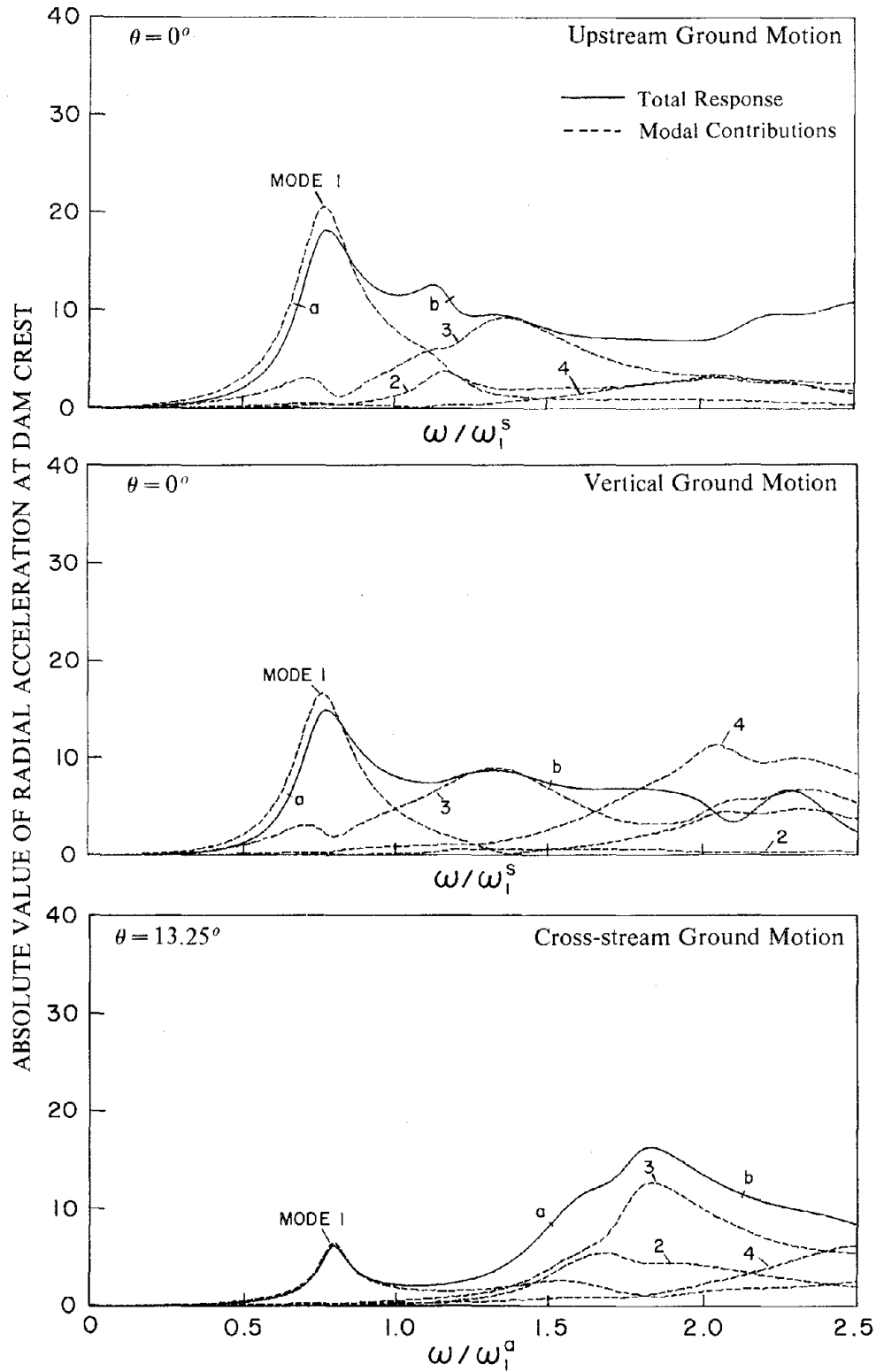


Figure 3.10 Modal contributions in the response of Morrow Point Dam to harmonic ground motion with full reservoir, rigid foundation rock and wave reflection coefficient, $\alpha = 0.5$.

response at all other frequencies within this frequency range is then computed from the interpolation equation (3.39):

$$\bar{Y}_j(\omega) = \frac{C_{1j}^n \omega^2 + C_{2j}^n}{\omega^4 + C_{3j}^n \omega^2 + C_{4j}^n} \quad (3.39)$$

Since the frequency response functions for all the J vibration modes are solved simultaneously from equation (3.5), each selected frequency range and the four frequencies chosen within a range should be the same for all the modes.

3.4.3 Selection of Frequencies for Exact Computation

The frequency response functions are computed exactly by solving equation (3.5) at selected frequencies and their values at other frequencies are obtained by interpolation. The selection of the frequencies at which response is exactly computed should obviously depend on the rapidity with which the response varies with excitation frequency; i.e., these frequencies should be closely spaced in the frequency range where the response varies rapidly and widely spaced if the response varies slowly. This may be achieved by imposing the objective that, over any frequency interval, the fractional change in the absolute value of response:

$$\left| \frac{\bar{Y}_{ji} - \bar{Y}_{j,i-1}}{\bar{Y}_{ji}} \right| = \left| \frac{\Delta \bar{Y}_{j,i-1}}{\bar{Y}_{ji}} \right|$$

should be kept fairly constant and close to a prescribed value b . Based on this objective, the i th frequency interval $(\Delta\omega)_i = \Omega_{i+1} - \Omega_i$ can be determined from the preceding frequency interval $(\Delta\omega)_{i-1} = \Omega_i - \Omega_{i-1}$ as follows:

$$(\Delta\omega)_i = (\Delta\omega)_{i-1} \frac{b}{\max_j \left| \frac{\Delta \bar{Y}_{j,i-1}}{\bar{Y}_{ji}} \right|} \quad (3.40)$$

Thus the selection of the next frequency interval is based on the current interval and the largest fractional change in modal response over the current interval. If the maximum variation in modal response over the current interval is larger than b , then the next frequency interval will be smaller than the current interval and vice versa. Because the frequency interval from equation (3.40) may be

impractically small or large depending on the values of $\Delta\bar{Y}_{j,i-1}$ and \bar{Y}_{ji} , each of which can vary over a very wide range, it is necessary to impose $(\Delta\omega)_{\max}$, the maximum value permitted for $\Delta\omega$, and $(\Delta\omega)_{\min}$, the minimum value permitted for $\Delta\omega$.

Starting with $(\Delta\omega)_{\min}$ for the first frequency interval, all the subsequent frequency intervals can be conveniently determined from equation (3.40) once the parameters b , $(\Delta\omega)_{\max}$ and $(\Delta\omega)_{\min}$ have been selected. After several numerical experiments it was concluded that the following parameter values would provide accurate results:

$$b = 0.5 \quad (3.41a)$$

$$\frac{(\Delta\omega)_{\max}}{\min(\omega_1^p, \omega_1)} = 0.2 \quad (3.41b)$$

$$\frac{(\Delta\omega)_{\min}}{\min(\omega_1^p, \omega_1)} = 0.01 \quad (3.41c)$$

where ω_1 is the fundamental frequency of the dam-foundation rock system with an empty reservoir, and ω_1^p is the fundamental frequency of an infinite reservoir of uniform depth computed by equation (3.23b) in which the maximum depth of the impounded water in the entire reservoir domain is used instead of H .

The effectiveness of the interpolation scheme for the frequency response functions, using the above mentioned parameters, is demonstrated in Figure 3.11. The absolute values of the frequency response functions for radial acceleration at the crest of Morrow Point Dam with full reservoir to harmonic ground motion are plotted against the normalized excitation frequency ω/ω_1^s or ω/ω_1^a , as appropriate. Reservoir boundary absorption is neglected, i.e. the wave reflection coefficient $\alpha = 1$, which leads to the most rapid variations in the frequency response functions, to provide the most severe test for the interpolation procedure. The response functions are computed using the interpolation procedure described earlier with the above mentioned parameters and compared with the exact values computed at selected frequencies. There is no observable difference between the response functions computed by the two procedures. Using interpolation of the frequency response functions, however, the required computational effort is only 50 to 60 % of that necessary without

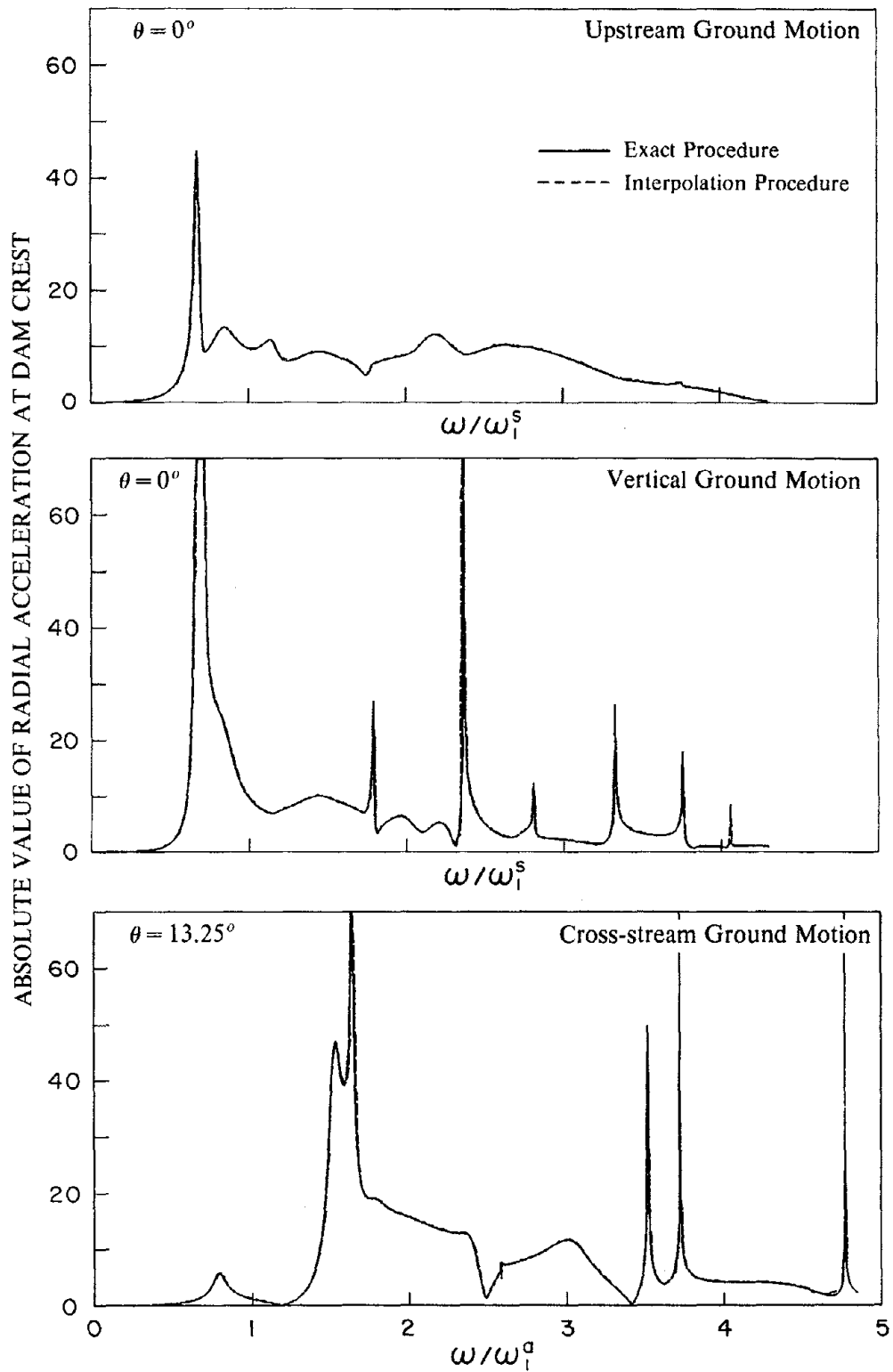


Figure 3.11 Accuracy of the response of Morrow Point Dam to harmonic ground motion computed by the interpolation procedure. Results presented for full reservoir, rigid foundation and wave reflection coefficient, $\alpha = 1$; were obtained with $J = 12$ and $N_\psi = 10$ or 9.

interpolation.

The interpolation parameters of equation (3.41) were derived from numerical experiments on response of dams supported on rigid foundation rock with no absorption of hydrodynamic pressure waves at the reservoir boundary. These assumptions lead to the most sharply peaked and rapidly varying response functions. These functions become much smoother if reservoir boundary absorption is considered (Chapter 4 and reference [19]), in which case the interpolation parameters of equation (3.41) would be conservative; in particular, the normalized $(\Delta\omega)_{\min}$ can be increased to 0.02 [equation (3.41c)].

Compared to the earlier application of the above described interpolation procedure to soil-structure interaction problems [23], the exact response is computed in the present application at 3 to 5 times the number of frequencies, because structure-fluid interaction leads to complicated response functions with sharp peaks and rapidly variation, if reservoir boundary absorption is not considered [9,20]. Because of these complications and because arch dams are complex structures having vibration modes with closely spaced frequencies, the conservative parameters of equation (3.41) are recommended. The computational cost can be further reduced by choosing larger $\Delta\omega$, tailored specifically for specific arch dams and assumptions used in the analysis.

An interpolation procedure such as the one described in this work should always be used with caution. Using the parameters of equation (3.41), the response function should be computed exactly at selected frequencies and then the response function at other frequencies obtained from the interpolation equation (3.39). The entire interpolated response should be plotted, and evaluated in light of the known characteristics (Chapter 4 and reference [9]) of frequency response functions of arch dams, including their behavior at or near characteristic frequencies -- the natural vibration frequencies of the dam, natural frequencies of the infinite channel of the fluid domain, and resonant frequencies of the dam including hydrodynamic effects -- to see if the initial choice of frequencies was adequate. The user can then select additional frequencies deemed necessary to compute additional values to describe the frequency response functions. The new results can then be combined with the initial results and new interpolations can be carried out.

3.4.4 Summary of Interpolation Procedure

The procedure for computing the frequency response functions $\bar{Y}_j^l(\omega)$ for the entire frequency range 0 to ω_{\max} is summarized below as a sequence of steps [23]:

1. Determine the values for parameters b , $(\Delta\omega)_{\min}$ and $(\Delta\omega)_{\max}$ from equation (3.41), with the normalized $(\Delta\omega)_{\min}$ in equation (3.41c) increased to 0.02 if reservoir boundary absorption is considered.

2. Starting with zero frequency and the initial frequency interval as $(\Delta\omega)_{\min}$, solve equation (3.5) to compute $\bar{Y}_j^l(\omega)$ at $\omega = 0$ and $\omega = (\Delta\omega)_{\min}$. From equation (3.40) determine the next frequency value, and solve equation (3.5) to exactly determine $\bar{Y}_j^l(\omega)$ at that frequency. This process of utilizing equation (3.40) to determine the next ω value and solving equation (3.5) at that frequency is repeated until $\bar{Y}_j^l(\omega)$ are computed for the frequency range 0 to ω_{\max} .

3. Subdivide the computed results into frequency ranges containing 4 computed values of the response function per range.

4. For each vibration mode j of the dam included in the response analysis, compute the constants $C_{1j}^n, C_{2j}^n, C_{3j}^n$ and C_{4j}^n for frequency range n from equation (3.38).

5. Compute the response for all other frequencies in the range n from equation (3.39).

6. Repeat steps 4 and 5 for all the frequency ranges defined in step 3.

7. If the last frequency range is not complete, i.e., does not contain values of the response function at four frequencies, it is necessary to include enough frequency points from the previous range in order to determine the constants in step 4 and to compute the responses in step 5 for this last range.

3.5 Efficient Response Analysis Procedure

Efficient methods were presented in Section 3.3 to minimize the computational effort required in evaluating the hydrodynamic terms that entered into the equations governing the frequency response functions for the generalized coordinates of the dam. In Section 3.4, a procedure for efficient interpolation of the frequency response functions was developed, in which these functions

were obtained exactly at fewer selected frequencies and their values at other frequencies were obtained by interpolation, thus further reducing the computational effort. Both of these concepts have been implemented in a computer program (Section 3.6) to obtain an efficient procedure for the earthquake analysis of arch dams. The effectiveness of this procedure is evaluated next to demonstrate its accuracy and the computational savings achieved.

The accuracy of the efficient procedure is demonstrated by analyzing the response of Morrow Point Dam supported on rigid foundation rock with full reservoir considering the hydrodynamic effects and reservoir boundary absorption effects with the wave reflection coefficient $\alpha = 0.5$. Presented in Figure 3.12 are the absolute values of frequency response functions for the radial acceleration at the crest of the dam due to the upstream, cross-stream, and vertical components of ground motion, plotted against the normalized excitation frequency, as appropriate. The frequency response functions are computed for two cases: (1) Standard Procedure: Number of eigenvectors of the infinite channel included in evaluation of hydrodynamic forces, $N_\psi = 30$; equation (3.11) is solved at each frequency to determine the eigenproperties of the infinite channel; and equation (3.5) is solved at each frequency to obtain the exact solution for the modal coordinates $\bar{Y}_j'(\omega)$; (2) Efficient Procedure: $N_\psi = 10$ or 9, determined from equation (3.15), for analysis of symmetric (x and y ground motion) and antisymmetric (z ground motion) problems, respectively; the eigenproperties of the infinite channel are determined by solving equation (3.11) at the frequency spacing ω^* given by equation (3.36), i.e. $\omega^*/\omega_1^y = 1.5$ and $\omega^*/\omega_1^z = 1.5$, combined with linear interpolation to obtain their values at intermediate frequencies; and $\bar{Y}_j'(\omega)$ are obtained by the interpolation procedures developed in Section 3.4 using the recommended interpolation parameters [equation (3.41)]. It is apparent from Figure 3.12 that there is no observable difference between the response functions computed by the standard and efficient procedures.

The computational efforts required in the standard and efficient analysis procedures are compared in Table 3.1. When the effects of hydrodynamic wave absorption at the reservoir boundary, due to the alluvium or sediments inevitably present in actual reservoirs, are included we note that the efficient analysis procedure is very effective compared to the standard analysis procedure. The

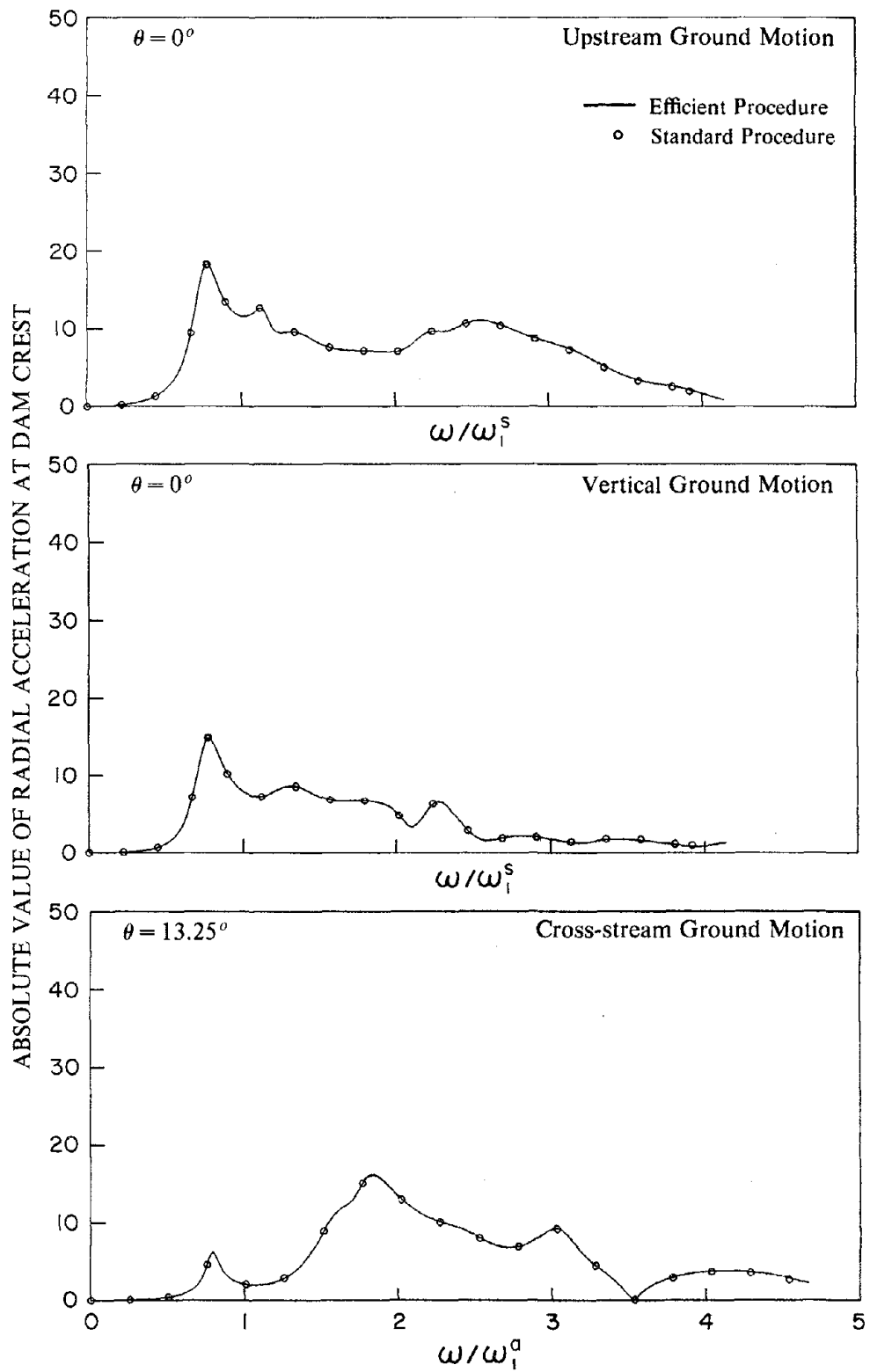


Figure 3.12 Comparison of dam responses obtained by efficient and standard procedures. Response of Morrow Point Dam to harmonic ground motion is presented for full reservoir, rigid foundation rock and wave reflection coefficient $\alpha = 0.5$.

Table 3.1 -- Comparison of Efficient and Standard Procedures
to Obtain Frequency Response Functions for Morrow Point Dam
on Rigid Foundation Rock with Full Reservoir

Case	N_{ψ}		No. of times eq. (3.11) is solved		No. of ω values $\bar{Y}(\omega)$ is exactly solved		Central Processor Time* (sec)				
	Reservoir Boundary	α	Standard	Efficient	Standard	Efficient	Standard	Efficient	Ratio		
RESPONSE TO UPSTREAM OR VERTICAL GROUND MOTION (SYMMETRIC ANALYSIS)											
Absorptive			30	10	361	17	361	136	520	64	12%
Absorptive			30	10	361	4	361	188	520	74	14%
Rigid			30	10	1	1	436	225	299	82	27%
RESPONSE TO CROSS STREAM GROUND MOTION (ANTISYMMETRIC ANALYSIS)											
Absorptive			30	9	361	14	361	93	357	39	11%
Absorptive			30	9	361	4	361	112	357	39	11%
Rigid			30	9	1	1	431	181	230	52	23%

* CDC 7600 Computer

efficient procedure requires much fewer, 5 % or less, solutions of the eigenproblem of the infinite channel; similarly solutions of equation (3.5) for the frequency response functions need to be computed at much fewer, half or less, excitation frequencies compared to the standard procedure. As a result the computation time required to obtain the response functions over the frequency range 0 to 18.3 Hz by the efficient procedure is a small fraction, 11 to 14 %, of that required in the standard procedure.

The computational savings are not as dramatic, but are still very significant, if the wave absorptive effects at the reservoir boundary are not considered, i.e. $\alpha = 1$. In this case, the eigenproperties of the infinite channel are independent of excitation frequency and need to be computed once in either, standard or efficient, procedure. Furthermore, because the response functions are sharply peaked and vary more rapidly with frequency, they need to be computed exactly at more frequencies (Table 3.1), requiring greater computational effort. The net result is that the computation time required to obtain the response functions by the efficient procedure is about one quarter, 23 to 27 %, of that required in the standard procedure.

In order to account for the wave absorption effects at the reservoir boundary, the computational time is increased by about 55 to 75 % in the standard procedure, but is decreased by about 10 to 25 % in the efficient procedure. Further reductions in the computation time should be possible in the efficient analysis procedure because, in many cases, the number of frequency values at which the response functions need to be exactly computed can be reduced below the number obtained using the parameters of equation (3.41) without any significant loss in accuracy. However, even with the present recommendations, which in many cases are overly conservative but reduce the risk of error in other cases, the efficient procedure is successful in eliminating the computational penalty to include wave absorption effects of the reservoir boundary.

3.6 Computer Program

The response analysis procedure described in Sections 3.1 and 3.2 is implemented in a computer program to numerically evaluate the earthquake responses of arch dam systems of the type described in Chapter 2. Various effects in the analysis procedure are included in the program: dam-water interaction, foundation-rock flexibility, water compressibility and reservoir boundary absorption. Efficient computational procedures described in Sections 3.3 and 3.4 have been incorporated into this computer program resulting in an effective tool to compute the earthquake responses of arch dams.

The computer program has different three-dimensional elements as described in Chapter 2 to model the dam, reservoir, and foundation rock. The FFT algorithm [18] used to evaluate the Fourier integrals in equations (3.7) and (3.8) takes advantage of the fact that the ground acceleration and displacement response are real-valued functions, thus reducing the computational and storage requirements. The computer program also evaluates the static displacements and stresses of the dam due to the gravity loads of the dam and the hydrostatic pressure; these static responses, which are evaluated in a separate run, can be combined with the earthquake responses if desired.

Input to the computer program consists of various control parameters, the finite element idealizations and properties of the arch dam, the foundation rock and the impounded water. In the dynamic run of the program, the following parameters are also input: the wave reflection coefficient for the absorptive reservoir boundary, the number of generalized coordinates of the dam included, the FFT parameters, and the upstream, vertical, and cross-stream components of the free-field ground acceleration. The output in the static run of the program consists of the static displacements at all nodal points and stresses in all elements of the dam. In the dynamic run, the output consists of the complex-valued frequency response functions for the generalized coordinates and the complete time-history of displacements and stresses at specified locations within the dam as well as the extreme values of stresses at all stress points. The computer program can also be run in several separate stages; the output from one stage is stored and subsequently used as input to the other stages.

4. FREQUENCY RESPONSE FUNCTIONS

4.1 Introduction

Presented in this chapter is the response of a selected arch dam to harmonic ground motion in the form of complex-valued frequency response functions. Response results, computed by the analytical procedure presented in Chapter 3, are presented for the upstream, vertical and cross-stream components of ground motion, and for a wide range of the important parameters characterizing the properties of the dam, foundation rock, impounded water and reservoir boundary materials. Based on the frequency response results, the effects of dam-water interaction, reservoir boundary absorption, and foundation-rock flexibility on the dynamic response of the dam are investigated.

4.2 System, Ground Motion, Cases Analyzed and Response Quantities

4.2.1 Dam-Water-Foundation Rock System

The dam selected for this study is Morrow Point Dam. The finite element idealizations selected for the dam and foundation-rock region, the idealization for the impounded water consisting of a finite element region combined with an infinite, uniform channel, and the properties of the dam-water-foundation rock system are the same as described in Section 2.6; except that in this study the Young's modulus of the dam is varied: $E_s = 2, 4$ or 5 million psi, and the Young's modulus of the foundation is also varied so that $E_f/E_s = \infty, 2, 1$ or $1/4$. One of the objectives of this study is to investigate the effects of reservoir boundary absorption (Section 2.4) on the earthquake response of arch dams; therefore, the wave reflection coefficient α is varied over a wide range. The values considered are: $\alpha = 1.0$ (rigid reservoir boundary), $0.75, 0.50$ and 0 .

4.2.2 Ground Motion

The excitation for the dam-water-foundation rock system is defined by three components of free-field ground motion: the upstream (x) component $a_g^x(t)$, the vertical (y) component $a_g^y(t)$, and the cross-stream (z) component $a_g^z(t)$. Each component of ground acceleration is assumed to be

harmonic, i.e. $= e^{i\omega t}$, with the excitation frequency ω to be varied over a wide range.

4.2.3 Cases Analyzed

The responses of the several dam-water-foundation rock systems shown in Table 4.1 are presented. These systems are defined by the chosen values for the important system parameters, $E_s, E_f/E_s, H/H_s$, and α . The complex frequency response functions for each case were determined. The responses of the various systems and their interpretation are organized to facilitate study of the effects of reservoir boundary absorption, dam-water interaction, and foundation-rock flexibility on the response of the dam.

4.2.4 Response Quantities

The complex-valued frequency response functions presented here are dimensionless response factors that represent the acceleration components in selected directions at a few locations in the dam due to unit, harmonic, free-field ground acceleration. For analysis cases assuming rigid foundation rock, the complex frequency response function for radial acceleration at one location at the dam crest is presented; the location is defined by an angle value θ measured from the crown (plane of symmetry) along the dam crest, which is selected as: $\theta = 0^\circ$ [nodal point 60 in Figure 2.3(a)] for x and y ground motion and $\theta = 13.25^\circ$ [nodal point 54 in Figure 2.3(a)] for z ground motion. When foundation flexibility is included, in addition to the radial accelerations at these crest locations, the vertical acceleration at the crest and the radial and vertical accelerations at the base for the same θ values are also presented for some cases. The frequency response functions are for acceleration relative to the free-field ground motion; they are not direct measures of deformation.

These functions, describing the response to harmonic upstream, vertical or cross-stream ground motion, were determined using the analytical procedure described in Chapter 3 with the excitation frequency ω varied over a relevant range of interest. In computing the response for the different cases in Table 4.1, different number of generalized coordinates [see equation (3.9)] were included. In analyzes assuming rigid foundation rock ($E_f/E_s = \infty$), 12 generalized coordinates were included for dams with $E_s = 4$ or 5 million psi and 15 generalized coordinates if $E_s = 2$ million psi. In analyzes

Table 4.1 -- Cases of Dam-Water-Foundation Rock System Analyzed

Case	E_s (million psi)	Foundation Rock		Impounded Water		Reservoir Boundary	
		Condition	E_f/E_s	Condition	H/H_s	Condition	α
1	any*	rigid	∞	empty	0	-	-
2	4	rigid	∞	full	1	rigid	1.0
3	4	rigid	∞	full	1	absorptive	0.75
4	4	rigid	∞	full	1	absorptive	0.50
5	4	rigid	∞	full	1	absorptive	0
6	5	rigid	∞	full	1	rigid	1.0
7	5	rigid	∞	full	1	absorptive	0.5
8	2	rigid	∞	full	1	rigid	1.0
9	2	rigid	∞	full	1	absorptive	0.5
10	any*	rigid	∞	full, incompressible	1	rigid	any†
11	any*	flexible	2	empty	0	-	-
12	any*	flexible	1	empty	0	-	-
13	any*	flexible	1/4	empty	0	-	-
14	4	flexible	1	full	1	rigid	1.0
15	4	flexible	1	full	1	absorptive	0.75
16	4	flexible	1	full	1	absorptive	0.50
17	4	flexible	1	full	1	absorptive	0
18	4	flexible	2	full	1	rigid	1.0
19	4	flexible	2	full	1	absorptive	0.50
20	4	flexible	1/4	full	1	rigid	1.0
21	4	flexible	1/4	full	1	absorptive	0.50

* Response results for these cases, when presented in normalized form, are valid for all E_s .

† Response results for the case neglecting water compressibility are independent of α .

considering foundation rock flexibility, with $E_f/E_s = 2, 1$ and $1/4, 16, 18$ and 20 generalized coordinates were included, respectively. The resulting frequency response functions should be accurate for excitation frequencies up to approximately four times the fundamental natural frequency ω_1 of the dam on rigid foundation rock with an empty reservoir.

For each case in Table 4.1 the absolute value of the complex-valued frequency response function for acceleration is plotted against the normalized excitation frequency parameter ω/ω_1 , where ω_1 is the fundamental resonant frequency of the dam without water on a rigid foundation rock; ω_1^s is used as the normalizing factor for symmetric (upstream or vertical) ground motion, and ω_1^a is used for antisymmetric (cross-stream) ground motion. If compressibility of the impounded water is neglected, or the reservoir is empty, these response results plotted in this manner are independent of E_s and α [21].

4.3 Hydrodynamic Forces on Rigid Dam

Before studying the response of the dam, it is useful to examine the hydrodynamic force due to a full reservoir ($H/H_s = 1$) on a rigid dam, with the foundation rock also assumed as rigid. The x-component of the total hydrodynamic force acting on half of the dam due to upstream, vertical and cross-stream ground motion, $\bar{F}_0^l(\omega)$, $l = x, y$ and z , are shown as frequency response functions in Figures 4.1, 4.2 and 4.3, respectively. The hydrodynamic force is presented considering water compressibility for five values of α : 1.0, 0.75, 0.50, 0.25, 0; and also for incompressible water in which case the force is independent of α . These frequency response functions for the hydrodynamic force are computed as the integral of the corresponding functions for the hydrodynamic pressures acting on the upstream face of the dam. The pressure functions are determined by solving the wave equation over the reservoir domain with appropriate boundary conditions at the free surface, upstream dam face and the reservoir boundary using the analytical procedure described in Chapter 3. The hydrodynamic force $\bar{F}_0^l(\omega)$ is normalized with respect to the hydrostatic force on half of the dam $F_{st} = 0.208 \rho g H^2$ and the excitation frequency is normalized with respect to $\omega_1^y = \pi C/2H$, the first natural vibration frequency of an infinite reservoir of uniform depth H with rigid reservoir bottom. When presented

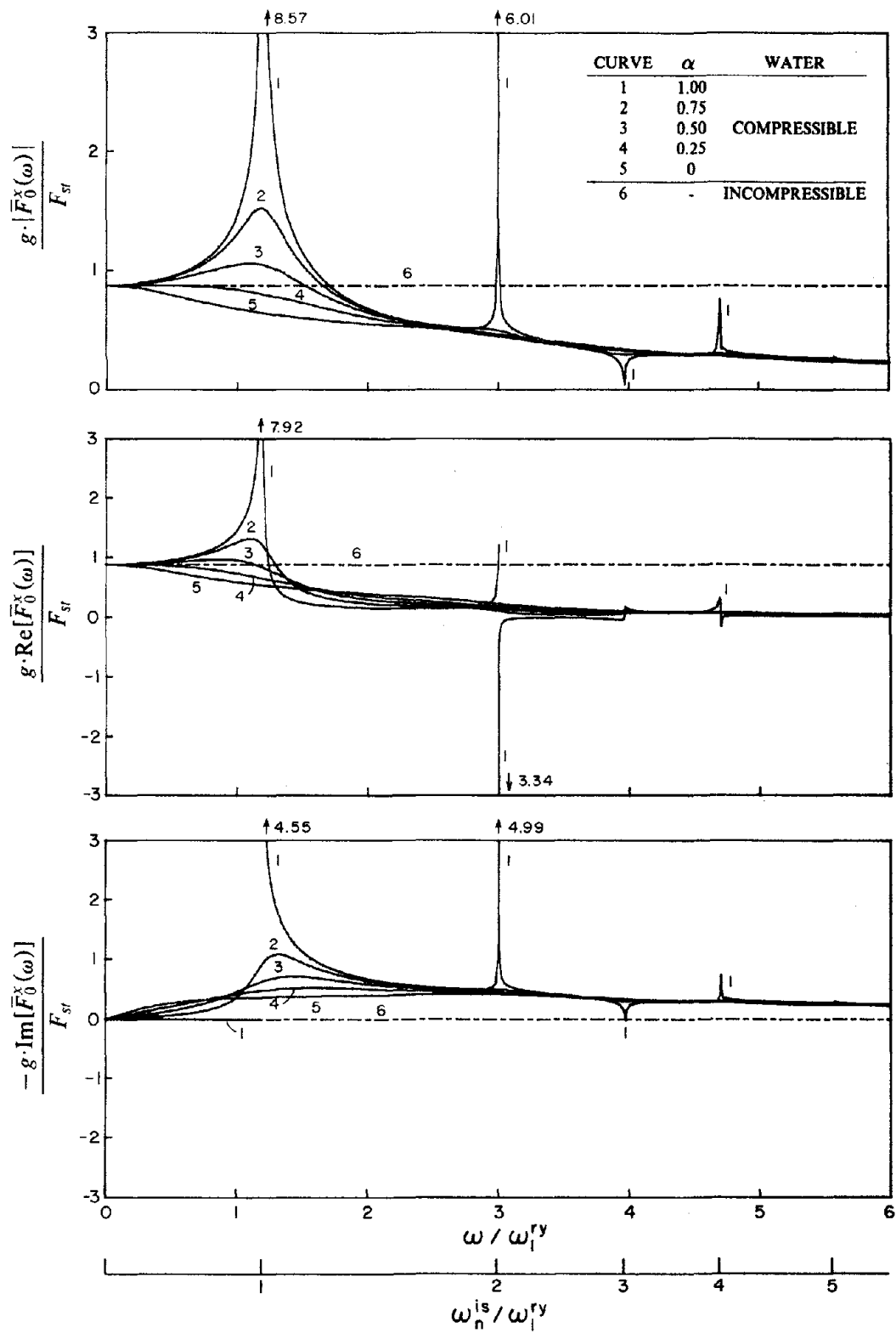


Figure 4.1 Influence of reservoir boundary absorption on the hydrodynamic force on rigid dam due to harmonic upstream ground motion.

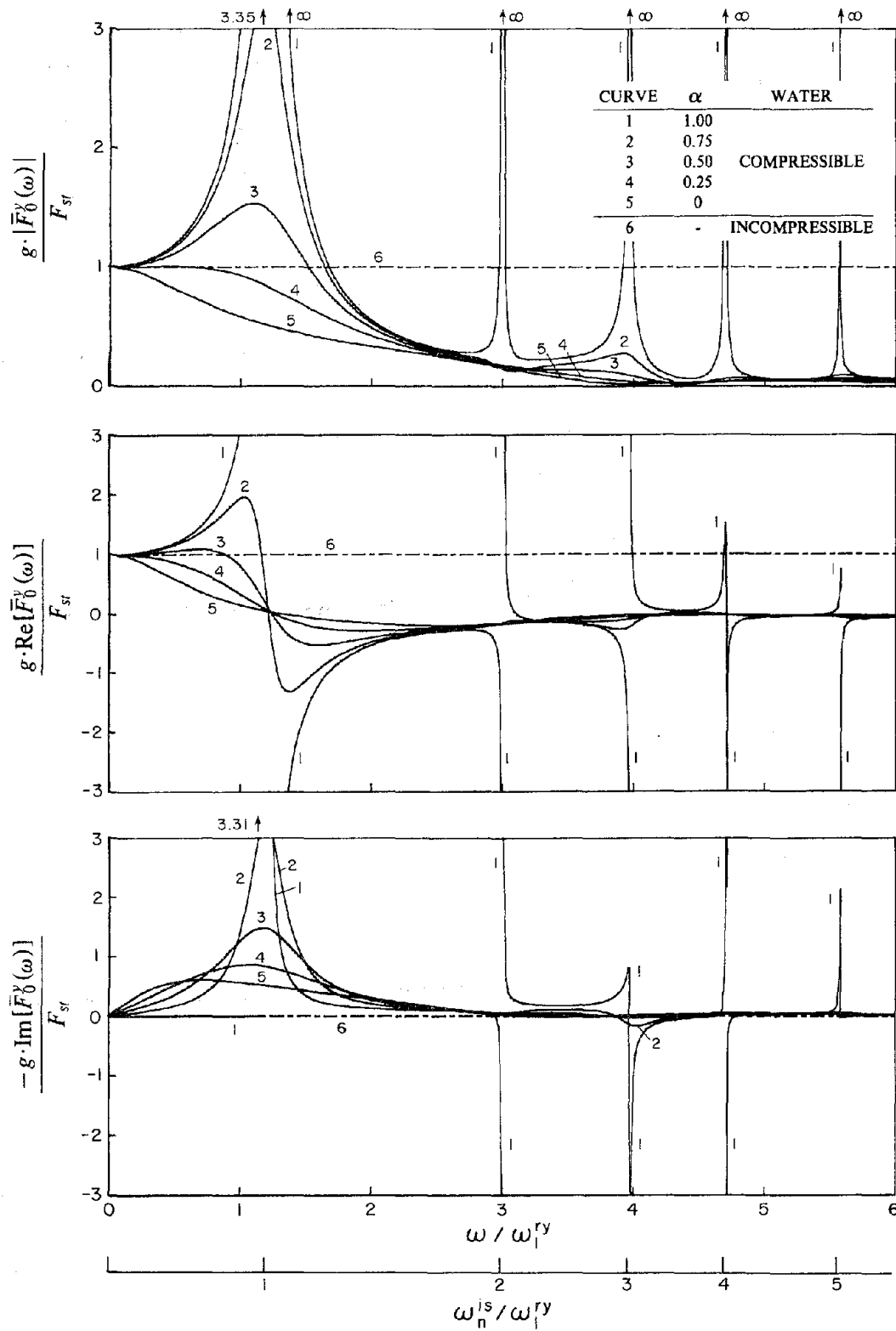


Figure 4.2 Influence of reservoir boundary absorption on the hydrodynamic force on rigid dam due to harmonic vertical ground motion.

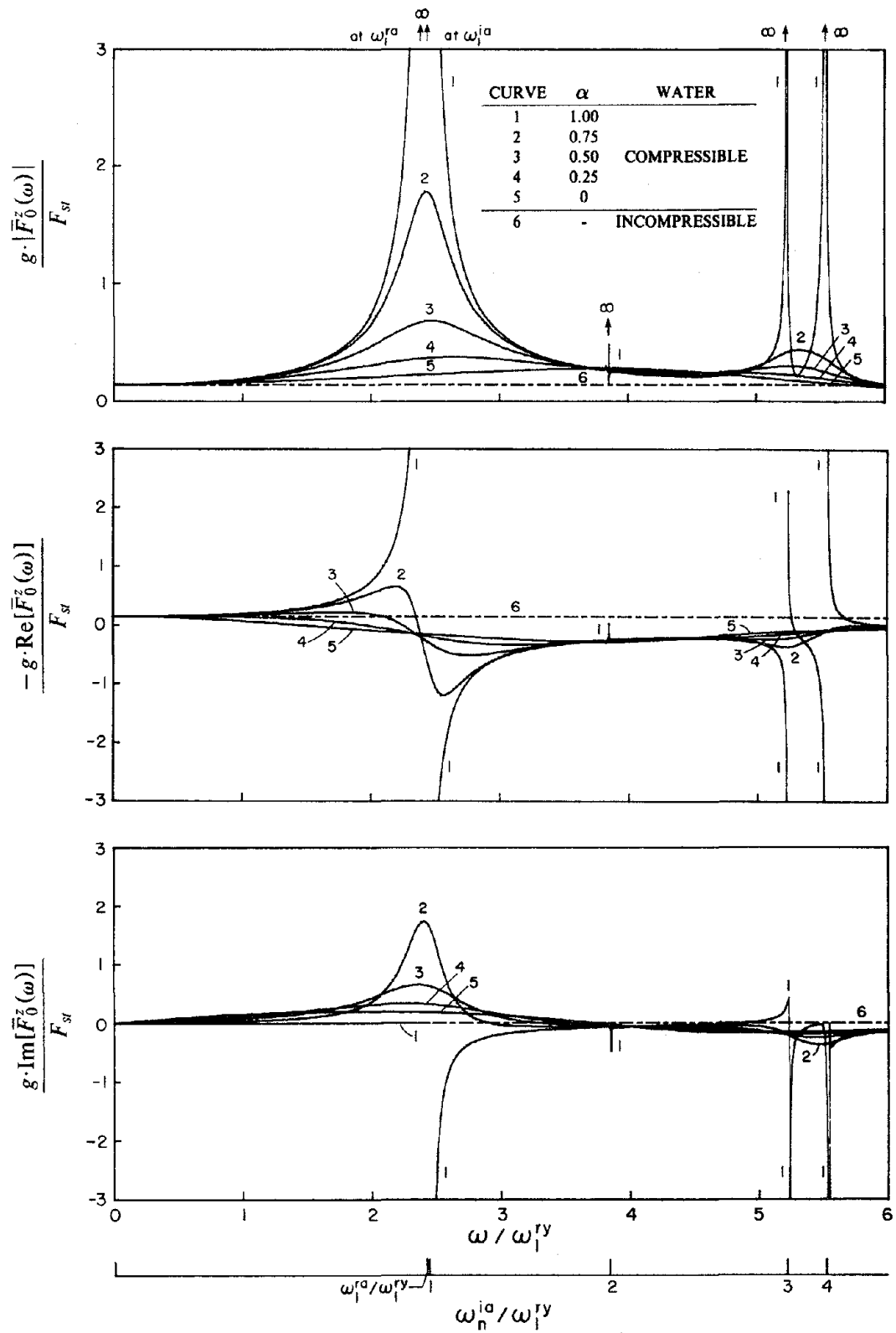


Figure 4.3 Influence of reservoir boundary absorption on the hydrodynamic force on rigid dam due to harmonic cross-stream ground motion.

in this form, the results apply to reservoir domains of any depth with the geometry shown in Figure 2.3. The real and imaginary components as well as the absolute value of the complex-valued frequency response functions are presented for each case. The real and imaginary components represent the in-phase and 90° -out-of-phase hydrodynamic forces relative to the harmonic ground acceleration, respectively.

If the reservoir boundary is rigid, i.e. $\alpha = 1$, the hydrodynamic force due to upstream ground motion is bounded for all excitation frequencies, while the hydrodynamic forces due to vertical and cross-stream ground motion are unbounded at the natural frequencies of the infinite uniform channel. Symmetric ground motion (vertical component) causes unbounded resonance at the natural frequencies ω_n^{is} of the symmetric modes; and antisymmetric ground motion (cross-stream component) at the natural frequencies ω_n^{ia} of the antisymmetric modes (Figures 4.1, 4.2 and 4.3). The hydrodynamic force due to upstream or vertical ground motion is opposite-phase relative to the ground acceleration for excitation frequencies less than the first natural frequency of the infinite channel ω_1^{is} , but a 90° -out-of-phase component exists for higher excitation frequencies indicating energy radiation due to propagation of hydrodynamic pressure wave in the upstream direction. For cross-stream ground motion, the hydrodynamic force on one-half of the dam is in-phase with the ground acceleration for excitation frequencies less than ω_1^{ra} , of opposite-phase between ω_1^{ra} and ω_1^{ia} ; but a 90° -out-of-phase component exists for higher frequencies; ω_1^{ra} is the fundamental natural frequency of the complete reservoir domain (infinite channel and irregular region) that exists just below ω_1^{ia} . Because the response to cross-stream ground motion is antisymmetric, at each excitation frequency the hydrodynamic force on one-half of the dam is of opposite-phase relative to the force on the other half. When reservoir boundary absorption is considered, i.e. $\alpha \neq 1$, the hydrodynamic forces are bounded, and a 90° -out-of-phase component exists for all excitation frequencies for all three components of ground motion.

The hydrodynamic pressure and hence force on rigid dam are determined by the hydrodynamic pressure responses in the reservoir domain which includes both the finite irregular region next to the dam and the infinite channel of uniform cross-section connected to the irregular region through the

transmitting plane. As indicated in the analytical procedure in Chapter 3, the hydrodynamic pressure in the infinite channel can be described as the sum of the contribution of N_ψ natural vibration modes of the infinite channel, with N_ψ chosen appropriately to accurately represent the hydrodynamic pressure over the desired frequency range.

The hydrodynamic pressures in the infinite channel due to upstream ground motion may be interpreted as the response to normal accelerations of the fluid at the fictitious transmitting plane. If the reservoir boundary is rigid, i.e. $\alpha = 1$, the contribution of the n th mode to the hydrodynamic pressures due to upstream ground motion is real-valued for excitation frequencies lower than ω_n^{is} ; but is imaginary-valued, i.e. 90° out-of-phase relative to the ground acceleration, for excitation frequencies higher than ω_n^{is} . If the excitation frequency is ω_n^{is} , the n th mode resonates in the infinite channel, but because of the existence of the irregular fluid region between the infinite channel and the dam, its contribution to the hydrodynamic pressure in the irregular region and hence to the force on a rigid dam has a bounded limit; though the response may be very large [Figure 4.1(a)]. In contrast, infinite hydrodynamic pressures would result at ω_n^{is} if the upstream face of dam is a vertical plane and the fluid domain is the infinite channel without any irregular region [9]. For excitation frequencies higher than ω_n^{is} , the pressure wave associated with the n th mode propagates in the upstream direction of the infinite channel resulting in radiation of energy and hence the imaginary component of the pressure response. With increasing excitation frequency, a larger number of modes are associated with the propagating pressure waves, leading to increased energy radiation and hence smaller hydrodynamic force [Figure 4.1(a)] -- except for the local resonance behavior near the natural vibration frequencies of the infinite channel. Because upstream radiation of energy does not occur for excitation frequencies below ω_1^{is} , the imaginary component is zero at these frequencies [Figure 4.1(c)].

If the reservoir boundary is absorptive, the natural vibration modes of the infinite channel are complex-valued and frequency-dependent. Consequently, the contribution of the n th mode to the hydrodynamic pressure and force due to upstream ground motion is complex-valued for all excitation frequencies. For excitation frequencies below ω_1^{is} , the imaginary component arises from the radiation of energy due to the refraction of pressure waves into the absorptive reservoir boundary; whereas for

excitation frequencies higher than ω_1^{is} , the imaginary component arises from the radiation of energy due to both the propagation of pressure waves in the upstream direction and their refraction into the absorptive reservoir boundary [Figure 4.1(c)]. Because of the additional energy radiation resulting from reservoir boundary absorption, the fundamental resonant peak is reduced and the response curve is smoothed [Figure 4.1(a)-(c)]. However, the additional energy radiation has little influence on the resonant frequencies of the impounded water.

The hydrodynamic pressures in the infinite channel due to vertical ground motion may be interpreted as the simultaneous response to normal accelerations of the fluid at the fictitious transmitting plane and to normal accelerations of the reservoir boundary due to the ground motion. If the reservoir boundary is rigid, i.e. $\alpha = 1$, the contribution of the n th natural vibration mode of the infinite channel to the hydrodynamic pressure due to the normal accelerations of the fluid across the transmitting plane behaves similarly as in the case of upstream ground motion, being real-valued below ω_n^{is} and imaginary-valued above ω_n^{is} because of energy radiation in the upstream direction. However, the modal contribution to the hydrodynamic pressures caused by normal accelerations of the reservoir boundary is always real-valued, behaving like a truly undamped system as the pressure waves do not propagate in the upstream direction [9]. At excitation frequency ω_n^{is} , the n th mode in the infinite channel has unbounded resonance due to the accelerations at the reservoir boundary like a truly undamped system, resulting in infinite values for the real and imaginary components and total hydrodynamic pressures in the irregular region and hence on the dam (Figure 4.2). Again, there is no upstream radiation of energy at excitation frequencies below ω_1^{is} , and so the imaginary component is zero at these frequencies [Figure 4.2(c)]. With increasing excitation frequency, there is increased energy radiation upstream and hence the hydrodynamic force is smaller [Figure 4.2(a)]; however, since the upstream radiation of energy arises only from the normal accelerations of the fluid across the transmitting plane, it does not prevent the unbounded resonances of the n th mode at ω_n^{is} due to the accelerations at the reservoir boundary. Reservoir boundary absorption leads to an imaginary component of hydrodynamic force associated with radiation of energy because pressure waves refract at the reservoir boundary for all excitation frequencies. This radiation damping reduces the response

for almost all frequencies and the resonant responses are now bounded.

The hydrodynamic pressures in the infinite channel due to cross-stream ground motion may be interpreted as the simultaneous response of the channel to normal accelerations of the fluid at the fictitious transmitting plane and to normal accelerations of the reservoir boundary due to the ground motion. The hydrodynamic force is unbounded at ω_n^{ia} if the reservoir boundary is rigid, i.e. $\alpha = 1$ because the n th vibration mode of the infinite channel has unbounded resonance [Figure 4.3(a)]. Again, there is no upstream radiation of energy below ω_1^{ia} , and so the imaginary component of the hydrodynamic force is zero at these frequencies [Figure 4.3(c)]. As in the response to vertical ground motion, both the real and imaginary components of the hydrodynamic force resonate to infinity at ω_n^{ia} [Figure 4.3(b)-(c)]. However, as mentioned earlier in this section, for this particular reservoir geometry, an eigenfrequency ω_1^{ra} of the complete reservoir domain (irregular region and infinite channel) exists just below ω_1^{ra} , resulting in an unbounded peak in the force at this frequency [Figure 4.3(a)]. Reservoir boundary absorption reduces the responses at ω_1^{ra} and ω_n^{ia} to finite values, smoothens the entire response curve, and gives complex-valued forces at all excitation frequencies [Figure 4.3(a)-(c)].

If water compressibility is neglected, the hydrodynamic forces are real-valued and independent of the excitation frequency (Figures 4.1, 4.2, 4.3). The hydrodynamic force due to upstream ground motion is slightly smaller than the hydrostatic force and of opposite phase relative to the ground acceleration (Figure 4.1); that due to vertical ground motion is equal to the hydrostatic force and also of opposite phase relative to the ground acceleration (Figure 4.2); and that due to cross-stream ground motion is much less than the hydrostatic force and in phase with the ground acceleration (Figure 4.3). The hydrodynamic effects are now equivalent to an added mass and, depending on the ground motion component, an added or reduced force.

4.4 Dam-Water Interaction Effects

4.4.1 Hydrodynamic Effects

The effects of interaction between the dam and the water on the dam response to upstream, vertical, and cross-stream ground motion are shown in Figure 4.4; where the results from the analyses of Cases 1, 2 and 10 (Table 4.1) are plotted. The response of the dam with an empty reservoir (Case 1) is characteristic of a multi-degree of freedom system with frequency-independent mass, stiffness, and damping properties. The response of the dam with a full reservoir (Cases 2 and 10) is affected by the hydrodynamic terms in the equations of motion for the dam. The hydrodynamic terms can be interpreted as modifying the properties of the dam by introducing an added mass, an added or subtracted hydrodynamic force, and an added damping. In the case of upstream and vertical ground motions, the hydrodynamic force is real-valued and additive for excitation frequencies ω less than ω_1^s because it has the same phase as the effective earthquake inertial force at these frequencies; whereas in the case of cross-stream ground motion, the hydrodynamic force is real-valued and subtractive for excitation frequencies ω less than ω_1^a because it has opposite phase compared to the effective earthquake inertial force at these frequencies. At higher excitation frequencies, the hydrodynamic force is complex-valued. These hydrodynamic terms depend on the excitation frequency and wave reflection coefficient α if water compressibility is considered, and on the ground motion component [9,20] with one exception: the added mass and added damping are the same for upstream and vertical ground motions.

Because of the strong frequency dependence of the hydrodynamic terms if the reservoir boundary is rigid and water compressibility effects are included, the response of the dam is quite complicated as seen in Figure 4.4. The response behavior is especially complicated at excitation frequencies in the neighborhood of the natural frequencies of the infinite reservoir channel. In particular, the response curve due to upstream or vertical ground motion has a double resonant peak at frequencies near ω_1^s and ω_1^s , the fundamental natural frequencies of the symmetric modes of dam and infinite channel, respectively [Figure 4.4(a)-(b)]; whereas the response curve due to cross-stream ground motion has a double resonant peak near ω_2^a , the natural frequency of the second antisymmetric

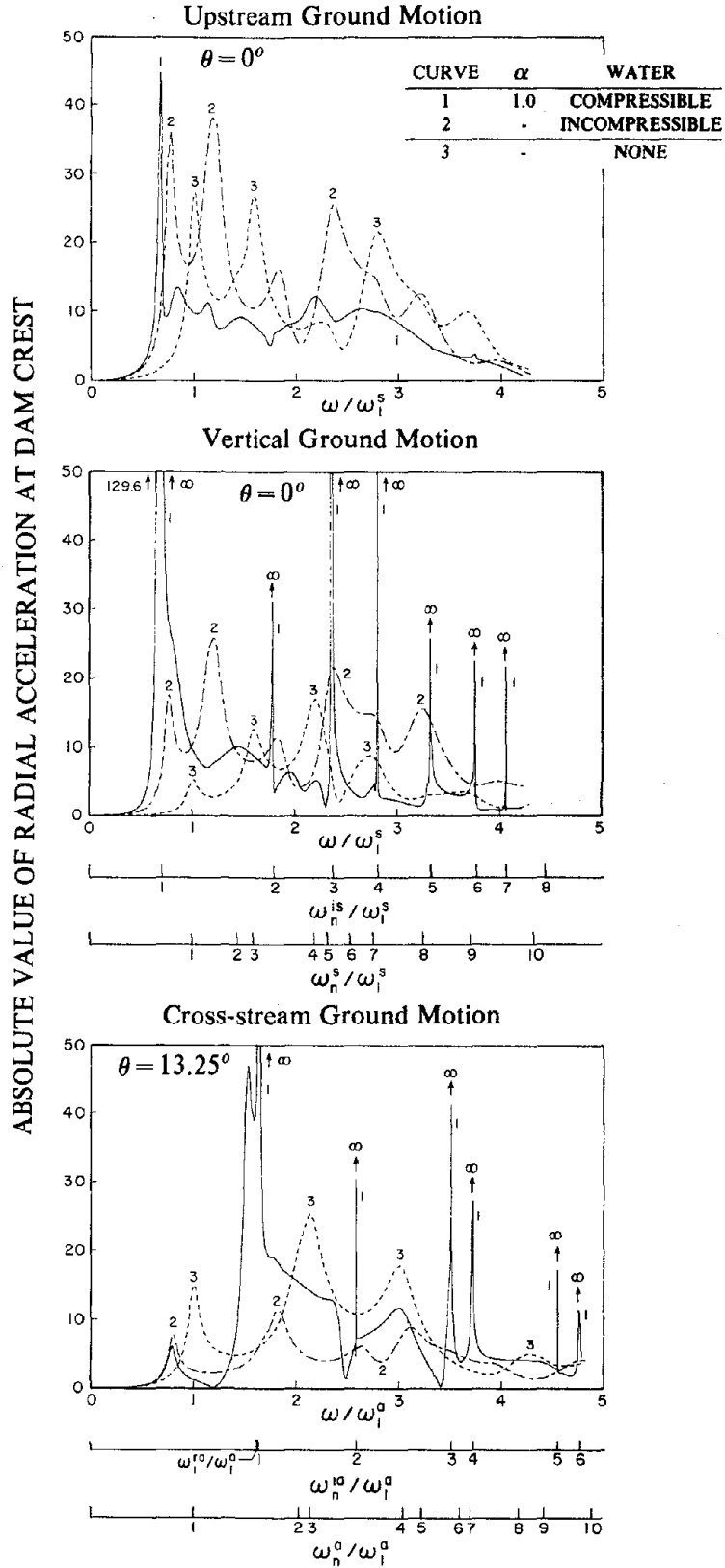


Figure 4.4 Hydrodynamic effects in response of dams to harmonic ground motion. Results presented for no water (Case 1 of Table 4.1), full reservoir with incompressible and compressible water (Cases 10 and 2).

vibration mode of the dam, and ω_1^a , the natural frequency of the fundamental antisymmetric mode of the infinite channel. The double resonant peak is especially pronounced when the excitation is vertical or cross-stream ground motion and the response is unbounded at ω_1^i as well as at higher ω_n^i . The superscripts s and a are dropped in this and subsequent statements if they are valid for both symmetric and antisymmetric modes.

As seen in Figure 4.4, the fundamental resonant frequency $\tilde{\omega}_r$ of the dam is reduced below both ω_1 and ω_1^i by the added mass of the water. The ratio \tilde{T}_r/T_1 of the resonant period \tilde{T}_r of the dam with reservoir filled to depth H to that period T_1 with empty reservoir is plotted in Figure 4.5 against normalized water depth H/H_s where H_s is the dam height. Results are presented for the resonant period of the fundamental symmetrical and antisymmetrical modes of vibration. Also presented is the period ratio for a concrete gravity dam from reference [24] which is comparable to the symmetric case for arch dams. These results are applicable to dams of any height with the specified geometry, and chosen values for Poisson's ratio, E_s and H/H_s ; and they are presented for a rigid reservoir boundary ($\alpha = 1$). As noted previously for gravity dams [24], dam-water interaction lengthens the vibration period also of arch dams, with the effect being very small for H/H_s less than 0.5, but increasing rapidly with water depth for H/H_s greater than 0.5. Dam-water interaction lengthens the vibration period of the symmetrical mode of arch dams more than that of gravity dams because the added hydrodynamic mass has more effect on the mass of a slender arch dam than of a massive gravity dam. Dam-water interaction lengthens the period of the fundamental antisymmetrical vibration mode of an arch dam to a lesser degree than the symmetric vibration mode of the arch dam or a gravity dam.

As shown in Table 4.2, dam-water interaction lengthens the periods of the higher vibration modes of the dam with the effect decreasing with mode number for symmetric vibration modes but is about the same for the first four antisymmetric vibration modes. The higher resonant periods of the symmetric vibration modes of the dam are affected not as much as the fundamental period by dam-water interaction because, just like the real part of the hydrodynamic force on rigid dam due to upstream ground motion [Figure 4.1(b)], the added mass decreases with increasing excitation

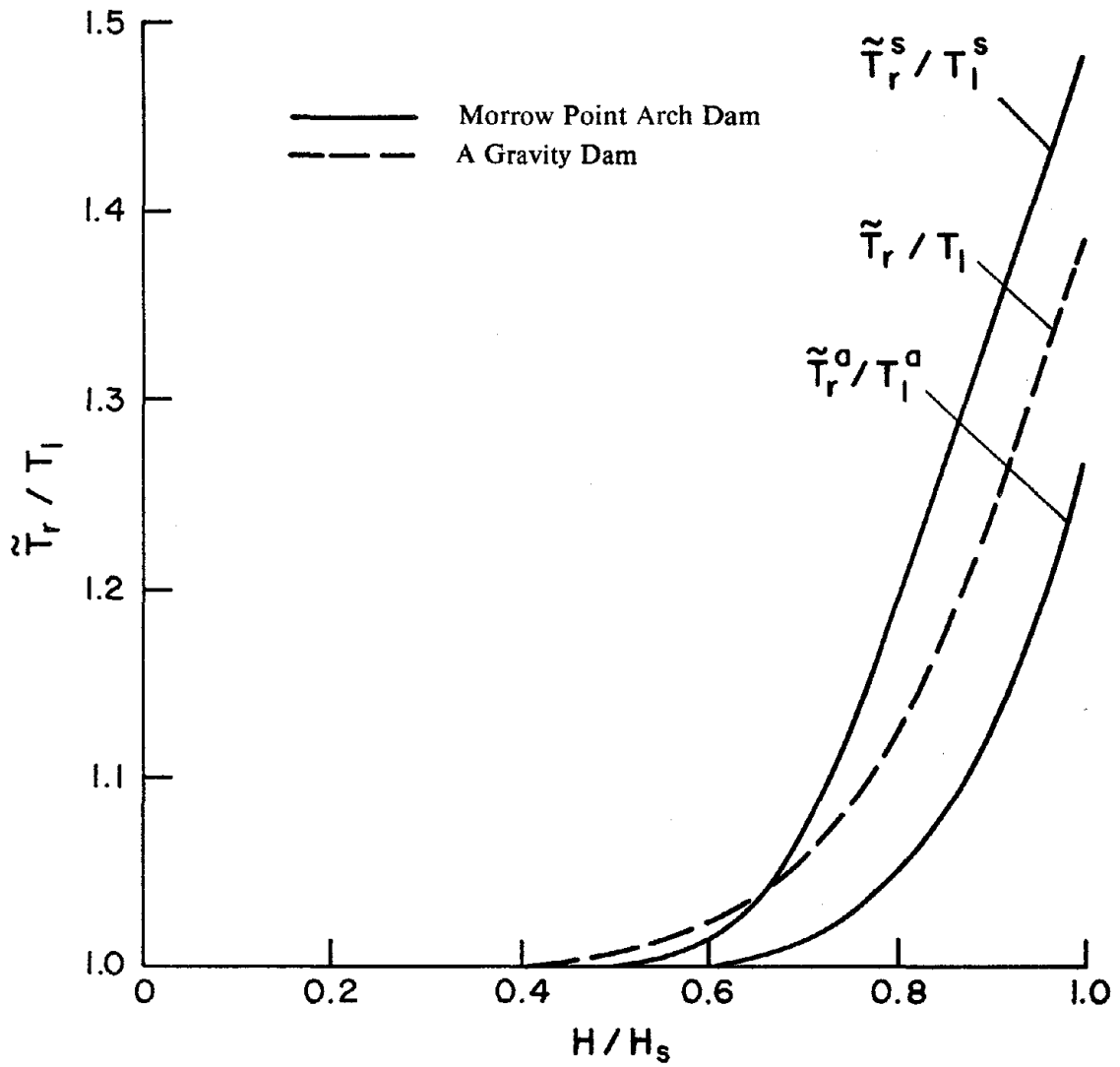


Figure 4.5 Variation of the fundamental period ratios, \tilde{T}_r/T_1 , \tilde{T}_r^s/T_1^s , and \tilde{T}_r^a/T_1^a , with the water depth ratio H/H_s , for dam on rigid foundation-rock. Results for the gravity dam are from Fenves and Chopra (1984).

Table 4.2 -- Ratio of the Resonant Period \tilde{T}_n of Dam on Rigid Foundation
with Water ($H/H_s = 1, \alpha = 1.0$) to T_n Without Water
for the First Five Symmetric and Antisymmetric Modes

Mode number n	Ratio \tilde{T}_n/T_n	
	Symmetric Modes	Antisymmetric Modes
1	1.48	1.27
2	1.24	1.33
3	1.16	1.21
4	1.09	1.26
5	1.10	1.06

frequency and is thus less effective in the higher vibration modes. However, the resonant periods of the first few antisymmetric modes of the dam are lengthened by about the same percentage because, unlike the symmetric vibration modes, the added mass associated with the higher antisymmetric vibration modes of the dam is as significant as that of the fundamental mode, as some of the higher resonant frequencies of the dam are quite close to the resonant frequencies of the impounded water in the infinite channel.

The fundamental resonant response due to upstream and vertical ground motions is increased due to dam-water interaction because of the added force at the resonant frequency. Furthermore, the bandwidth of the fundamental resonant response decreases [Figure 4.4(a)-(b)]. This apparent decrease in the effective damping ratio is due to the interaction of the dam and water and the rapid variation of the added force near the fundamental resonant frequency resulting in a double resonant peak in the response curve. This apparent decrease in damping occurs although propagation of hydrodynamic pressure waves in the upstream direction does not occur at the fundamental resonant frequency because the resonant frequency is smaller than ω_1^{is} , and in spite of the fact that the damping ratio associated with a constant hysteretic damping model for the dam is not affected by the hydrodynamic added mass [25]. The fundamental response to cross-stream ground motion is reduced by dam-water interaction because of the subtracted hydrodynamic force at this frequency; while the bandwidth is essentially unaffected. Dam-water interaction effects in the response to cross-stream ground motion differ from those in the response to upstream or vertical ground motions because of the relative values of the natural frequencies of the dam and impounded water. The double resonant peak due to dam-water interaction occurs because of interaction between the neighboring natural frequencies of the dam and infinite channel; in case of the upstream or vertical ground motion these are the fundamental frequencies, ω_1^d and ω_1^{is} , of the two systems; but in case of the cross-stream ground motion these are the second frequency ω_2^d of the dam and the fundamental frequency ω_1^{ia} of the infinite channel. The resonant response at higher resonant frequencies to upstream or vertical ground motion is much smaller than that for the dam with an empty reservoir [Figure 4.4(a)-(b)] because, for excitation frequencies greater than ω_1^d , the energy radiation due to propagation of hydrodynamic

pressure waves in the upstream direction leads to added damping. The resonant response at higher-than-the-second resonant frequencies to cross-stream ground motion is also smaller than that for the dam with an empty reservoir [Figure 4.4(c)] for the same reason.

When water compressibility is neglected, the hydrodynamic terms are independent of excitation frequency and the response of the dam is much less complicated. It is like that of a standard multi-degree of freedom system with modified natural frequencies and effective earthquake force. When the excitation is upstream or vertical ground motion, the decrease in the resonant frequency of the dam and the increase in earthquake force is apparent from the dam response [Figure 4.4(a)-(b)]. When the excitation is cross-stream ground motion, the decrease in the resonant frequency and in the earthquake force is apparent from the dam response [Figure 4.4(c)].

4.4.2 *Effects of Reservoir Boundary Absorption*

The effects of hydrodynamic pressure wave absorption at the reservoir boundary on the dynamic response of the dam with full reservoir (Cases 1 to 5) are shown in Figure 4.6. As in the case of gravity dams [19], with increasing wave absorption at the reservoir boundary, i.e. decreasing wave reflection coefficient α , the amplitude of the fundamental resonant peak due to upstream ground motion decreases whereas the second, smaller peak increases, resulting in a single fundamental resonant peak at an intermediate frequency value. Because of reservoir boundary absorption, the frequency response functions become smoother near the fundamental resonant peak with reduced resonant amplitude and wider frequency bandwidth in the case of upstream or vertical ground motions. But with increasing wave absorption (decreasing α from 0.75 to 0), the resonant peak in upstream ground motion increases -- contrary to intuition -- because the added damping decreases at this frequency. This decrease in added damping with increasing wave absorption is dependent on the particular problem analyzed and has also been observed in response of a gravity dam [24]. For cross-stream ground motion, however, the fundamental resonant amplitude slightly increases with reservoir boundary absorption; because the "added" hydrodynamic force, being of opposite phase relative to the effective earthquake inertia force, is reduced by wave absorption. The fundamental resonant frequency is, in general, not much affected by reservoir boundary absorption for all three

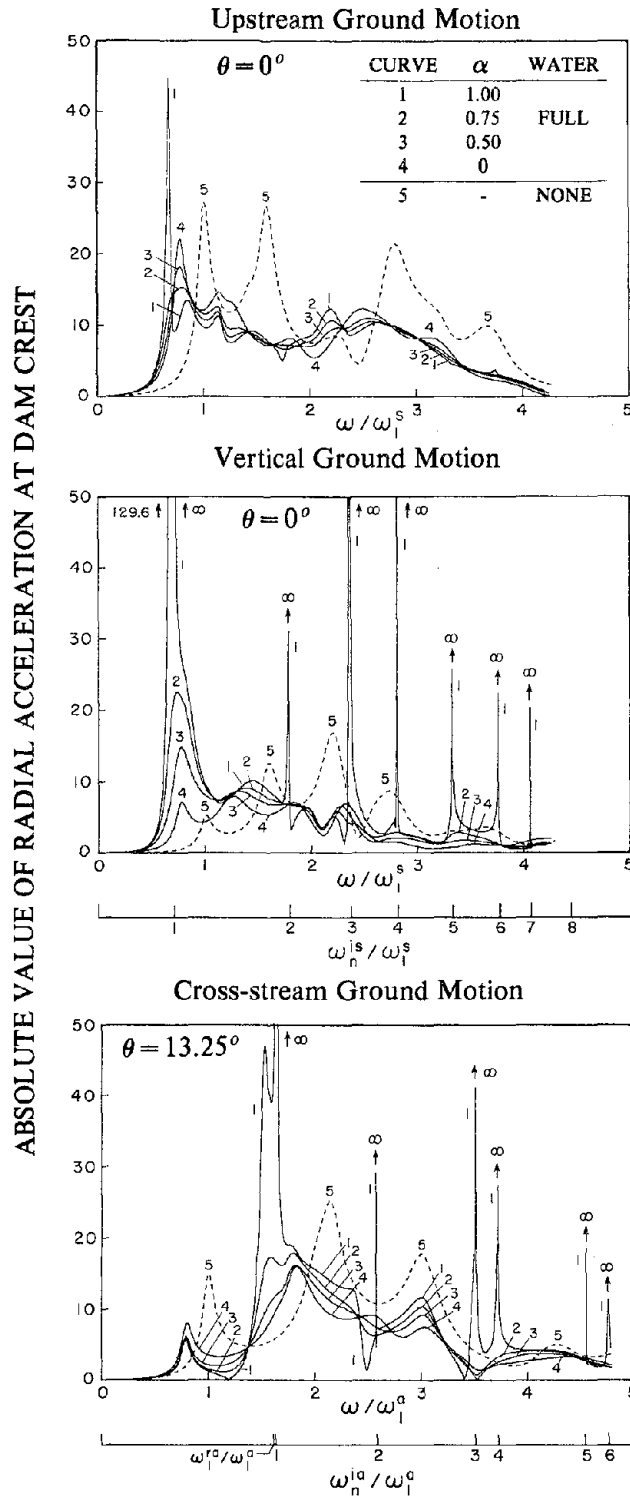


Figure 4.6 Hydrodynamic effects in response of dams to harmonic ground motion. Results presented for full reservoir with varying values of the wave reflection coefficient α (Cases 2, 3, 4 and 5 of Table 4.1), and for no water (Case 1).

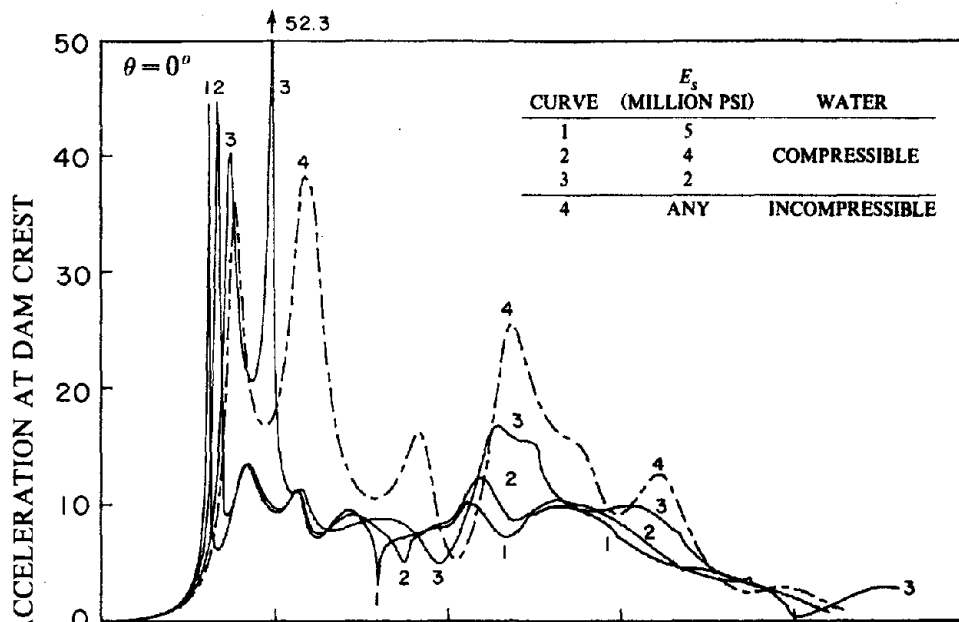
components of ground motion.

Reservoir boundary absorption reduces the added mass and added or subtracted force for all three ground motion components (Figures 4.1 to 4.3) at all excitation frequencies; in particular these hydrodynamic quantities associated with vertical and cross-stream ground motions are reduced to finite values at excitation frequencies ω_1^{is} and ω_1^{ia} , respectively. Consequently, at these excitation frequencies the unbounded response to vertical or cross-stream ground motions is eliminated. The effects of reservoir boundary absorption are relatively less significant for excitation frequencies greater than ω_1^i -- except locally near ω_n^i . This is because, at these higher frequencies, the energy radiation due to refraction of hydrodynamic pressure waves into the reservoir boundary is small compared to the energy radiation due to pressure waves propagating in the upstream direction. Reservoir boundary absorption eliminates the unbounded responses at excitation frequencies equal to ω_n^i due to vertical or cross-stream ground motion.

4.4.3 Influence of Young's Modulus E_s

The response of the dam with water when presented in the form of Figures 4.7 to 4.9 is independent of the Young's modulus E_s of the dam concrete if water compressibility is neglected [21]. However, the results from analysis of Cases 2, 6 and 8 (Table 4.1) presented in Figures 4.7(a), 4.8(a) and 4.9(a) demonstrate that the E_s value affects the response functions when water compressibility is considered. This effect is most pronounced on the fundamental resonant frequency $\tilde{\omega}_r$, associated with the symmetric vibration mode and on the response to upstream and vertical ground motions in the neighborhood of this frequency. For the larger values of E_s , when the reservoir boundary is rigid, the fundamental resonant frequency of the dam decreases due to hydrodynamic effects to a greater degree and the response is amplified more but over a narrower frequency band. The amplitude of resonant response to upstream ground motion is affected little by variations in E_s but is influenced substantially for vertical ground motion. At higher excitation frequencies the response functions are less affected by E_s except for the location of the sharp unbounded spikes at ω_n^{is} in the response to vertical ground motion. The E_s value has little effect on the fundamental resonant frequency $\tilde{\omega}_r$, associated with the antisymmetric vibration mode and on the resonant response to cross-

Rigid Reservoir Boundary, $\alpha = 1.0$



Absorptive Reservoir Boundary, $\alpha = 0.5$

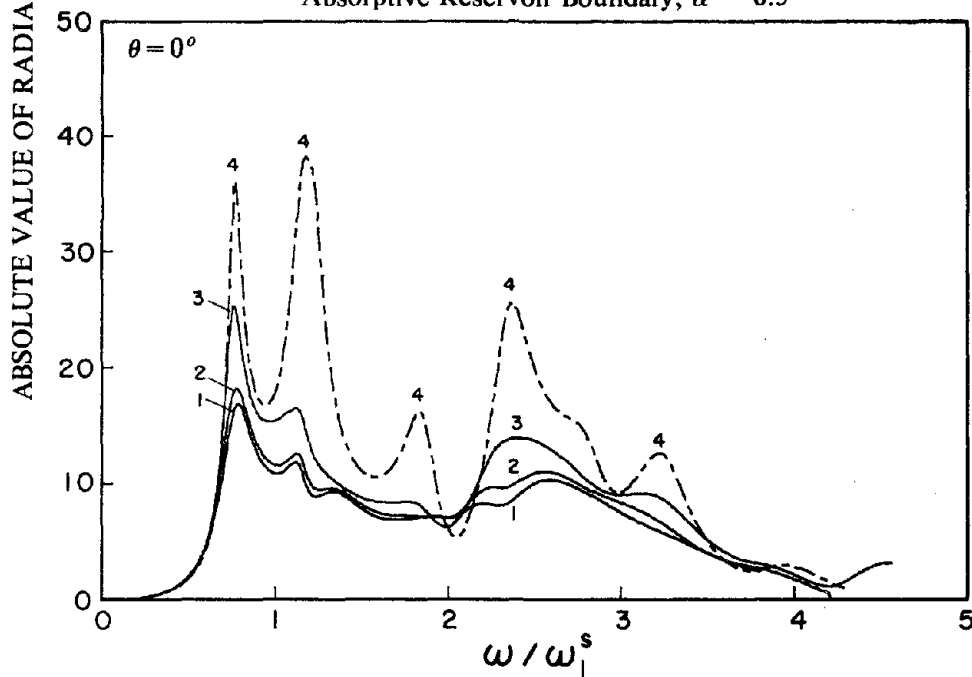


Figure 4.7 Influence of Young's modulus E_s of dam concrete on response of dams with full reservoir to harmonic upstream ground motion. Results presented for rigid reservoir boundary (Cases 2, 6 and 8 of Table 4.1), absorptive reservoir boundary (Cases 4, 7 and 9) and incompressible water (Case 10).

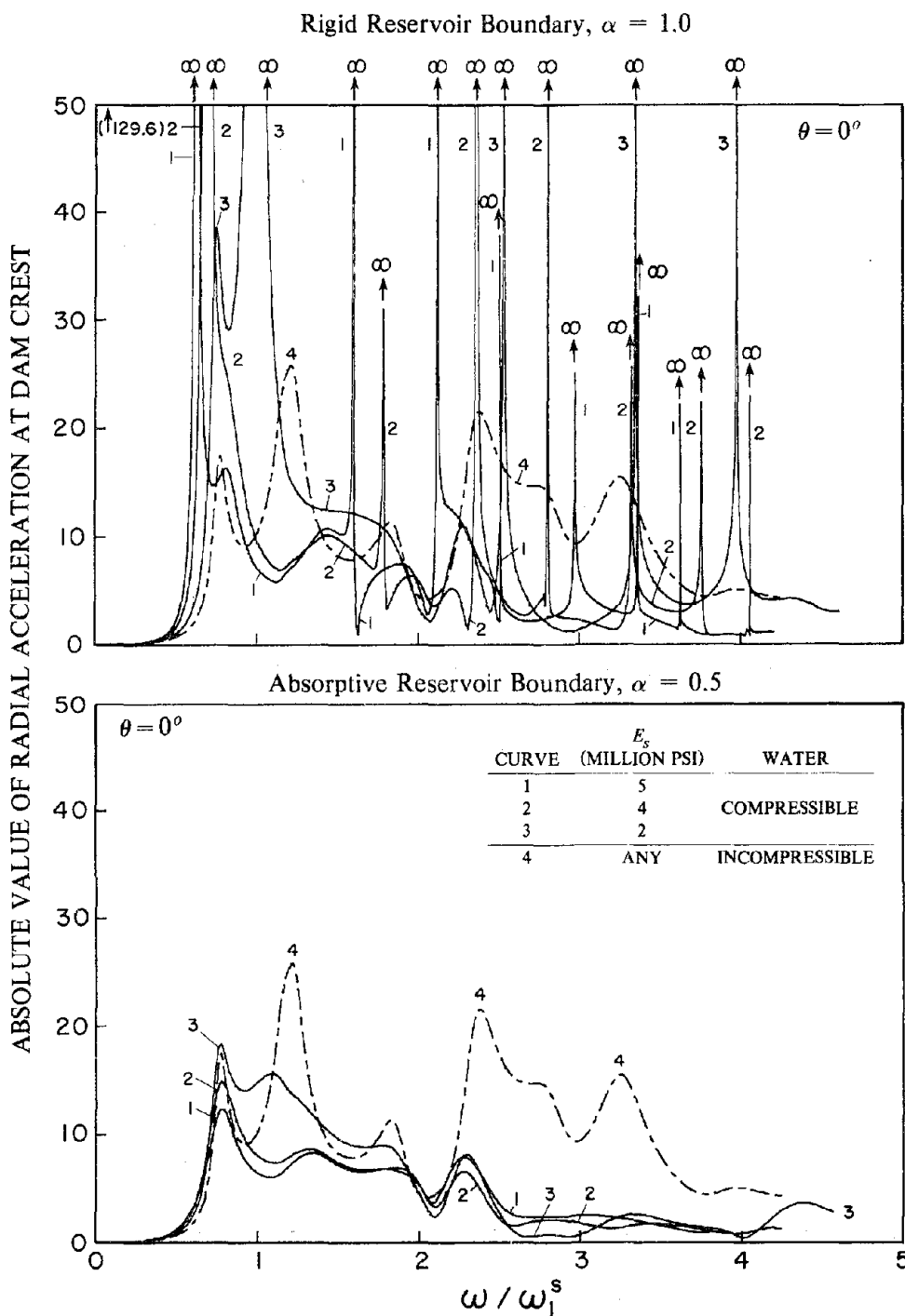


Figure 4.8 Influence of Young's modulus E_s of dam concrete on response of dams with full reservoir to harmonic vertical ground motion. Results presented for rigid reservoir boundary (Cases 2, 6 and 8 of Table 4.1), absorptive reservoir boundary (Cases 4, 7 and 9) and incompressible water (Case 10).

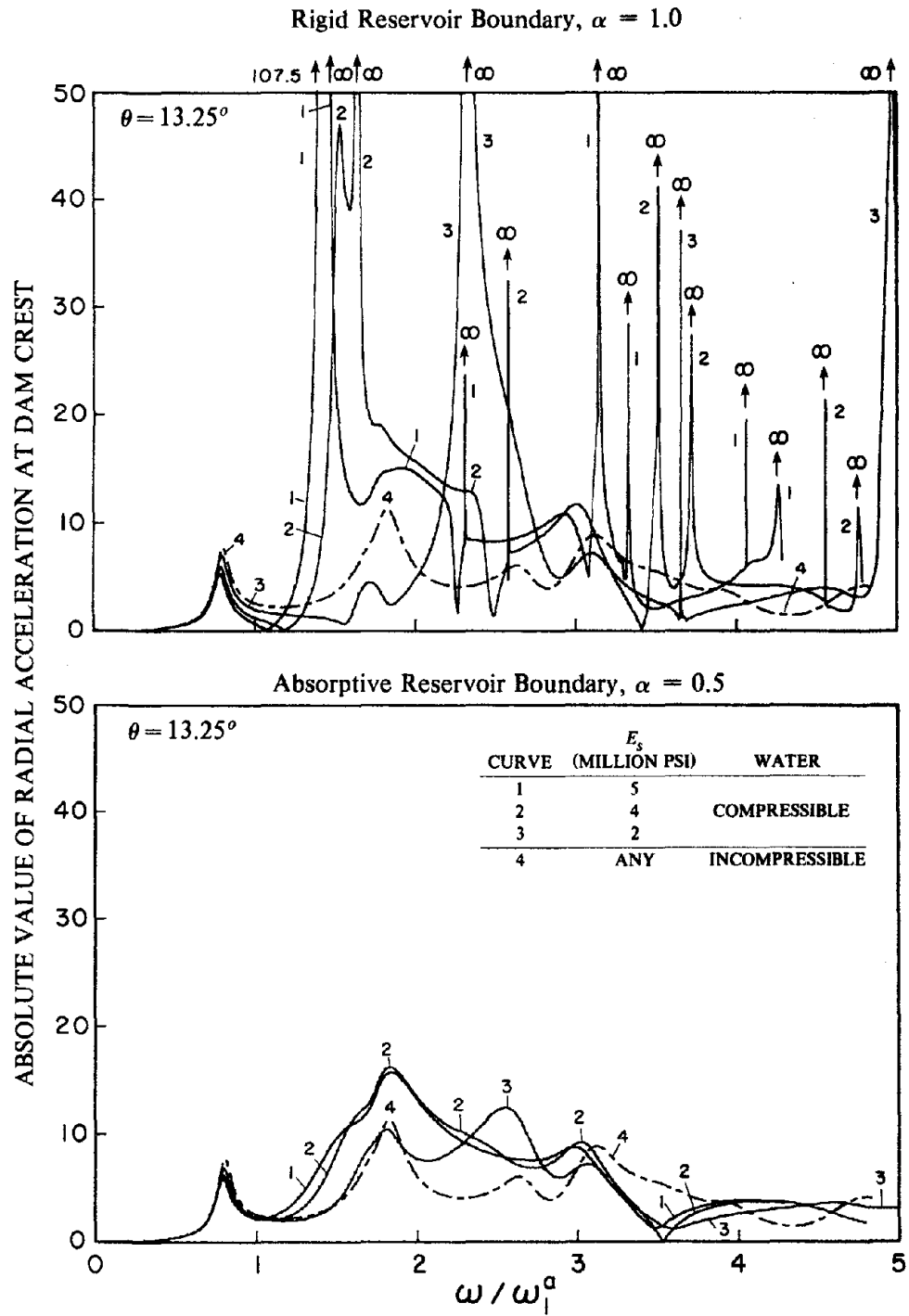


Figure 4.9 Influence of Young's modulus E_s of dam concrete on response of dams with full reservoir to harmonic cross-stream ground motion. Results presented for rigid reservoir boundary (Cases 2, 6 and 8 of Table 4.1), absorptive reservoir boundary (Cases 4, 7 and 9) and incompressible water (Case 10).

stream ground motion [Figure 4.9(a)]. At higher excitation frequencies, the effect of E_s on response is dominated by its influence on the location of the unbounded peaks.

Reservoir boundary absorption affects in an especially significant way how the amplitude and frequency bandwidth of the fundamental resonant peak varies with E_s . As discussed and interpreted for gravity dams [19], increasing E_s now causes smaller resonant peak over a wider bandwidth in the response to upstream or vertical ground motions [Figures 4.7(b) and 4.8(b)], with comparatively little influence on the amplitude of resonant response to vertical ground motion [Figure 4.8(b)]. Just as for rigid reservoir boundary, the fundamental resonant frequency and amplitude of response to cross-stream ground motion are essentially unaffected by E_s . However, at higher excitation frequencies, reservoir boundary absorption eliminates the unbounded spikes in the response to cross-stream or vertical ground motions and the responses to all three ground motions are less affected by E_s .

With decreasing E_s , the effects of water compressibility on the fundamental resonant response due to upstream, vertical, or cross-stream ground motion become smaller, and the response approaches the incompressible case. This trend is readily apparent in Figures 4.7 - 4.9 except in the response to vertical or cross-stream ground motions with rigid reservoir boundary in which case the trend is masked by the unbounded response peaks at excitation frequencies equal to ω_n^{is} or ω_n^{ia} .

As noted in a study on gravity dams [19], the effects of wave absorption on dam response are not properly represented by analyses neglecting water compressibility [Figures 4.7(b), 4.8(b) and 4.9(b)]. Although such an analysis provides a good approximation to the fundamental resonant frequency $\tilde{\omega}_r$, the fundamental resonant response to upstream ground motion is overestimated because there is no radiation of energy upstream or through the reservoir boundary if water is incompressible; the amplitude of higher resonant peaks due to upstream or vertical ground motion are overestimated by even a greater margin. However, the higher resonant peaks due to cross-stream ground motion are underestimated because the "added" hydrodynamic force is really a subtracted force as it is of opposite-phase compared to the effective earthquake force associated with the ground acceleration at all excitation frequencies if water is incompressible, whereas the added force has an in-phase component at some higher frequencies if water compressibility and wave absorption are considered.

4.4.4 Comparison of Responses to Three Ground Motion Components

Comparing the responses of the dam with an empty reservoir to the three components of ground motion, it is apparent that the fundamental resonant response to vertical or cross-stream ground motion is relatively small. However, with a full reservoir, the response to vertical ground motion is much larger, even exceeding the response to horizontal ground motion for the larger values of α . For the smaller values of α , the resonant response to vertical ground motion, although smaller than that due to upstream ground motion, is relatively significant because of hydrodynamic effects. The fundamental resonant response to cross-stream ground motion remains small even for a full reservoir irrespective of the α value.

4.5 Foundation Flexibility Effects

The frequency response functions for the dam on flexible foundation rock are presented in Figures 4.10, 4.11 and 4.12 for varying foundation modulus E_f (Cases 1, 11, 12 and 13 in Table 4.1). When presented in this form, these functions do not depend separately on E_s or E_f but only on the ratio E_f/E_s . Results are presented for four values of $E_f/E_s = \infty, 2, 1, 1/4$. The first represents rigid foundation rock, whereas in the last case the elastic modulus for the foundation rock is a fraction of the modulus for dam concrete, an assumption appropriate in many practical situations because of joints in the foundation rock.

Unlike impounded water, the foundation rock does not have any resonant frequencies because it is assumed to be massless. As a result, foundation flexibility affects the response of the dam in a simpler manner than does dam-water interaction. As the E_f/E_s ratio decreases, which for a fixed concrete modulus E_s implies decrease of foundation modulus E_f , the fundamental resonant frequency of the dam decreases because of foundation flexibility; the response at the crest of the dam at this frequency increases and the frequency bandwidth at resonance decreases, implying a decrease in the apparent damping of the structure resulting, in part, from the undamped foundation rock region. The increase in response is, in part, due to the increase in the effective earthquake forces in individual vibration modes arising from modifications in the mode shape due to foundation flexibility.

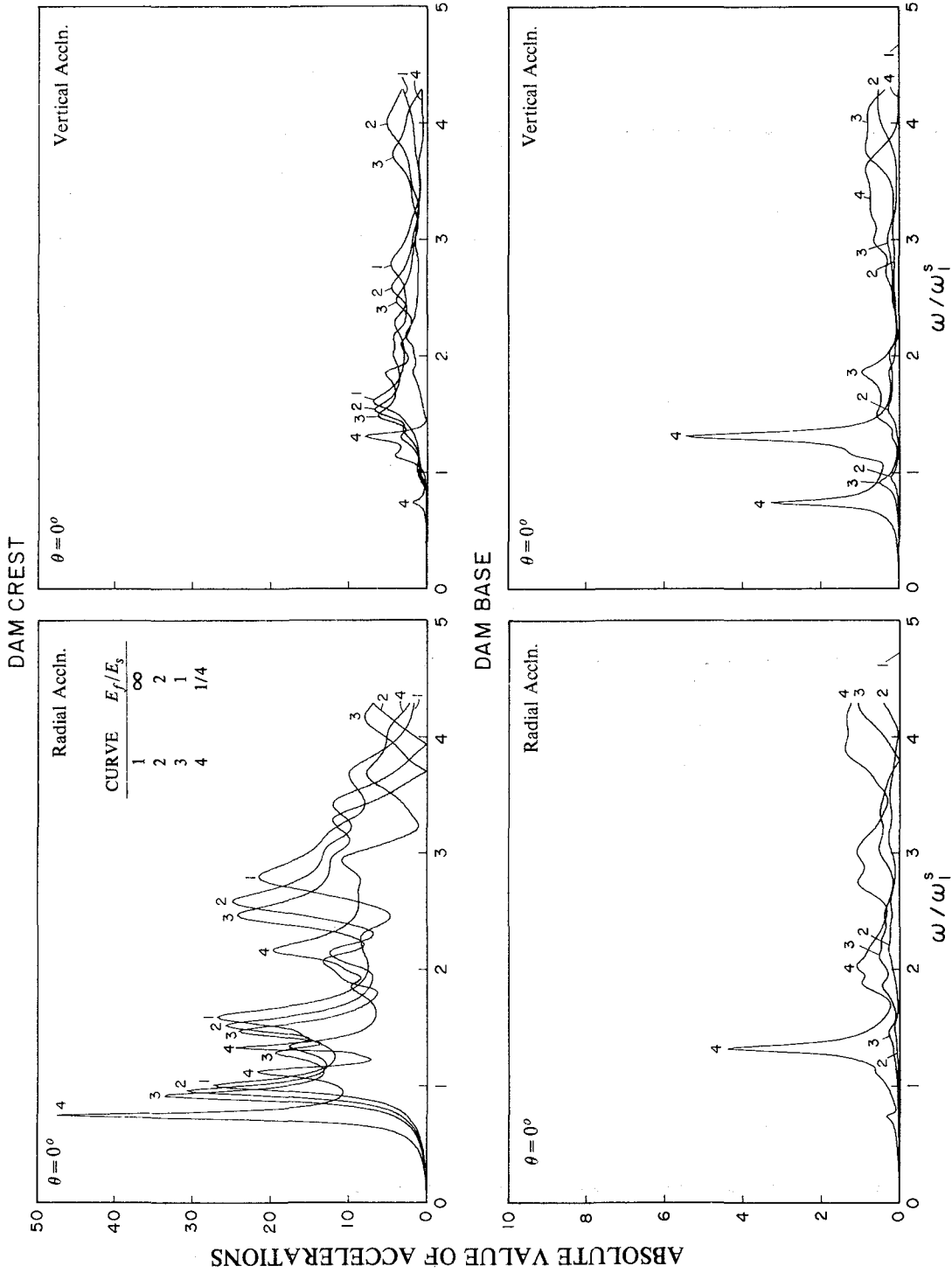


Figure 4.10 Influence of moduli ratio E_f/E_s on response of dams with no water to harmonic upstream ground motion (Cases 1, 11, 12 and 13 of Table 4.1).

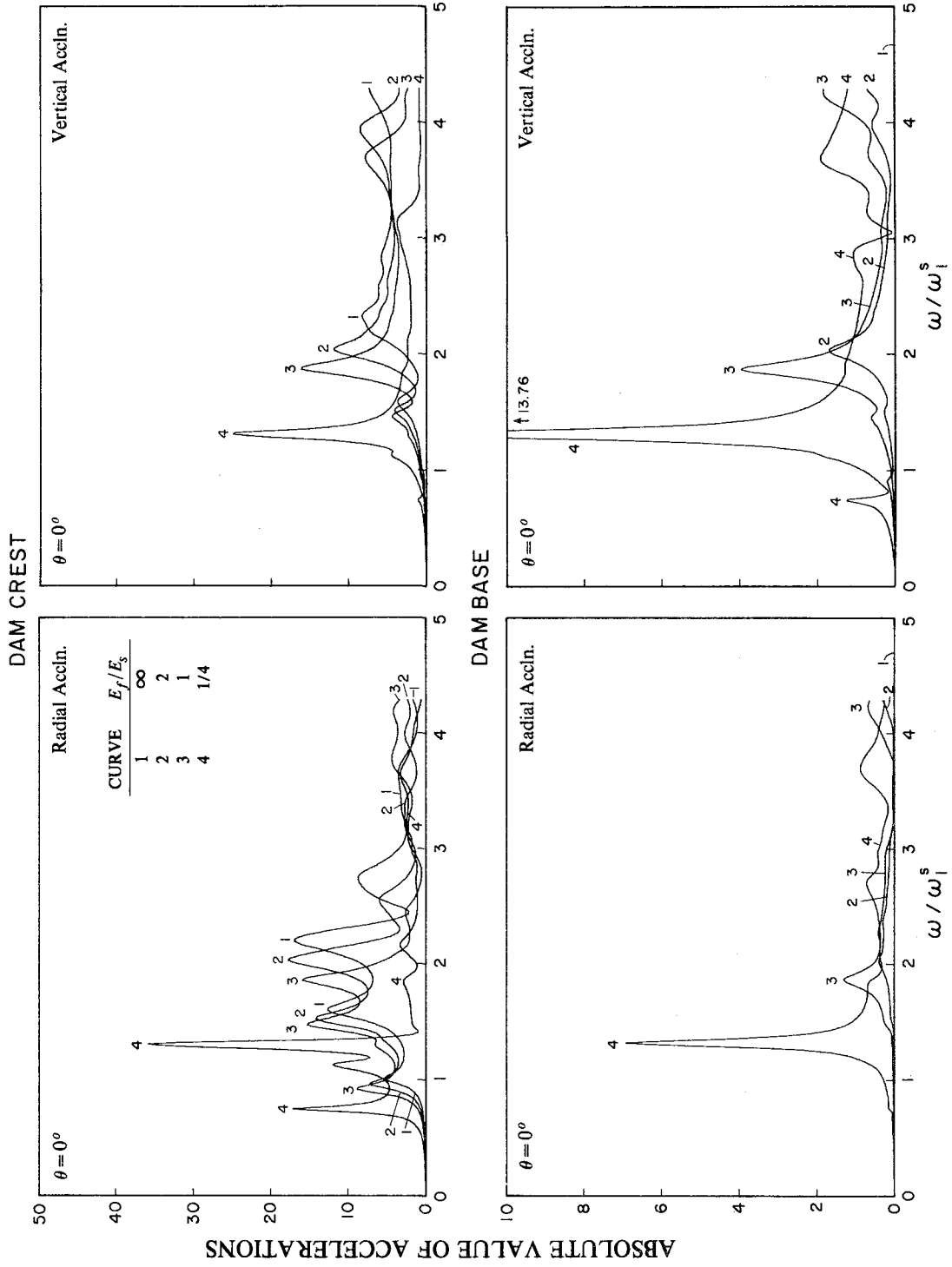


Figure 4.11 Influence of moduli ratio E_f/E_s on response of dams with no water to harmonic vertical ground motion (Cases 1, 11, 12 and 13 of Table 4.1).

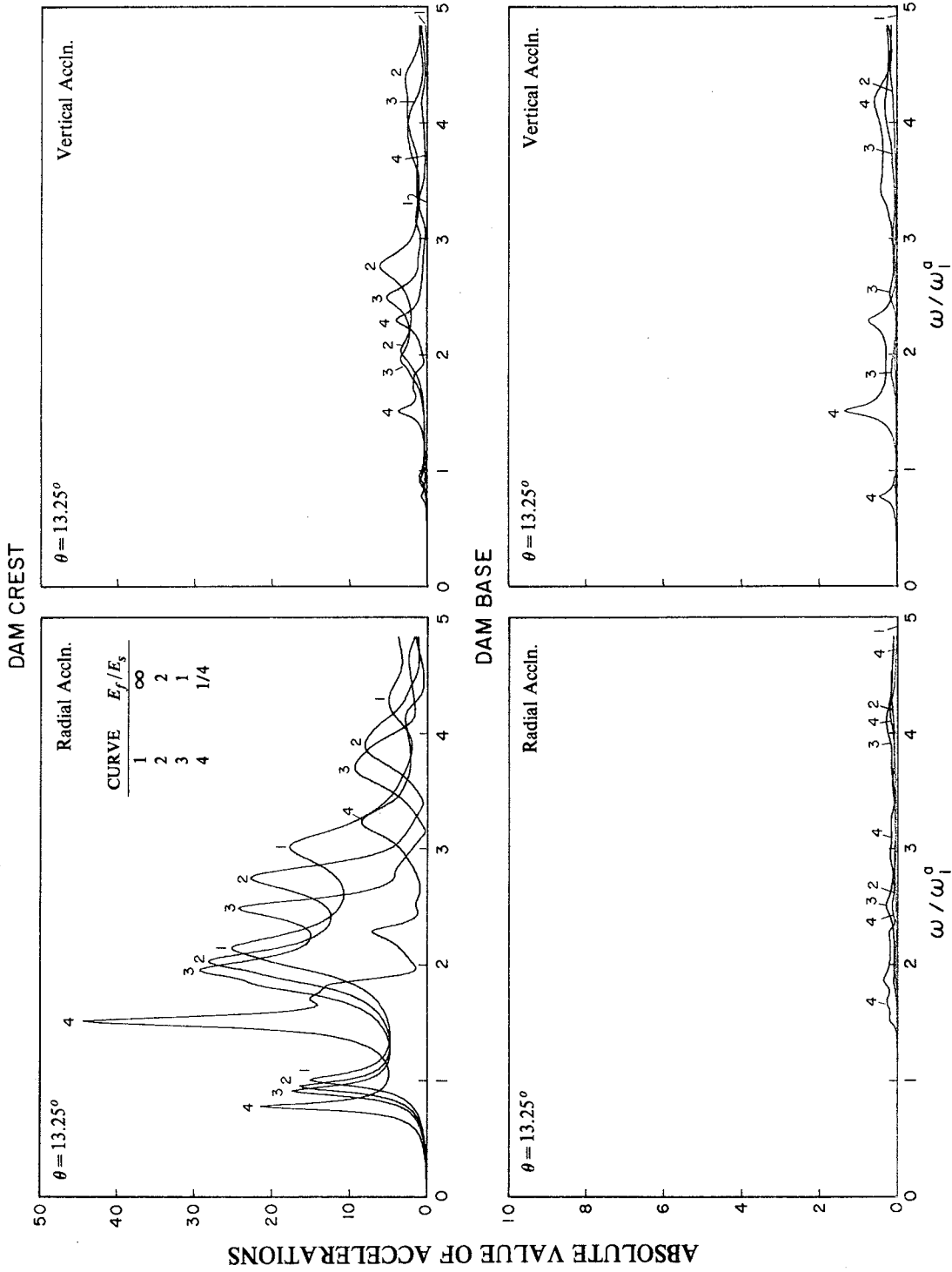


Figure 4.12 Influence of moduli ratio E_f/E_s on response of dams with no water to harmonic cross-stream ground motion (Cases 1, 11, 12 and 13 of Table 4.1).

Accompanying this change in the resonant response at the crest of the dam is an increasing response at the base of the dam -- which is however, a small fraction of the response at the crest -- with increasingly flexible rock (Figures 4.10 - 4.12). Similar but somewhat smaller effects of decreasing E_f/E_s are observed at higher resonant frequencies; in particular, the higher resonant frequencies are decreased to a lesser degree by foundation rock flexibility. The above mentioned effects of foundation-rock flexibility are qualitatively similar in the response to the three components of ground motion.

The effect of foundation-rock flexibility on the fundamental vibration period of the dam is displayed in Figure 4.13 wherein the ratio \tilde{T}_f/T_1 of the resonant period \tilde{T}_f of the dam on flexible foundation rock to that on rigid foundation rock is plotted as a function of E_f/E_s . Also presented is the period ratio for a gravity dam [24]. These results are applicable to dams of any height with the specified geometry and chosen values for Poisson's ratio and density of materials. As expected, the period ratio \tilde{T}_f/T_1 increases, i.e. the fundamental period lengthens, as the foundation-rock becomes increasingly flexible. The increase in vibration period can be significant and it is about the same for the symmetric and antisymmetric modes, but much less than the period increase for gravity dams. Dam-foundation rock interaction effects are more significant for gravity dams because they are massive compared to arch dams. Part of the differences in the interaction effects are, however, due to the use of different foundation idealizations, half-plane in the case of gravity dams and a massless, finite element system for arch dams.

4.6 Dam-Water Interaction and Foundation Flexibility Effects

4.6.1 Hydrodynamic and Reservoir Boundary Absorption Effects

The simultaneous effects of interaction between the dam and impounded water and of foundation flexibility on the dynamic response of arch dams can be examined from Figures 4.14 - 4.16, wherein response results are presented for four systems: dam on rigid foundation rock with no water (Case 1); dam on flexible foundation rock with no water (Case 12); dam on rigid foundation rock with full reservoir (Cases 2 and 4); and dam on flexible foundation rock with full reservoir (Cases 14 and

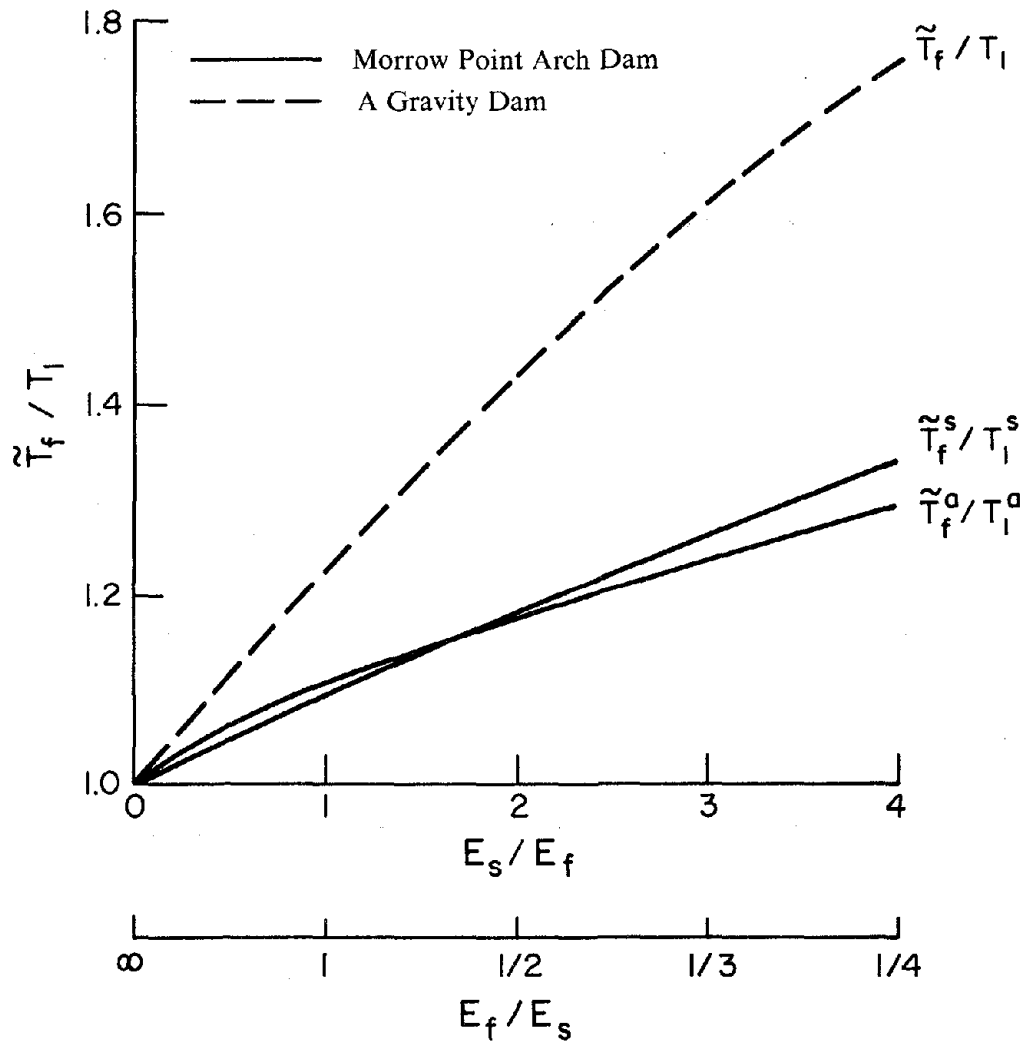
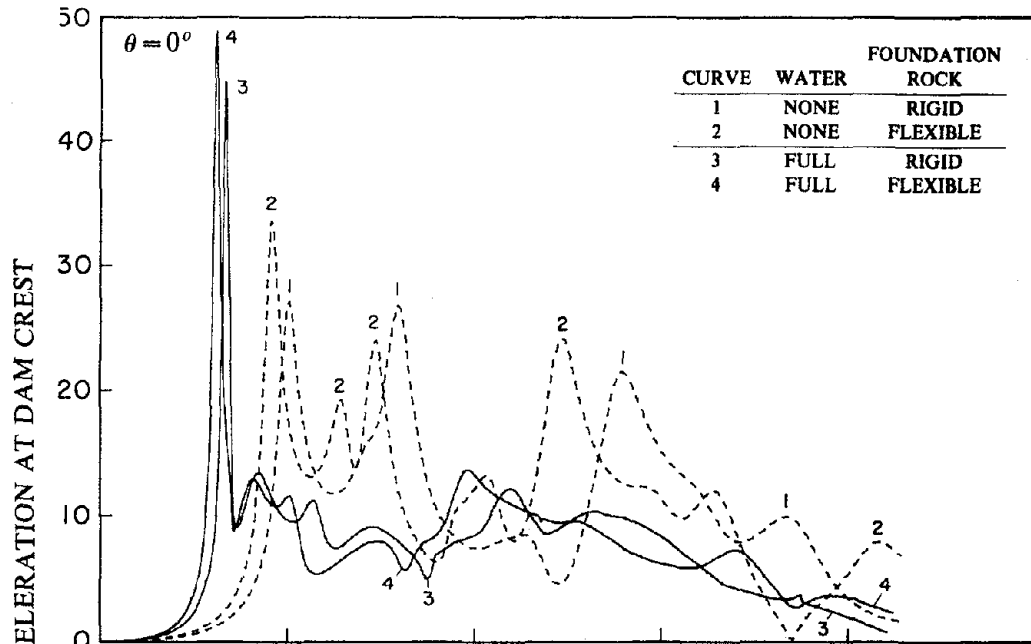


Figure 4.13 Variation of the fundamental period ratios, \tilde{T}_f / T_1 , \tilde{T}_f^s / T_1^s and \tilde{T}_f^a / T_1^a , with the moduli ratio E_f / E_s , for dam with an empty reservoir. Results for the gravity dam are from Fenves and Chopra (1984).

Rigid Reservoir Boundary, $\alpha = 1.0$



Absorptive Reservoir Boundary, $\alpha = 0.5$

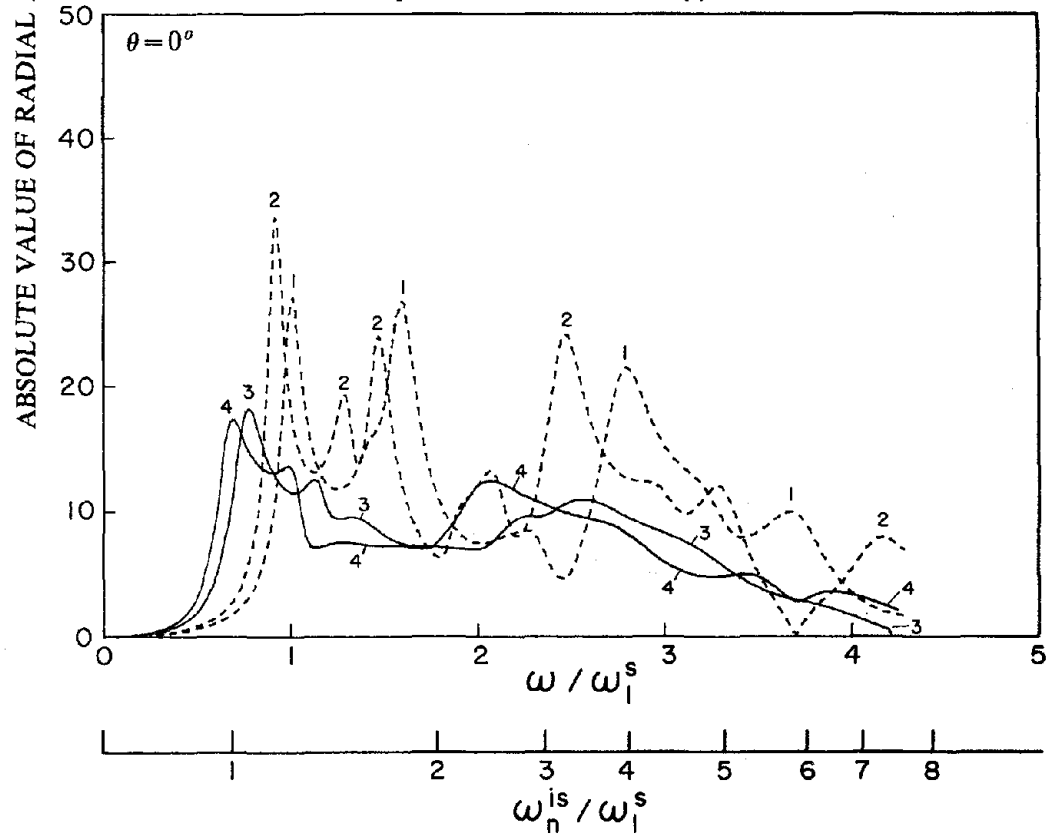
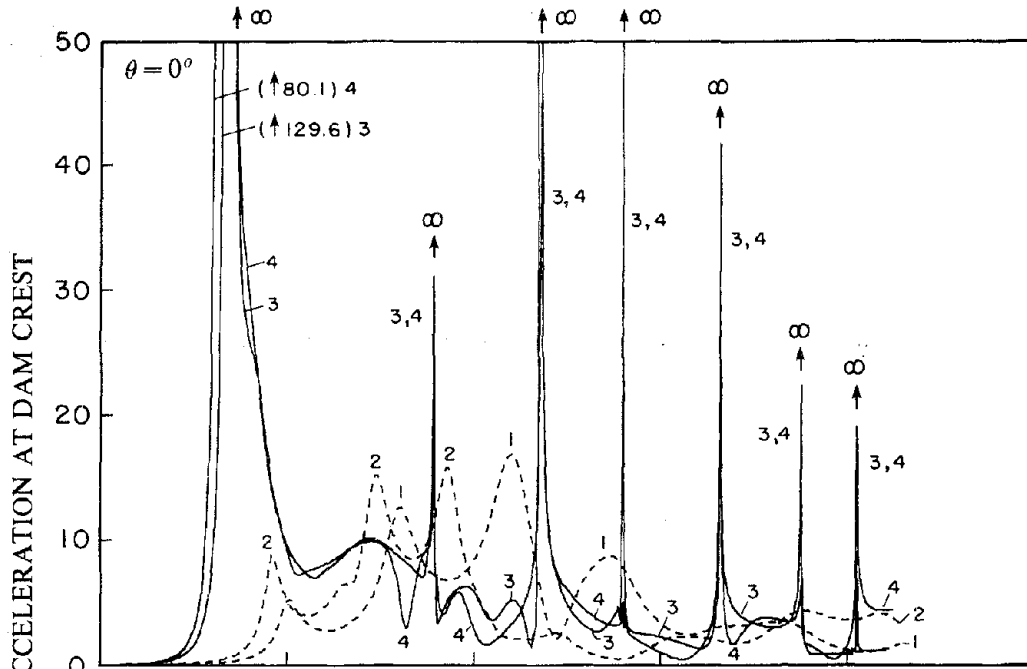


Figure 4.14 Response of dams to harmonic upstream ground motion for four conditions: dam on rigid foundation rock with no water (Case 1 of Table 4.1); dam on flexible foundation rock with no water (Case 12); dam on rigid foundation rock with full reservoir (Cases 2 and 4); and dam on flexible foundation rock with full reservoir (Cases 14 and 16).

Rigid Reservoir Boundary, $\alpha = 1.0$



Absorptive Reservoir Boundary, $\alpha = 0.5$

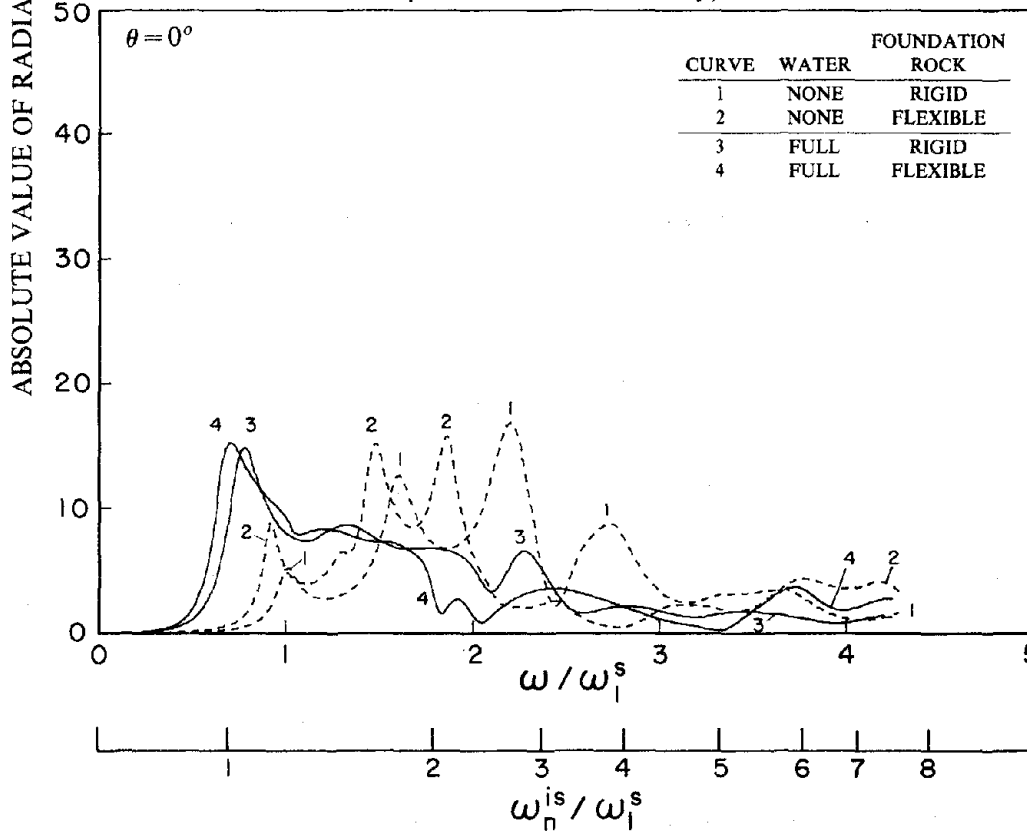
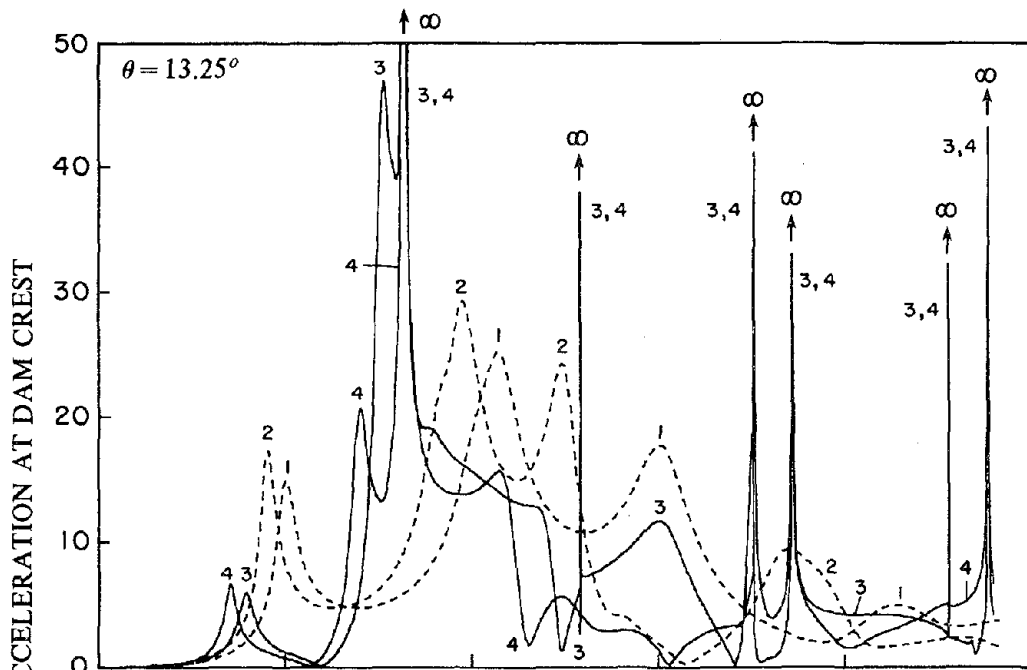


Figure 4.15 Response of dams to harmonic vertical ground motion for four conditions: dam on rigid foundation rock with no water (Case 1 of Table 4.1); dam on flexible foundation rock with no water (Case 12); dam on rigid foundation rock with full reservoir (Cases 2 and 4); and dam on flexible foundation rock with full reservoir (Cases 14 and 16).

Rigid Reservoir Boundary, $\alpha = 1.0$



Absorptive Reservoir Boundary, $\alpha = 0.5$

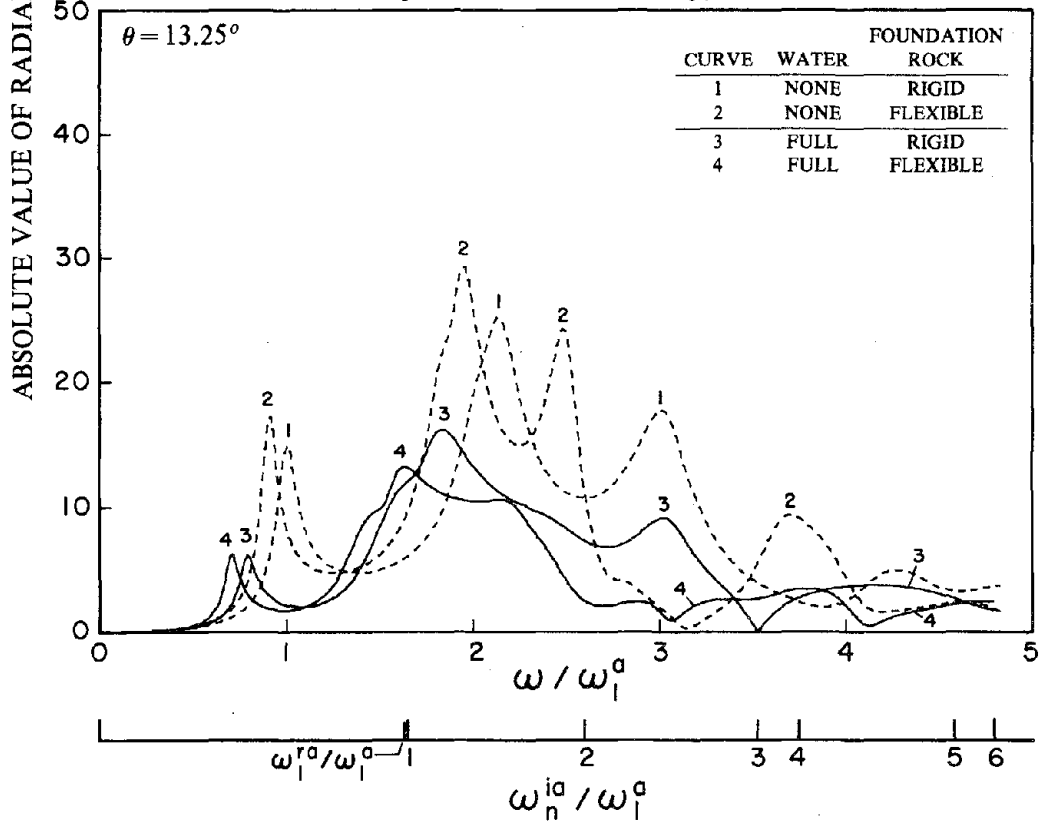


Figure 4.16 Response of dams to harmonic cross-stream ground motion for four conditions: dam on rigid foundation rock with no water (Case 1 of Table 4.1); dam on flexible foundation rock with no water (Case 12); dam on rigid foundation rock with full reservoir (Cases 2 and 4); and dam on flexible foundation rock with full reservoir (Cases 14 and 16).

16). The effects of dam-water interaction on the dam response to any of the three ground motion components are qualitatively similar for rigid rock (Section 4.4) and flexible foundation rock, whether the reservoir boundary is rigid [Figures 4.14(a), 4.15(a) and 4.16(a)] or absorptive [Figures 4.14(b), 4.15(b) and 4.16(b)]. It is apparent from Figures 4.14 - 4.16 that the fundamental natural or resonant frequency ω_1^\dagger of the dam alone (without water, supported on rigid foundation rock) is reduced to $\tilde{\omega}_r$ due to dam-water interaction, to $\tilde{\omega}_f^\dagger$ due to foundation flexibility, and to $\tilde{\omega}$ due to both effects simultaneously. The vibration periods corresponding to these frequencies are denoted as T_1 , \tilde{T}_r , \tilde{T}_f and \tilde{T} , respectively. To examine how the increase in period due to dam-water interaction is affected by foundation rock flexibility, the ratio \tilde{T}/\tilde{T}_f is plotted in Figure 4.17(a) against normalized water depth H/H_s where H_s is the dam height. Results are presented for the resonant period of the fundamental symmetrical and antisymmetrical modes of vibration for four values of E_f/E_s , with a rigid reservoir boundary ($\alpha = 1$). It is apparent that the E_f/E_s value has relatively small influence on the period ratio, especially if the reservoir is close to full. The data of Figure 4.17(a) is replotted in Figure 4.17(b) where the period ratio \tilde{T}/\tilde{T}_f is plotted against the E_f/E_s ratio for different values of H/H_s . For a fixed H/H_s , this plot would have been a horizontal line if the increase in period due to dam-water interaction was completely independent of foundation flexibility. It is apparent that the effects of foundation flexibility on the period ratio are small. This observation was made earlier for gravity dams, suggesting the following equation [19]:

$$\frac{\tilde{\omega}}{\omega_1} \approx \frac{\tilde{\omega}_r}{\omega_1} \frac{\tilde{\omega}_f}{\omega_1}$$

This approximate relationship is valid for arch dams with rigid reservoir boundary (Figure 4.17) as well as absorptive reservoir boundary (Figure not presented here).

The trends in the amplitude of the fundamental resonant peak depend on the modification of the effective damping ratio and effective modal earthquake force due to foundation rock flexibility and dam-water interaction, on the contribution of damping from reservoir boundary absorption, and

† In equation (3.1) the symbol ω_j was used for vibration frequency of the dam, whether the foundation rock is rigid or flexible. However, different symbols ω_1 and $\tilde{\omega}_f$ are used for the fundamental frequency to emphasize the effects of foundation-rock flexibility on this frequency.

on the added hydrodynamic forces. The effects of the various damping changes in the response of the dam to upstream ground motion can be identified in Figure 4.14. When the reservoir boundary is rigid [Figure 4.14(a)], dam-water interaction reduces the effective damping as a result of the double resonant peak and increases the added force at the fundamental resonant frequency, resulting in increased fundamental resonant response whether the foundation rock is rigid or flexible. This decrease in the effective damping and the added hydrodynamic force dominate the corresponding effects of foundation flexibility and therefore have about the same influence on the dam response whether the foundation rock is rigid or flexible. When the effects of reservoir boundary absorption are included [Figure 4.14(b)], the opposite trend occurs: dam-water interaction increases the effective damping at the fundamental resonant frequency resulting in reduced resonant response whether the foundation rock is rigid or flexible. This increase in effective damping dominates the total damping resulting in approximately the same resonant amplitude irrespective of the foundation rock condition.

The amplitude of the fundamental resonant peak due to vertical ground motion (Figure 4.15) is mainly affected by the added hydrodynamic force, and less by the previously discussed trends in damping. When the reservoir boundary is rigid [Figure 4.15(a)], dam-water interaction increases the added force and reduces the effective damping ratio at the fundamental resonant frequency, leading to increased resonant response and a double resonant peak, of which one peak is unbounded, whether foundation rock is rigid or flexible. When the reservoir boundary is absorptive [Figure 4.15(b)], dam-water interaction still increases the fundamental resonant response because of the large added force for vertical ground motion, whether the foundation rock is flexible or rigid. However, the increase in resonant response is less pronounced for flexible foundation rock than for rigid foundation rock (compare the change from curve 2 to 4 with the change from curve 1 to 3), because the significance of the added hydrodynamic force relative to the inertia force of the dam is less for flexible compared to rigid foundation rock, resulting in approximately the same resonant amplitude irrespective of the foundation rock condition.

The amplitude of the fundamental resonant peak due to cross-stream ground motion (Figure 4.16) is also mainly affected by the "added" hydrodynamic force, and less by the previously discussed

trends in damping. In this case the total earthquake force decreases at the fundamental resonant frequency because the hydrodynamic force is of opposite-phase relative to the inertia force of the dam. When the reservoir boundary is rigid [Figure 4.16(a)], dam-water interaction reduces the earthquake force at the fundamental resonant frequency, leading to reduced resonant peak whether the foundation rock is rigid or flexible, because the reduction in force dominates the effects of foundation flexibility. However, the unbounded hydrodynamic force dominates the dam response at excitation frequencies near ω_n^{ia} , leading to increased response, and a double resonant peak near ω_1^{ia} , of which one peak is unbounded, whether the foundation rock is rigid or flexible. When the reservoir boundary is absorptive [Figure 4.16(b)], the fundamental resonant peak is essentially unaffected but the higher resonant peaks, those associated with ω_n^{ia} , are reduced to bounded values.

The effects of reservoir boundary absorption on the response of the dam, supported on flexible foundation rock, due to the three components of ground motion, are shown in Figure 4.18. The response of systems with moduli ratio $E_f/E_s = 1$ is presented for four values of the wave reflection coefficient: $\alpha = 1.0$ (rigid reservoir boundary), 0.75, 0.5, and 0 (Cases 14, 15, 16 and 17 in Table 4.1). Comparison of Figure 4.18 with Figure 4.6, which shows the corresponding results for rigid foundation rock, indicates that the effects of reservoir boundary absorption on dam response are about the same whether the foundation rock is rigid or flexible.

4.6.2 Influence of Moduli Ratio E_f/E_s

The response of the dam with full reservoir and rigid or absorptive reservoir boundary to upstream, vertical, and cross-stream ground motions is presented in Figures 4.19 - 4.21 for four values of $E_f/E_s = \infty, 2, 1$ and $1/4$. The response results for the rigid reservoir boundary, presented in Figures 4.19(a) - 4.21(a), were obtained by analyzing Cases 2, 14, 18 and 20 of Table 4.1; and those for absorptive reservoir boundary, presented in Figures 4.19(b) - 4.21(b), were obtained by analyzing Cases 4, 16, 19 and 21 of Table 4.1.

As E_f/E_s decreases, which for a fixed E_s means an increasingly flexible foundation rock, the fundamental resonant frequency decreases, irrespective of whether the reservoir boundary is rigid or absorptive; the dam response to upstream ground motion at this frequency increases slightly if the

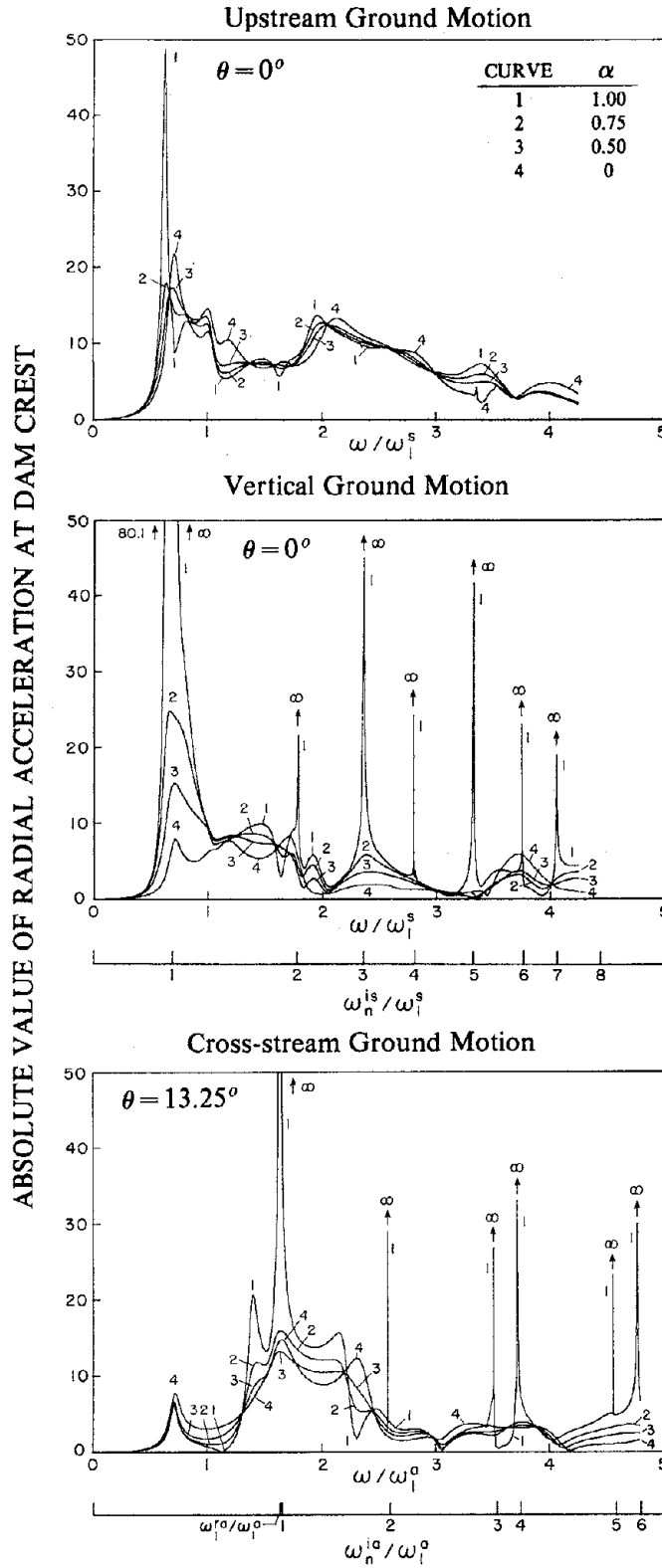
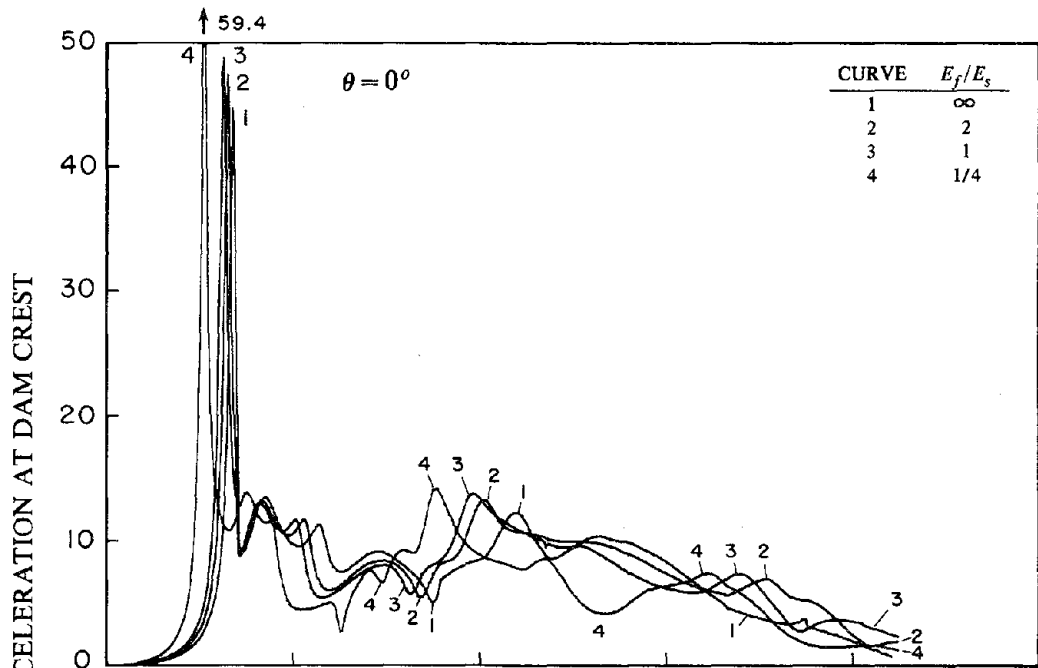


Figure 4.18 Influence of wave reflection coefficient α on response of dams on flexible foundation rock with full reservoir to harmonic ground motion (Cases 14, 15, 16 and 17 of Table 4.1).

Rigid Reservoir Boundary, $\alpha = 1.0$



Absorptive Reservoir Boundary, $\alpha = 0.5$

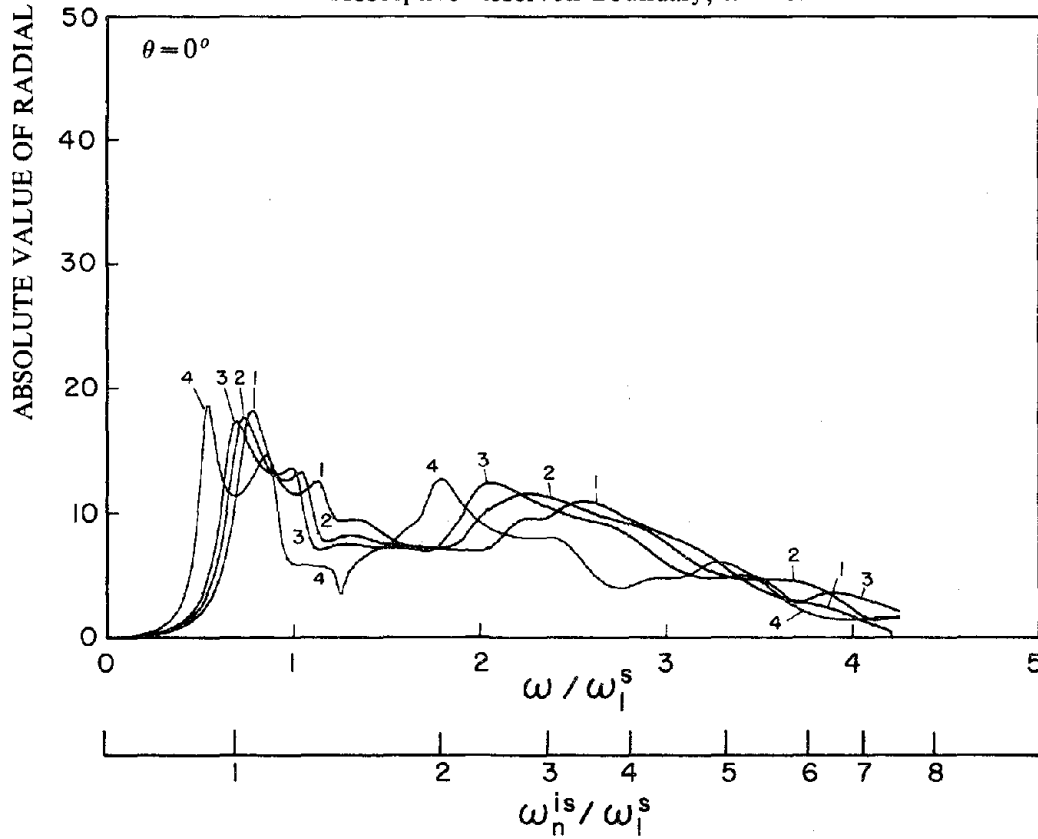
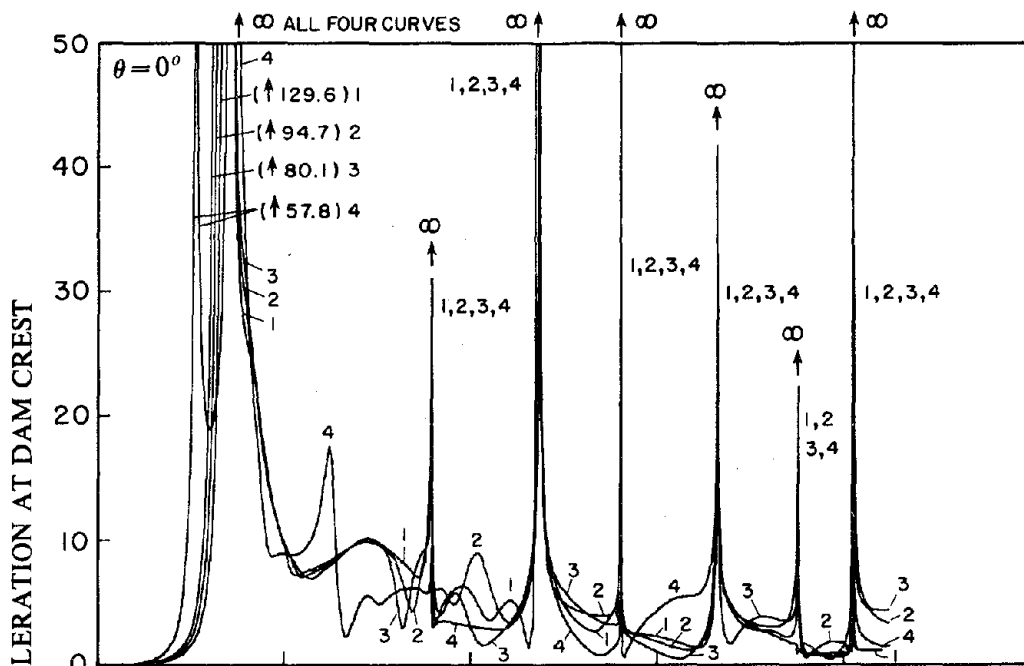


Figure 4.19 Influence of moduli ratio E_f/E_s on response of dams with full reservoir to harmonic upstream ground motion. Results presented for rigid reservoir boundary (Cases 2, 14, 18 and 20 of Table 4.1), and absorptive reservoir boundary (Cases 4, 16, 19 and 21).

Rigid Reservoir Boundary, $\alpha = 1.0$



Absorptive Reservoir Boundary, $\alpha = 0.5$

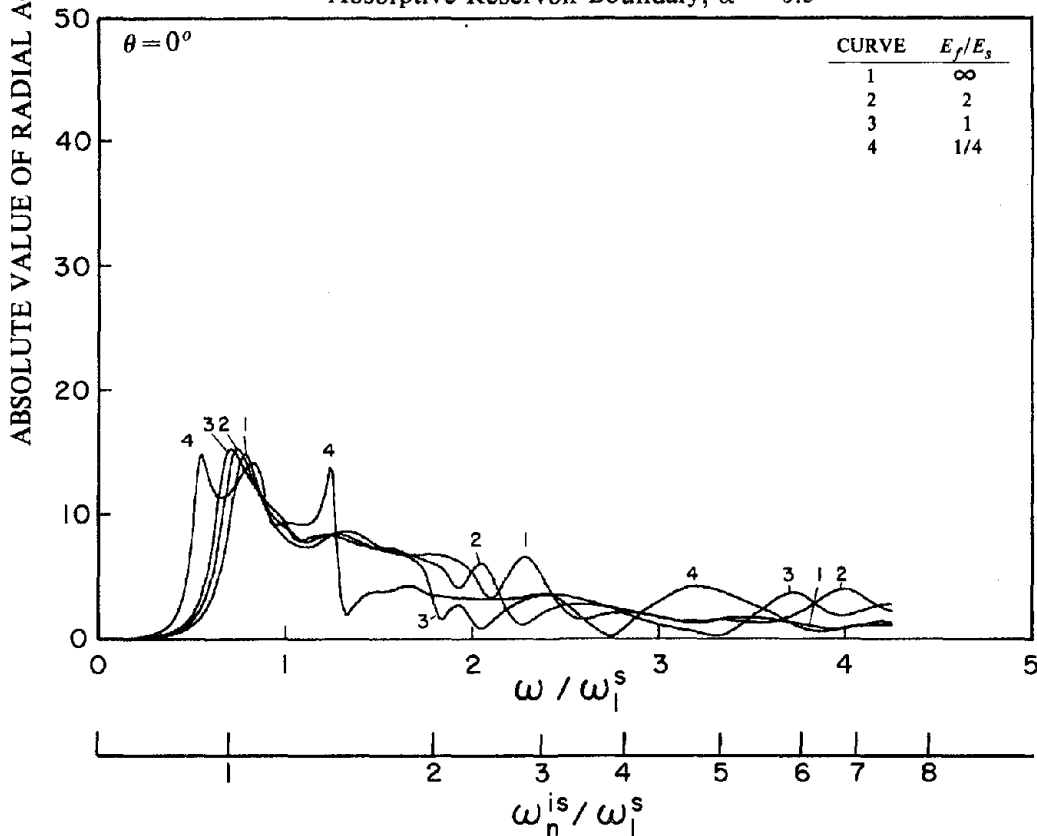
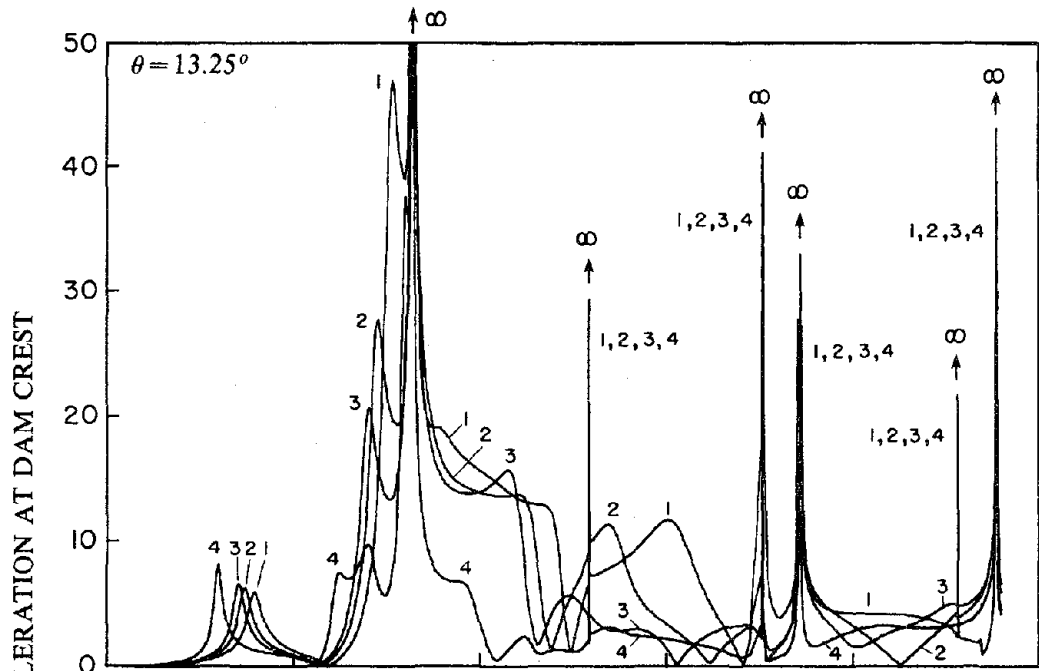


Figure 4.20 Influence of moduli ratio E_f/E_s on response of dams with full reservoir to harmonic vertical ground motion. Results presented for rigid reservoir boundary (Cases 2, 14, 18 and 20 of Table 4.1), and absorptive reservoir boundary (Cases 4, 16, 19 and 21).

Rigid Reservoir Boundary, $\alpha = 1.0$



Absorptive Reservoir Boundary, $\alpha = 0.5$

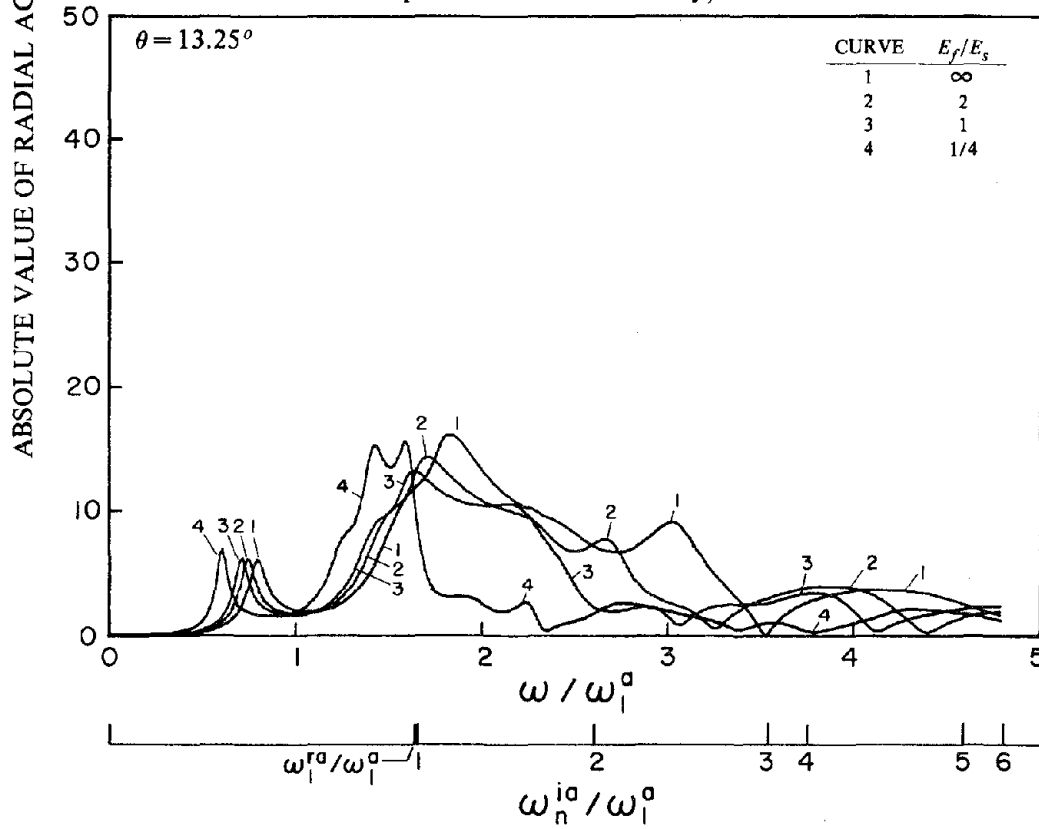


Figure 4.21 Influence of moduli ratio E_f/E_s on response of dams with full reservoir to harmonic cross-stream ground motion. Results presented for rigid reservoir boundary (Cases 2, 14, 18 and 20 of Table 4.1), and absorptive reservoir boundary (Cases 4, 16, 19 and 21).

reservoir boundary is rigid [Figure 4.19(a)] and stays about the same if the reservoir boundary is absorptive [Figure 4.19(b)]; the dam response to vertical ground motion at this frequency decreases if the reservoir boundary is rigid [Figure 4.20(a)] and stays about the same if the reservoir boundary is absorptive [Figure 4.20(b)]; and the dam response to cross-stream ground motion at this frequency increases slightly irrespective of whether the reservoir boundary is rigid [Figure 4.21(a)] or absorptive [Figure 4.21(b)].

As the moduli ratio E_f/E_s decreases, the higher resonant peaks due to upstream ground motion usually increase, especially if the reservoir boundary is rigid (Figure 4.19). The response to vertical ground motion, is dominated by the unbounded peaks at frequencies ω_n^{is} irrespective of the E_f/E_s value if the reservoir boundary is rigid; but the resonant peaks are affected little by the foundation flexibility if the reservoir boundary is absorptive. The response to cross-stream ground motion is dominated by the unbounded peaks at frequencies ω_n^{ia} irrespective of the E_f/E_s value if the reservoir boundary is rigid; but the resonant peaks are affected little by the E_f/E_s value if the reservoir boundary is absorptive.

5. EARTHQUAKE RESPONSE OF MORROW POINT DAM

5.1 Introduction

Presented in this chapter is the response of a selected arch dam to Taft ground motion. Response results, computed by the analytical procedure presented in Chapter 3, are presented for a wide range of the important parameters characterizing the properties of the dam, foundation rock, impounded water and reservoir boundary materials. Based on these response results, the effects of dam-water interaction, reservoir boundary absorption, and foundation-rock flexibility on the earthquake induced displacements and stresses in the dam, and the relative significance of the response to the three components of ground motion, are investigated.

5.2 System and Ground Motion

5.2.1 Dam-Water-Foundation Rock System

The dam selected for this investigation is Morrow Point Dam, the same as in Chapter 4 for the study based on frequency response functions. The finite element idealizations selected for the dam and foundation-rock region, the special finite-element cum continuum idealization for the impounded water, and the properties of the dam-water-foundation rock system are the same as described in Section 2.6. As in the frequency response function study presented in Chapter 4, the wave reflection coefficient α is varied over a wide range in this study; the values considered are: $\alpha = 1.0$ (rigid reservoir boundary), 0.50 and 0.

5.2.2 Ground Motion

The ground motion recorded at Taft Lincoln School Tunnel during the Kern County, California, earthquake of 21 July 1952 is selected as the free-field ground acceleration for the analysis of Morrow Point Dam. The ground motion acting in the upstream (x), vertical (y), and cross-stream (z) directions is defined as the S69E, vertical, and S21W components of the recorded ground motion, respectively. These three components of ground motion and their maximum accelerations are shown in

Figure 5.1.

5.3 Response Results

The response of Morrow Point Dam was analyzed for the eight sets of assumptions and conditions listed in Table 5.1 for the dam, foundation rock, impounded water and reservoir boundary materials, with the objective of studying the effects of dam-water interaction, reservoir boundary absorption, and foundation-rock flexibility on the earthquake responses. For each of these eight cases, the response of the dam was computed for four excitations: upstream ground motion, only; vertical ground motion, only; cross-stream ground motion, only; and all three ground motion components, simultaneously, of Taft ground motion.

The earthquake response of the dam was computed under the assumption of linear behavior of the dam-water-foundation rock system, using the analytical procedure developed in Chapter 3, where the displacement history was obtained by Fourier synthesis of the complex-valued frequency response functions for the generalized coordinates. These response functions were computed for the excitation frequency range 0 to approximately 20 Hz, which had been tested to be adequate for the recorded Taft ground motion. To accurately represent the response of the dam in this frequency range, the first 12 generalized coordinates were included in the analyses for Cases 1 to 4 with rigid foundation rock, and the first 18 generalized coordinates were included in the analyses for Cases 5 to 8 with flexible foundation rock.

The fundamental resonant period and effective damping ratio at that period, determined by the half-power bandwidth method from the frequency response function for crest acceleration due to each of the three ground motion components, are presented in Table 5.1. Strictly speaking, the half-power bandwidth method does not apply to dams because dam-water interaction introduces frequency-dependent added mass, damping and force. However, the method is employed here to obtain a rough measure of damping to assist in the interpretation of response results. As seen in Table 5.1, the fundamental resonant period obtained from the responses to upstream (x) or vertical (y) ground motions is the same; it is the period of the fundamental, symmetric mode of vibration, modified by the added

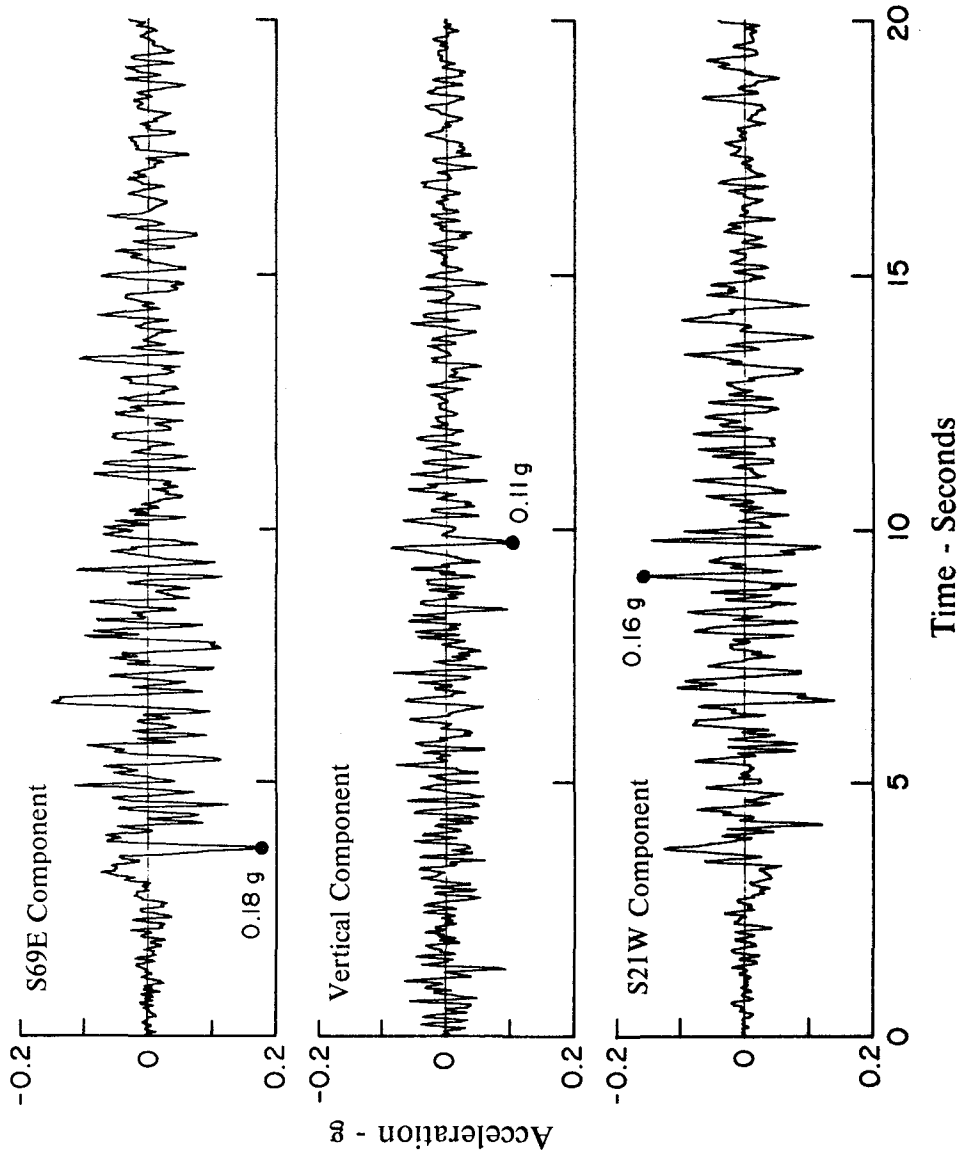


Figure 5.1 Ground motion at Taft Lincoln School Tunnel, Kern County, California, Earthquake, 21 July 1952.

Table 5.1 -- Cases of Morrow Point Dam Analyzed, Fundamental Resonant Periods of Vibration, Damping Ratios, and Response Spectrum Ordinates for the Three Components of Taft Ground Motion

Case	Foundation	Water	α	Fundamental Mode Properties											
				Upstream Ground Motion				Vertical Ground Motion				Cross-stream Ground Motion			
				Resonant Period (sec)	Damping Ratio ξ_1^u (%)	$S_a(T, \xi_1^u)$ (g)	Resonant Period (sec)	Damping Ratio ξ_1^v (%)	$S_a(T, \xi_1^v)$ (g)	Resonant Period (sec)	Damping Ratio ξ_1^c (%)	$S_a(T, \xi_1^c)$ (g)	Resonant Period (sec)	Damping Ratio ξ_1^s (%)	$S_a(T, \xi_1^s)$ (g)
1	Rigid	None	-	0.235	5.0	0.43	0.235	5.0	0.30	0.264	5.0	0.37			
2	Rigid	Full	1.0	0.347	2.2	0.60	0.347	3.7	0.41	0.336	4.9	0.50			
3	Rigid	Full	0.5	0.302	13.4	0.30	0.302	11.8	0.21	0.331	5.7	0.44			
4	Rigid	Full	0	0.301	7.9	0.35	0.301	8.5	0.21	0.330	6.7	0.39			
5	Flexible	None	-	0.256	4.6	0.37	0.256	4.6	0.24	0.292	4.4	0.33			
6	Flexible	Full	1.0	0.376	2.6	0.47	0.376	3.0	0.31	0.375	4.1	0.49			
7	Flexible	Full	0.5	0.338	19.2	0.25	0.338	19.4	0.18	0.373	5.0	0.47			
8	Flexible	Full	0	0.331	8.5	0.34	0.331	9.1	0.28	0.369	6.4	0.45			

mass from dam-water interaction and the flexibility of the foundation rock. The frequency-dependent hydrodynamic load which is not the same for the two ground motions slightly influences the resonant period in some cases. The damping ratios ξ_1^x and ξ_1^y corresponding to the upstream and vertical ground motions have the same value if the reservoir is empty, as it represents the damping property of the dam-foundation system in its fundamental, symmetric mode of vibration, which is the same for upstream and vertical ground motions. However, the damping values ξ_1^x and ξ_1^y obtained from the two response functions are slightly different if the reservoir is not empty (Table 5.1), because they are affected more by the fact that the frequency-dependent added hydrodynamic load is not the same for the two ground motions. The fundamental resonant period and damping ratio ξ_1^z , obtained from the response to cross-stream ground motion, are the period and damping ratio of the fundamental, antisymmetric mode of vibration, modified by dam-water interaction and foundation flexibility. For each of the eight cases, the pseudo-acceleration corresponding to the vibration period and damping ratio, determined from the response to each ground motion component, is obtained from the response spectrum for that particular ground motion and is listed in Table 5.1.

The response results selected to illustrate the different effects in this study consist of displacement time histories and contours of maximum stresses. The radial component of the displacement at the dam crest nodal point defined by $\theta = 13.25^\circ$ [nodal point 54 in Figure 2.3(a)], where θ is an angle measured from the x-y plane along the dam crest arch, is presented in Figures 5.2, 5.10, 5.17, 5.18, 5.27, and 5.28. The distributions of envelope values of the maximum tensile stresses in the arch and cantilever directions are presented for both the upstream and downstream dam faces in Figures 5.3 to 5.8, 5.11 to 5.16, 5.19 to 5.26 and 5.29 to 5.36. Except for the maximum tensile stresses due to the three components of Taft ground motion acting simultaneously, the envelope values of maximum tensile stresses are shown in these figures for the right half of the dam when looking from the downstream side in the upstream direction. The maximum radial displacement at the dam crest nodal point 54 ($\theta = 13.25^\circ$) [Figure 2.3(a)], and maximum tensile values of arch and cantilever stresses over the upstream and downstream faces, are summarized in Table 5.2 for the dam supported on rigid foundation rock (Cases 1 to 4), and in Table 5.3 for the dam supported on flexible foundation rock

Table 5.2 -- Summary of Responses* of Morrow Point Dam,
on Rigid Foundation Rock, to Taft Ground Motion

Case	Water	α	Maximum Radial Crest Displacement (inches)	Maximum Tensile Stress (psi)			
				Upstream Face		Downstream Face	
				Arch Stress	Cantilever Stress	Arch Stress	Cantilever Stress
(a) Response to Upstream (S69E Component of Taft) Ground Motion							
1	None	-	0.38	268	101	247	62
2	Full	1.0	0.81	735	268	641	189
3	Full	0.5	0.63	525	165	443	118
4	Full	0	0.64	517	154	431	106
(b) Response to Vertical Component of Taft Ground Motion							
1	None	-	0.068	57	48	43	41
2	Full	1.0	1.98	1572	571	1412	361
3	Full	0.5	0.33	263	130	229	59
4	Full	0	0.14	113	60	86	43
(c) Response to Cross-stream (S21W Component of Taft) Ground Motion							
1	None	-	0.37	177	104	194	88
2	Full	1.0	0.68	410	313	382	212
3	Full	0.5	0.38	200	106	201	93
4	Full	0	0.45	245	120	227	105
(d) Response to Upstream, Vertical, and Cross-stream Components, Simultaneously, of Ground Motion							
1	None	-	0.50	325	116	275	123
2	Full	1.0	2.45	1976	712	1751	521
3	Full	0.5	0.67	556	193	480	163
4	Full	0	0.73	540	184	474	163

* Effects of static loads are excluded.

(Cases 5 to 8).

A point worth mentioning here concerns the stress contour presentation in this chapter. Because the Morrow Point Dam system is assumed to be symmetric about the x-y plane (Figure 2.3), the displacement and stress responses due to the upstream (x) or vertical (y) ground motions are symmetric about the x-y plane, while the responses due to the cross-stream (z) ground motion are antisymmetric about this plane. As a result, the envelope of maximum tensile stresses on both faces of the dam due to upstream or vertical ground motion are symmetric about this plane. However, the maximum tensile stresses due to cross-stream ground motion are not symmetric about this plane, because the maximum tensile stresses on one-half of the dam are actually the minimum tensile stresses or maximum compressive stresses on the other half. However, the maximum tensile stress distribution was determined to be approximately the same for the two halves of the selected dam subjected to the selected ground motion. Because of this approximate symmetry and in order to simplify the presentation, the maximum stresses due to cross-stream ground motion are also shown for only one-half of the dam, as it is for upstream and vertical ground motions. However, the maximum tensile stresses due to the three components of Taft ground motion acting simultaneously, which are not symmetric about the x-y plane, are shown for the whole dam.

In a practical earthquake analysis of a dam, the displacements and stresses due to static loads (weight of the dam and hydrostatic pressure) would be included in the total responses. However, the static effects are not included in most of the results presented here because they complicate the interpretation of the effects of dam-water interaction, reservoir boundary absorption, and foundation-rock flexibility on the dynamic response of the dam. However, an example of a practical earthquake analysis, including the effects of the static loads, is presented towards the end of this chapter.

5.4 Dam-Water Interaction Effects

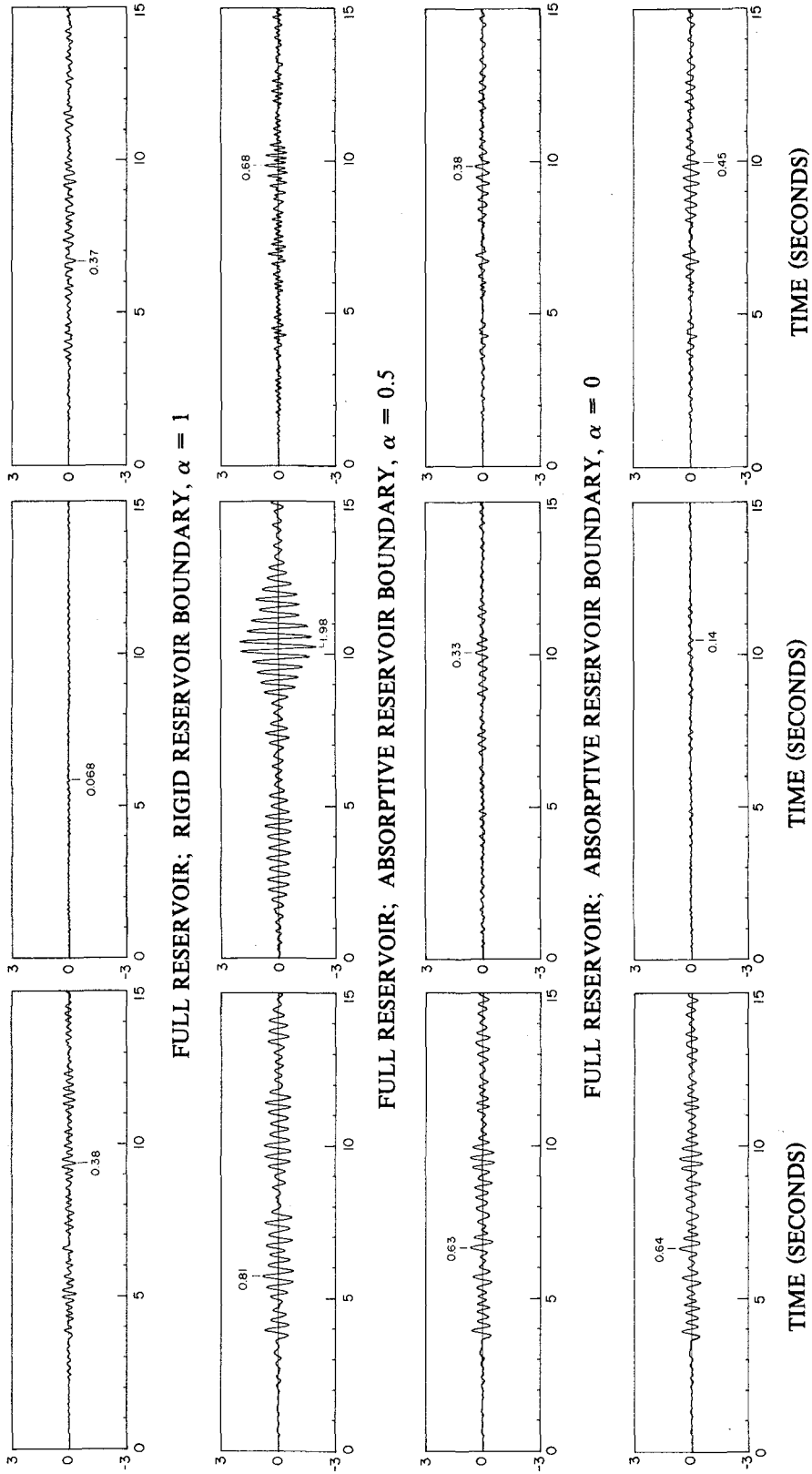
5.4.1 Hydrodynamic Effects

Hydrodynamic effects on the earthquake responses of dams can be visualized as arising partly from the change in the complex-valued frequency response functions of the dam (Chapter 4) and,

CROSS-STREAM COMPONENT

VERTICAL COMPONENT

UPSTREAM COMPONENT



RADIAL DISPLACEMENT AT DAM CREST, $\theta = 13.25^\circ$ (INCHES)

Figure 5.2 Displacement response of Morrow Point Dam on rigid foundation rock due to upstream, vertical and cross-stream components, separately, of Taft ground motion.

partly from the change in the response spectrum ordinates corresponding to the resonant peaks, especially the fundamental resonant peak, corresponding to the change in the resonant period and damping. These changes are due to the frequency-dependent hydrodynamic terms that result from dam-water interaction with compressible water. The hydrodynamic terms can be interpreted as an added mass, an added damping (both are different for symmetric and antisymmetric ground motions), and an added force (different for the three components of ground motion).

The displacement history of Morrow Point Dam supported on rigid foundation rock with an empty reservoir is shown in Figure 5.2(a), and that with a full reservoir and rigid reservoir boundary is shown in Figure 5.2(b), for the three components of ground motion. The maximum crest displacement due to upstream ground motion increases from 0.38 in. to 0.81 in. [Table 5.2(a)] due to hydrodynamic effects because of the increase in fundamental resonant peak of the frequency response function [Figure 4.4(a)], and because the fundamental period lengthens from 0.235 sec. to 0.347 sec. (Table 5.1), the damping ratio decreases resulting in the pseudo-acceleration $S_a(T, \xi_i^d)$ increasing from 0.43g to 0.60g. The increase in the fundamental period can also be observed from the displacement histories [compare the responses to upstream ground motion in Figures 5.2(a) and 5.2(b)]. The effects of dam-water interaction with rigid reservoir boundary on the maximum arch and cantilever stresses can be seen by comparison of Figures 5.3(a) with 5.3(b) and 5.4(a) with 5.4(b). The maximum arch stress increases from 268 psi to 735 psi on the upstream face, and from 247 psi to 641 psi on the downstream face; the maximum cantilever stress increases from 101 psi to 268 psi on the upstream face, and from 62 psi to 189 psi on the downstream face [Table 5.2(a)]. The area enclosed by a particular stress contour increases, indicating that tensile stresses exceed the value corresponding to that contour over a larger portion of the dam face because of hydrodynamic effects. The distribution pattern for the arch stress does not change substantially. Dam-water interaction especially increases the cantilever stresses at the base of the dam and along the abutment, with these areas becoming the most-stressed areas instead of the upper, central portion of the dam.

If the reservoir boundary is rigid, the added hydrodynamic force for vertical ground motion at the fundamental resonant period is especially large compared to the small effective earthquake force

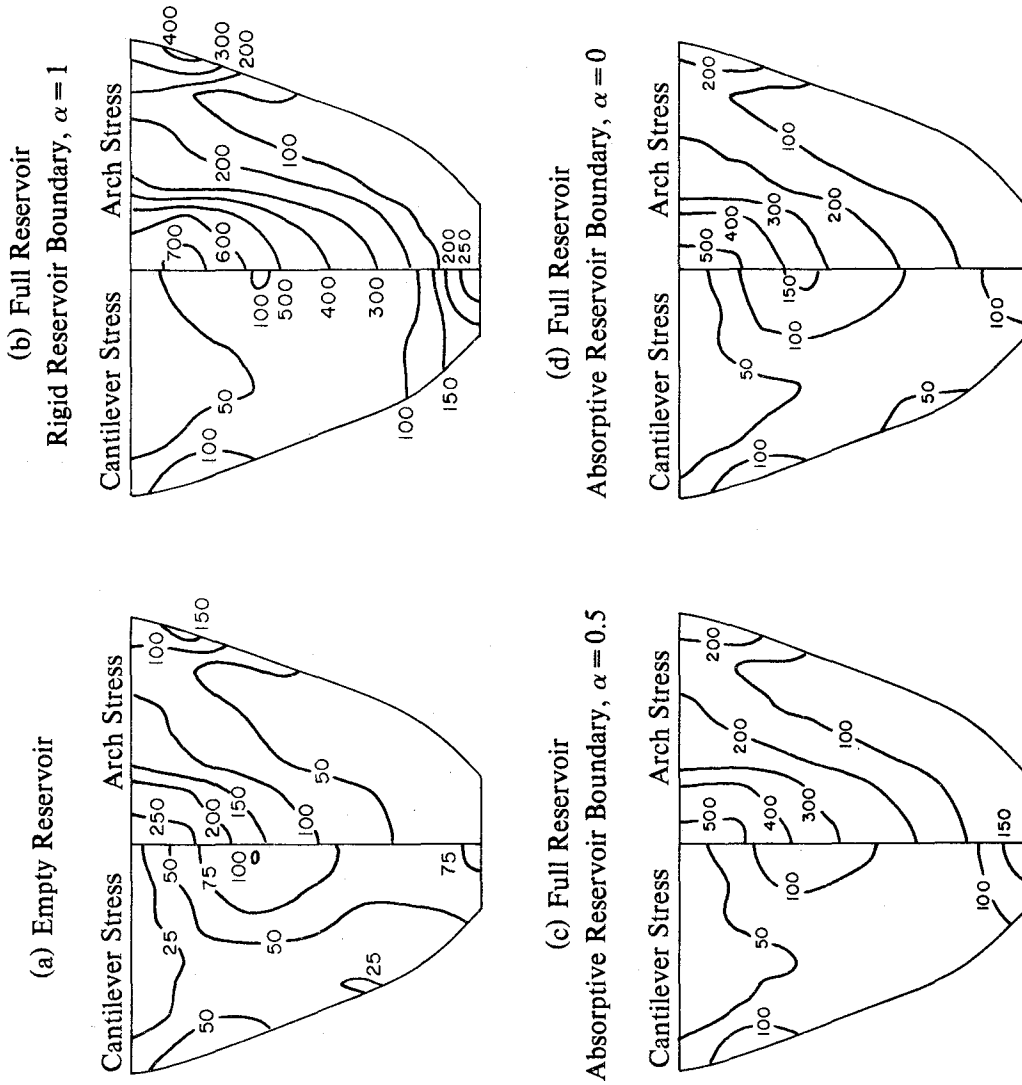


Figure 5.3 Envelope values of maximum tensile stresses (in psi) on upstream face of Morrow Point Dam on rigid foundation rock due to upstream component, only, of Taft ground motion. Initial static stresses are excluded.

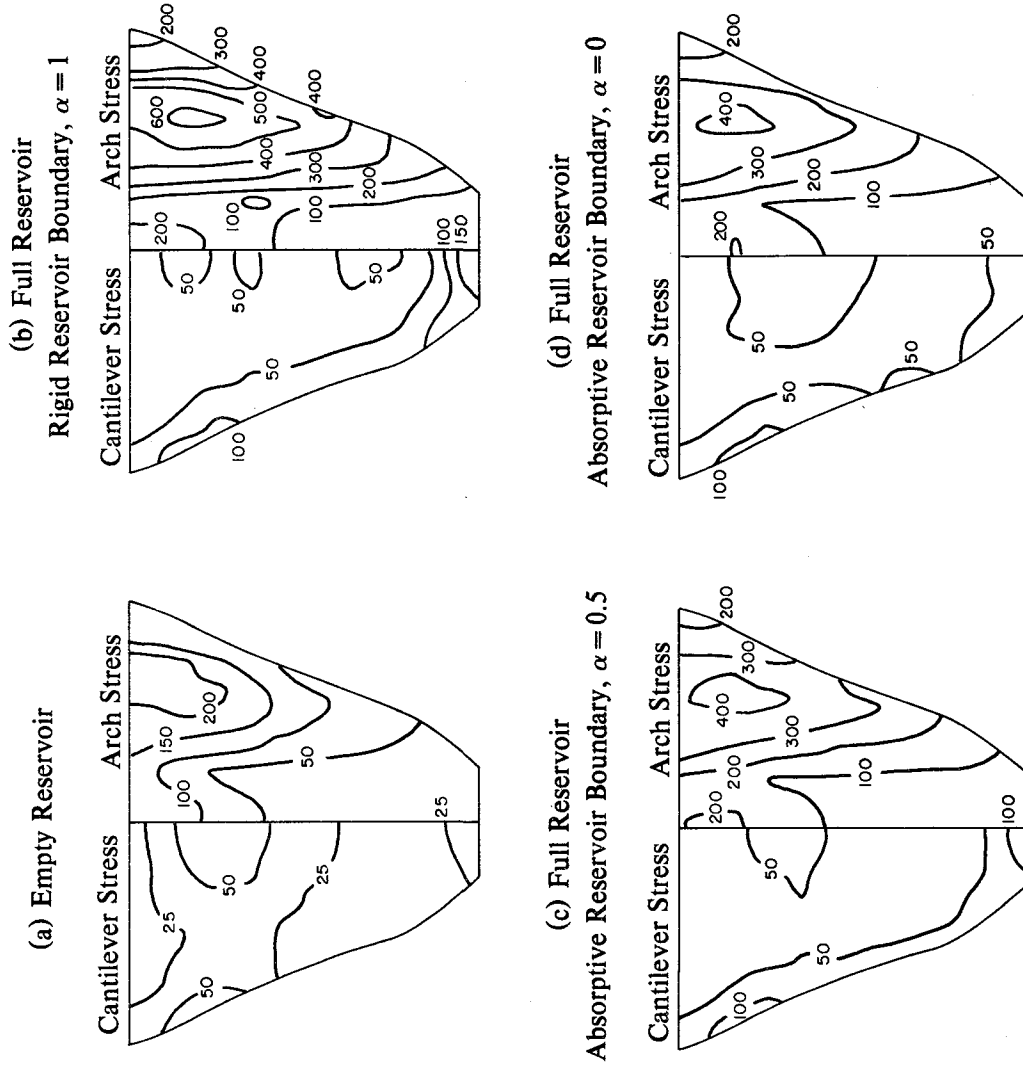


Figure 5.4 Envelope values of maximum tensile stresses (in psi) on downstream face of Morrow Point Dam on rigid foundation rock due to upstream component, only, of Taft ground motion. Initial static stresses are excluded.

associated with the mass of the dam, and it is unbounded at the natural frequencies ω_n^{is} of the infinite uniform channel of the reservoir. Therefore, the frequency response function has a greatly amplified fundamental resonant peak and unbounded peaks at ω_n^{is} due to hydrodynamic effects (Chapter 4). Consequently, the response of the dam increases greatly because of dam-water interaction when the reservoir boundary is rigid, with the maximum displacement increasing from 0.068 in. to 1.98 in., the maximum arch stress from 57 psi to 1572 psi on the upstream face, and from 43 psi to 1412 psi on the downstream face; the maximum cantilever stress from 48 psi to 571 psi on the upstream face, and from 41 psi to 361 psi on the downstream face [Table 5.2(b)]. Only a very small part of these large increases in responses is due to the increase in pseudo-acceleration ordinate associated with lengthening of the vibration period and reduction in effective damping due to dam-water interaction. The general distribution pattern of the maximum arch and cantilever stresses due to vertical ground motion is affected by dam-water interaction in a manner similar to the case of upstream ground motion [Figures 5.5(a) and 5.5(b), 5.6(a) and 5.6(b)].

In contrast to upstream and vertical ground motions, the amplitude of the fundamental resonant peak in the frequency response function for the dam subjected to cross-stream ground motion is reduced by dam-water interaction, because the "added" hydrodynamic force is of opposite-phase compared to the effective earthquake force associated with the mass of the dam (Chapter 4). However, the response of the dam to cross-stream ground motion increases due to dam-water interaction, in part, because the added hydrodynamic force is infinite at the natural frequencies ω_n^{ia} of the antisymmetric modes of infinite uniform channel of the reservoir, causing unbounded peaks in the frequency response function for the dam at these frequencies (Chapter 4). Moreover, comparing the displacement histories of Figures 5.2(a) and 5.2(b) due to cross-stream ground motion, it is apparent that dam-water interaction has the effect of increasing the relative significance of the contributions of the second mode to the response; because the second resonant frequency is quite close to ω_1^{ia} , the fundamental resonant frequency of the infinite uniform channel, resulting in dam-water interaction causing a large increase in the resonant peak in the frequency response function (Figure 4.6). In addition, dam-water interaction lengthens the fundamental period and the corresponding pseudo-acceleration

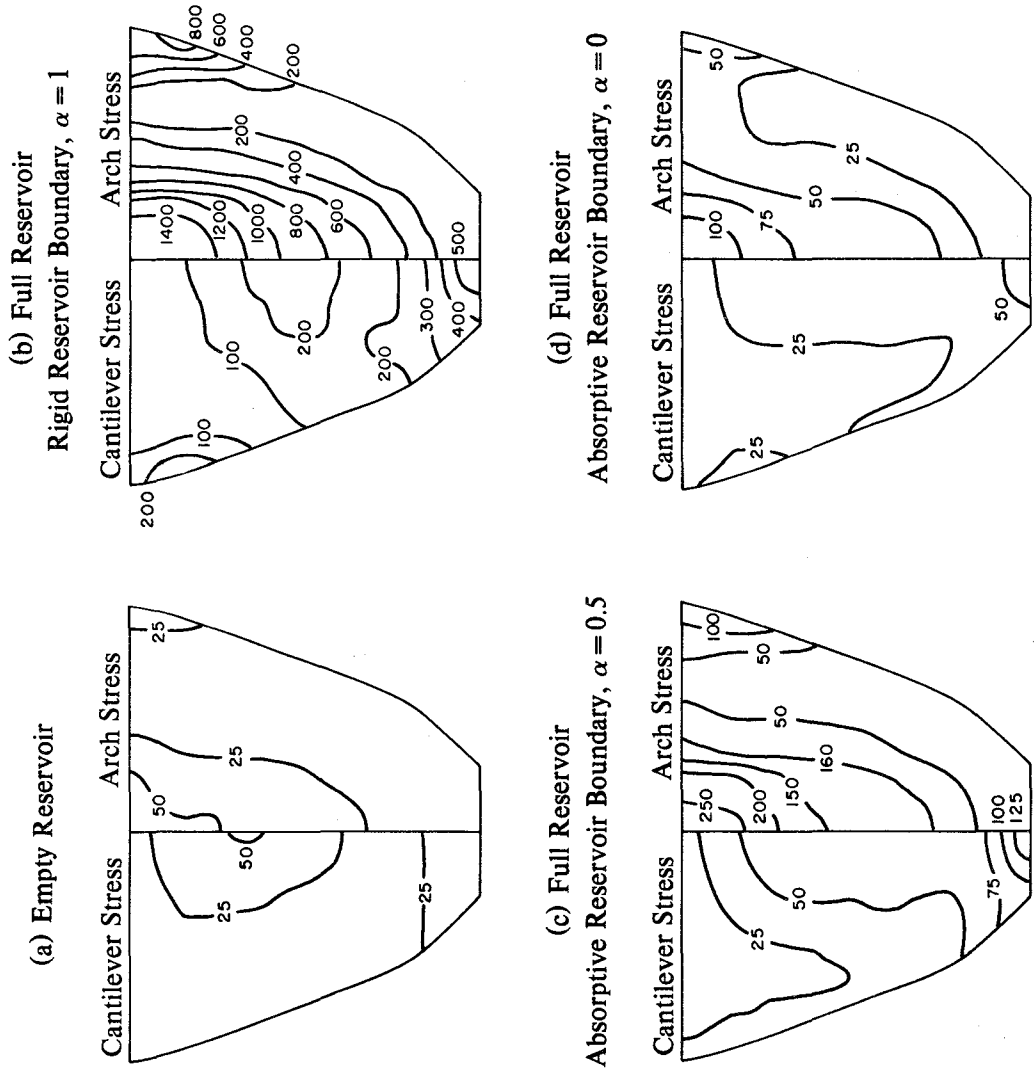


Figure 5.5 Envelope values of maximum tensile stresses (in psi) on upstream face of Morrow Point Dam on rigid foundation rock due to vertical component, only, of Taft ground motion. Initial static stresses are excluded.

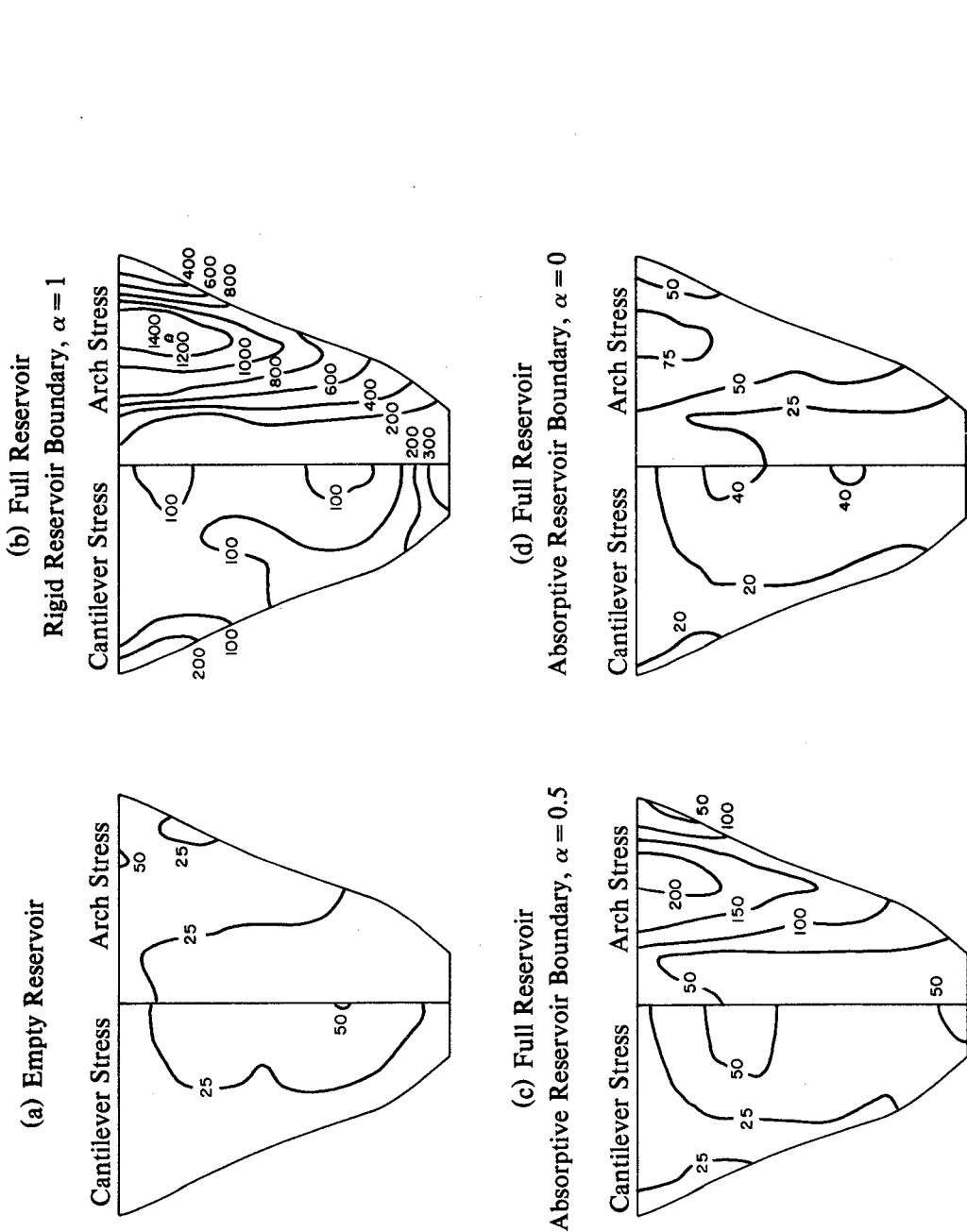


Figure 5.6 Envelope values of maximum tensile stresses (in psi) on downstream face of Morrow Point Dam on rigid foundation rock due to vertical component, only, of Taft ground motion. Initial static stresses are excluded.

$S_a(T, \xi_f^2)$ increases (Table 5.1). The response of the dam with full reservoir and rigid reservoir boundary due to cross-stream ground motion clearly shows the resulting increase in response, where the maximum radial crest displacement increases from 0.37 in. to 0.68 in. [Figure 5.2(a)-(b)]; the maximum arch stress increases from 177 psi to 410 psi on the upstream face [Figure 5.7(a)-(b)], and from 194 psi to 382 psi on the downstream face [Figure 5.8(a)-(b)]; and the maximum cantilever stress increases from 104 psi to 313 psi on the upstream face [Figure 5.7(a)-(b)], and from 88 psi to 212 psi on the downstream face [Figure 5.8(a)-(b)] [see also Table 5.2(c)]. Comparing these figures also shows how the pattern of stresses is affected by dam-water interaction. The locations of the larger arch stress at 1/4 span points from the abutments at or near the dam crest and along the abutment in the upper half of the dam when there is no impounded water shift lower toward the mid-height of the dam due to dam-water interaction. Similarly the locations of the larger cantilever stress along the abutments in the upper half of the dam with an empty reservoir are shifted to 1/4 span points from the abutments in the upper portion of the dam.

The arch action in the response of the dam to each of the three ground motion components is quite pronounced, whether the reservoir is full or empty, as illustrated by the much larger values of arch stresses compared to the cantilever stresses over both faces of the dam (Table 5.2). The only exception is in the relatively small response of the dam with an empty reservoir to vertical ground motion in which case the arch stresses are only slightly larger than the cantilever stresses. The relative significance of arch and cantilever actions varies, of course, with the geometry of the dam.

It is useful to examine how dam-water interaction affects the response of arch dams compared to that of gravity dams. For this purpose, the displacement response of Pine Flat gravity dam on rigid foundation rock to S69E (upstream) and vertical components of Taft ground motion is reproduced in Figure 5.9 from reference [24]. Comparison with Figure 5.2 indicates that dam-water interaction has greater influence on the response of the arch dam compared to the gravity dam. With a rigid reservoir boundary ($\alpha = 1$), dam-water interaction increases the maximum displacement of the arch dam due to upstream ground motion by 113% and that due to cross-stream ground motion by 84%; whereas the displacement of a gravity dam due to upstream ground motion is increased only by

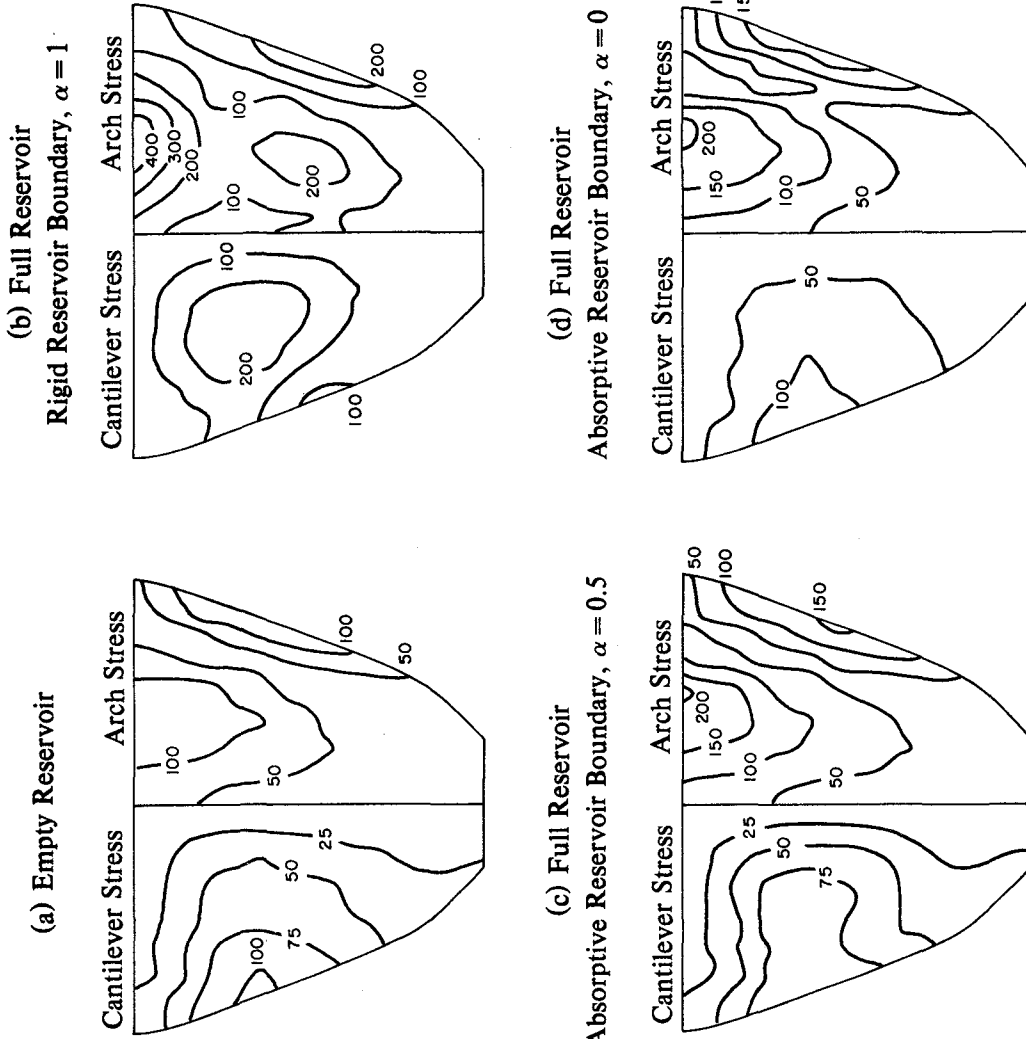


Figure 5.7 Envelope values of maximum tensile stresses (in psi) on upstream face of Morrow Point Dam on rigid foundation rock due to cross-stream component, only, of Taft ground motion. Initial static stresses are excluded.

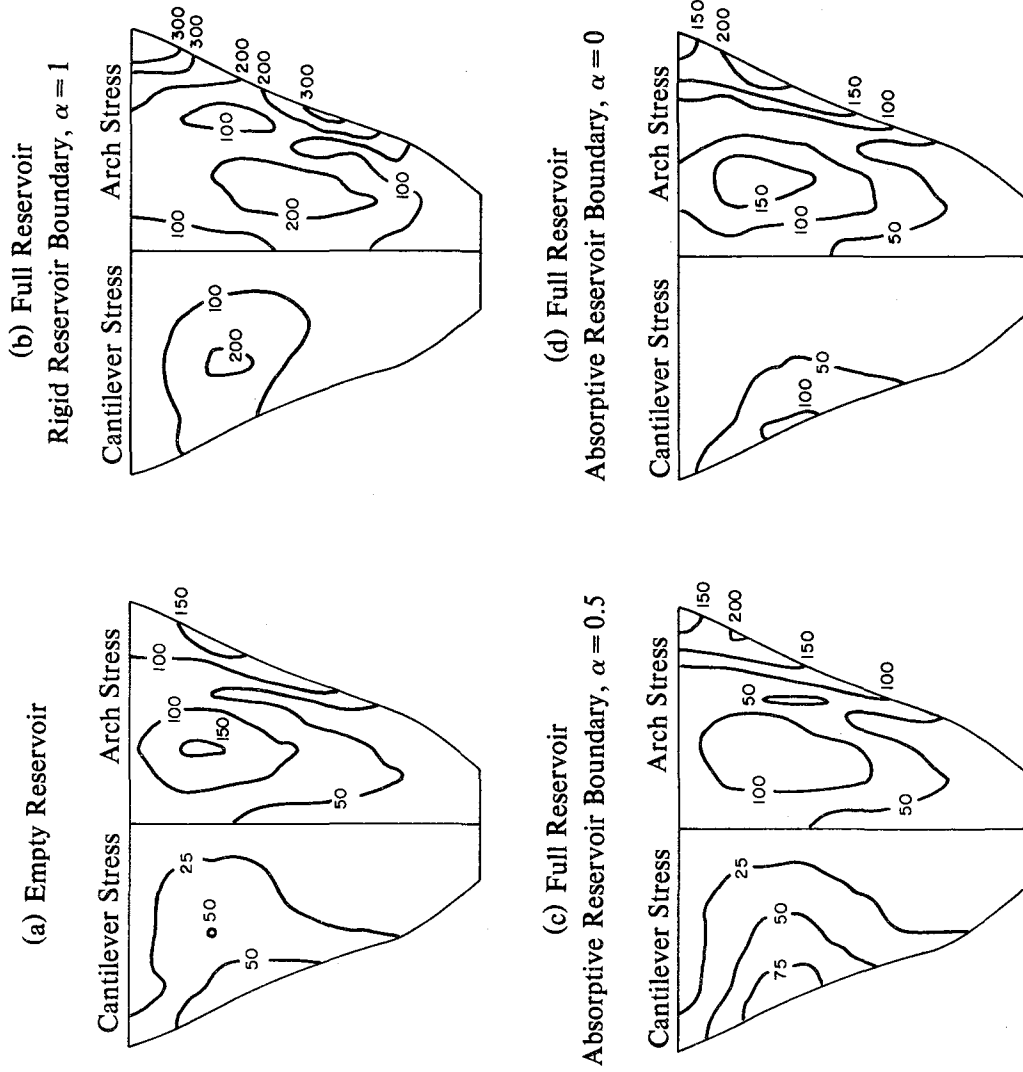


Figure 5.8 Envelope values of maximum tensile stresses (in psi) on downstream face of Morrow Point Dam on rigid foundation rock due to cross-stream motion, only, of Taft ground motion. Initial static stresses are excluded.

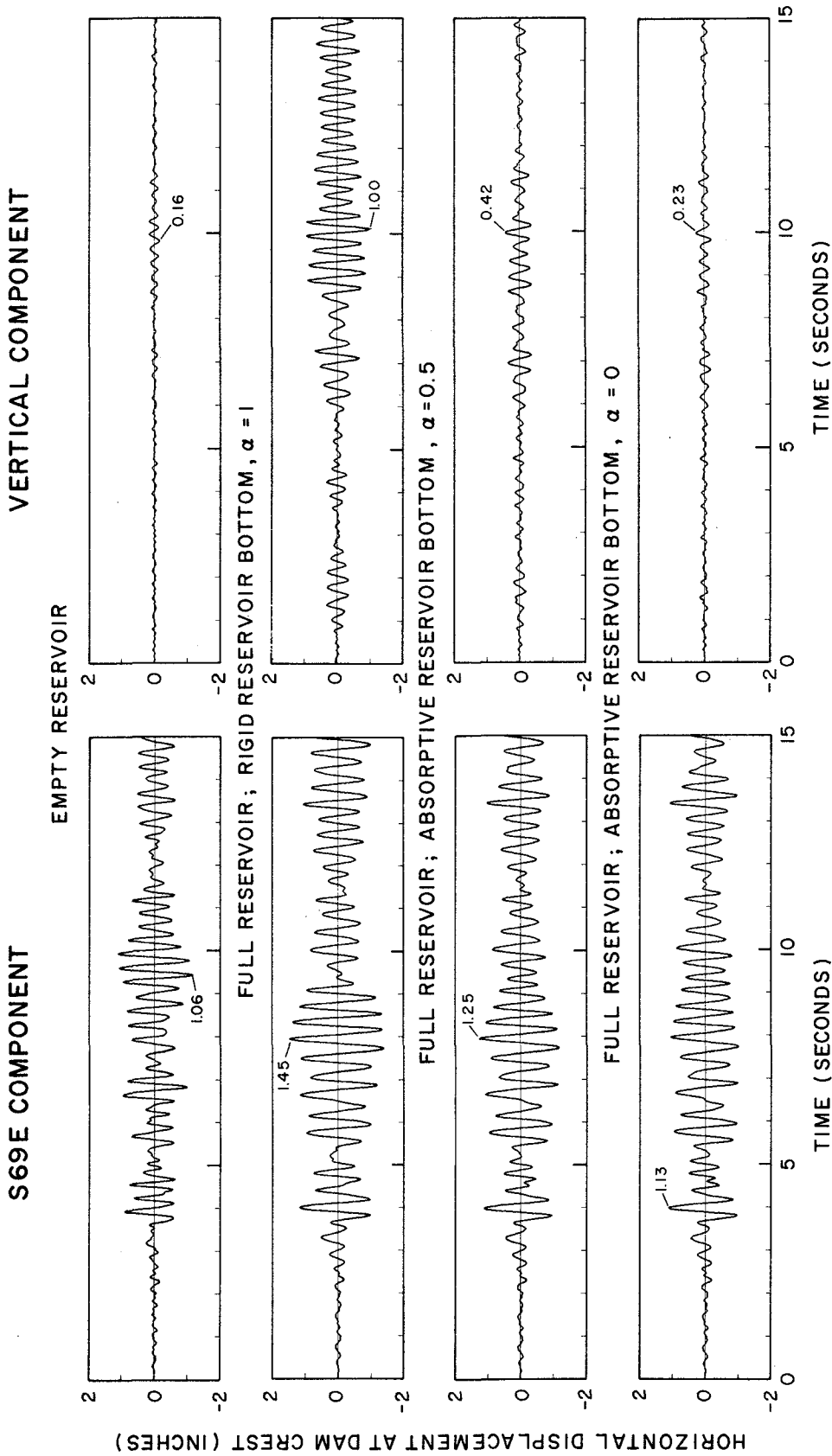


Figure 5.9 Displacement response of Pine Flat Dam on rigid foundation rock due to S69E and vertical components, separately, of Taft ground motion. From Fenves and Chopra (1984).

37%. Dam-water interaction has an especially strong influence in the response of dams to vertical ground motion with the maximum response of the arch dam magnified 30 times and of the gravity dam 6 times. Dam-water interaction effects are more significant in the response of arch dams than that of gravity dams because the added hydrodynamic mass, damping, and force have more effect on the response of a slender arch dam than on a massive gravity dam.

5.4.2 *Effects of Reservoir Boundary Absorption*

The alluvium and sediments usually present at the boundary of a reservoir are approximately modelled by a boundary that partially absorbs the incident hydrodynamic pressure waves. As shown in Chapter 4, reservoir boundary absorption affects all the hydrodynamic terms in the equations of motion for dams and hence their earthquake responses. The fundamental resonant period of the dam with a full reservoir is reduced due to reservoir boundary absorption but it is still longer than the period of the dam without water. As the reservoir boundary becomes more absorptive, i.e. as α decreases, the added damping at the fundamental resonant period increases because of increasing refraction of hydrodynamic pressure waves into the reservoir boundary materials and propagation of hydrodynamic pressure waves in the upstream direction, resulting in the tendency for the effective damping ratio to increase (Table 5.1). However, in contrast to gravity dams [24], the effective damping does not increase monotonically with decreasing α , because the added damping at the fundamental resonant period actually decreases -- contrary to intuition -- as α decreases from 0.5 to 0 (Chapter 4).

As shown in Chapter 4, reservoir boundary absorption primarily affects the fundamental resonant response to upstream or vertical ground motions, and has little effect on the response at higher excitation frequencies. On the other hand, the fundamental resonant response to cross-stream ground motion is essentially unaffected but the second resonant response is affected most as it occurs at a frequency close to the fundamental resonant frequency of the infinite channel (Figure 4.6).

The displacement response of the dam with full reservoir due to upstream ground motion is shown in Figures 5.2(c) and 5.2(d) for $\alpha = 0.5$ and $\alpha = 0$. These results demonstrate that the main effect of reservoir boundary absorption is to reduce the larger displacement peaks without

significantly changing the frequency content of the response [compare Figure 5.2(c)-(d) to Figure 5.2(b)]. Primarily because of added hydrodynamic damping due to reservoir boundary absorption and the resulting decrease in the pseudo-acceleration ordinate, the maximum crest displacement of the dam with full reservoir decreases from 0.81 in. (for rigid reservoir boundary) to 0.63 in. for $\alpha = 0.5$; the maximum arch stress decreases from 735 psi to 525 psi on the upstream face and from 641 psi to 443 psi on the downstream face; the maximum cantilever stress decreases from 268 psi to 165 psi on the upstream face and from 189 psi to 118 psi on the downstream face. However, the general pattern of maximum stresses is not substantially altered. As the wave reflection coefficient α decreases from 0.5 to 0, the maximum responses are essentially unaffected. Hydrodynamic pressure wave absorption, while decreasing the maximum stresses over the face of the dam, also eliminates the redistribution of cantilever stresses due to hydrodynamic effects mentioned in Section 5.4.1 [compare Figures 5.3(a), 5.3(b) and 5.3(d); 5.4(a), 5.4(b) and 5.4(d)].

Reservoir boundary absorption eliminates the unbounded peaks in the added hydrodynamic force, and in the dam response, due to vertical ground motion for excitation frequencies equal to the natural vibration frequencies ω_n^{is} of the infinite channel. Also the fundamental resonant peak in the dam response which is bounded is greatly reduced [Figure 4.6(b)]. The resulting effect on the response of the dam with full reservoir to vertical ground motion is apparent from Figures 5.2(b)-(d), 5.5(b)-(d), and 5.6(b)-(d) and Table 5.2(b). Reservoir boundary absorption drastically reduces the maximum displacement from 1.98 in. (for rigid reservoir boundary) to 0.33 in. for $\alpha = 0.5$, and to 0.14 in. for $\alpha = 0$ [Table 5.2(b)], similarly reduces the maximum arch stress from 1572 psi to 263 psi, and to 113 psi on the upstream face [Figure 5.5(b)-(d)]; and from 1412 psi to 229 psi, and to 86 psi on the downstream face [Figure 5.6(b)-(d)]; and also the maximum cantilever stress from 571 psi to 130 psi, and to 60 psi on the upstream face [Figure 5.5(b)-(d)]; and from 361 psi to 59 psi, and to 43 psi on the downstream face [Figure 5.6(b)-(d)][see also Table 5.2(b)]. These drastic decreases in the responses are, in part, due to the decrease in $S_a(T, \xi_f)$ as α decreases from 1.0 to 0.5 (Table 5.1). Although the apparent damping ratio ξ_f decreases as α decreases from 0.5 to 0 (Table 5.1), the dam response decreases because of the decrease in the added hydrodynamic force due to reservoir

boundary absorption. As in the case of upstream ground motion, wave absorption eliminates the redistribution of cantilever stresses caused by hydrodynamic effects [compare Figures 5.5(a), 5.5(b) and 5.5(d); 5.6(a), 5.6(b) and 5.6(d)].

As mentioned in Section 5.4.1, dam-water interaction has the effect of increasing the relative significance of the contributions of the second mode to the response to cross-stream ground motion, because it greatly increases the response amplitude at the second resonant frequency which is close to ω_1^a , the fundamental resonant frequency of the infinite uniform channel. Reservoir boundary absorption reduces the second resonant peak, thus decreasing the relative significance of the second mode response, and also reduces the unbounded peaks at ω_n^{ia} in the frequency response function. This can be observed from the change in frequency content of the displacement history due to the cross-stream component of Taft ground motion as α changes from 1.0 to 0.5 [Figures 5.2(b) and 5.2(c)]. As a result of this decrease in the second mode response, and the decrease in the pseudo-acceleration ordinate for the fundamental mode (Table 5.1), the displacement and stress responses are reduced as α decreases from 1.0 to 0.5 [compare Figures 5.2(b) and 5.2(c), 5.7(b) and 5.7(c), 5.8(b) and 5.8(c)]. As α decreases from 1.0 to 0.5, the maximum displacement decreases from 0.68 in. to 0.38 in.; the maximum arch stress decreases from 410 psi to 200 psi on the upstream face, and from 382 psi to 201 psi on the downstream face; the maximum cantilever stress decreases from 313 psi to 106 psi on the upstream face, and from 212 psi to 93 psi on the downstream face [Table 5.2(c)]. As in the case of upstream and vertical ground motion, absorption of hydrodynamic pressure waves also eliminates the changes, due to hydrodynamic effects, in the patterns of maximum arch and cantilever stresses over the dam face [compare Figures 5.7(a), 5.7(b) and 5.7(c); 5.8(a), 5.8(b) and 5.8(c)]. With increasing absorptiveness of the reservoir boundary materials from $\alpha = 0.5$ to 0, however, the displacement and stress responses increase slightly with little change in the stress patterns [compare Figures 5.2(c) and 5.2(d), 5.7(c) and 5.7(d), 5.8(c) and 5.8(d)]. As α decreases from 0.5 to 0, the maximum displacement increases from 0.38 in. to 0.45 in.; the maximum arch stress increases from 200 psi to 245 psi on the upstream face, and from 201 psi to 227 psi on the downstream face; the maximum cantilever stress increases from 106 psi to 120 psi on the upstream face, and from 93 psi to 105 psi on the

downstream face [Table 5.2(c)]. As mentioned in Section 5.4.1, the added hydrodynamic force is opposite in phase compared to the effective earthquake force associated with the mass of the dam at the fundamental resonant frequency. Reservoir boundary absorption decreases somewhat the added hydrodynamic force and thus increases slightly the fundamental resonant peak in the frequency response function (Chapter 4); and therefore the earthquake responses increase slightly when α decreases from 0.5 to 0.

It is apparent from the preceding results and discussion that the effects of reservoir boundary absorption are least pronounced in the response to upstream ground motion, they have a dominant effect in the response to vertical ground motion and somewhat less in the case of cross-stream ground motion. In general, assuming a rigid reservoir boundary leads to an unrealistically large response for dams with impounded water, particularly due to vertical and cross-stream ground motions. Reservoir boundary absorption does not alter the earlier observation that the arch stresses are greater than the cantilever stresses over both faces of the dam (Table 5.2).

The effects of reservoir boundary absorption on the earthquake response of arch dams identified in the preceding discussion are generally similar to those presented earlier [24] for gravity dams. However, as the wave reflection coefficient α decreases from 1.0 to 0.5, the reduction in response of the arch dam is greater compared to the gravity dam. As α decreases from 0.5 to 0, the response of arch as well as gravity dams to horizontal ground motion is affected little whereas the response to vertical ground motion is significantly affected for both types of dams, with the reduction being greater in the response of arch dams.

5.5 Foundation Flexibility Effects

The response of Morrow Point Dam supported on flexible foundation rock with an empty reservoir to three components of ground motion is presented in Figures 5.10(a) to 5.16(a) and summarized as Case 5 in Table 5.3. A comparison of these results with those for the dam on rigid foundation with an empty reservoir, presented in Figures 5.2(a) to 5.8(a) and summarized as Case 1 in Table 5.2, provides an indication of effects of foundation flexibility on dam response.

Table 5.3 -- Summary of Responses* of Morrow Point Dam,
on Flexible Foundation Rock, to Taft Ground Motion

Case	Water	α	Maximum Radial Crest Displacement (inches)	Maximum Tensile Stress (psi)			
				Upstream Face		Downstream Face	
				Arch Stress	Cantilever Stress	Arch Stress	Cantilever Stress
(a) Response to Upstream (S69E Component of Taft) Ground Motion							
5	None	-	0.49	308	117	273	115
6	Full	1.0	1.11	760	275	721	188
7	Full	0.5	0.79	555	171	519	176
8	Full	0	0.91	618	173	561	178
(b) Response to Vertical Component of Taft Ground Motion							
5	None	-	0.11	92	62	67	49
6	Full	1.0	2.10	1435	427	1332	182
7	Full	0.5	0.54	380	123	333	69
8	Full	0	0.27	180	79	147	61
(c) Response to Cross-stream (S21W Component of Taft) Ground Motion							
5	None	-	0.46	211	106	205	106
6	Full	1.0	0.60	340	212	237	164
7	Full	0.5	0.49	257	107	216	109
8	Full	0	0.68	345	143	290	149
(d) Response to Upstream, Vertical, and Cross-stream Components, Simultaneously, of Ground Motion							
5	None	-	0.71	337	143	281	151
6	Full	1.0	2.61	1821	522	1684	377
7	Full	0.5	0.85	624	214	558	212
8	Full	0	0.90	652	228	537	237

* Effects of static loads are excluded.

As mentioned in Section 4.5, foundation flexibility affects the response of the dam in a simpler manner than does dam-water interaction because, unlike impounded water, the foundation rock does not have any resonant frequencies as it is assumed to be massless. As seen by comparing Cases 1 and 5 in Table 5.1, the fundamental period is slightly lengthened and the effective damping is reduced, in part, because the foundation region is undamped. In this particular case the combined change in the vibration period and damping ratio results in a slight reduction of the pseudo-acceleration response spectrum ordinate for each of the three components of ground motion.

In spite of this reduction of the spectrum ordinate, the response of the dam increases slightly because of foundation flexibility. Most of the responses are increased, primarily because of the increase in effective earthquake forces in individual vibration modes arising from modification in the mode shapes due to foundation flexibility. However, foundation flexibility does not significantly alter the general pattern of maximum stresses, presumably because the relative values of the various modal contributions are not significantly affected by foundation flexibility. The arch stresses are greater than the cantilever stresses over both faces of the dam (Table 5.3), another observation that is not affected by foundation flexibility.

5.6 Dam-Water Interaction Effects with Flexible Foundation Rock

5.6.1 Hydrodynamic Effects

As demonstrated in Chapter 4, the effects of dam-water interaction on the response of dam to harmonic ground motion in the upstream, vertical or cross-stream directions are qualitatively similar for rigid and flexible foundation rock. In particular, the percentage increase in the fundamental period due to hydrodynamic effects is approximately the same whether the foundation rock is rigid or flexible. This is further demonstrated for the symmetric vibration period and antisymmetric vibration period by comparing the results for Cases 1 and 2 with 5 and 6 in Table 5.1.

The displacement and stress responses of Morrow Point Dam on a flexible foundation to the three components of Taft ground motion are presented in Figures 5.10 to 5.16. As seen by comparing part (a) with (b) in each of these figures and the summarized results in Cases 5 and 6 of Table 5.3,

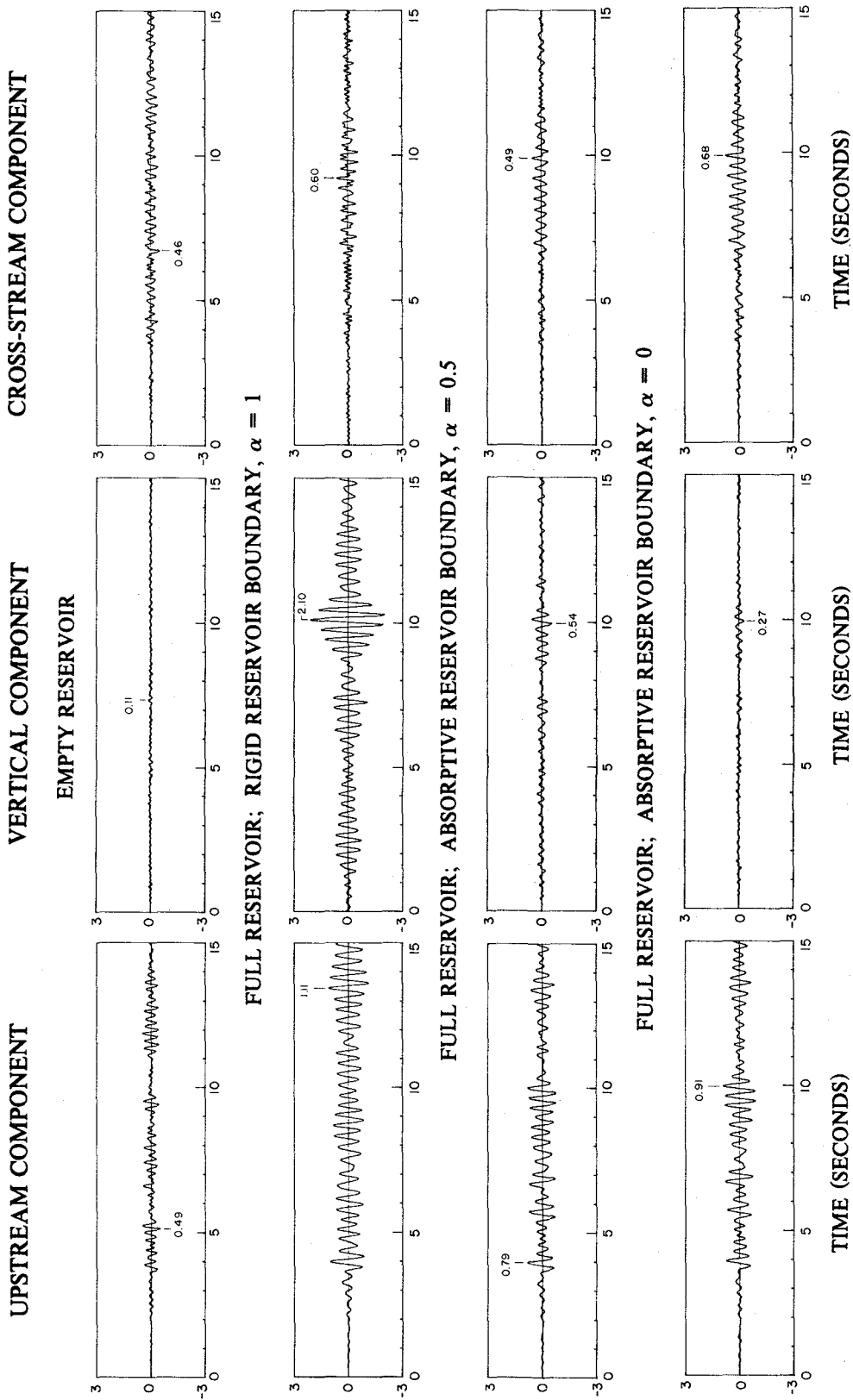


Figure 5.10 Displacement response of Morrow Point Dam on flexible foundation rock due to upstream, vertical and cross-stream components, separately, of Taft ground motion.

hydrodynamic effects generally increase the displacement and stress responses to all three components of ground motion. For example, the maximum crest displacement of the dam due to the upstream component of ground motion increases from 0.49 in. to 1.11 in.; the maximum arch stress increases from 308 psi to 760 psi on the upstream face, and from 273 psi to 721 psi on the downstream face; the maximum cantilever stress increases from 117 psi to 275 psi on the upstream face, and from 115 psi to 188 psi on the downstream face [Table 5.3(a)]. In general, hydrodynamic effects influence the distribution pattern of the maximum stresses for the dam similarly whether the foundation rock is flexible or rigid, except for some differences. For example, the distribution of the arch stress over both the upstream and downstream faces of the dam due to the cross-stream component of ground motion is not much affected by hydrodynamic effects, unlike the case of rigid foundation [compare Figures 5.15(a), (b) and 5.16(a), (b) with Figures 5.7(a), (b) and 5.8(a), (b)]. However, as in the case of a rigid foundation rock, the arch stresses are generally much larger than the cantilever stresses over both faces of the dam on flexible foundation rock, irrespective of the reservoir condition (Table 5.3).

The earthquake response results presented here confirm the conclusions of Chapter 4 based on frequency response functions that foundation flexibility does not have much influence on the hydrodynamic effects in the dam response. The hydrodynamic effects influence the dam response similarly whether the foundation rock is rigid or flexible [compare parts (a) and (b) of Figures 5.10 to 5.16 with parts (a) and (b) of Figures 5.2 to 5.8, and Cases 5 and 6 in Table 5.3 with Cases 1 and 2 in Table 5.2].

5.6.2 *Effects of Reservoir Boundary Absorption*

The effects of absorption of hydrodynamic pressure waves at the reservoir boundary on the response of the dam supported on flexible foundation to the three components of Taft ground motion can be seen from the results shown in parts (b), (c), and (d) of Figures 5.10 to 5.16, and from Cases 6, 7, and 8 in Table 5.3. From these results, it is apparent that with increasing wave absorption, with α decreasing from 1.0 to 0.5, reduces the response of the dam to all three components of ground motion, similar to the case of rigid foundation rock discussed earlier [compare parts (b) and (c) of Figures 5.10 - 5.16 with Figures 5.2 - 5.8]. As discussed in Section 5.4.2, the reduction in response

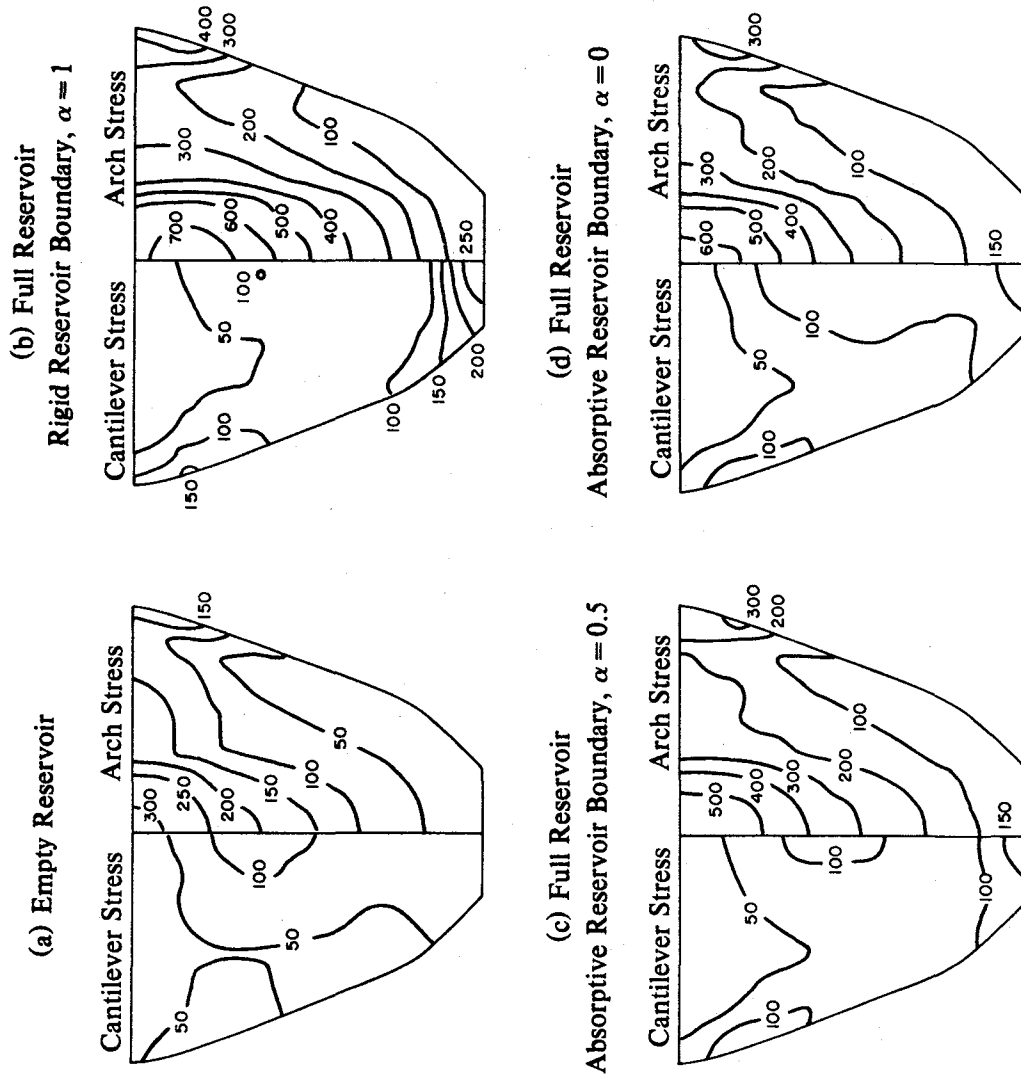


Figure 5.11 Envelope values of maximum tensile stresses (in psi) on upstream face of Morrow Point Dam on flexible foundation rock due to upstream component, only, of Taft ground motion. Initial static stresses are excluded.

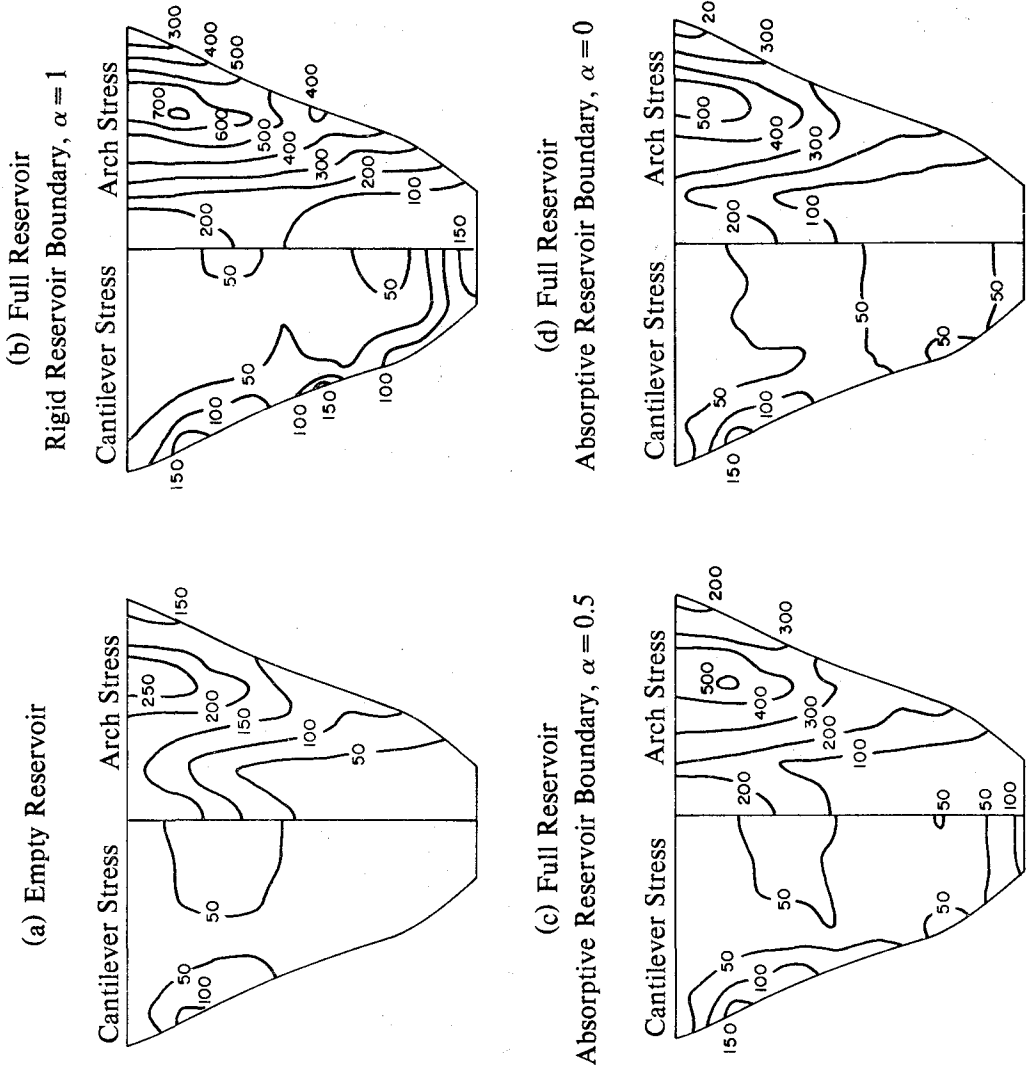


Figure 5.12 Envelope values of maximum tensile stresses (in psi) on downstream face of Morrow Point Dam on flexible foundation rock due to upstream component, only, of Taft ground motion. Initial static stresses are excluded.

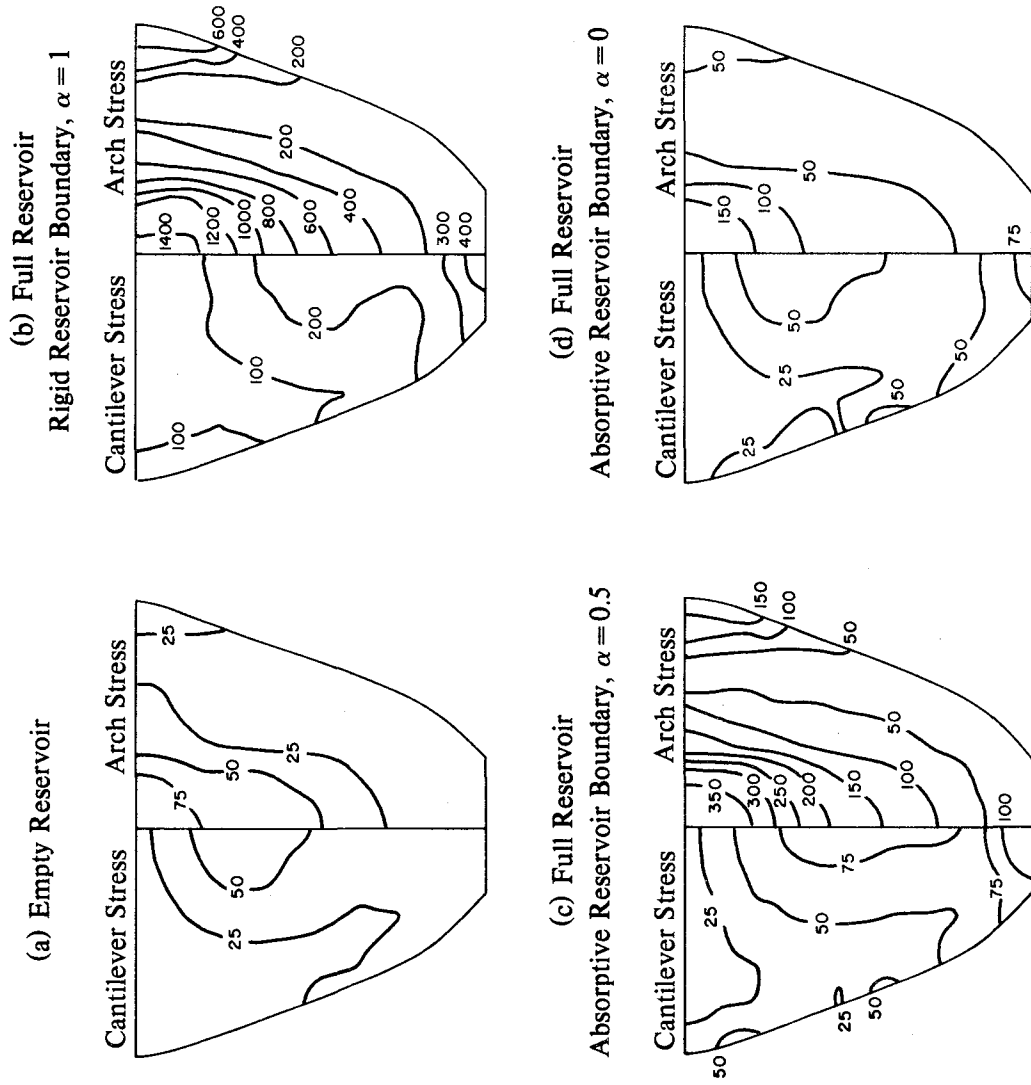


Figure 5.13 Envelope values of maximum tensile stresses (in psi) on upstream face of Morrow Point Dam on flexible foundation rock due to vertical component, only, of Taft ground motion. Initial static stresses are excluded.

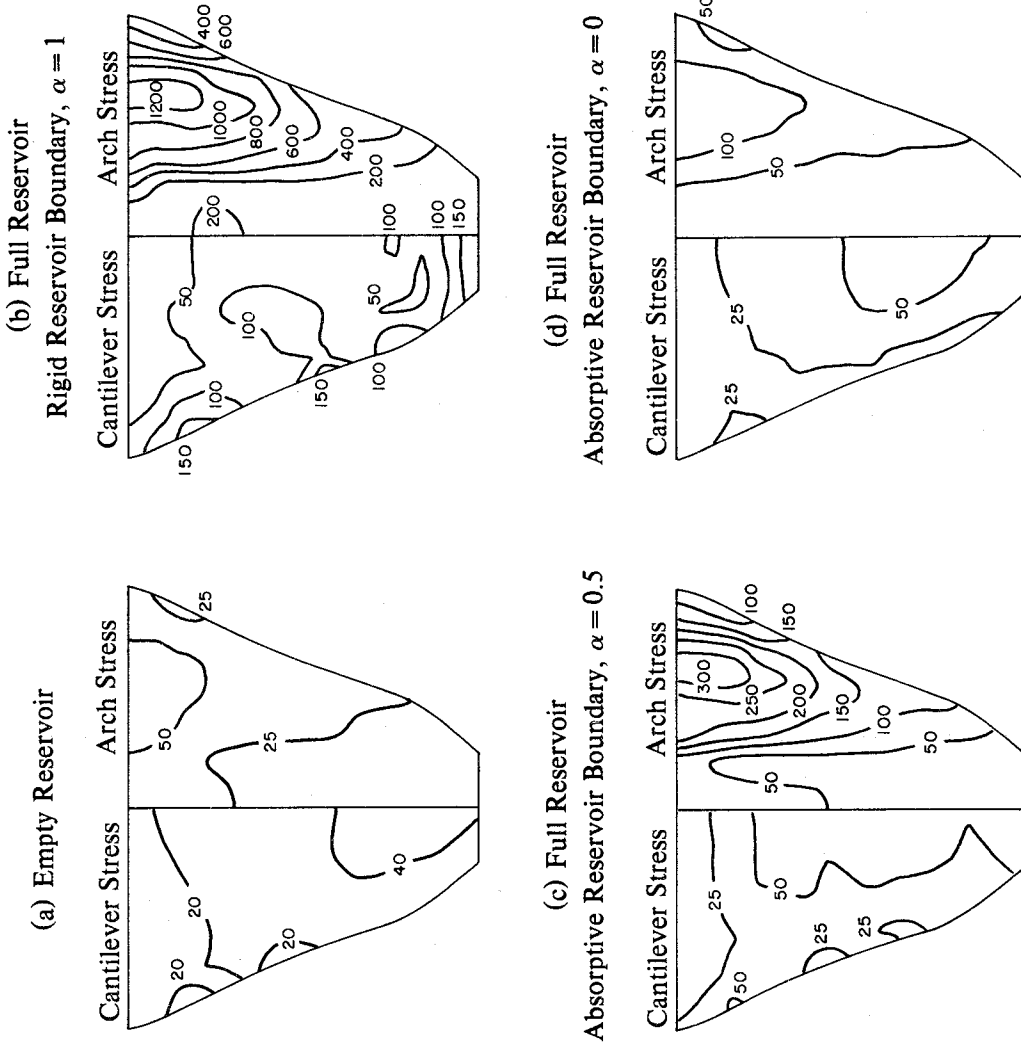


Figure 5.14 Envelope values of maximum tensile stresses (in psi) on downstream face of Morrow Point Dam on flexible foundation rock due to vertical component, only, of Taft ground motion. Initial static stresses are excluded.

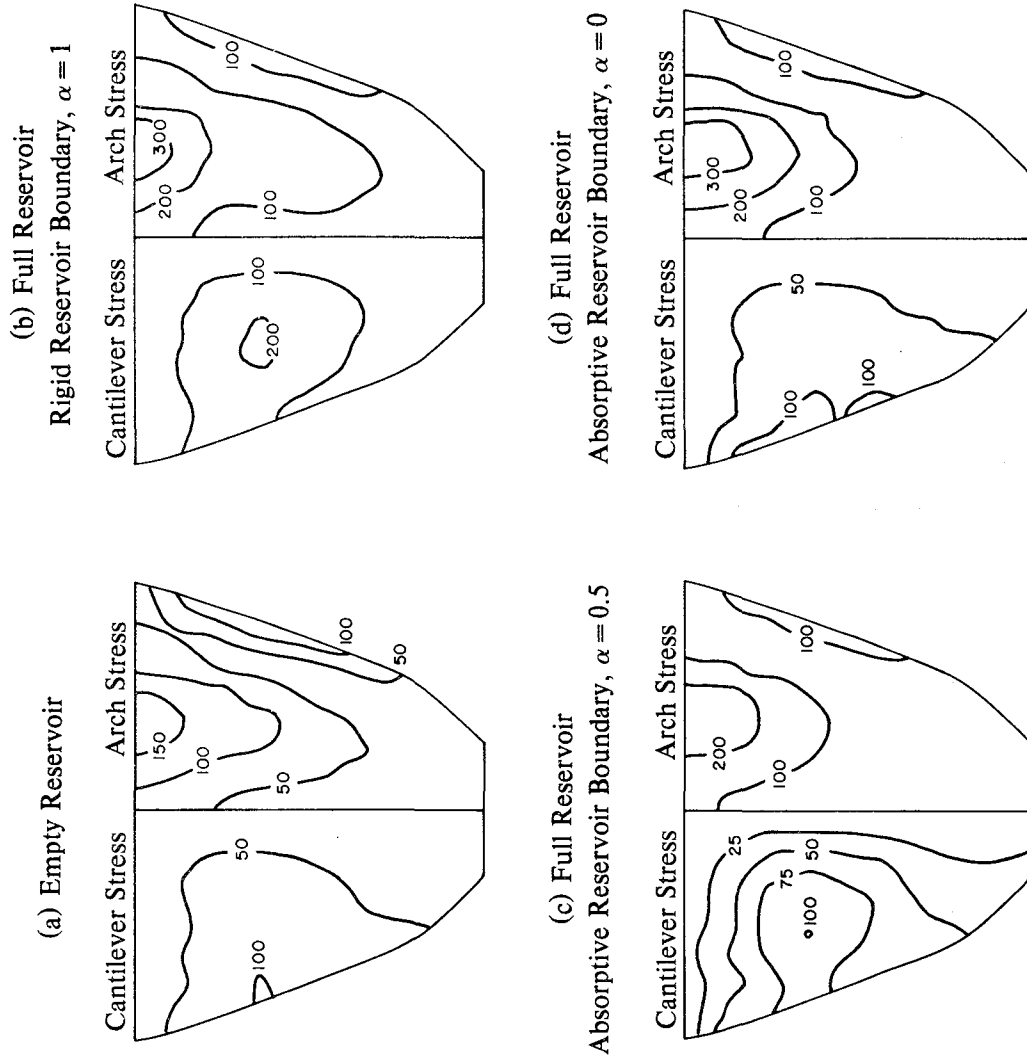


Figure 5.15 Envelope values of maximum tensile stresses (in psi) on upstream face of Morrow Point Dam on flexible foundation rock due to cross-stream component, only, of Taft ground motion. Initial static stresses are excluded.

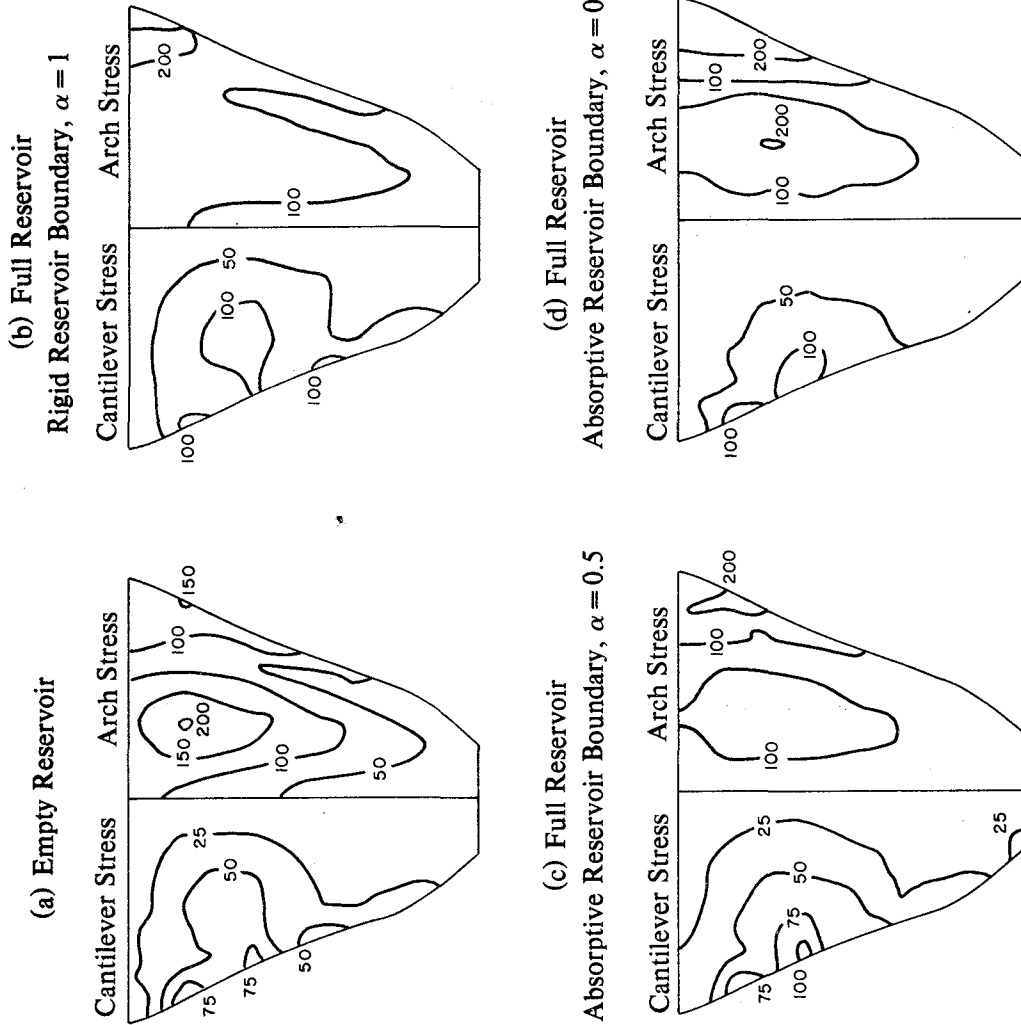


Figure 5.16 Envelope values of maximum tensile stresses (in psi) on downstream face of Morrow Point Dam on flexible foundation rock due to cross-stream component, only, of Taft ground motion. Initial static stresses are excluded.

arises in part from the reduction in the ordinate of the pseudo-acceleration spectrum due to increased effective damping arising from reservoir boundary absorption (Table 5.1).

However, with further increase in the absorptiveness of the reservoir boundary materials, with α decreasing from 0.5 to 0, the response of the dam to upstream and cross-stream ground motions generally increases contrary to intuition, while the responses to vertical ground motion decrease as expected [compare parts (c) and (d) of Figures 5.10 to 5.16 and Cases 7 and 8 in Table 5.3]. This increase in responses to cross-stream ground motion is similar to what was observed earlier with a rigid foundation rock [compare parts (c) and (d) of Figures 5.10, 5.15, 5.16 with Figures 5.2, 5.7, 5.8; and Cases 7 and 8 in Table 5.3(c) with Cases 3 and 4 in Table 5.2(c)]. As mentioned in Section 5.4.2, reservoir boundary absorption reduces the second resonant peak, thus decreasing the relative significance of the second mode response in case of cross-stream ground motion. However, as also mentioned in Section 5.4.2, reservoir boundary absorption decreases somewhat the "added" hydrodynamic force, which is opposite in phase compared to the effective earthquake force associated with the mass of the dam at the fundamental resonant frequency, thus increasing the fundamental resonant peak. This increase in the fundamental mode contribution becomes more significant with increase in the absorptiveness of the reservoir boundary materials so that the response increases as α decreases from 0.5 to 0. For the selected dam-foundation system and ground motion, this increase in the fundamental mode contribution with increase in the absorptiveness of the reservoir boundary materials may completely offset the above-mentioned decrease in the second mode contribution so that some of the responses with $\alpha = 0$ are greater than the corresponding responses with $\alpha = 1.0$ [compare Figures 5.10(b) and 5.10(d), 5.15(b) and 5.15(d), 5.16(b) and 5.16(d), and Cases 6 and 8 in Table 5.3(c)].

The slight increases in the response to upstream ground motion as α decreases from 0.5 to 0 are, for the most part, in contrast to the trend with a rigid foundation [compare parts (c) and (d) of Figures 5.10, 5.11, 5.12 with Figures 5.2, 5.3, 5.4; and Cases 7 and 8 in Table 5.3(a) with Cases 3 and 4 in Table 5.2(a)]. The added damping decreases, contrary to intuition, with increasing wave absorption at the fundamental resonant frequency (Chapter 4), resulting in a decrease in the effective damping ratio (Table 5.1) and a corresponding increase in $S_a(T, \xi_1^x)$ (Table 5.1), and thus slight increases

in the responses.

As in the case of rigid foundation rock, the response to vertical ground motion is greatly decreased by wave absorption even if the foundation rock is flexible; and reservoir boundary absorption eliminates somewhat the cantilever stress redistribution due to hydrodynamic effects for all three components of ground motion. However, as in the case of a rigid foundation rock, reservoir boundary absorption does not alter the observation that the arch stresses are greater than the cantilever stresses over both faces of the dam (Table 5.3).

5.7 Relative Significance of Response to Ground Motion Components

As seen in the preceding sections of this chapter, the earthquake response of Morrow Point Dam is increased by dam-water interaction and generally decreased by reservoir boundary absorption with the magnitude of these effects depending little on the condition of foundation rock, rigid or flexible, but significantly on the component of ground motion. In particular, both dam-water interaction and reservoir boundary absorption profoundly affect the response of the dam to vertical ground motion, but have relatively less -- although significant -- effect on the response to upstream or cross-stream ground motion. Stated differently, the response of the dam with an empty reservoir due to vertical ground motion expressed as a percentage of the response to one of the horizontal ground motion components is small; the percentage greatly increases because of dam-water interaction with a rigid reservoir boundary; and from this increased value it decreases significantly because of reservoir boundary absorption.

The response of the dam to the three components, separately and simultaneously, of Taft ground motion is presented in Figures 5.17 to 5.36 to evaluate the significance of the various ground motion components in the total dynamic response of the dam. All the conclusions stated in the preceding paragraph would be fully applicable to the total response if the individual responses to the three components of ground motion were exactly in phase and the maximum responses were directly additive. But this is not the case as is apparent from the response history of crest displacement in Figures 5.17 and 5.18 for rigid foundation rock and Figures 5.27 and 5.28 for flexible foundation

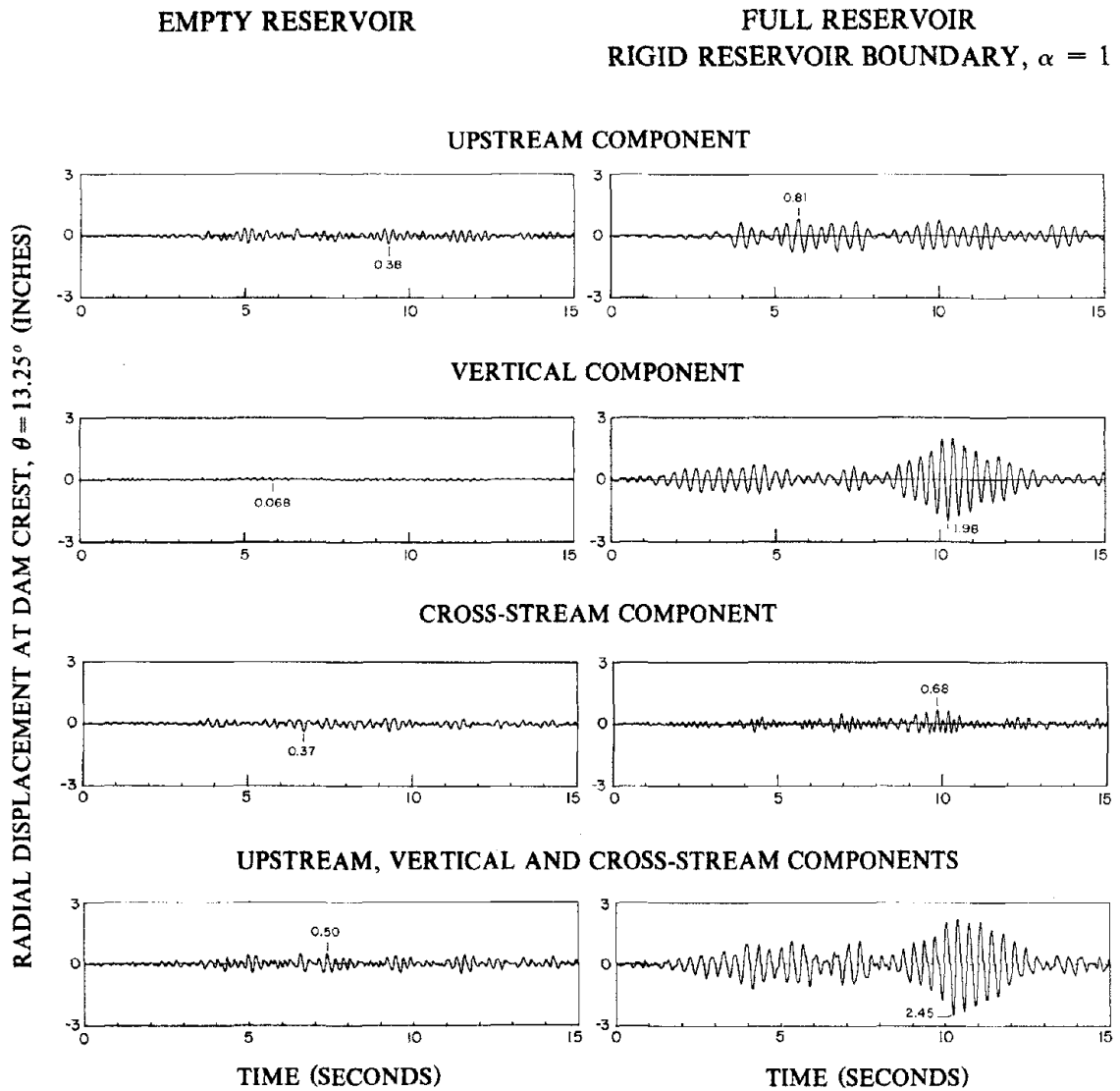


Figure 5.17 Displacement response of Morrow Point Dam on rigid foundation rock due to upstream, vertical and cross-stream components, separately and simultaneously, of Taft ground motion: (i) empty reservoir, and (ii) full reservoir with rigid reservoir boundary ($\alpha = 1$).

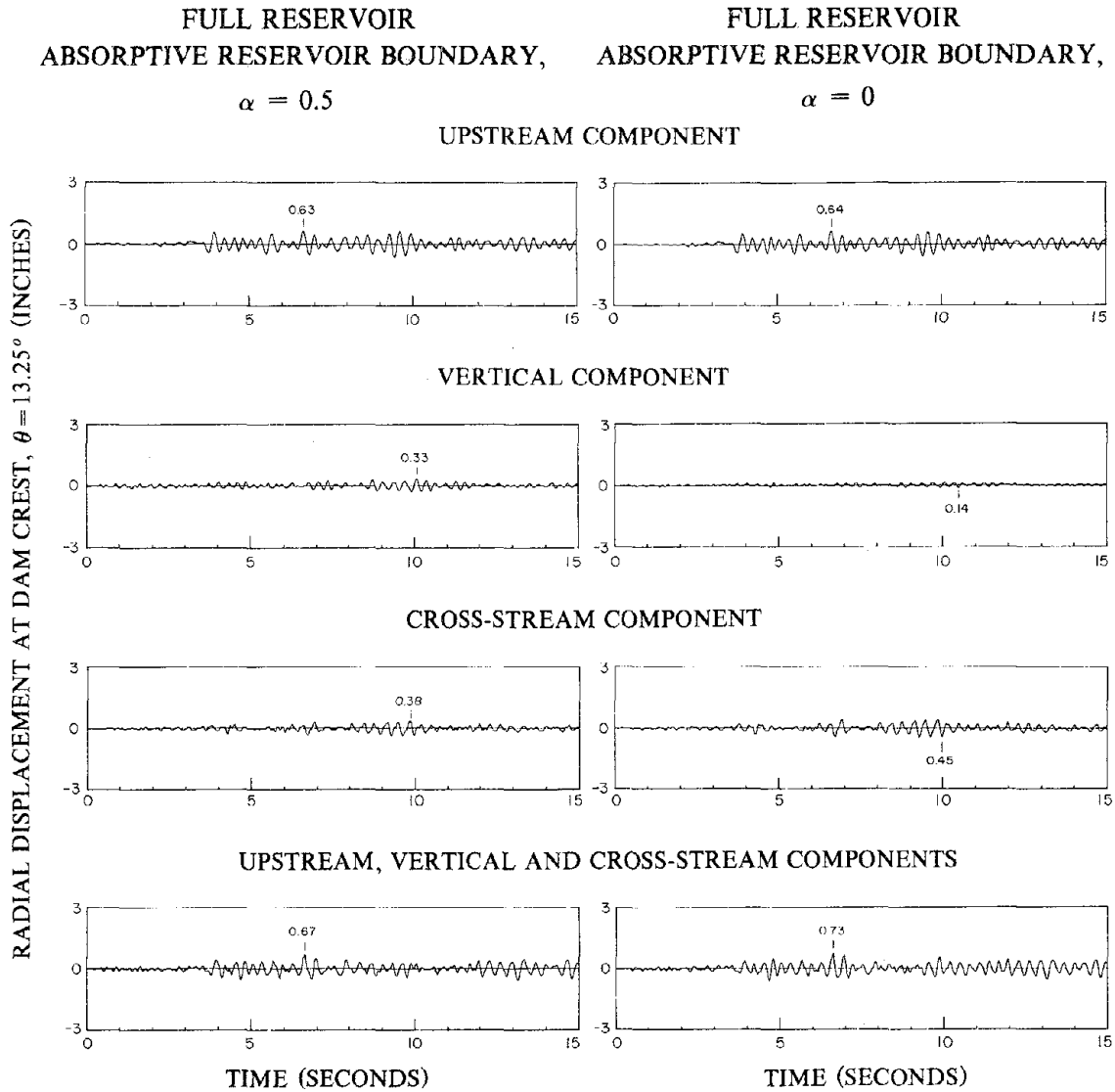


Figure 5.18 Displacement response of Morrow Point Dam on rigid foundation rock with full reservoir and absorptive reservoir boundary due to upstream, vertical and cross-stream components, separately and simultaneously, of Taft ground motion: (i) $\alpha = 0.5$, and (ii) $\alpha = 0$.

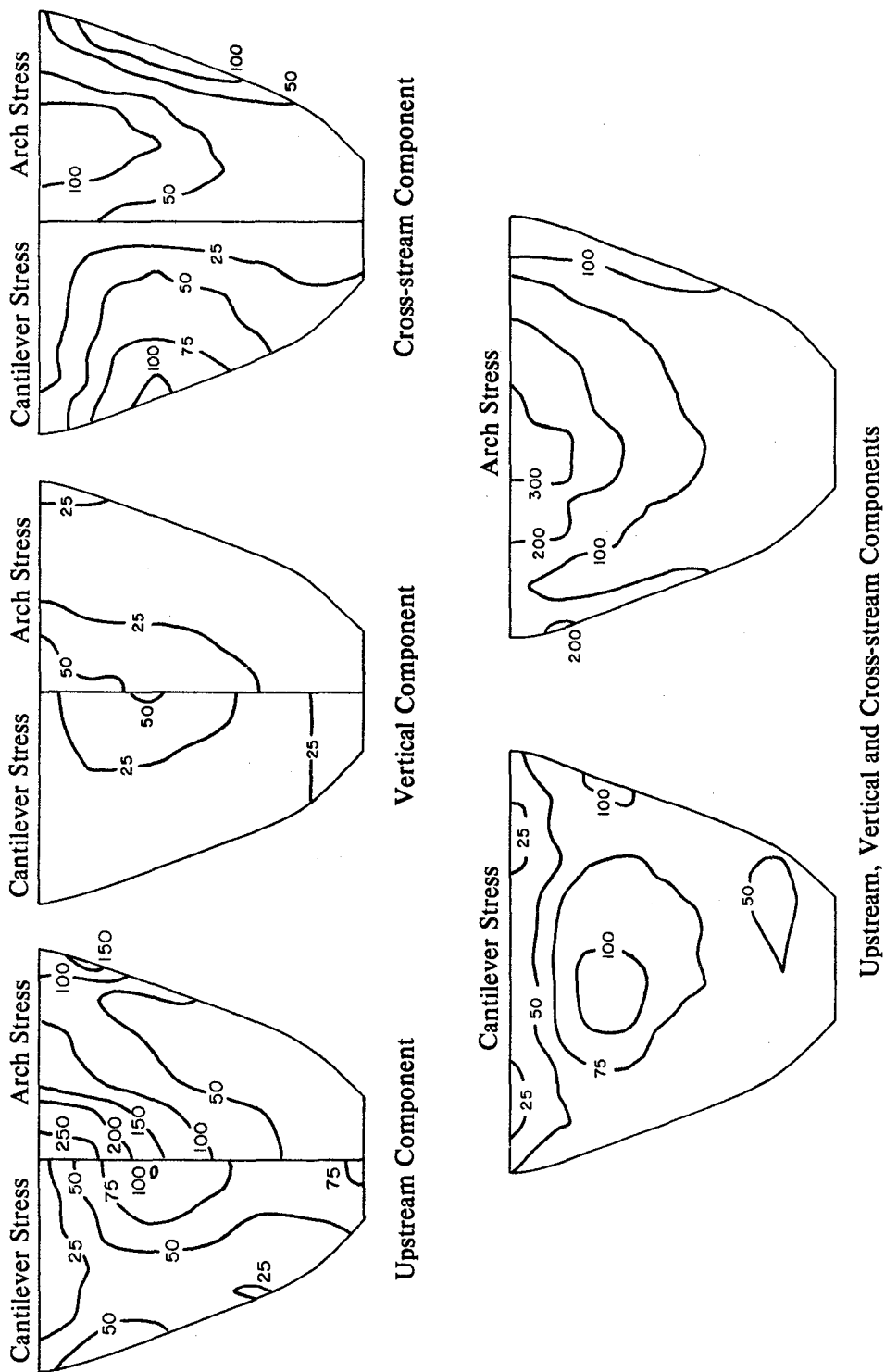


Figure 5.19 Envelope values of maximum tensile stresses (in psi) on upstream face of Morrow Point Dam on rigid foundation rock with empty reservoir due to upstream, vertical and cross-stream components, separately and simultaneously, of Taft ground motion. Initial static stresses are excluded.

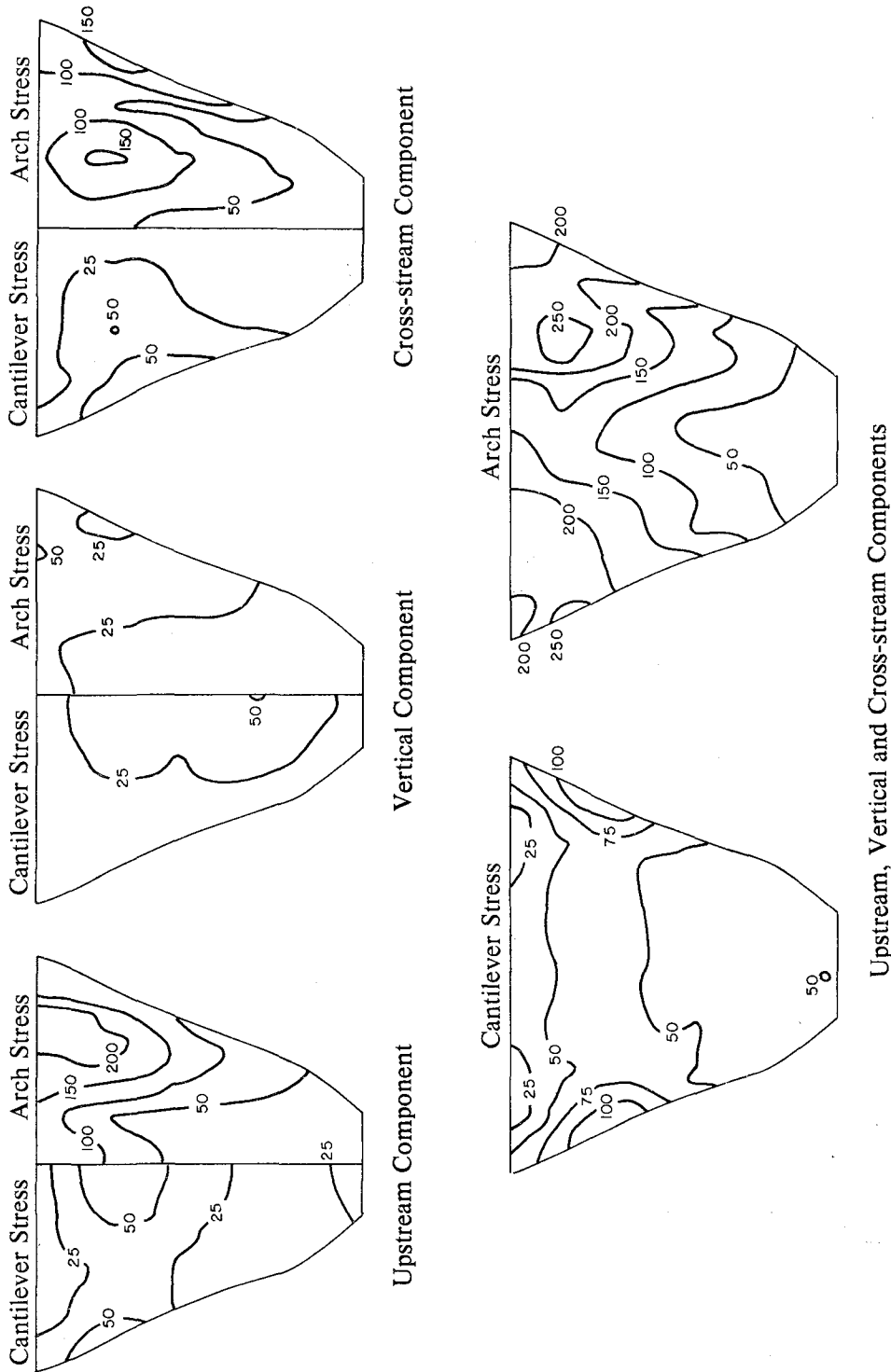


Figure 5.20 Envelope values of maximum tensile stresses (in psi) on downstream face of Morrow Point Dam on rigid foundation rock with empty reservoir due to upstream, vertical and cross-stream components, separately and simultaneously, of Taft ground motion. Initial static stresses are excluded.

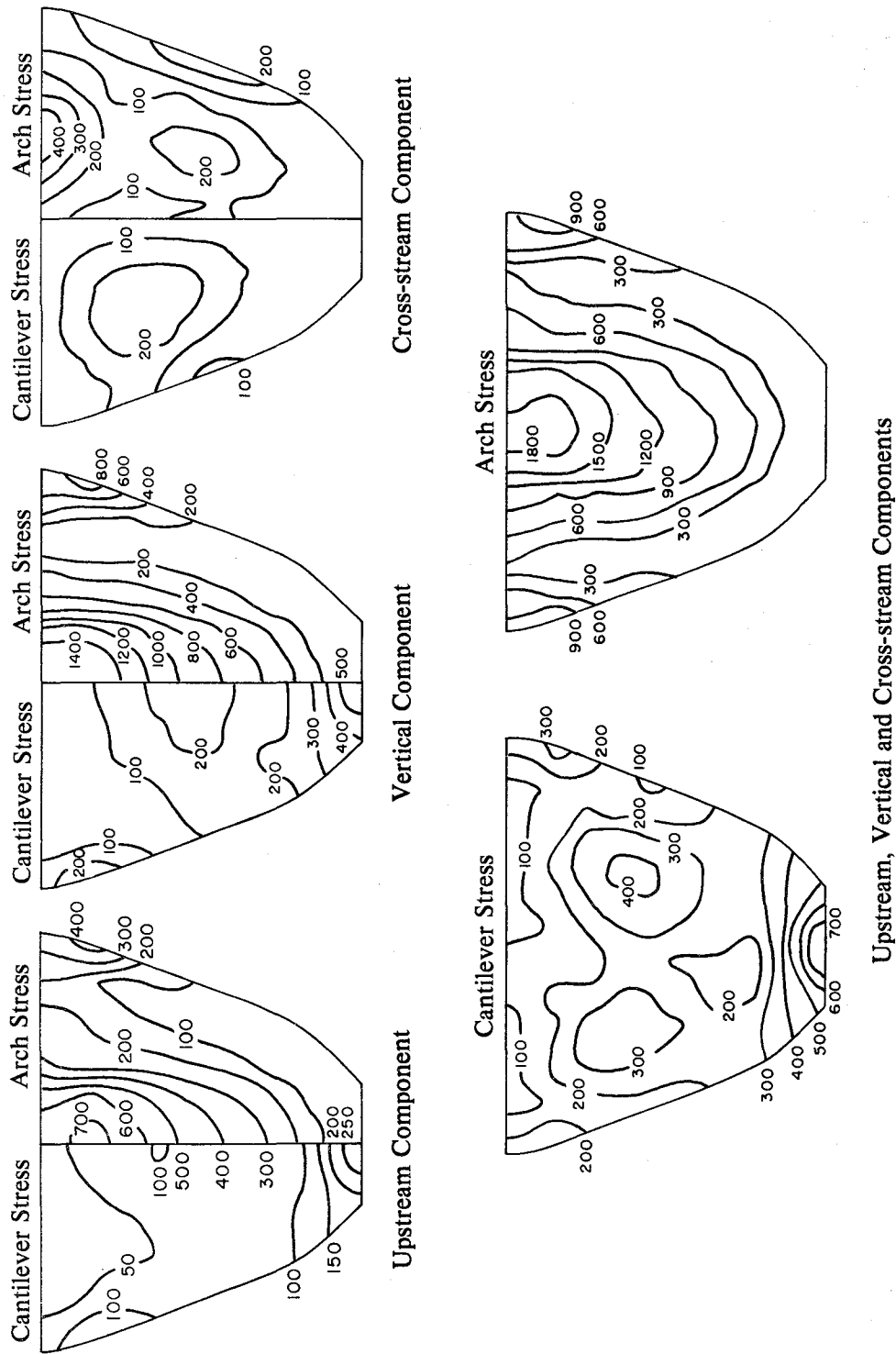


Figure 5.21 Envelope values of maximum tensile stresses (in psi) on upstream face of Morrow Point Dam on rigid foundation rock with full reservoir and rigid reservoir boundary ($\alpha = 1$) due to upstream, vertical and cross-stream components, separately and simultaneously, of Taft ground motion. Initial static stresses are excluded.

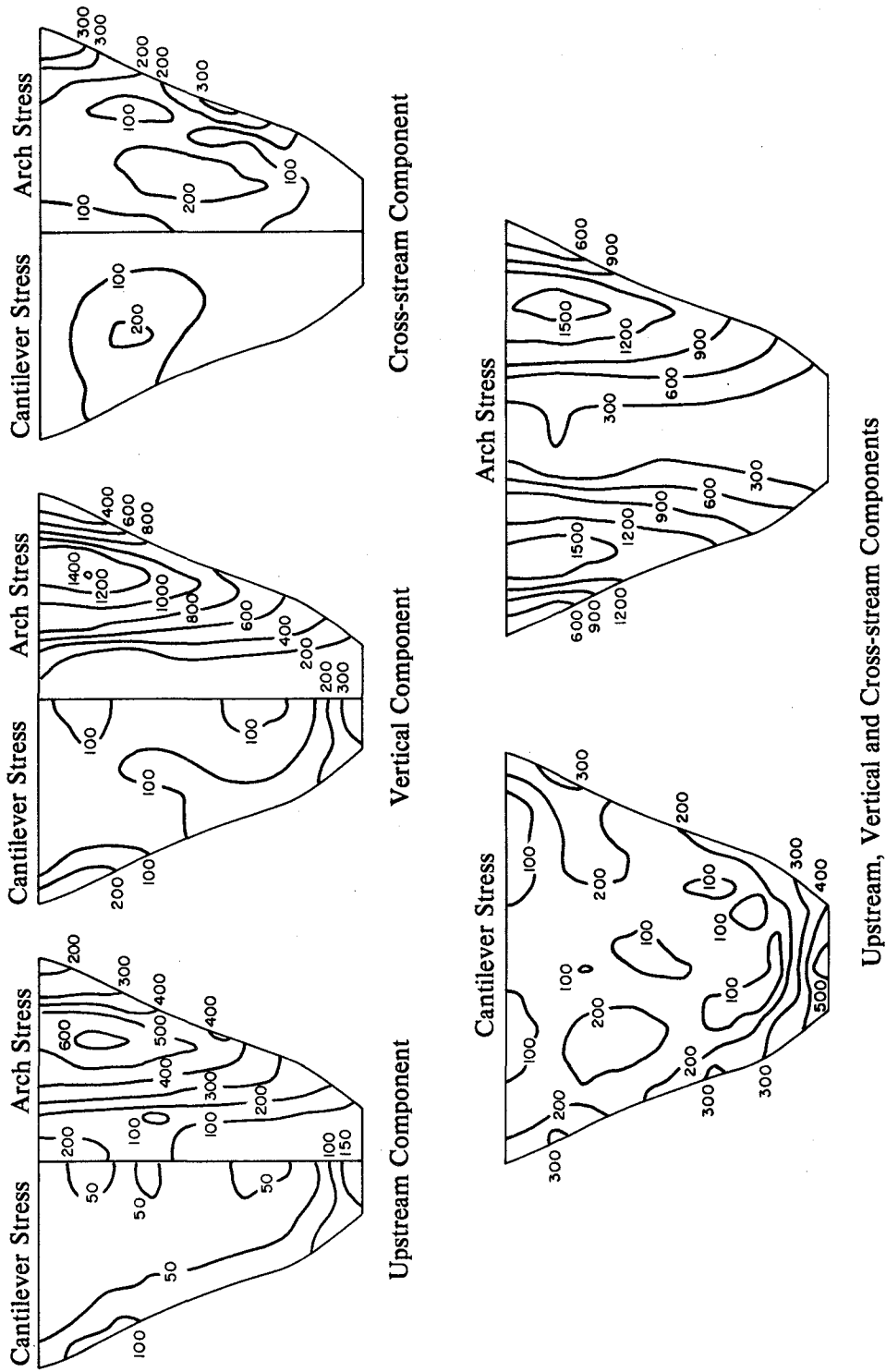


Figure 5.22 Envelope values of maximum tensile stresses (in psi) on downstream face of Morrow Point Dam on rigid foundation rock with full reservoir and rigid reservoir boundary ($\alpha = 1$) due to upstream, vertical and cross-stream components, separately and simultaneously, of Taft ground motion. Initial static stresses are excluded.

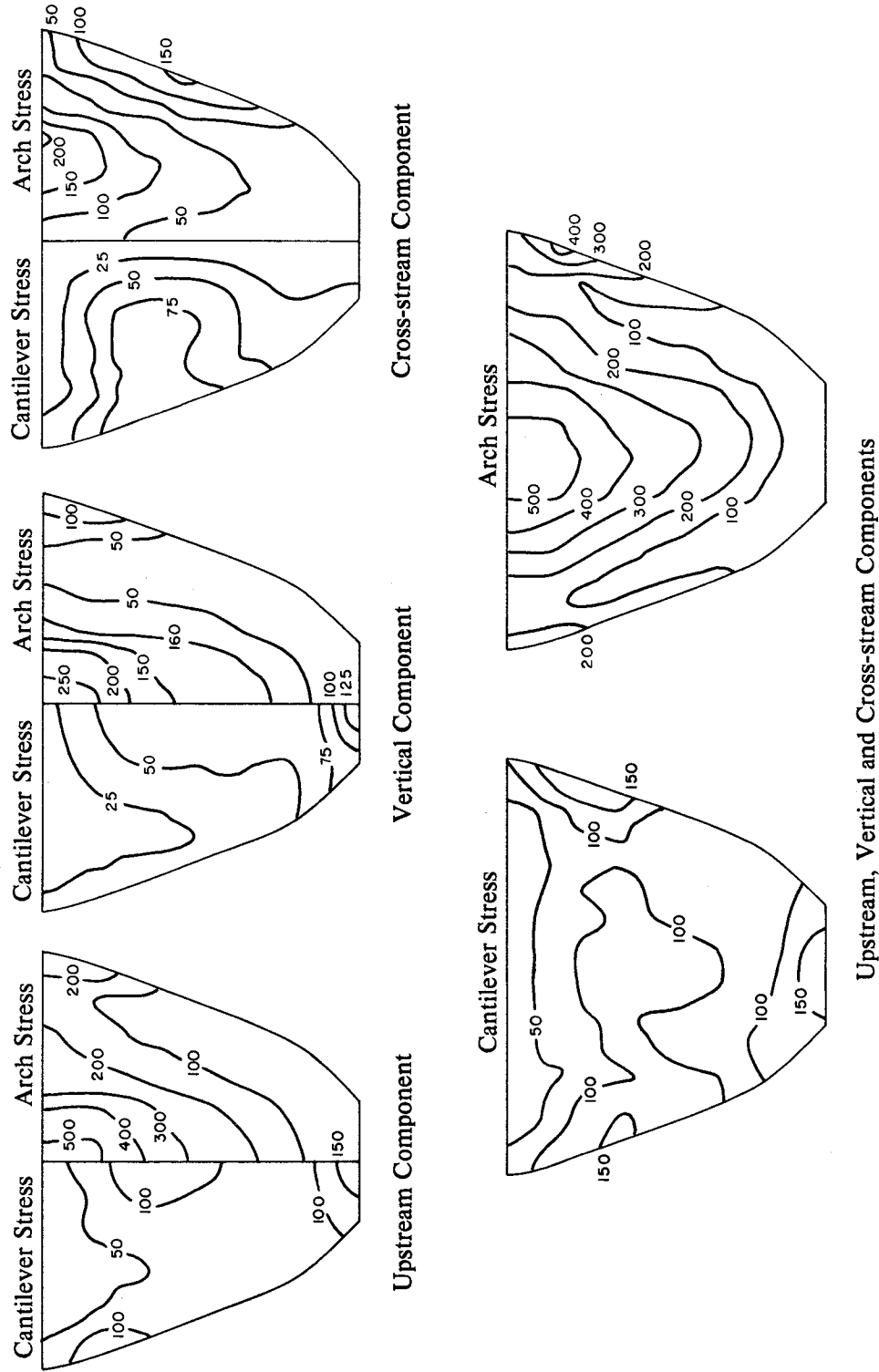


Figure 5.23 Envelope values of maximum tensile stresses (in psi) on upstream face of Morrow Point Dam on rigid foundation rock with full reservoir and absorptive reservoir boundary ($\alpha = 0.5$) due to upstream, vertical and cross-stream components, separately and simultaneously, of Taft ground motion. Initial static stresses are excluded.

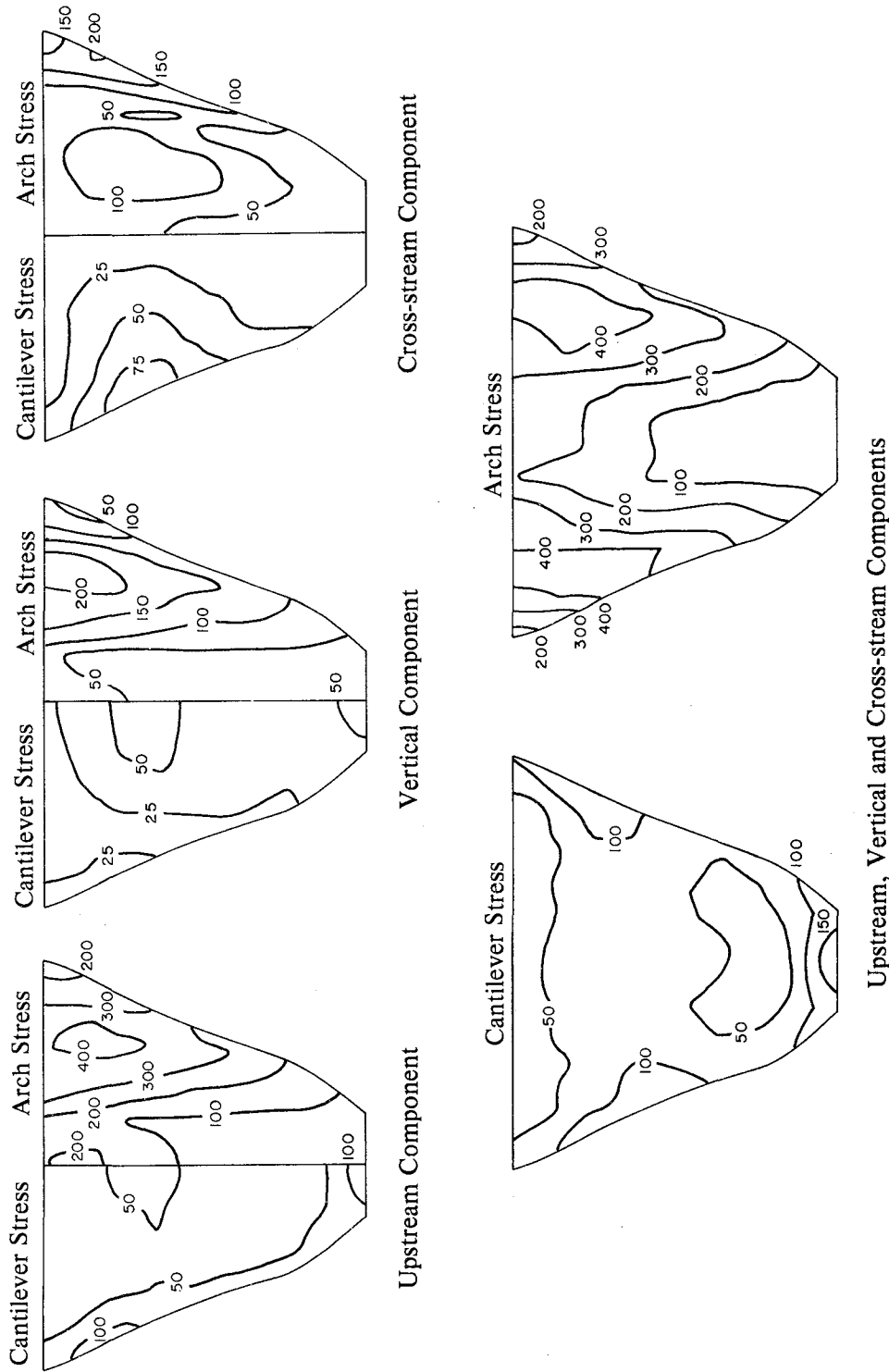


Figure 5.24 Envelope values of maximum tensile stresses (in psi) on downstream face of Morrow Point Dam on rigid foundation rock with full reservoir and absorptive reservoir boundary ($\alpha = 0.5$) due to upstream, vertical and cross-stream components, separately and simultaneously, of Taft ground motion. Initial static stresses are excluded.

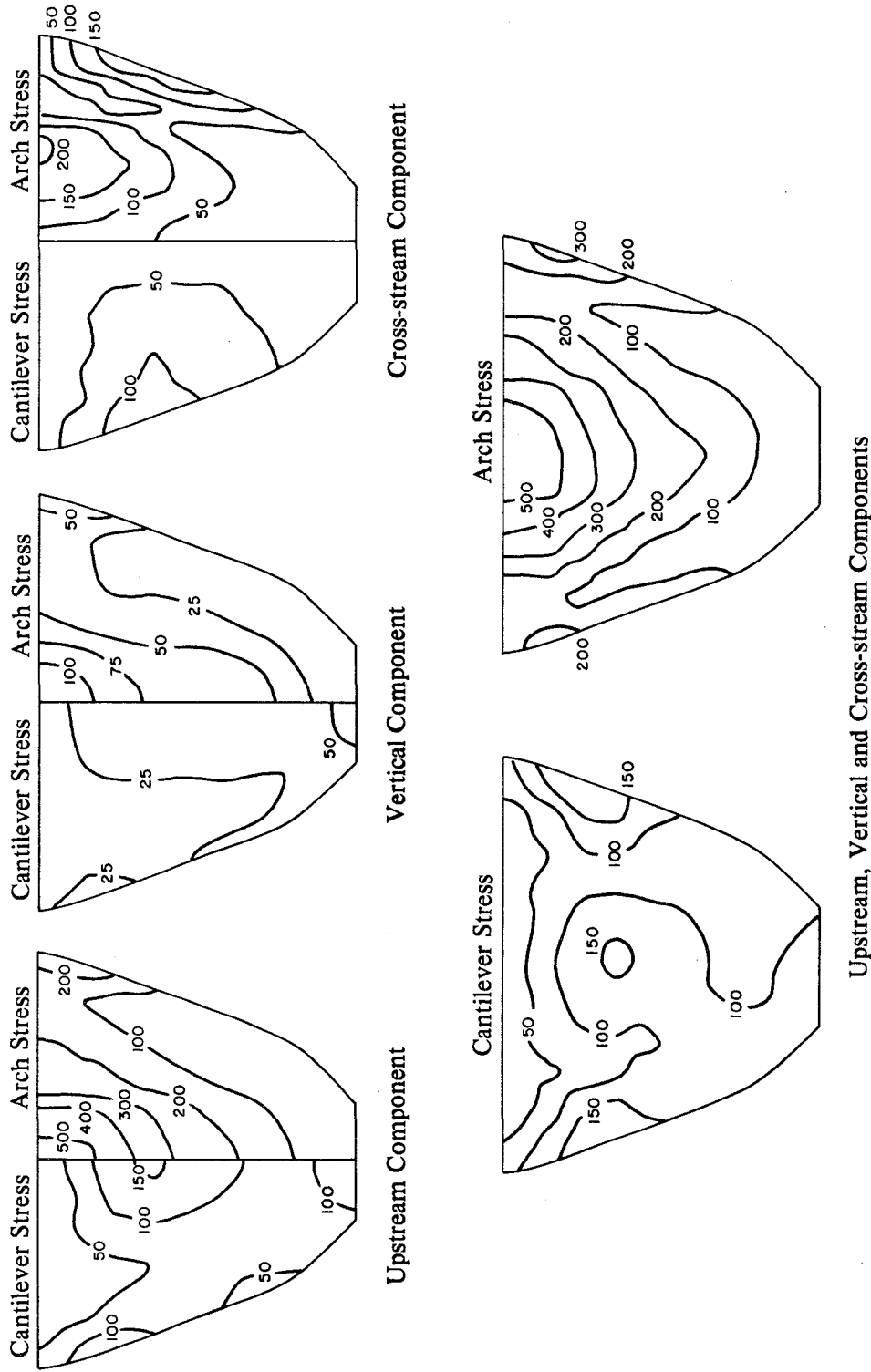


Figure 5.25 Envelope values of maximum tensile stresses (in psi) on upstream face of Morrow Point Dam on rigid foundation rock with full reservoir and absorptive reservoir boundary ($\alpha = 0$) due to upstream, vertical and cross-stream components, separately and simultaneously, of Taft ground motion. Initial static stresses are excluded.

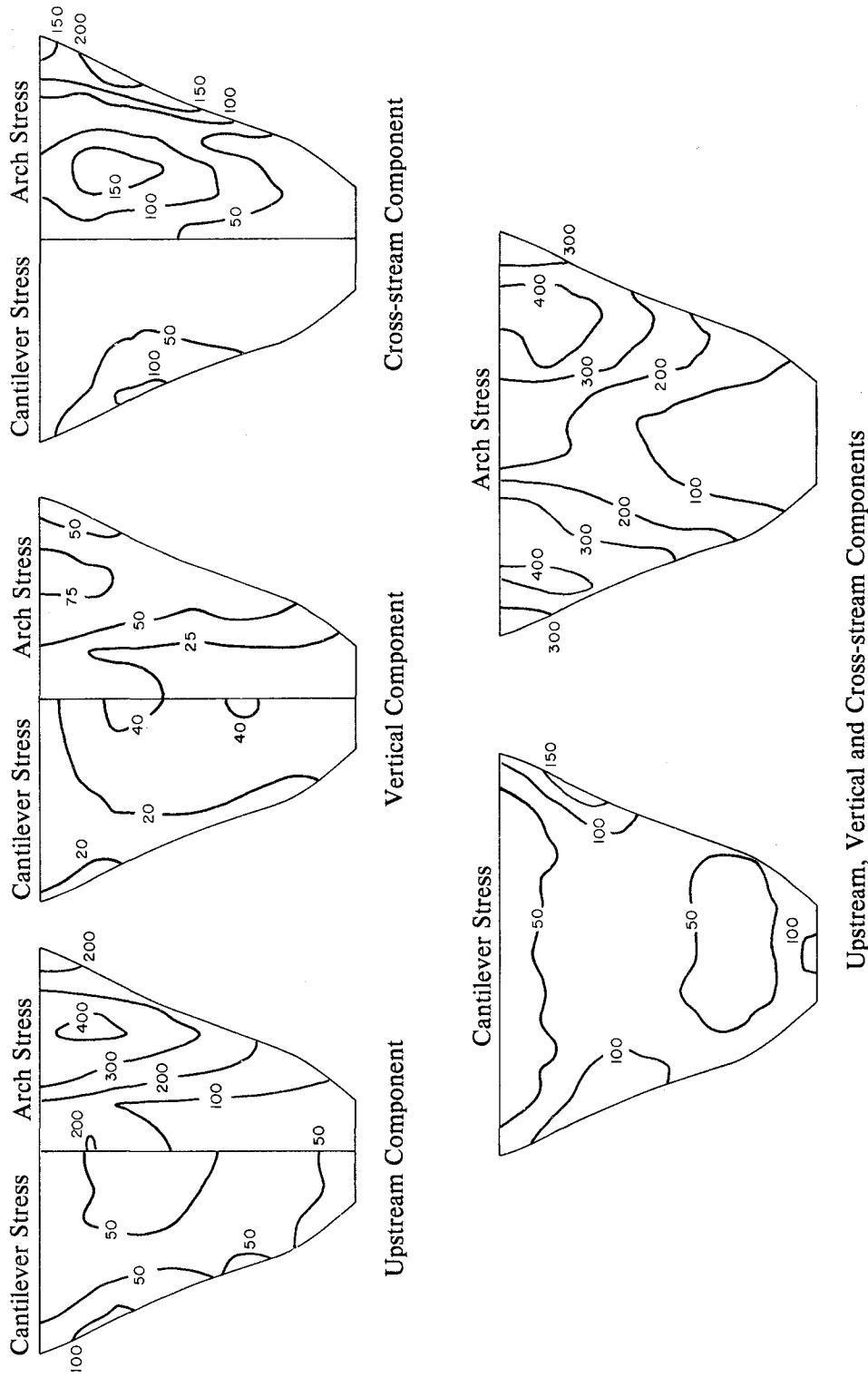


Figure 5.26 Envelope values of maximum tensile stresses (in psi) on downstream face of Morrow Point Dam on rigid foundation rock with full reservoir and absorptive reservoir boundary ($\alpha = 0$) due to upstream, vertical and cross-stream components, separately and simultaneously, of Taft ground motion. Initial static stresses are excluded.

rock. If the reservoir is empty, the contribution of the response to the vertical component is very small whether the foundation rock is rigid [Figure 5.17(a) for crest displacement and Figures 5.19 and 5.20 for stresses] or flexible [Figure 5.27(a) for crest displacement and Figures 5.29 and 5.30 for stresses]; and the contribution of the response to cross-stream ground motion is generally smaller than that due to upstream ground motion whether the foundation rock is rigid [Figure 5.17(a) for crest displacement and Figures 5.19 and 5.20 for stresses] or flexible [Figure 5.27(a) for crest displacement and Figures 5.29 and 5.30 for stresses].

For dams with impounded water, however, the main implication of the phase difference between the responses to the three components of ground motion is that the contribution to the maximum response from the vertical component may not be as significant as noted earlier from the dam responses to the individual ground motion components. For example, if the reservoir boundary is absorptive with $\alpha = 0.5$, the increase of the maximum stresses in the dam with full reservoir is not as large (Figures 5.23 and 5.24 for rigid foundation rock and Figures 5.33 and 5.34 for flexible foundation rock) as would be expected from the significant stresses due to vertical component alone. However, when the reservoir boundary is rigid, the response to the vertical component is so large that it dominates the total response irrespective of the phase differences among responses to the individual components [Figures 5.17(b), 5.21 and 5.22 for rigid foundation rock and Figures 5.27(b), 5.31 and 5.32 for flexible foundation rock].

The most important implication of these response results and their interpretation is that the assumption of a rigid reservoir boundary overestimates the significance of the response of the dam to vertical ground motion. The large amplification of response to vertical ground motion for excitation frequencies equal to the natural vibration frequencies of the infinite uniform channel of the reservoir predicted by the assumption of a rigid reservoir boundary are unlikely because of the alluvium and sediments invariably present at the reservoir boundary. An absorptive reservoir boundary that models the alluvium and sediments gives a more realistic estimate of the earthquake response of concrete arch dams, especially of the response to vertical ground motion and its contribution to the total dynamic response.

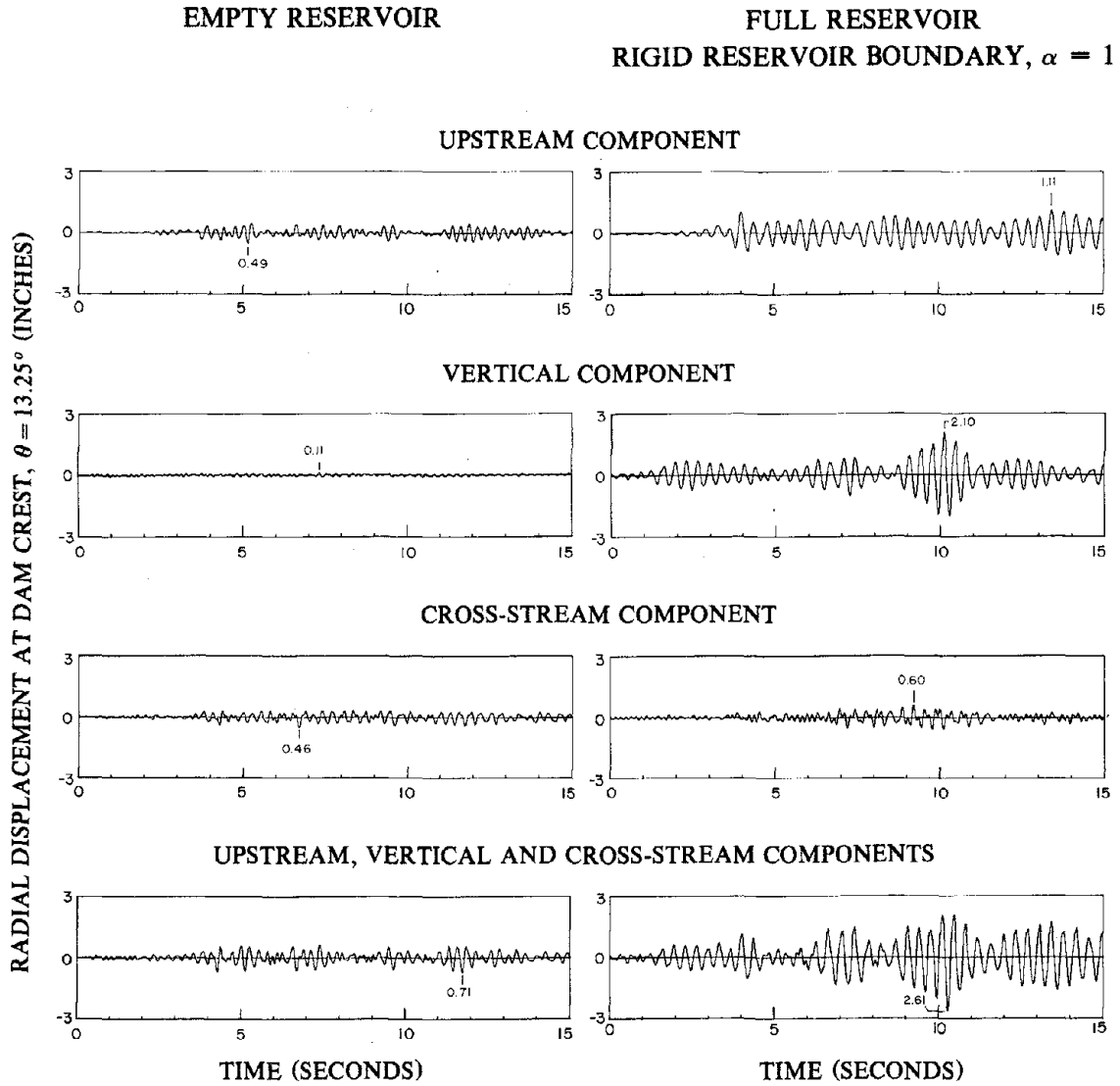


Figure 5.27 Displacement response of Morrow Point Dam on flexible foundation rock due to upstream, vertical and cross-stream components, separately and simultaneously, of Taft ground motion: (i) empty reservoir, and (ii) full reservoir with rigid reservoir boundary ($\alpha = 1$).

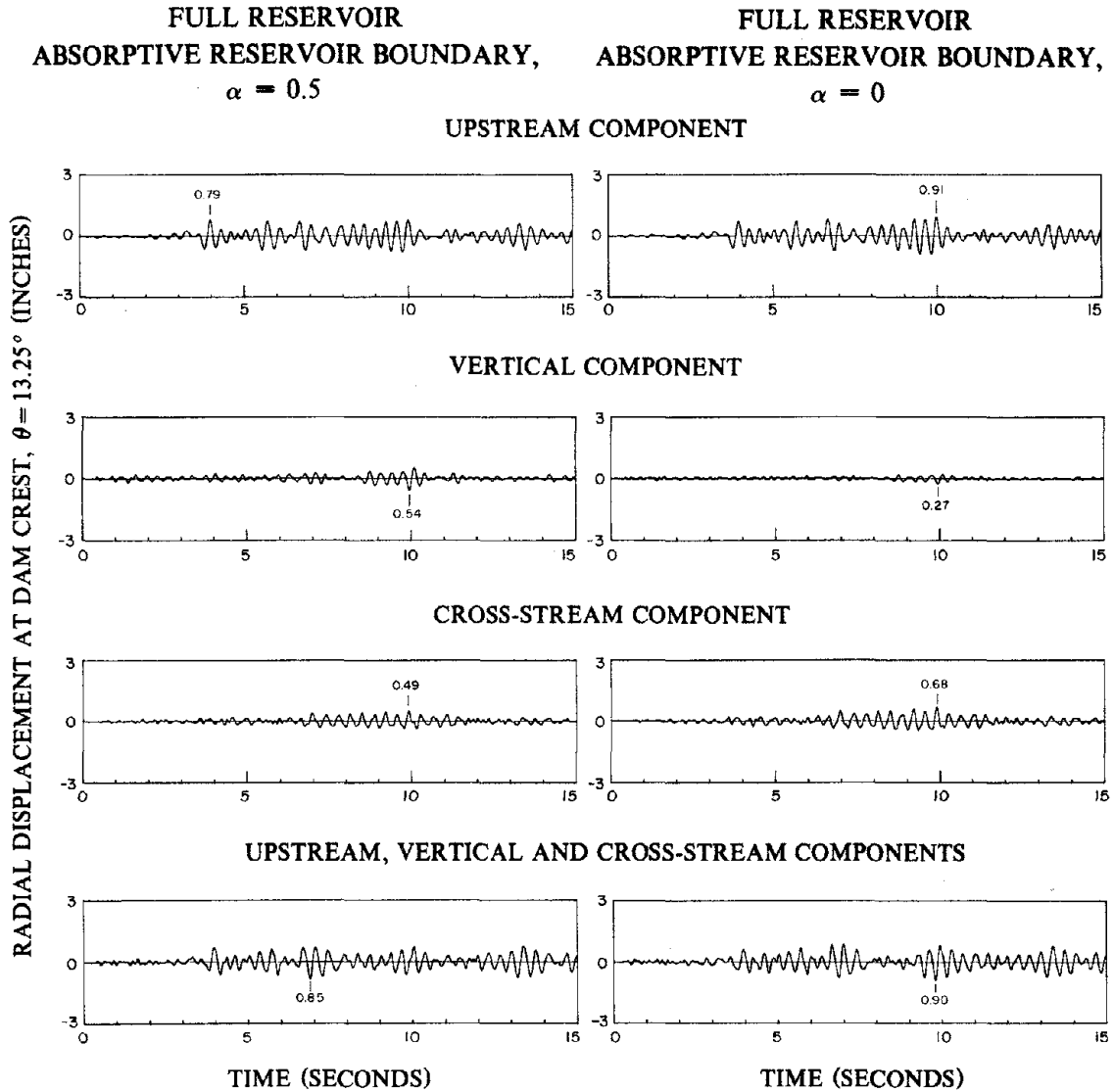


Figure 5.28 Displacement response of Morrow Point Dam on flexible foundation rock with full reservoir and absorptive reservoir boundary due to upstream, vertical and cross-stream components, separately and simultaneously, of Taft ground motion: (i) $\alpha = 0.5$, and (ii) $\alpha = 0$.

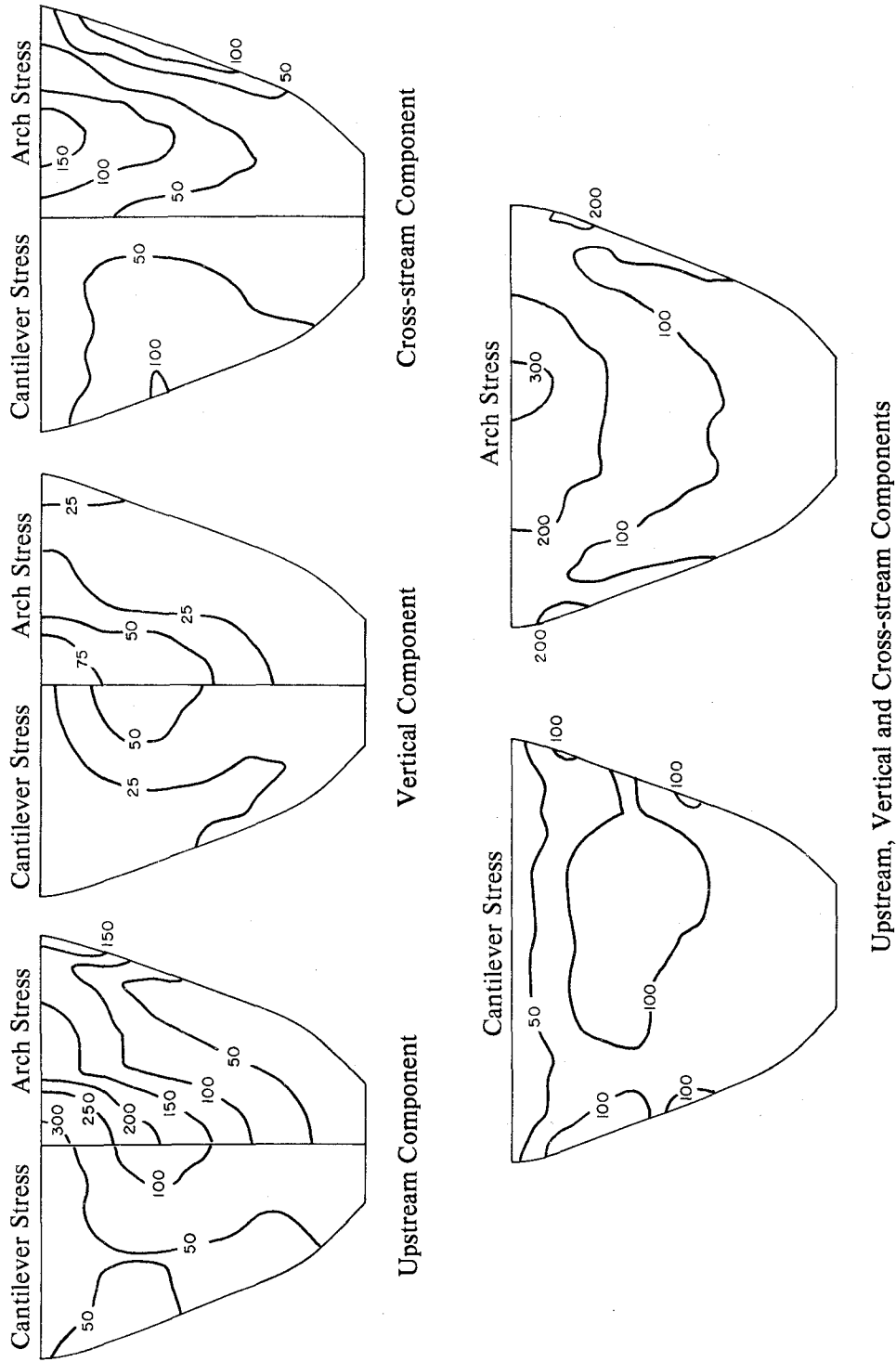


Figure 5.29 Envelope values of maximum tensile stresses (in psi) on upstream face of Morrow Point Dam on flexible foundation rock with empty reservoir due to upstream, vertical and cross-stream components, separately and simultaneously, of Taft ground motion. Initial static stresses are excluded.

Upstream, Vertical and Cross-stream Components

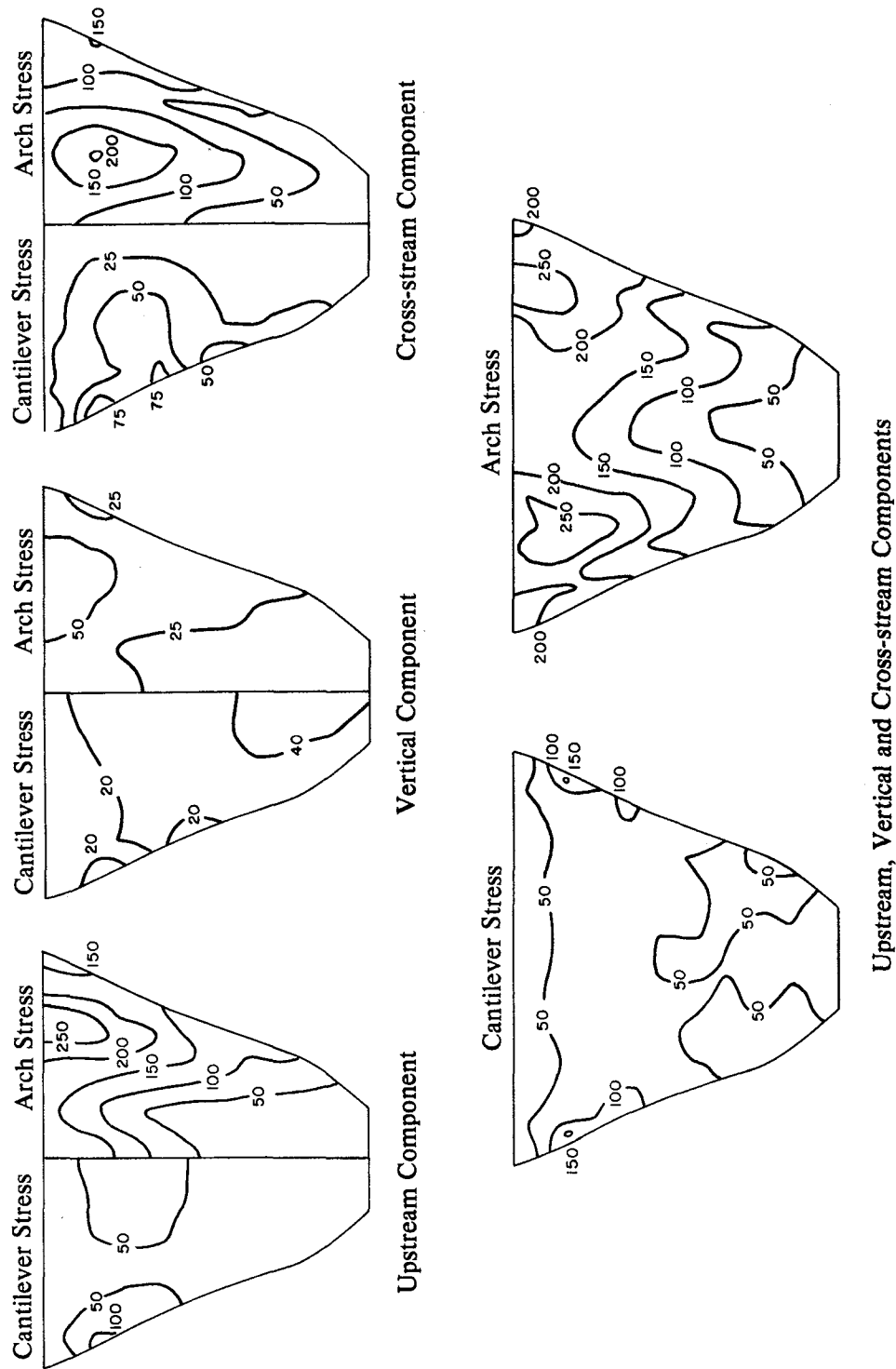


Figure 5.30 Envelope values of maximum tensile stresses (in psi) on downstream face of Morrow Point Dam on flexible foundation rock with empty reservoir due to upstream, vertical and cross-stream components, separately and simultaneously, of Taft ground motion. Initial static stresses are excluded.

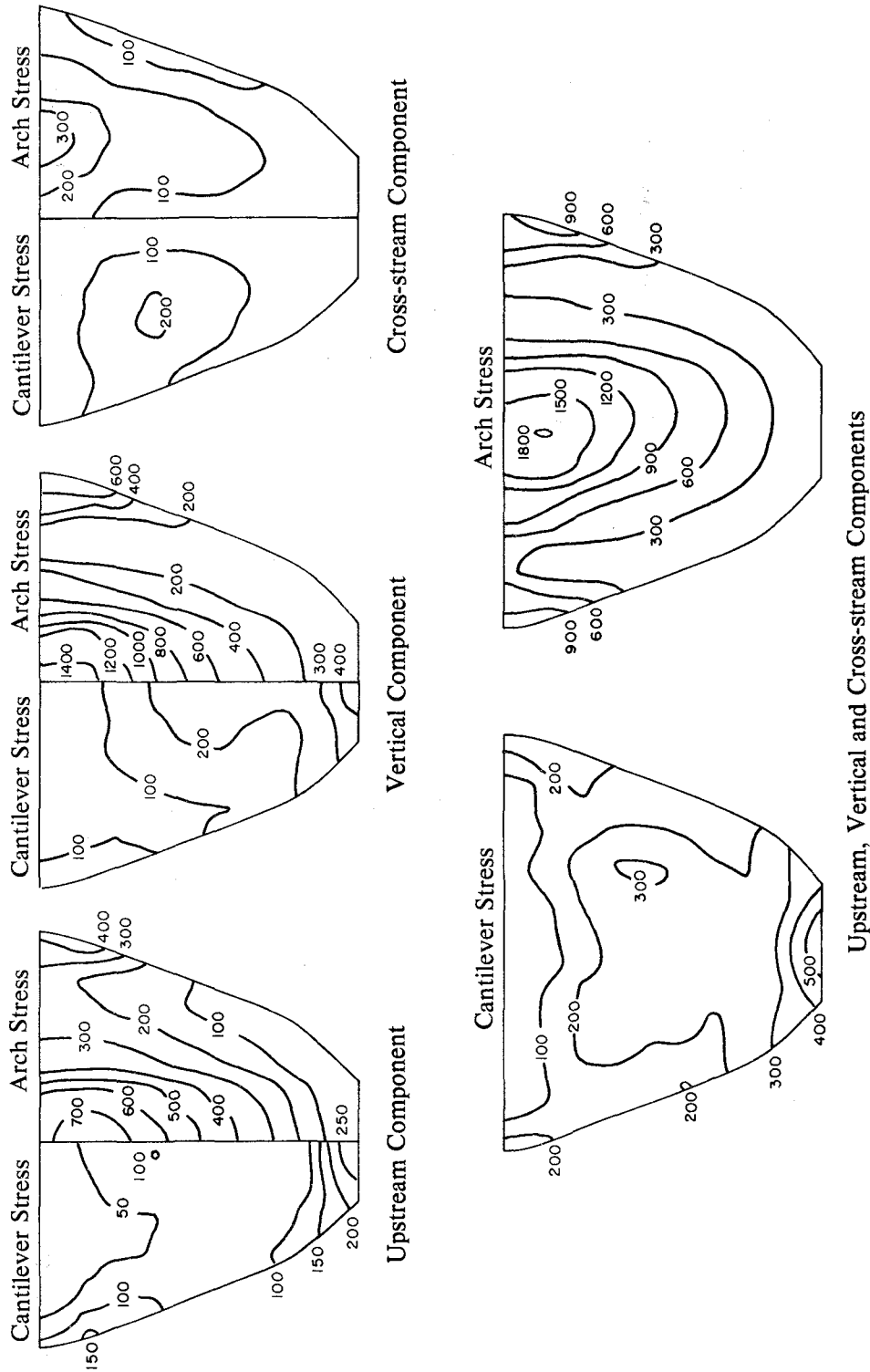


Figure 5.31 Envelope values of maximum tensile stresses (in psi) on upstream face of Morrow Point Dam on flexible foundation rock with full reservoir and rigid reservoir boundary ($\alpha = 1$) due to upstream, vertical and cross-stream components, separately and simultaneously, of Taft ground motion. Initial static stresses are excluded.

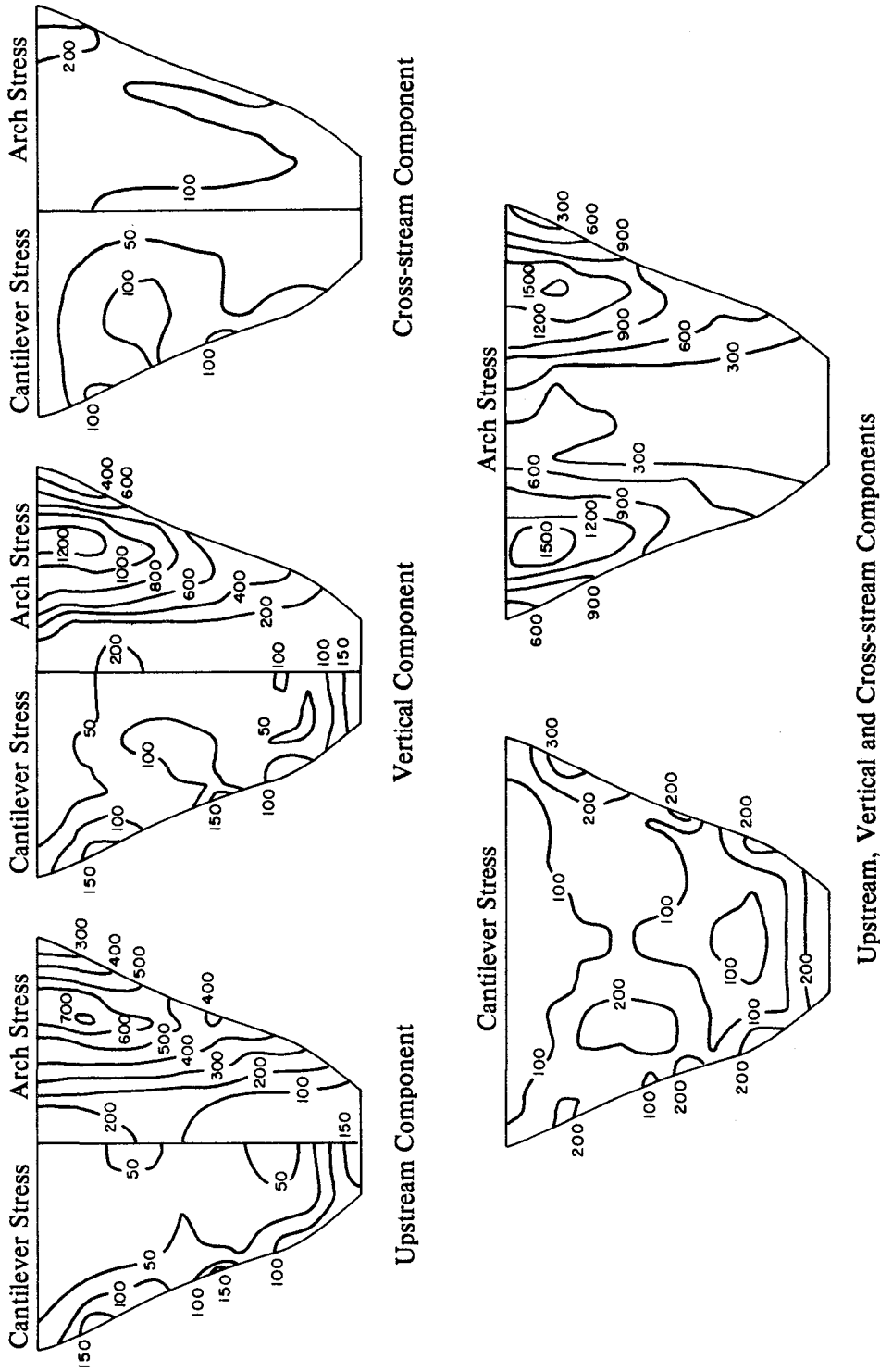


Figure 5.32 Envelope values of maximum tensile stresses (in psi) on downstream face of Morrow Point Dam on flexible foundation rock with full reservoir and rigid reservoir boundary ($\alpha = 1$) due to upstream, vertical and cross-stream components, separately and simultaneously, of Taft ground motion. Initial static stresses are excluded.

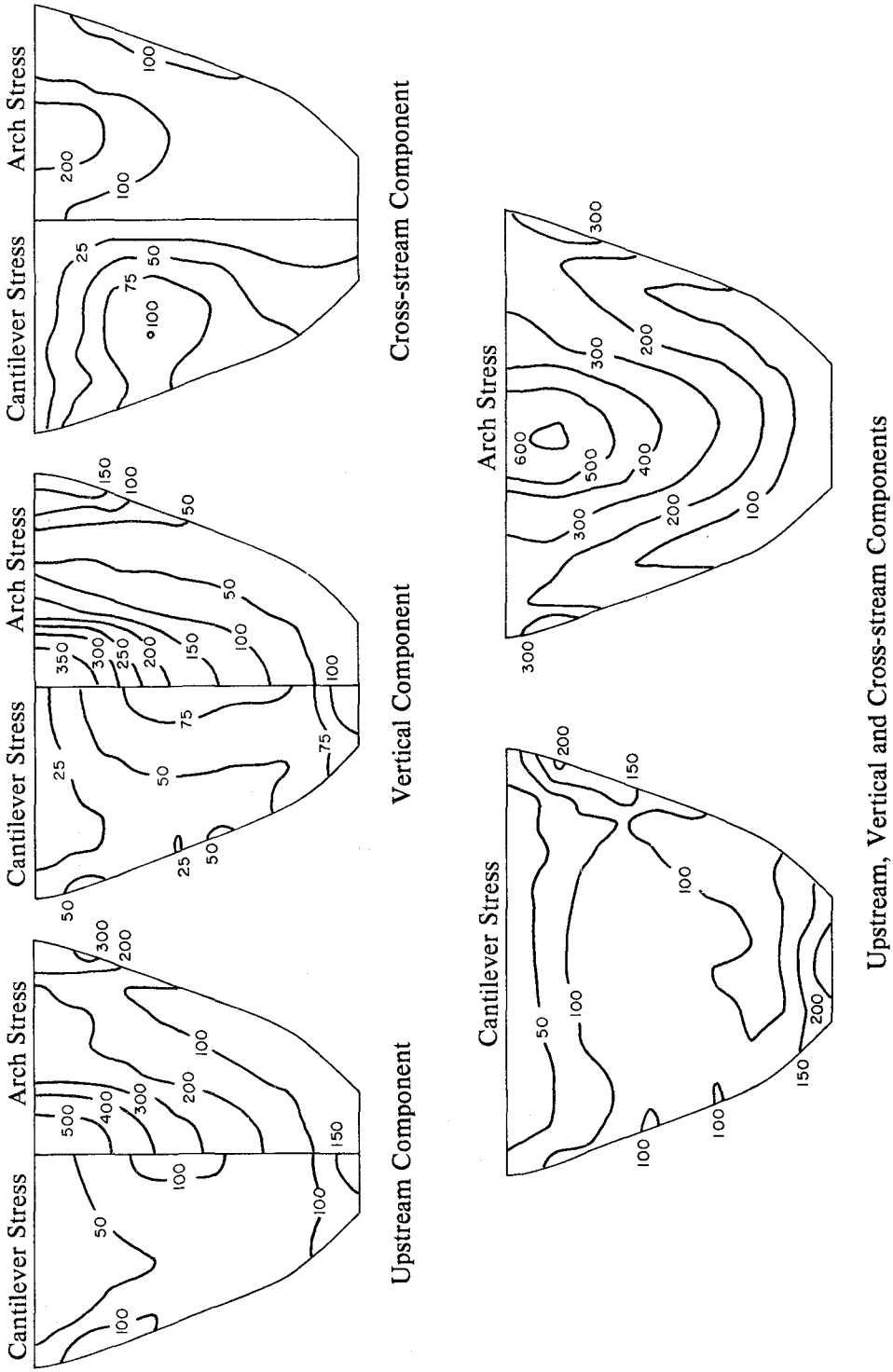


Figure 5.33 Envelope values of maximum tensile stresses (in psi) on upstream face of Morrow Point Dam on flexible foundation rock with full reservoir and absorptive reservoir boundary ($\alpha = 0.5$) due to upstream, vertical and cross-stream components, separately and simultaneously, of Taft ground motion. Initial static stresses are excluded.

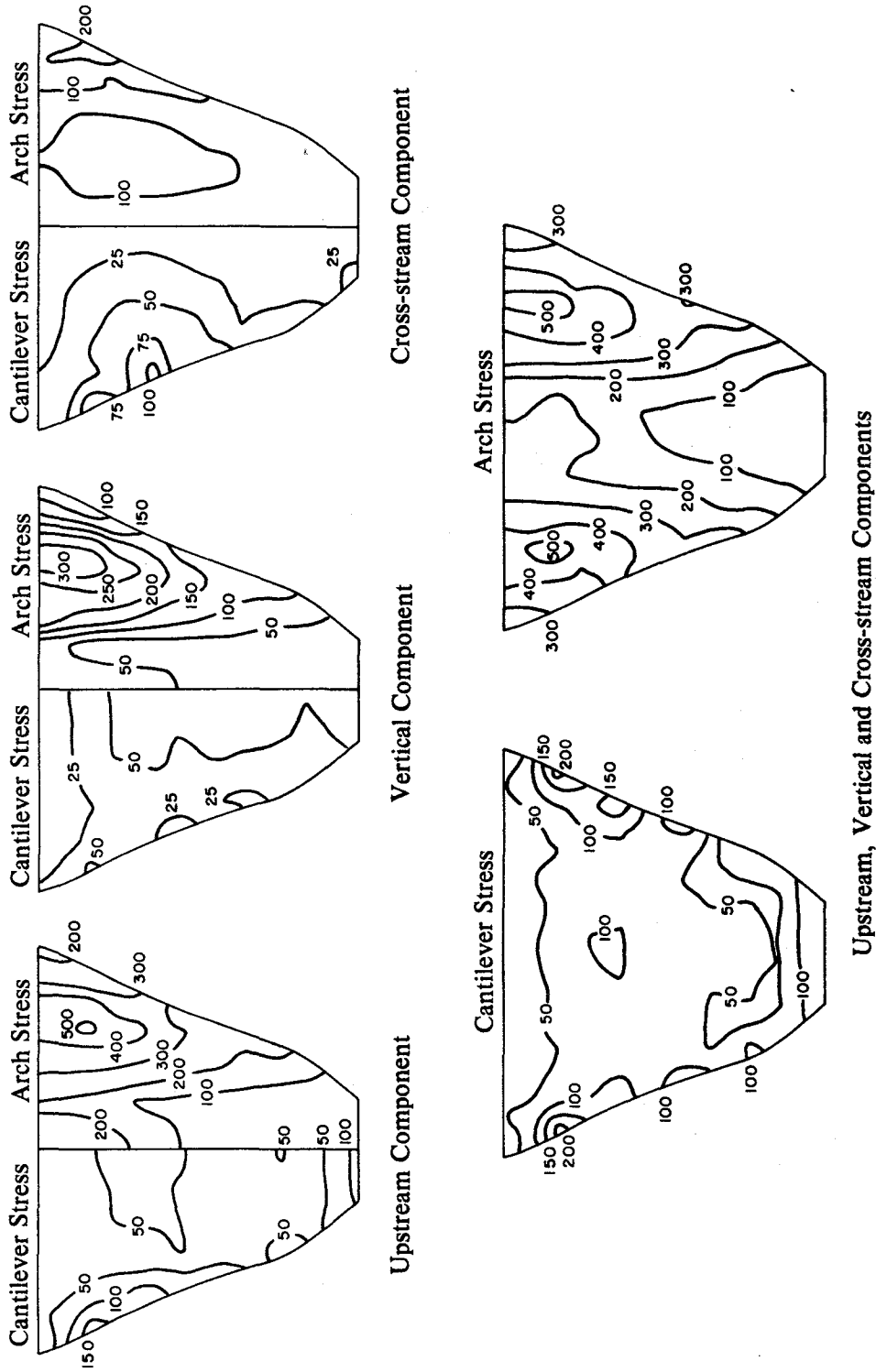


Figure 5.34 Envelope values of maximum tensile stresses (in psi) on downstream face of Morrow Point Dam on flexible foundation rock with full reservoir and absorptive reservoir boundary ($\alpha = 0.5$) due to upstream, vertical and cross-stream components, separately and simultaneously, of Taft ground motion. Initial static stresses are excluded.

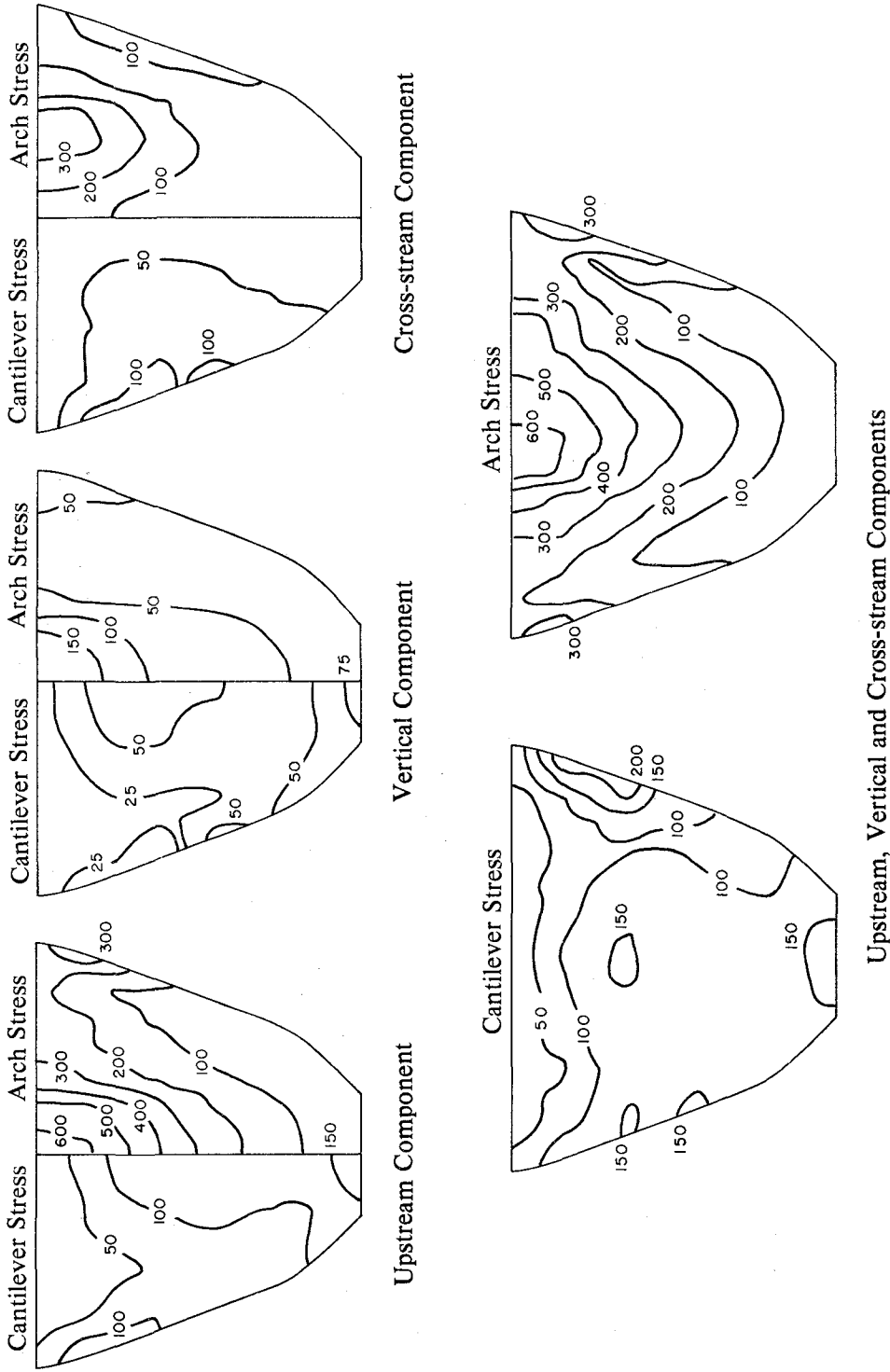


Figure 5.35 Envelope values of maximum tensile stresses (in psi) on upstream face of Morrow Point Dam on flexible foundation rock with full reservoir and absorptive reservoir boundary ($\alpha = 0$) due to upstream, vertical and cross-stream components, separately and simultaneously, of Taft ground motion. Initial static stresses are excluded.

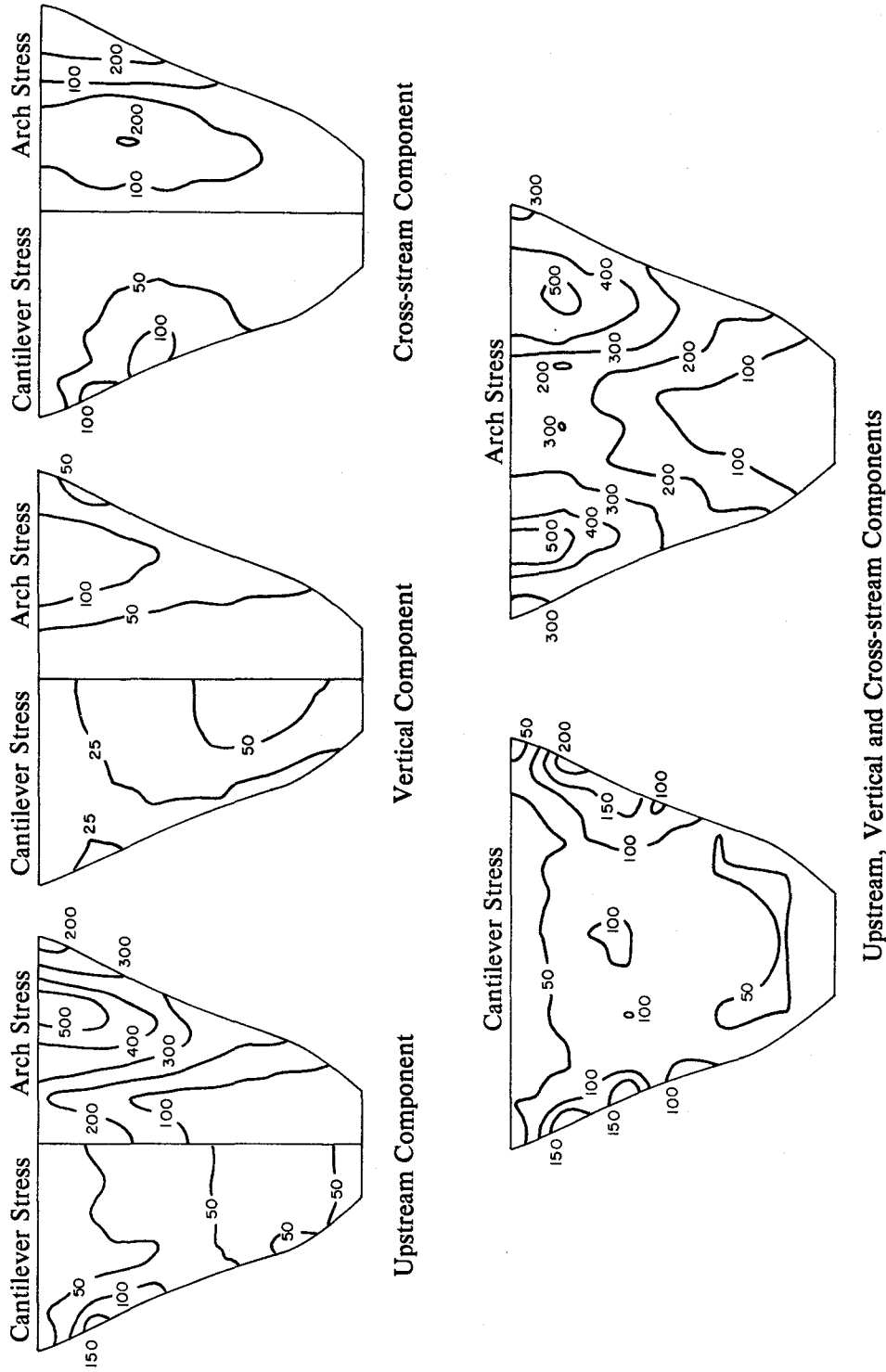


Figure 5.36 Envelope values of maximum tensile stresses (in psi) on downstream face of Morrow Point Dam on flexible foundation rock with full reservoir and absorptive reservoir boundary ($\alpha = 0$) due to upstream, vertical and cross-stream components, separately and simultaneously, of Taft ground motion. Initial static stresses are excluded.

5.8 Practical Earthquake Analysis of Arch Dams

The analytical procedure and computer program is very efficient in obtaining the earthquake response results presented in the preceding sections. Therefore, it is an effective tool in the design of new arch dams and in the evaluation of the safety of existing arch dams. However, in such practical application, the effects of the static loads should be included into the earthquake response of the dam to the three components of ground motion considering dam-water interaction, reservoir boundary absorption, and foundation rock flexibility.

A complete analysis of the response of Morrow Point Dam due to its weight, the hydrostatic pressure and the simultaneous action of the S69E, vertical, and S21W components of Taft ground motion was performed. A wave reflection coefficient $\alpha = 0.5$ at the reservoir boundary was selected. Figure 5.37 shows the time history of radial, vertical, and tangential displacements at nodal points 44 and 60 located at the dam crest, and at nodal points 1 and 13 located at the dam-foundation rock interface [Figure 2.3(a)]. Figure 5.38 shows the time history of arch and cantilever stresses on the upstream face at stress points 1 and 10 and on the downstream face at stress points 31 and 53 [Figure 2.3(a)]. Figure 5.39 shows the distribution of envelope values of the maximum arch and cantilever stresses on the upstream and downstream faces of the dam. Such stress results, which include the stresses due to the static loads, aid in identifying areas in the dam that may crack during an earthquake.

The computation time required for a complete earthquake analysis of this selected dam is shown as Case 7 in Table 5.4. Also included in Table 5.4 are the computation times required for response analyses of the dam under alternative assumptions for the effects of impounded water, foundation rock and the reservoir boundary materials. The additional computation time required to consider dam-water interaction is significant because of the complications associated with the evaluation of hydrodynamic terms for three-dimensional fluid domains. Also consideration of foundation rock flexibility in the analysis increases the computational time because of the additional effort required for computing the foundation-rock stiffness matrix, the additional DOF at the dam-foundation rock interface, and the larger number of generalized coordinates required. In earlier analyses [9], the

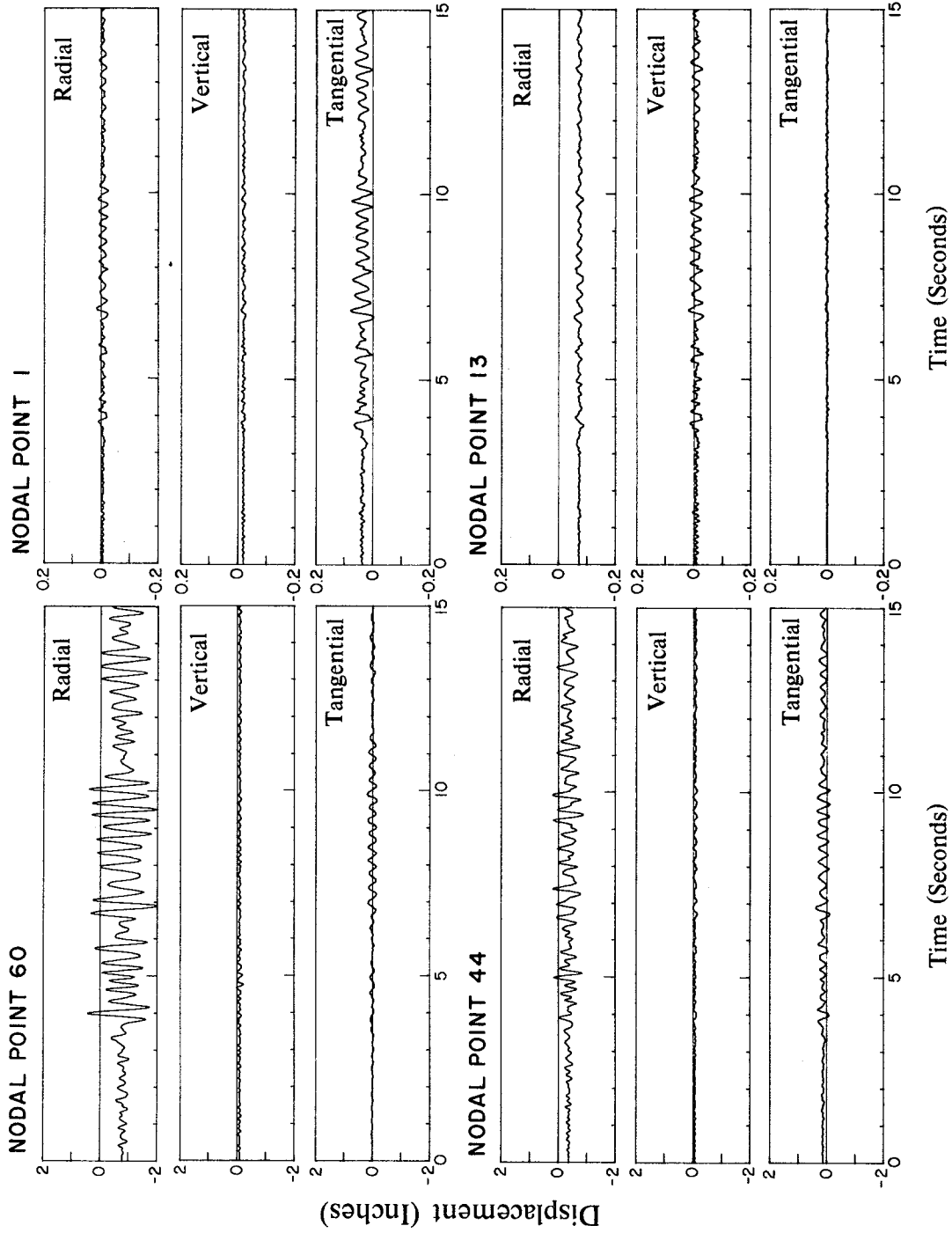


Figure 5.37 Displacement response of Morrow Point Dam on flexible foundation rock with full reservoir and absorptive reservoir boundary ($\alpha = 0.5$) due to upstream, vertical, and cross-stream components, simultaneously, of Taft ground motion.

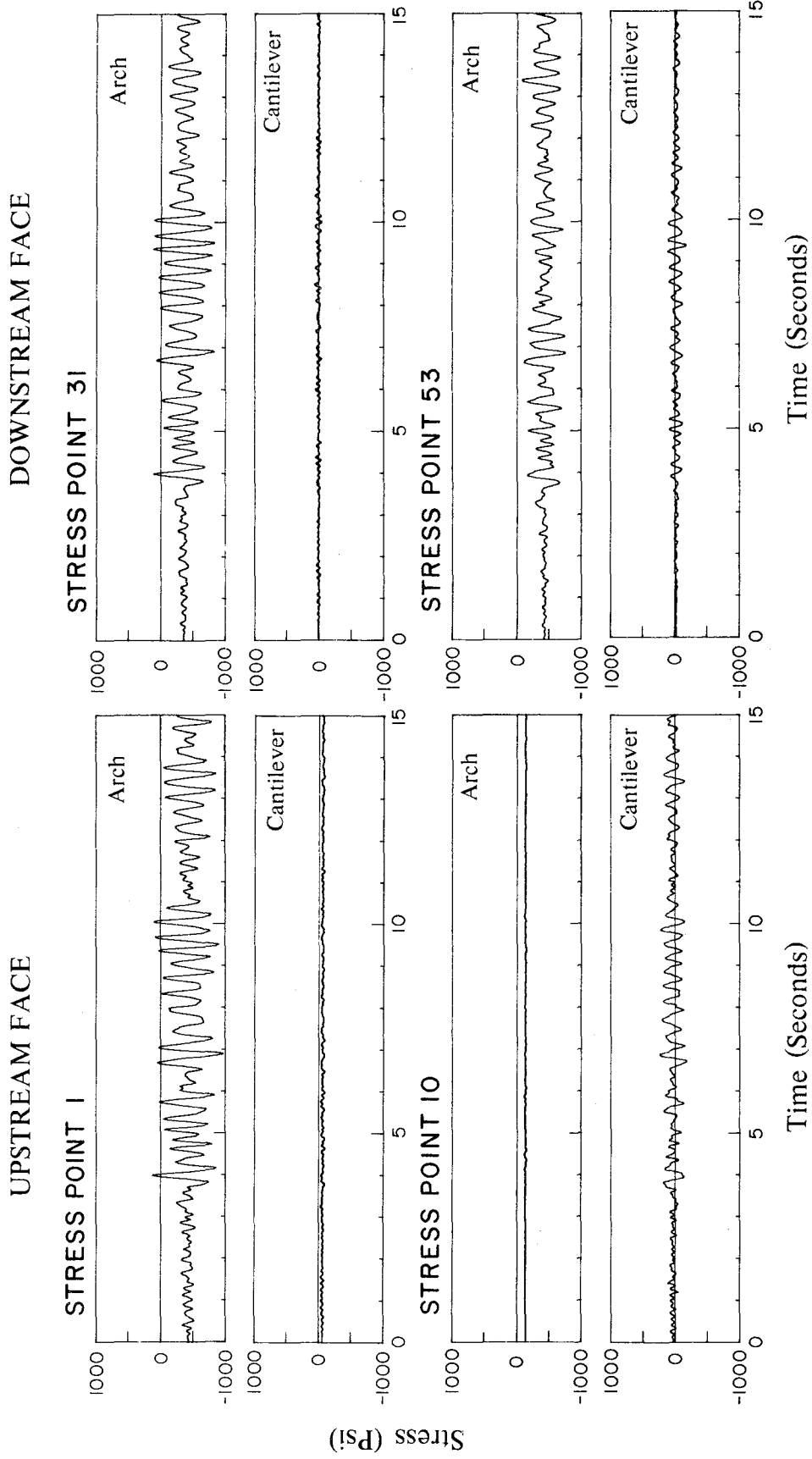


Figure 5.38 Stress response of Morrow Point Dam on flexible foundation rock with full reservoir and absorptive reservoir boundary ($\alpha = 0.5$) due to upstream, vertical, and cross-stream components, simultaneously, of Taft ground motion.

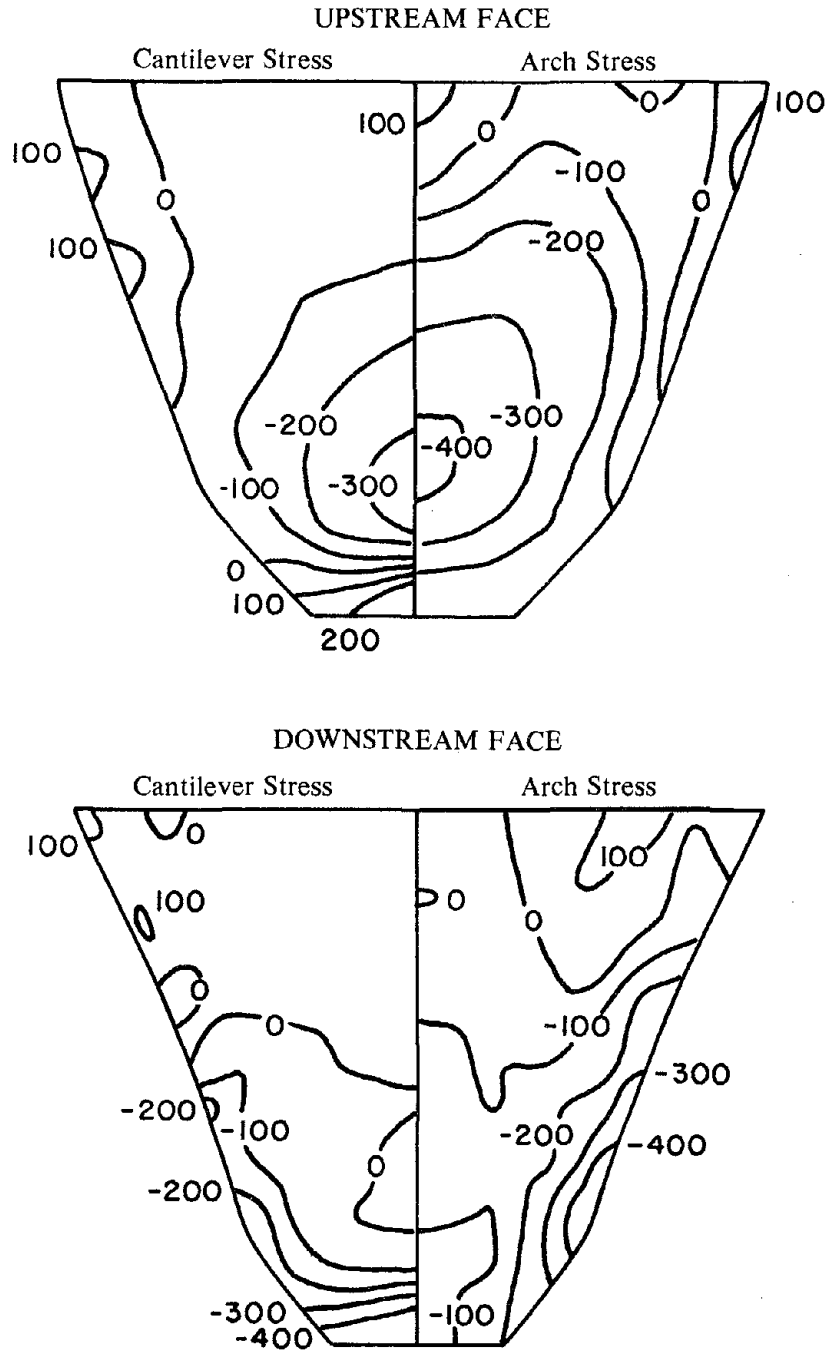


Figure 5.39 Envelope values of maximum arch and cantilever stresses (in psi) in Morrow Point Dam on flexible foundation rock with full reservoir and absorptive reservoir boundary ($\alpha = 0.5$) due to upstream, vertical, and cross-stream components, simultaneously, of Taft ground motion. Initial static stresses are included.

Table 5.4 -- Computation Times for Complete Analysis of
Morrow Point Dam to Upstream, Vertical and Cross-stream Components,
Simultaneously, of Taft Ground Motion

Case	Foundation Rock	Water	Reservoir Boundary	No. of Generalized Coordinates	Central Processor Time* (sec)		
					Efficient	Standard	Ratio
1	rigid	empty	-	12	47	47	100%
2	rigid	full	rigid	12	152	544	28%
3-4	rigid	full	absorptive	12	113	892	13%
5	flexible†	empty	-	18	113	113	100%
6	flexible†	full	rigid	18	249	652	38%
7-8	flexible†	full	absorptive	18	204	993	21%

* CDC 7600 Computer

† Foundation rock region shown in Figure 2.3(b) with $R_f = H_s$

computational effort increased by a factor of 7 to 8 to include wave absorption at reservoir boundary. However, the efficient evaluation of hydrodynamic terms developed in this work, the interpolation of the frequency response functions, and more efficient computer programming make it possible to include this effect without any increase in the computational effort. For Cases 2, 3, 4, 6, 7, and 8 of Table 5.4 wherein dam-water interaction effects are considered, the total computational time required by the efficient procedure presented in Section 3.5 varies between 13 % and 38 %, approximately, of that required in the standard procedure (see also Section 3.5).

6. CONCLUSIONS

The earlier analytical procedure [5,9] to evaluate the steady-state response of arch dams to harmonic ground motion, including the effects of impounded water and of alluvium and sediments usually found at the bottom and sides of the reservoir, has been extended to consider the flexibility of the foundation rock and to include Fourier synthesis of harmonic responses to obtain earthquake responses. In addition, this earlier analytical procedure has been improved by incorporating more efficient analytical formulations and computational procedures for evaluating the hydrodynamic terms. Moreover, rational expressions are used as interpolating functions for the frequency response functions for the generalized coordinates of the dam-foundation system, thus reducing the number of frequency points at which a response function must be computed exactly. As a result of these improvements, the computational costs for analyzing arch dams have been reduced by an order of magnitude. Thus, the resulting analytical procedure and computer program described in Chapter 3 is an effective tool for computing the earthquake response of proposed designs for new arch dams and in evaluating the seismic safety of existing dams.

Utilizing this analytical procedure, the effects of dam-water interaction, reservoir boundary absorption, and foundation-rock flexibility on the response of a selected arch dam to harmonic ground motion have been investigated. The results for the frequency response functions presented for a wide range of system parameters lead to the following conclusions:

1. The hydrodynamic pressures and hence forces on a rigid dam are significantly influenced by water compressibility and reservoir boundary absorption. With a rigid (non-absorptive) reservoir boundary, the hydrodynamic force is unbounded due to harmonic vertical or cross-stream ground motions with excitation frequency equal to one of the natural frequencies, ω_n^{is} of the symmetric modes, or ω_n^{ia} of the antisymmetric modes, of the infinite uniform channel, respectively; however, the force due to upstream ground motion is finite at ω_n^{is} . Reservoir boundary absorption eliminates the unbounded peaks of the frequency response function at ω_n^{is} or ω_n^{ia} , and generally smoothens the frequency response curve.

2. Dam-water interaction reduces the fundamental resonant frequency of the dam to $\tilde{\omega}_r$, a value below both ω_1 and ω_1^i , the fundamental natural frequencies of the dam (on rigid foundation rock without water) and of the infinite uniform channel. These are the frequencies associated with the symmetric vibration modes in the case of upstream or vertical ground motion, or with the antisymmetric modes in case of cross-stream ground motion.* Dam-water interaction increases the fundamental resonant peak due to upstream or vertical ground motion because of an added hydrodynamic force which is in-phase with the effective earthquake inertial force, but decreases that due to cross-stream ground motion because of a subtracted hydrodynamic force which is opposite-phase with the effective earthquake inertial force. At higher excitation frequencies, energy radiation due to propagation of hydrodynamic pressure waves in the upstream direction reduces the response of the dam to below that for the dam with an empty reservoir, for all three components of ground motion.
3. Reservoir boundary absorption generally reduces the fundamental resonant response due to upstream or vertical ground motion, because it reduces the added hydrodynamic force and introduces an added damping; but it slightly increases the fundamental resonant response to cross-stream ground motion because it reduces the subtracted hydrodynamic force. It also reduces the unbounded peaks in the frequency response function at excitation frequencies equal to ω_n^i for vertical and cross-stream ground motion, and generally smoothens the response curve. At excitation frequencies greater than ω_1^i , the radiation of energy through upstream propagation of hydrodynamic pressure waves dominates the energy radiation into the absorptive reservoir boundary materials, thus reducing their effect.
4. The effects of water compressibility on the fundamental resonant response of the dam become smaller with increasing flexibility of the dam. However, the effects of reservoir

* The superscripts *S* and *a* are dropped in this and subsequent statements if they are valid for both symmetric and antisymmetric modes.

boundary absorption on dam response are not properly represented by analyses neglecting water compressibility, although such an analysis provides a good approximation to the fundamental resonant frequency $\tilde{\omega}_r$.

5. Foundation-rock flexibility affects the frequency response functions for the dam in a simpler manner than does dam-water interaction. It reduces the resonant frequencies of the dam, and increases the fundamental resonant peak with narrower bandwidth.
6. Dam-water interaction lengthens the vibration periods of the dam, especially for the vibration period associated with the fundamental symmetrical mode. Its effect is very small when the reservoir is less than half full, but increases rapidly with water depth thereafter. Foundation-rock flexibility has little effect on the percentage increase in vibration period due to dam-water interaction, especially if the reservoir is close to full.
7. The effects of dam-water interaction on the dam response to any of the three ground motion components are qualitatively similar for rigid and flexible foundation rock, whether the reservoir boundary is absorptive or not, because dam-water interaction effects generally dominate those of foundation-rock flexibility. In particular, the effects of reservoir boundary absorption on dam response are about the same whether the foundation rock is rigid or flexible.
8. Dam-water interaction lengthens the vibration period of the fundamental symmetrical mode of the arch dam more than that of a gravity dam because the added hydrodynamic mass has more effect on the mass of the slender arch dam than of the massive gravity dam. Dam-water interaction lengthens the period of the fundamental antisymmetrical vibration mode of an arch dam to a lesser degree than the symmetrical vibration mode of the arch dam or a gravity dam. Foundation-rock flexibility, on the other hand, lengthens the vibration period of the fundamental symmetrical or antisymmetrical mode of the arch dam less than that of the gravity dam, because dam-foundation rock interaction effects are less significant for arch dams because they are less massive compared to gravity dams.

Utilizing the analytical procedure of Chapter 3, the earthquake response of Morrow Point Dam to Taft ground motion was presented in Chapter 5 for a wide range of properties of the reservoir boundary materials and various assumptions for the impounded water and foundation rock. These results lead to the following conclusions:

1. The earthquake response of the dam is increased by dam-water interaction and decreased by reservoir boundary absorption with the magnitude of these effects depending little on the condition of the foundation rock, rigid or flexible, but significantly on the component of ground motion.
2. Both dam-water interaction and reservoir boundary absorption have profound effect on the response of the dam to vertical ground motion, somewhat less in the case of cross-stream ground motion, and least -- although significant -- in the response to upstream ground motion. In general, assuming a rigid (non-absorptive) reservoir boundary leads to unrealistically large response for dams with impounded water, particularly due to vertical ground motion.
3. Dam-water interaction and reservoir boundary absorption have more significant effect on the response of the arch dam than on the response of a gravity dam to both horizontal and vertical components of ground motion. This is because the added hydrodynamic mass, damping, and force have more effect on the response of a slender arch dam than for a massive gravity dam.

Since the effects of dam-water interaction, reservoir boundary absorption, and foundation-rock flexibility depend, in part, on the particular dam and earthquake ground motion, the above conclusions deduced from the computed responses of Morrow Point Dam to Taft ground motion may not apply in their entirety to all arch dams and ground motions. Whereas the detailed observations may be problem dependent, the broad conclusions should apply to many cases.

The response of the selected arch dam to harmonic and earthquake ground motion demonstrates that dam-water interaction, water compressibility, reservoir boundary absorption, and foundation-rock flexibility may significantly affect the earthquake response of arch dams. The earthquake

analysis of arch dams including these effects can be effectively accomplished by the analytical procedure and computer program described in Chapter 3.

REFERENCES

1. R. W. Clough, J. M. Raphael, and S. Mojtahedi, "ADAP - A Computer Program for Static and Dynamic Analysis of Arch Dams," *Report No. EERC 73-14*, Earthquake Engineering Research Center, University of California, Berkeley, June 1973.
2. J. S.-H. Kuo, "Fluid-Structure Interactions: Added Mass Computations for Incompressible Fluid," *Report No. UCB/EERC-82/09*, Earthquake Engineering Research Center, University of California, Berkeley, August 1982.
3. B. Nath, "Hydrodynamic Pressure on Arch Dams -- By a Mapping Finite Element Method," *Earthquake Engineering and Structural Dynamics*, Vol. 9, 1981, pp. 117-131.
4. C. S. Porter and A. K. Chopra, "Dynamic Response of Simple Arch Dams Including Hydrodynamic Interaction," *Report No. UCB/EERC-80/17*, Earthquake Engineering Research Center, University of California, Berkeley, July 1980.
5. J. F. Hall and A. K. Chopra, "Dynamic Analysis of Arch Dams Including Hydrodynamic Effects," *Journal of the Engineering Mechanics Division*, ASCE, Vol. 109, No. EM1, February 1983, pp. 149-167.
6. C. S. Porter and A. K. Chopra, "Dynamic Analysis of Simple Arch Dams Including Hydrodynamic Interaction," *Earthquake Engineering and Structural Dynamics*, Vol. 9, 1981, pp. 573-597.
7. R. Priscu, A. Popovici, L. Ilie, and D. Stematiu, "New Aspects in the Earthquake Analysis of Arch Dams," in *Criteria and Assumptions for Numerical Analysis of Dams*, Ed. by D. N. Naylor, et al., Proceedings of an International Symposium, Swansea, United Kingdom, September 1975, pp. 709-725.
8. C. S. Porter and A. K. Chopra, "Hydrodynamic Effects in Dynamic Response of Simple Arch Dams," *Earthquake Engineering and Structural Dynamics*, Vol. 10, 1982, pp. 417-431.

9. J. F. Hall and A. K. Chopra, "Dynamic Response of Embankment Concrete-Gravity and Arch Dams Including Hydrodynamic Interaction," *Report No. UCB/EERC-80/39*, Earthquake Engineering Research Center, University of California, Berkeley, October 1980.
10. S. F. Pawsey, "The Analysis of Moderately Thick to Thin Shells by the Finite Element Method," *Report No. UC SESM 70-12*, Structural Engineering Laboratory, University of California, Berkeley, August 1970.
11. G. Dasgupta and A. K. Chopra, "Dynamic Stiffness Matrices for Viscoelastic Half Planes," *Journal of the Engineering Mechanics Division*, ASCE, Vol. 105, No. EM5, October 1979, pp. 729-745.
12. J. Lysmer and G. Waas, "Shear Waves in Plane Infinite Structures," *Journal of the Engineering Mechanics Division*, ASCE, Vol. 98, No. EM1, February 1972, pp. 85-105.
13. R. W. Clough, "Nonlinear Mechanisms in the Seismic Response of Arch Dams," presented at the 1980, International Conference on Earthquake Engineering, held at Skopje, Yugoslavia.
14. G. Fenves and A. K. Chopra, "Earthquake Analysis of Concrete Gravity Dams Including Dam-Water-Foundation Rock Interaction and Reservoir Bottom Absorption," *Earthquake Engineering and Structural Dynamics*, Vol. 12, 1984, pp. 663-680.
15. E. Rosenblueth, "Presión Hidrodinámica en Presas Debida a la Aceleración Vertical con Refracción en el Fondo," presented at the 1968, 2nd Congreso Nacional de Ingeniería Sísmica, held at Veracruz, Mexico.
16. R. W. Clough and J. Penzien, *Dynamics of Structures*, McGraw-Hill Book Co., New York, N.Y., 1975.
17. U.S. Dept. of the Interior, Bureau of Reclamation, *Design of Arch Dams*, U.S. Government Printing Office, Denver, Colorado, 1977.
18. J. F. Hall, "An FFT Algorithm for Structural Dynamics," *Earthquake Engineering and Structural Dynamics*, Vol. 10, 1982, pp. 797-811.

19. G. Fenves and A. K. Chopra, "Effects of Reservoir Bottom Absorption and Dam-Water-Foundation Rock Interaction on Frequency Response Functions for Concrete Gravity Dams," *Earthquake Engineering and Structural Dynamics*, Vol. 13, 1985, pp. 13-31.
20. G. Fenves and A. K. Chopra, "Effects of Reservoir Bottom Absorption on Earthquake Response of Concrete Gravity Dams," *Earthquake Engineering and Structural Dynamics*, Vol. 11, 1983, pp. 809-829.
21. A. K. Chopra, "Earthquake Behavior of Reservoir-Dam Systems," *Journal of the Engineering Mechanics Division*, ASCE, Vol. 94, No. EM6, December 1968, pp. 1475-1500.
22. B. N. Parlett, *The Symmetric Eigenvalue Problem*, Prentice-Hall, Inc., Englewood Cliffs, N.J., 1980.
23. F. F. Tajirian, "Impedance Matrices and Interpolation Techniques for 3-D Interaction Analysis by the Flexible Volume Method," *Ph.D. Dissertation*, Department of Civil Engineering, University of California, Berkeley, September 1981.
24. G. Fenves and A. K. Chopra, "Earthquake Analysis and Response of Concrete Gravity Dams," *Report No. UCB/EERC-84/10*, Earthquake Engineering Research Center, University of California, Berkeley, August 1984.
25. A. K. Chopra, P. Chakrabarti, and S. Gupta, "Earthquake Response of Concrete Gravity Dams Including Hydrodynamic and Foundation Interaction Effects," *Report No. UCB/EERC-80/01*, Earthquake Engineering Research Center, University of California, Berkeley, January 1980.

APPENDIX A: NOTATION

$a_g^l(t)$	$l = x, y, z$ l -component of free-field ground acceleration
$A_g^l(\omega)$	Fourier transform of $a_g^l(t)$
b	parameter used in equation (3.40) to determine the frequency increment for interpolation of $\bar{Y}_j^l(\omega)$
B	$= 2D$, horizontal width of a rectangular cross-section of the infinite fluid channel
\mathbf{B}	fluid "damping" matrix for the irregular finite element region, with submatrices \mathbf{B}_{11} , \mathbf{B}_{12} , \mathbf{B}_{21} , and \mathbf{B}_{22} ; where subscripts 1 and 2 refer to subscript-1 and subscript-2 nodal points, respectively
\mathbf{B}^i	fluid "damping" matrix for the finite element idealization of the infinite channel cross-section
C	velocity of pressure waves in water
C_r	velocity of compression waves in the materials at reservoir boundary
C_{ij}	$i = 1, 2, 3, 4$ the four complex constants used in the interpolation equation (3.37) to determine the generalized coordinate $\bar{Y}_j^l(\omega)$
C_{ij}^n	$i = 1, 2, 3, 4$ the four constants C_{ij} used in equation (3.39) to determine the generalized coordinate $\bar{Y}_j^l(\omega)$ in frequency range n
d	duration of free-field ground motion
D	half-width of a rectangular cross-section of the infinite fluid channel
\mathbf{D}	vector of normal accelerations for the irregular fluid finite element region, with sub-vectors \mathbf{D}_1 and \mathbf{D}_2 corresponding to subscript-1 and subscript-2 nodal points, respectively
$\{\mathbf{D}\}_\delta^l$	vector D computed from the rigid-body motion $\epsilon^l(s, r)$ at the upstream face of the dam and $\epsilon^l(s', r')$ at the reservoir boundary
$\{\mathbf{D}\}_j$	vector D computed from the modal acceleration $\phi_j(s, r)$ at the upstream face of the dam

\mathbf{D}^i	vector of normal accelerations for the finite element idealization of the infinite channel cross-section
$\{\mathbf{D}^i\}_0^l$	vector \mathbf{D}^i computed from $\epsilon^l(s',r')$ at the reservoir boundary
$\{\mathbf{D}^i\}_j$	vector \mathbf{D}^i computed from zero boundary accelerations due to the modal acceleration $\phi_j(s,r)$ at the dam-water interface, i.e. a zero vector
E_f	Young's modulus of the foundation rock
E_r	Young's modulus of the materials at reservoir boundary
E_s	Young's modulus of the dam
$\bar{F}_0^l(\omega)$	x component of the total hydrodynamic force acting on half of the dam assumed rigid due to unit harmonic free-field ground motion in the l direction, $l = x, y, z$
F_{st}	x component of the total hydrostatic force acting on half of the dam
g	the acceleration due to gravity
\mathbf{G}	fluid "mass" matrix for the irregular finite element region, with submatrices \mathbf{G}_{11} , \mathbf{G}_{12} , \mathbf{G}_{21} , and \mathbf{G}_{22} ; where subscripts 1 and 2 refer to subscript-1 and subscript-2 nodal points, respectively
\mathbf{G}^i	fluid "mass" matrix for the finite element idealization of the infinite channel cross-section
H	= y coordinate of the free surface of water measured from the base of the dam; also the maximum depth of the water in the infinite channel
H_s	Height of the dam
\mathbf{H}	fluid "stiffness" matrix for the irregular finite element region, with submatrices \mathbf{H}_{11} , \mathbf{H}_{12} , \mathbf{H}_{21} , and \mathbf{H}_{22} ; where subscripts 1 and 2 refer to subscript-1 and subscript-2 nodal points, respectively
\mathbf{H}^i	fluid "stiffness" matrix for the finite element idealization of the infinite channel cross-section
i	= $\sqrt{-1}$
J	number of vibration modes of the dam included in the analysis

\mathbf{k}_c	stiffness matrix of the finite element idealization of the dam
\mathbf{k}_f	stiffness matrix of the finite element idealization of the foundation rock condensed to the dam-foundation interface degrees of freedom
$\tilde{\mathbf{k}}_f$	expanded matrix of \mathbf{k}_f containing \mathbf{k}_f as the only non-zero submatrix
l	= x, y, z , direction of the free-field ground motion
$\mathbf{L}^l(\omega)$	forcing vector of the dam-water-foundation rock system containing terms $L_n^l(\omega)$ defined in equation (3.6)
\mathbf{m}_c	mass matrix of the finite element idealization of the dam
n	inward normal direction at the free surface, upstream dam face or reservoir boundary as illustrated in Figure 3.2
N_ψ	number of eigenvectors of the infinite channel included in the analysis in matrix Ψ
$\bar{p}(x, y, z, \omega)$	frequency response function for the hydrodynamic pressure distribution
$\bar{p}_0^l(s, r, \omega)$	$\bar{p}(x, y, z, \omega)$ at the upstream face of the dam due to boundary condition of equation (3.3)
$\bar{p}_j(s, r, \omega)$	$\bar{p}(x, y, z, \omega)$ at the upstream face of the dam due to boundary condition of equation (3.4)
$\bar{\mathbf{p}}_1(\omega), \bar{\mathbf{p}}_2(\omega)$	vectors of the hydrodynamic pressures $\bar{p}(x, y, z, \omega)$ at subscript-1 and subscript-2 nodal points
$\bar{\mathbf{p}}_0^l(\omega)$	vector of the hydrodynamic pressures $\bar{p}_0^l(s, r, \omega)$
$\bar{\mathbf{p}}_j^f(\omega)$	vector of the hydrodynamic pressures $\bar{p}_j^f(s, r, \omega)$
q	damping coefficient of the reservoir boundary materials
$\bar{\mathbf{Q}}_0^l(\omega)$	hydrodynamic force vector of pressure $\bar{\mathbf{p}}_0^l(\omega)$
$\bar{\mathbf{Q}}_j^f(\omega)$	hydrodynamic force vector of pressure $\bar{\mathbf{p}}_j^f(\omega)$
R_f	radius parameter describing the size of the foundation rock
s, r	spacial coordinates on the upstream dam face boundary of the fluid domain as illustrated in Figure 3.2

s', r'	spacial coordinates on the reservoir boundary as illustrated in Figure 3.2
$Sa(T, \xi_1)$	pseudo-acceleration value of a component of ground motion at period T and damping ratio ξ_1 ; T is the fundamental vibration period, associated with the symmetric mode for x or y ground motion, or associated with the antisymmetric mode for z ground motion; $\xi_1 = \xi_1^x, \xi_1^y, \text{ or } \xi_1^z$ respectively for x, y, or z ground motions
$S(\omega)$	matrix of the dam-water-foundation rock system containing terms $S_{nj}(\omega)$ defined in equation (3.6)
t	time
T_1	fundamental vibration period of the dam on rigid foundation rock with no water; T_1^s and T_1^a denote periods associated with symmetric and antisymmetric modes, respectively
T_n	nth vibration period of the dam on rigid foundation rock with no water
\tilde{T}	fundamental vibration period of the dam on flexible foundation rock including dam-water interaction; \tilde{T}^s and \tilde{T}^a denote periods associated with symmetric and antisymmetric modes, respectively
\tilde{T}_f	fundamental vibration period of the dam on flexible foundation rock with no water; \tilde{T}_f^s and \tilde{T}_f^a denote periods associated with symmetric and antisymmetric modes, respectively
\tilde{T}_r	fundamental vibration period of the dam on rigid foundation rock including dam-water interaction; \tilde{T}_r^s and \tilde{T}_r^a denote periods associated with the symmetric and antisymmetric modes, respectively
\tilde{T}_{nr}	nth vibration period of the dam on rigid foundation rock including dam-water interaction
T_p	stress-displacement transformation matrix for finite element p of the dam
u	distance used in defining the connection surface [Figure 2.7(b)] in the modelling of the foundation-rock region
$v_p(t)$	nodal relative displacement vector for finite element p of the dam
$v_c(t)$	nodal relative displacement vector for the dam
w_s	unit weight of the dam

w_w	unit weight of water
$Y_j^l(t)$	jth generalized coordinate response time function to $a_g^l(t)$
\bar{Y}_{ji}	$= \bar{Y}_j(\Omega_i) = \bar{Y}_j^l(\Omega_i)$; the superscript l is dropped for convenience
$\bar{Y}^l(\omega)$	vector of frequency response of generalized coordinates $\bar{Y}_j^l(\omega)$ of the dam-foundation rock system
α	wave reflection coefficient of the reservoir boundary materials as computed in equation (2.1)
β_1	coefficient describing the static displacement along the crown cantilever due to the dead weight of the dam
β_2	coefficient describing the static displacement along the crown cantilever due to the hydrostatic pressure with a full reservoir
$\gamma_j(\omega)$	square root of the jth eigenvalue of the y-eigenvalue problem of a rectangular section
δ_{nj}	Kronecker delta function
$\delta_k(\omega)$	square root of the kth eigenvalue of the z-eigenvalue problem of a rectangular section; $\delta_k^s(\omega)$ and $\delta_k^a(\omega)$ denote $\delta_k(\omega)$ corresponding to symmetric and antisymmetric eigenfunctions, respectively
$\epsilon^l(s, r)$	function illustrated in Figure 3.2; when represented by $\epsilon^l(s', r')$, it refers to s', r' coordinates
$\zeta_k(z, \omega)$	kth eigenfunction of the z-eigenvalue problem of a rectangular section given by equations (3.20) or (3.22); $\zeta_k^s(z, \omega)$ and $\zeta_k^a(z, \omega)$ denote symmetric and antisymmetric eigenfunctions, respectively
η_s	constant hysteretic damping factor of the dam
$\bar{\mathbf{q}}_2(\omega)$	vector related to $\bar{\mathbf{p}}_2(\omega)$ by equation (3.13)
θ	angle describing the position along the dam crest measured from the x-y plane
κ_n	$= \sqrt{\lambda_n^2 - \frac{\omega^2}{C^2}}$, nth diagonal term in matrix $\mathbf{\kappa}$
$\mathbf{\kappa}$	fluid infinite channel diagonal matrix containing diagonal terms $\kappa_n, n = 1, 2, \dots, N_\psi$

$\lambda_j^2(\omega)$	jth eigenvalue of an infinite fluid channel of an arbitrary section as determined in equation (3.11)
$\lambda_{jk}^2(\omega)$	the eigenvalue of a rectangular section infinite channel given by equation (3.16a)
$\lambda_{jl}^2(\omega), \lambda_{j\mu}^2(\omega)$	jth eigenvalues of the lower and upper bound rectangular sections for an arbitrary section
μ_1	coefficient describing the static arch stress adjacent to the crown cantilever due to the dead weight of the dam
μ_2	coefficient describing the static arch stress adjacent to the crown cantilever due to the hydrostatic pressure with a full reservoir
ν_s	Poisson's ratio for the dam
ν_f	Poisson's ratio for the foundation rock
ξ_1	damping ratio at the fundamental period estimated using the half-power bandwidth method; ξ_1^x , ξ_1^y , and ξ_1^z denote respectively the fundamental damping ratio associated with the x, y, and z ground motions
ρ	mass density of water
ρ_r	mass density of the materials at reservoir boundary
$\sigma_p(l)$	stress vector for finite element p of the dam
$\phi_j(s, r)$	function representing the normal component of the jth mode shape ϕ_j at the dam-water interface
ϕ_j	jth natural mode shape vector of the dam-foundation rock system
ϕ_n^b	subvector of ϕ_n corresponding to the degrees of freedom on the dam-foundation interface
ϕ_n^f	subvector of ϕ_n corresponding to the degrees of freedom on the dam-water interface
$\chi_j(y, \omega)$	jth eigenfunction of the y-eigenvalue problem of a rectangular section given by equation (3.18)
$\psi_{jk}(y, z, \omega)$	the eigenfunction of a rectangular section infinite channel given by equation (3.16b)
ψ_n	nth eigenvector of an infinite fluid channel of an arbitrary section as determined in equation (3.11)

Ψ	matrix containing the N_ψ eigenvectors ψ_n of an infinite fluid channel
ω	frequency
ω^*	frequency interval given by equations (3.36a) or (3.36b) over which the eigenproperties of the infinite channel are linearly interpolated
ω^{**}	frequency at which the fundamental eigenvalue $\lambda_1^2(\omega)$ has reached close to its limiting value at infinite ω
ω_n^i	n th natural frequency of the infinite fluid channel; ω_n^{is} and ω_n^{ia} denote frequencies associated with symmetric and antisymmetric eigenfunctions, respectively
ω_{\max}	maximum frequency in the frequency range of analysis
ω_j	j th natural frequency of the dam on rigid or flexible foundation rock; ω_j^s and ω_j^a denote natural frequencies associated with symmetric and antisymmetric modes, respectively
$\tilde{\omega}$	fundamental natural frequency of the dam on flexible foundation rock including dam-water interaction
$\tilde{\omega}_f$	fundamental natural frequency of the dam on flexible foundation rock with no water
$\tilde{\omega}_r$	fundamental natural frequency of the dam on rigid foundation rock including dam-water interaction
ω_1^{ra}	fundamental natural frequency of the complete reservoir domain (irregular region and infinite channel) associated with the antisymmetric modes
ω_j^{ry}	j th natural frequency of the vertical height H of water of a rectangular section
ω_k^{rz}	k th natural frequency of the horizontal width D of water of a rectangular section
$\Delta\omega$	frequency interval for interpolation of $\bar{Y}^l(\omega)$; $(\Delta\omega)_{\min}$ and $(\Delta\omega)_{\max}$ denote its minimum and maximum values, respectively
Ω_i	i th frequency at which equation (3.5) is solved exactly for subsequent interpolation
1_c^l	$l = x, y, z$ vector containing ones in the positions corresponding to the l translational DOF of the dam, and zeros elsewhere

APPENDIX B: FLUID EIGENVALUE PROBLEM

The two-dimensional, y - z , eigenvalue problem of equation (3.11) for an infinitely long channel cross-section can be represented in continuum form by the following equation [9]:

$$\frac{\partial^2 \psi}{\partial y^2} + \frac{\partial^2 \psi}{\partial z^2} + \lambda^2 \psi = 0 \quad (\text{B.1})$$

where $\psi(y, z, \omega)$ is the eigenfunction (related to the hydrodynamic pressure) and $\lambda^2(\omega)$ is the eigenvalue, subjected to the following boundary conditions:

$$\psi(H, z, \omega) = 0 \quad (\text{B.2a})$$

$$\left[\frac{\partial}{\partial n} - i \omega q \right] \psi(r', \omega) = 0 \quad (\text{B.2b})$$

where $y = H$ represents the free surface of the water inside the infinitely long channel and r' is the spacial coordinate along the reservoir boundary of the channel cross-section (see Figure 3.2).

B.1 Fluid Eigenvalue Problem of a Rectangular Section Channel

For a rectangular section channel of depth H and width $B = 2D$, the eigenvalue problem represented by equations (B.1) and (B.2) can be uncoupled into two, y and z , one-dimensional eigenvalue problems by the separation of variables:

$$\psi(y, z, \omega) = \chi(y, \omega) \zeta(z, \omega) \quad (\text{B.3})$$

Substituting equation (B.3) into equations (B.1) and (B.2) results in the following two sets of equations governing $\chi(y, \omega)$ and $\zeta(z, \omega)$:

(a)

$$\frac{d^2\chi}{dy^2} + \gamma^2\chi = 0 \quad (\text{B.4a})$$

$$\chi(H, \omega) = 0 \quad (\text{B.4b})$$

$$\frac{d\chi}{dy}(0, \omega) = i\omega q \chi(0, \omega) \quad (\text{B.4c})$$

(b)

$$\frac{d^2\zeta}{dz^2} + \delta^2\zeta = 0 \quad (\text{B.5a})$$

$$\frac{d\zeta}{dz}(-D, \omega) = i\omega q \zeta(-D, \omega) \quad (\text{B.5b})$$

$$-\frac{d\zeta}{dz}(D, \omega) = i\omega q \zeta(D, \omega) \quad (\text{B.5c})$$

with the following equation relating the separation constants γ^2 and δ^2 to the eigenvalue λ^2 :

$$\lambda^2(\omega) = \gamma^2(\omega) + \delta^2(\omega) \quad (\text{B.6})$$

Equation (B.4) represents a one-dimensional eigenvalue problem in y with eigenvalue $\gamma^2(\omega)$ and eigenfunction $\chi(y, \omega)$, and equation (B.5) represents a one-dimensional eigenvalue problem in z with eigenvalue $\delta^2(\omega)$ and eigenfunction $\zeta(z, \omega)$.

For the y -eigenvalue problem, the j th eigenfunction, $\chi_j(y, \omega)$, that satisfies equation (B.4a) is of the form:

$$\chi_j(y, \omega) = A_j(\omega)e^{-i\gamma_j(\omega)y} + B_j(\omega)e^{i\gamma_j(\omega)y} \quad (\text{B.7})$$

where $\gamma_j^2(\omega)$ is the j th eigenvalue. Substituting equation (B.7) into equation (B.4c) requires that

$$B_j(\omega) = A_j(\omega) \frac{\gamma_j(\omega) + \omega q}{\gamma_j(\omega) - \omega q} \quad (\text{B.8})$$

With $A_j(\omega)$ chosen as $[\gamma_j(\omega) - \omega q]/2\gamma_j(\omega)$ and substituting equation (B.8) into equation (B.7), the eigenfunction $\chi_j(y, \omega)$ is then given by:

$$\chi_j(y, \omega) = \frac{1}{2\gamma_j(\omega)} \left\{ [\gamma_j(\omega) + \omega q]e^{i\gamma_j(\omega)y} + [\gamma_j(\omega) - \omega q]e^{-i\gamma_j(\omega)y} \right\} \quad (\text{B.9})$$

which is the same as equation (3.18). Boundary condition of equation (B.4b) then yields the following transcendental equation governing the eigenvalue $\gamma_j^2(\omega)$:

$$e^{2i\gamma_j(\omega)H} = -\frac{\gamma_j(\omega) - \omega q}{\gamma_j(\omega) + \omega q} \quad (\text{B.10})$$

which is the same as equation (3.17).

For the z-eigenvalue problem, the kth eigenfunction, $\zeta_k(z, \omega)$, that satisfies equation (B.5a) is of the form similar to equation (B.7):

$$\zeta_k(z, \omega) = A_k(\omega)e^{-i\delta_k(\omega)z} + B_k(\omega)e^{i\delta_k(\omega)z} \quad (\text{B.11})$$

where $\delta_k^2(\omega)$ is the kth eigenvalue. Substituting equation (B.11) into equation (B.5b) requires that:

$$A_k(\omega)e^{i\delta_k(\omega)D}[\delta_k(\omega) + \omega q] = B_k(\omega)e^{-i\delta_k(\omega)D}[\delta_k(\omega) - \omega q] \quad (\text{B.12})$$

Substituting equation (B.11) into equation (B.5c) requires that:

$$A_k(\omega)e^{-i\delta_k(\omega)D}[\delta_k(\omega) - \omega q] = B_k(\omega)e^{i\delta_k(\omega)D}[\delta_k(\omega) + \omega q] \quad (\text{B.13})$$

Comparing equations (B.12) and (B.13) reveals that $A_k(\omega)$ and $B_k(\omega)$ are related by:

$$A_k(\omega) = \pm B_k(\omega) \quad (\text{B.14})$$

which means that $\zeta_k(z, \omega)$ in equation (B.11) is:

$$\zeta_k^s(z, \omega) = \cos[\delta_k^s(\omega)z] \quad \text{when } A_k(\omega) = B_k(\omega) = 1/2 \quad (\text{B.15a})$$

$$\zeta_k^a(z, \omega) = \sin[\delta_k^a(\omega)z] \quad \text{when } A_k(\omega) = -B_k(\omega) = -1/2 \quad (\text{B.15b})$$

which are the same as equations (3.20) and (3.22). Equation (B.15) shows that the eigenfunctions of the z-eigenvalue problem are either symmetric or antisymmetric about the $z = 0$ axis. The superscripts s and a denote respectively the symmetric and antisymmetric eigenfunction and the associated eigenvalue. For the kth symmetric eigenfunction $\zeta_k^s(z, \omega)$, the associated eigenvalue $[\delta_k^s(\omega)]^2$ is governed by equation (B.12) for $A_k(\omega) = B_k(\omega)$, resulting in:

$$e^{2i\delta_k^s(\omega)D} = \frac{\delta_k^s(\omega) - \omega q}{\delta_k^s(\omega) + \omega q} \quad (\text{B.16})$$

which is the same as equation (3.19). The k th eigenvalue, $\left[\delta_k^p(\omega)\right]^2$, associated with the antisymmetric eigenfunction $\zeta_k^p(z, \omega)$, is governed by equation (B.12) for $A_k(\omega) = -B_k(\omega)$, resulting in:

$$e^{2i\delta_k^p(\omega)D} = -\frac{\delta_k^p(\omega) - \omega q}{\delta_k^p(\omega) + \omega q} \quad (\text{B.17})$$

which is the same as equation (3.21).

Therefore, the eigenfunctions ψ and eigenvalues λ^2 of the rectangular section channel are related to the eigenfunctions and eigenvalues of the two one-dimensional eigenvalue problems by rewriting equations (B.3) and (B.6) as:

$$\psi_{jk}(y, z, \omega) = \chi_j(y, \omega)\zeta_k(z, \omega) \quad (\text{B.18a})$$

$$\lambda_{jk}^2(\omega) = \gamma_j^2(\omega) + \delta_k^2(\omega) \quad (\text{B.18b})$$

where the subscript jk for ψ and λ^2 refer to the particular eigenfunction and eigenvalue corresponding to the j th eigenfunction of the y -eigenvalue problem and the k th eigenfunction of the z -eigenvalue problem. Because of the symmetry or antisymmetry of $\zeta_k(z, \omega)$, $\psi_{jk}(y, z, \omega)$ is either symmetric or antisymmetric about the $z = 0$ axis; superscripts s or a can be added to ζ_k , δ_k^2 , ψ_{jk} and λ_{jk}^2 in equation (B.18).

B.2 Boundary Condition at the Absorptive Reservoir Boundary of the Fluid Eigenvalue Problem As the Excitation Frequency Tends to Infinity

The boundary condition at the reservoir boundary of the eigenvalue problem with wave absorption included as given in equation (B.2b) can be rewritten as:

$$\frac{\partial \psi}{\partial n}(r', \omega) = i \omega q \psi(r', \omega) \quad (\text{B.19})$$

As $\omega \rightarrow \infty$, for non-zero q (absorptive reservoir boundary), $\omega q \rightarrow \infty$. In order to maintain the normal gradient of ψ to a finite value on the left hand side of equation (B.19), the value of ψ must vanish at the reservoir boundary so that the product of ωq and ψ is a finite value. That is,

$$\lim_{\omega \rightarrow \infty} \psi(r', \omega) = 0 \quad (\text{B.20})$$

Since the hydrodynamic pressure \bar{p} in the infinite channel is a linear combination of the eigenfunctions ψ [9] [see equation (3.13) at the transmitting plane], equation (B.20) leads to:

$$\lim_{\omega \rightarrow \infty} \bar{p}(s', r', \omega) = 0 \quad (\text{B.21})$$

in the infinite channel. Therefore, as the excitation frequency approaches infinity, the absorptive reservoir boundary behaves like a free surface in this fluid eigenvalue problem.

**APPENDIX C: TWO MODE FREQUENCY RESPONSE FUNCTION FOR
THE DAM-FOUNDATION SYSTEM WITH INCOMPRESSIBLE WATER**

Including only two generalized coordinates of the dam-foundation system in equation (3.5) and neglecting water compressibility, which leads to hydrodynamic terms independent of excitation frequency; equation (3.5) can be written as:

$$\begin{bmatrix} -\omega^2 \bar{M}_1 + (1 + i\eta_s)K_1 - i\eta_s K_{f11} & \omega^2 Q - i\eta_s K_{f12} \\ \omega^2 Q - i\eta_s K_{f12} & -\omega^2 \bar{M}_2 + (1 + i\eta_s)K_2 - i\eta_s K_{f22} \end{bmatrix} \begin{bmatrix} \bar{Y}_1^l(\omega) \\ \bar{Y}_2^l(\omega) \end{bmatrix} = \begin{bmatrix} L_1^l \\ L_2^l \end{bmatrix} \quad (C.1)$$

where $\bar{M}_1, \bar{M}_2, K_1, K_2, K_{f11}, K_{f12}, K_{f22}, Q, L_1^l$, and L_2^l are real constants independent of the excitation frequency and they are defined as:

$$\begin{aligned} \bar{M}_j &= 1 - \{\phi_j^f\}^T \bar{Q}_j^f \\ K_j &= \omega_j^2 \\ K_{fij} &= \{\phi_i^b\}^T \mathbf{k}_f \{\phi_j^b\} = \{\phi_j^b\}^T \mathbf{k}_f \{\phi_i^b\} \\ Q &= \{\phi_1^f\}^T \bar{Q}_2^f = \{\phi_2^f\}^T \bar{Q}_1^f \\ L_j^l &= -\phi_j^T \mathbf{m}_c 1_c^l + \{\phi_j^f\}^T \bar{Q}_0^l \quad i=1,2, \quad j=1,2 \end{aligned} \quad (C.2)$$

Subscripts 1 and 2 in equations (C.1) and (C.2) refer to the two generalized coordinates included. Comparing with equation (3.6), it can be seen that the frequency dependency of the hydrodynamic terms is neglected here.

Equation (C.1) can be solved using Cramer's rule, resulting in the following expressions for $\bar{Y}_1^l(\omega)$ and $\bar{Y}_2^l(\omega)$:

$$\bar{Y}_1^l(\omega) = \frac{\omega^2(L_2^l Q - \bar{M}_2 L_1^l) + (1 + i\eta_s)K_2 L_1^l + i\eta_s(K_{f12} L_2^l - K_{f22} L_1^l)}{\Delta} \quad (\text{C.3a})$$

$$\bar{Y}_2^l(\omega) = \frac{\omega^2(L_1^l Q - \bar{M}_1 L_2^l) + (1 + i\eta_s)K_1 L_2^l + i\eta_s(K_{f12} L_1^l - K_{f11} L_2^l)}{\Delta} \quad (\text{C.3b})$$

where

$$\begin{aligned} \Delta = & \omega^4(\bar{M}_1 \bar{M}_2 - Q^2) - \omega^2[(1 + i\eta_s)(\bar{M}_1 K_2 + \bar{M}_2 K_1) - i\eta_s(\bar{M}_1 K_{f22} + \bar{M}_2 K_{f11} - 2QK_{f12})] \\ & + (1 + i\eta_s)^2 K_1 K_2 - i\eta_s(1 + i\eta_s)(K_1 K_{f22} + K_2 K_{f11}) + \eta_s^2(K_{f12}^2 - K_{f11} K_{f22}) \end{aligned}$$

An observation of equation (C.3) indicates that $\bar{Y}_j^l(\omega)$, $j = 1, 2$, can be expressed in the following form:

$$\bar{Y}_j^l(\omega) = \frac{C_{1j}\omega^2 + C_{2j}}{\omega^4 + C_{3j}\omega^2 + C_{4j}} \quad j = 1, 2 \quad (\text{C.4})$$

which is the same as equation (3.37). The constant C_{1j} is real-valued; and the constants C_{2j} , C_{3j} , and C_{4j} are complex-valued, in which the imaginary parts come from the constant hysteretic damping in the dam represented by the factor η_s . Just like $\bar{Y}_j^l(\omega)$, these constants also depend on the ground motion component, $l = x, y$ or z , but this superscript is dropped for convenience.

EARTHQUAKE ENGINEERING RESEARCH CENTER REPORTS

NOTE: Numbers in parentheses are Accession Numbers assigned by the National Technical Information Service; these are followed by a price code. Copies of the reports may be ordered from the National Technical Information Service, 5285 Port Royal Road, Springfield, Virginia, 22161. Accession Numbers should be quoted on orders for reports (PB --- ---) and remittance must accompany each order. Reports without this information were not available at time of printing. The complete list of EERC reports (from EERC 67-1) is available upon request from the Earthquake Engineering Research Center, University of California, Berkeley, 47th Street and Hoffman Boulevard, Richmond, California 94804.

- UCB/EERC-79/01 "Hysteretic Behavior of Lightweight Reinforced Concrete Beam-Column Subassemblages," by B. Forzani, E.P. Popov and V.V. Bertero - April 1979(PB 298 267)A06
- UCB/EERC-79/02 "The Development of a Mathematical Model to Predict the Flexural Response of Reinforced Concrete Beams to Cyclic Loads, Using System Identification," by J. Stanton & H. McNiven - Jan. 1979(PB 295 875)A10
- UCB/EERC-79/03 "Linear and Nonlinear Earthquake Response of Simple Torsionally Coupled Systems," by C.L. Kan and A.K. Chopra - Feb. 1979(PB 298 262)A06
- UCB/EERC-79/04 "A Mathematical Model of Masonry for Predicting its Linear Seismic Response Characteristics," by Y. Mengi and H.D. McNiven - Feb. 1979(PB 298 266)A06
- UCB/EERC-79/05 "Mechanical Behavior of Lightweight Concrete Confined by Different Types of Lateral Reinforcement," by M.A. Manrique, V.V. Bertero and E.P. Popov - May 1979(PB 301 114)A06
- UCB/EERC-79/06 "Static Tilt Tests of a Tall Cylindrical Liquid Storage Tank," by R.W. Clough and A. Niwa - Feb. 1979 (PB 301 167)A06
- UCB/EERC-79/07 "The Design of Steel Energy Absorbing Restrainers and Their Incorporation into Nuclear Power Plants for Enhanced Safety: Volume 1 - Summary Report," by P.N. Spencer, V.F. Zackay, and E.R. Parker - Feb. 1979(UCB/EERC-79/07)A09
- UCB/EERC-79/08 "The Design of Steel Energy Absorbing Restrainers and Their Incorporation into Nuclear Power Plants for Enhanced Safety: Volume 2 - The Development of Analyses for Reactor System Piping," "Simple Systems" by M.C. Lee, J. Penzien, A.K. Chopra and K. Suzuki "Complex Systems" by G.H. Powell, E.L. Wilson, R.W. Clough and D.G. Row - Feb. 1979(UCB/EERC-79/08)A10
- UCB/EERC-79/09 "The Design of Steel Energy Absorbing Restrainers and Their Incorporation into Nuclear Power Plants for Enhanced Safety: Volume 3 - Evaluation of Commercial Steels," by W.S. Owen, R.M.N. Pelloux, R.O. Ritchie, M. Faral, T. Ohashi, J. Toplosky, S.J. Hartman, V.F. Zackay and E.R. Parker - Feb. 1979(UCB/EERC-79/09)A04
- UCB/EERC-79/10 "The Design of Steel Energy Absorbing Restrainers and Their Incorporation into Nuclear Power Plants for Enhanced Safety: Volume 4 - A Review of Energy-Absorbing Devices," by J.M. Kelly and M.S. Skinner - Feb. 1979(UCB/EERC-79/10)A04
- UCB/EERC-79/11 "Conservatism In Summation Rules for Closely Spaced Modes," by J.M. Kelly and J.L. Sackman - May 1979(PB 301 328)A03
- UCB/EERC-79/12 "Cyclic Loading Tests of Masonry Single Piers; Volume 3 - Height to Width Ratio of 0.5," by P.A. Hidalgo, R.L. Mayes, H.D. McNiven and R.W. Clough - May 1979(PB 301 321)A08
- UCB/EERC-79/13 "Cyclic Behavior of Dense Course-Grained Materials in Relation to the Seismic Stability of Dams," by N.G. Banerjee, H.B. Seed and C.K. Chan - June 1979(PB 301 373)A13
- UCB/EERC-79/14 "Seismic Behavior of Reinforced Concrete Interior Beam-Column Subassemblages," by S. Viathanatepa, E.P. Popov and V.V. Bertero - June 1979(PB 301 326)A10
- UCB/EERC-79/15 "Optimal Design of Localized Nonlinear Systems with Dual Performance Criteria Under Earthquake Excitations," by M.A. Bhatti - July 1979(PB 80 167 109)A06
- UCB/EERC-79/16 "OPTDYN - A General Purpose Optimization Program for Problems with or without Dynamic Constraints," by M.A. Bhatti, E. Polak and K.S. Pister - July 1979(PB 80 167 091)A05
- UCB/EERC-79/17 "ANSR-II, Analysis of Nonlinear Structural Response, Users Manual," by D.P. Mondkar and G.H. Powell July 1979(PB 80 113 301)A05
- UCB/EERC-79/18 "Soil Structure Interaction in Different Seismic Environments," A. Gomez-Masso, J. Lysmer, J.-C. Chen and H.B. Seed - August 1979(PB 80 101 520)A04
- UCB/EERC-79/19 "ARMA Models for Earthquake Ground Motions," by M.K. Chang, J.W. Kwiatkowski, R.F. Nau, R.M. Oliver and K.S. Pister - July 1979(PB 301 166)A05
- UCB/EERC-79/20 "Hysteretic Behavior of Reinforced Concrete Structural Walls," by J.M. Vallenias, V.V. Bertero and E.P. Popov - August 1979(PB 80 165 905)A12
- UCB/EERC-79/21 "Studies on High-Frequency Vibrations of Buildings - I: The Column Effect," by J. Lubliner - August 1979 (PB 80 158 553)A03
- UCB/EERC-79/22 "Effects of Generalized Loadings on Bond Reinforcing Bars Embedded in Confined Concrete Blocks," by S. Viathanatepa, E.P. Popov and V.V. Bertero - August 1979(PB 81 124 018)A14
- UCB/EERC-79/23 "Shaking Table Study of Single-Story Masonry Houses, Volume 1: Test Structures 1 and 2," by P. Gülkan, R.L. Mayes and R.W. Clough - Sept. 1979 (HUD-000 1763)A12
- UCB/EERC-79/24 "Shaking Table Study of Single-Story Masonry Houses, Volume 2: Test Structures 3 and 4," by P. Gülkan, R.L. Mayes and R.W. Clough - Sept. 1979 (HUD-000 1836)A12
- UCB/EERC-79/25 "Shaking Table Study of Single-Story Masonry Houses, Volume 3: Summary, Conclusions and Recommendations," by R.W. Clough, R.L. Mayes and P. Gülkan - Sept. 1979 (HUD-000 1837)A06

- UCB/EERC-79/26 "Recommendations for a U.S.-Japan Cooperative Research Program Utilizing Large-Scale Testing Facilities," by U.S.-Japan Planning Group - Sept. 1979(PB 301 407)A06
- UCB/EERC-79/27 "Earthquake-Induced Liquefaction Near Lake Amatitlan, Guatemala," by H.B. Seed, I. Arango, C.K. Chan, A. Gomez-Masso and R. Grant de Ascoli - Sept. 1979(NUREG-CRI341)A03
- UCB/EERC-79/28 "Infill Panels: Their Influence on Seismic Response of Buildings," by J.W. Axley and V.V. Bertero Sept. 1979(PB 80 163 371)A10
- UCB/EERC-79/29 "3D Truss Bar Element (Type 1) for the ANSR-II Program," by D.P. Mondkar and G.H. Powell - Nov. 1979 (PB 80 169 709)A02
- UCB/EERC-79/30 "2D Beam-Column Element (Type 5 - Parallel Element Theory) for the ANSR-II Program," by D.G. Row, G.H. Powell and D.P. Mondkar - Dec. 1979(PB 80 167 224)A03
- UCB/EERC-79/31 "3D Beam-Column Element (Type 2 - Parallel Element Theory) for the ANSR-II Program," by A. Riahi, G.H. Powell and D.P. Mondkar - Dec. 1979(PB 80 167 216)A03
- UCB/EERC-79/32 "On Response of Structures to Stationary Excitation," by A. Der Kiureghian - Dec. 1979(PB 80166 929)A03
- UCB/EERC-79/33 "Undisturbed Sampling and Cyclic Load Testing of Sands," by S. Singh, H.B. Seed and C.K. Chan Dec. 1979(ADA 087 298)A07
- UCB/EERC-79/34 "Interaction Effects of Simultaneous Torsional and Compressional Cyclic Loading of Sand," by P.M. Griffin and W.N. Houston - Dec. 1979(ADA 092 352)A15
- UCB/EERC-80/01 "Earthquake Response of Concrete Gravity Dams Including Hydrodynamic and Foundation Interaction Effects," by A.K. Chopra, P. Chakrabarti and S. Gupta - Jan. 1980(AD-A087297)A10
- UCB/EERC-80/02 "Rocking Response of Rigid Blocks to Earthquakes," by C.S. Yim, A.K. Chopra and J. Penzien - Jan. 1980 (PB80 166 002)A04
- UCB/EERC-80/03 "Optimum Inelastic Design of Seismic-Resistant Reinforced Concrete Frame Structures," by S.W. Zagajeski and V.V. Bertero - Jan. 1980(PB80 164 635)A06
- UCB/EERC-80/04 "Effects of Amount and Arrangement of Wall-Panel Reinforcement on Hysteretic Behavior of Reinforced Concrete Walls," by R. Iliya and V.V. Bertero - Feb. 1980(PB81 122 525)A09
- UCB/EERC-80/05 "Shaking Table Research on Concrete Dam Models," by A. Niwa and R.W. Clough - Sept. 1980(PB81 122 368)A06
- UCB/EERC-80/06 "The Design of Steel Energy-Absorbing Restrainers and their Incorporation into Nuclear Power Plants for Enhanced Safety (Vol 1A): Piping with Energy Absorbing Restrainers: Parameter Study on Small Systems," by G.H. Powell, C. Oughourlian and J. Simons - June 1980
- UCB/EERC-80/07 "Inelastic Torsional Response of Structures Subjected to Earthquake Ground Motions," by Y. Yamazaki April 1980(PB81 122 327)A08
- UCB/EERC-80/08 "Study of X-Braced Steel Frame Structures Under Earthquake Simulation," by Y. Ghanaat - April 1980 (PB81 122 335)A11
- UCB/EERC-80/09 "Hybrid Modelling of Soil-Structure Interaction," by S. Gupta, T.W. Lin, J. Penzien and C.S. Yeh May 1980(PB81 122 319)A07
- UCB/EERC-80/10 "General Applicability of a Nonlinear Model of a One Story Steel Frame," by B.I. Sveinsson and H.D. McNiven - May 1980(PB81 124 877)A06
- UCB/EERC-80/11 "A Green-Function Method for Wave Interaction with a Submerged Body," by W. Kioka - April 1980 (PB81 122 269)A07
- UCB/EERC-80/12 "Hydrodynamic Pressure and Added Mass for Axisymmetric Bodies," by F. Nilrat - May 1980(PB81 122 343)A08
- UCB/EERC-80/13 "Treatment of Non-Linear Drag Forces Acting on Offshore Platforms," by B.V. Dao and J. Penzien May 1980(PB81 153 413)A07
- UCB/EERC-80/14 "2D Plane/Axisymmetric Solid Element (Type 3 - Elastic or Elastic-Perfectly Plastic) for the ANSR-II Program," by D.P. Mondkar and G.H. Powell - July 1980(PB81 122 350)A03
- UCB/EERC-80/15 "A Response Spectrum Method for Random Vibrations," by A. Der Kiureghian - June 1980(PB81 122 301)A03
- UCB/EERC-80/16 "Cyclic Inelastic Buckling of Tubular Steel Braces," by V.A. Zayas, E.P. Popov and S.A. Mahin June 1980(PB81 124 885)A10
- UCB/EERC-80/17 "Dynamic Response of Simple Arch Dams Including Hydrodynamic Interaction," by C.S. Porter and A.K. Chopra - July 1980(PB81 124 000)A13
- UCB/EERC-80/18 "Experimental Testing of a Friction Damped Aseismic Base Isolation System with Fail-Safe Characteristics," by J.M. Kelly, K.E. Beucke and M.S. Skinner - July 1980(PB81 148 595)A04
- UCB/EERC-80/19 "The Design of Steel Energy-Absorbing Restrainers and their Incorporation into Nuclear Power Plants for Enhanced Safety (Vol 1B): Stochastic Seismic Analyses of Nuclear Power Plant Structures and Piping Systems Subjected to Multiple Support Excitations," by M.C. Lee and J. Penzien - June 1980
- UCB/EERC-80/20 "The Design of Steel Energy-Absorbing Restrainers and their Incorporation into Nuclear Power Plants for Enhanced Safety (Vol 1C): Numerical Method for Dynamic Substructure Analysis," by J.M. Dickens and E.L. Wilson - June 1980
- UCB/EERC-80/21 "The Design of Steel Energy-Absorbing Restrainers and their Incorporation into Nuclear Power Plants for Enhanced Safety (Vol 2): Development and Testing of Restraints for Nuclear Piping Systems," by J.M. Kelly and M.S. Skinner - June 1980
- UCB/EERC-80/22 "3D Solid Element (Type 4-Elastic or Elastic-Perfectly-Plastic) for the ANSR-II Program," by D.P. Mondkar and G.H. Powell - July 1980(PB81 123 242)A03
- UCB/EERC-80/23 "Gap-Friction Element (Type 5) for the ANSR-II Program," by D.P. Mondkar and G.H. Powell - July 1980 (PB81 122 285)A03

- UCB/EERC-80/24 "U-Bar Restraint Element (Type 11) for the ANSR-II Program," by C. Oughourlian and G.H. Powell July 1980(PB81 122 293)A03
- UCB/EERC-8J/25 "Testing of a Natural Rubber Base Isolation System by an Explosively Simulated Earthquake," by J.M. Kelly - August 1980(PB81 201 360)A04
- UCB/EERC-80/26 "Input Identification from Structural Vibrational Response," by Y. Hu - August 1980(PB81 152 308)A05
- UCB/EERC-80/27 "Cyclic Inelastic Behavior of Steel Offshore Structures," by V.A. Zayas, S.A. Mahin and E.P. Popov August 1980(PB81 196 180)A15
- UCB/EERC-80/28 "Shaking Table Testing of a Reinforced Concrete Frame with Biaxial Response," by M.G. Oliva October 1980(PB81 154 304)A10
- UCB/EERC-80/29 "Dynamic Properties of a Twelve-Story Prefabricated Panel Building," by J.G. Bouwkamp, J.P. Kollegger and R.M. Stephen - October 1980(PB82 117 128)A06
- UCB/EERC-80/30 "Dynamic Properties of an Eight-Story Prefabricated Panel Building," by J.G. Bouwkamp, J.P. Kollegger and R.M. Stephen - October 1980(PB81 200 313)A05
- UCB/EERC-80/31 "Predictive Dynamic Response of Panel Type Structures Under Earthquakes," by J.P. Kollegger and J.G. Bouwkamp - October 1980(PB81 152 316)A04
- UCB/EERC-80/32 "The Design of Steel Energy-Absorbing Restrainers and their Incorporation into Nuclear Power Plants for Enhanced Safety (Vol 3): Testing of Commercial Steels in Low-Cycle Torsional Fatigue," by P. Spencer, E.R. Parker, E. Jongewaard and M. Drory
- UCB/EERC-80/33 "The Design of Steel Energy-Absorbing Restrainers and their Incorporation into Nuclear Power Plants for Enhanced Safety (Vol 4): Shaking Table Tests of Piping Systems with Energy-Absorbing Restrainers," by S.F. Stiemer and W.G. Godden - Sept. 1980
- UCB/EERC-80/34 "The Design of Steel Energy-Absorbing Restrainers and their Incorporation into Nuclear Power Plants for Enhanced Safety (Vol 5): Summary Report," by P. Spencer
- UCB/EERC-80/35 "Experimental Testing of an Energy-Absorbing Base Isolation System," by J.M. Kelly, M.S. Skinner and K.E. Beucke - October 1980(PB81 154 072)A04
- UCB/EERC-80/36 "Simulating and Analyzing Artificial Non-Stationary Earthquake Ground Motions," by R.F. Nau, R.M. Oliver and K.S. Pister - October 1980(PB81 153 397)A04
- UCB/EERC-80/37 "Earthquake Engineering at Berkeley - 1980," - Sept. 1980(PB61 205 874)A09
- UCB/EERC-80/38 "Inelastic Seismic Analysis of Large Panel Buildings," by V. Schricker and G.H. Powell - Sept. 1980 (PB81 154 338)A13
- UCB/EERC-80/39 "Dynamic Response of Embankment, Concrete-Gravity and Arch Dams Including Hydrodynamic Interaction," by J.F. Hall and A.K. Chopra - October 1980(PB81 152 324)A11
- UCB/EERC-80/40 "Inelastic Buckling of Steel Struts Under Cyclic Load Reversal," by R.G. Black, W.A. Wenger and E.P. Popov - October 1980(PB81 154 312)A08
- UCB/EERC-80/41 "Influence of Site Characteristics on Building Damage During the October 3, 1974 Lima Earthquake," by P. Repetto, I. Arango and H.B. Seed - Sept. 1980(PB81 161 739)A05
- UCB/EERC-80/42 "Evaluation of a Shaking Table Test Program on Response Behavior of a Two Story Reinforced Concrete Frame," by J.M. Blondet, R.W. Clough and S.A. Mahin
- UCB/EERC-80/43 "Modelling of Soil-Structure Interaction by Finite and Infinite Elements," by F. Medina - December 1980(PB81 229 270)A04
- UCB/EERC-81/01 "Control of Seismic Response of Piping Systems and Other Structures by Base Isolation," edited by J.M. Kelly - January 1981 (PB81 200 735)A05
- UCB/EERC-81/02 "OPTNSR - An Interactive Software System for Optimal Design of Statically and Dynamically Loaded Structures with Nonlinear Response," by M.A. Bhatti, V. Ciampi and K.S. Pister - January 1981 (PB81 218 851)A09
- UCB/EERC-81/03 "Analysis of Local Variations in Free Field Seismic Ground Motions," by J.-C. Chen, J. Lysmer and H.B. Seed - January 1981 (AD-A099508)A13
- UCB/EERC-81/04 "Inelastic Structural Modeling of Braced Offshore Platforms for Seismic Loading," by V.A. Zayas, P.-S.B. Shing, S.A. Mahin and E.P. Popov - January 1981(PB82 138 777)A07
- UCB/EERC-81/05 "Dynamic Response of Light Equipment in Structures," by A. Der Kiureghian, J.L. Sackman and B. Nour-Omid - April 1981 (PB81 218 497)A04
- UCB/EERC-81/06 "Preliminary Experimental Investigation of a Broad Base Liquid Storage Tank," by J.G. Bouwkamp, J.P. Kollegger and R.M. Stephen - May 1981(PB82 140 385)A03
- UCB/EERC-81/07 "The Seismic Resistant Design of Reinforced Concrete Coupled Structural Walls," by A.E. Aktan and V.V. Bertero - June 1981(PB82 113 358)A11
- UCB/EERC-81/08 "The Undrained Shearing Resistance of Cohesive Soils at Large Deformations," by M.R. Pyles and H.B. Seed - August 1981
- UCB/EERC-81/09 "Experimental Behavior of a Spatial Piping System with Steel Energy Absorbers Subjected to a Simulated Differential Seismic Input," by S.F. Stiemer, W.G. Godden and J.M. Kelly - July 1981

- UCB/EERC-81/10 "Evaluation of Seismic Design Provisions for Masonry in the United States," by B.L. Sveinsson, R.L. Mayes and H.D. McNiven - August 1981 (PB82 166 075)A08
- UCB/EERC-81/11 "Two-Dimensional Hybrid Modelling of Soil-Structure Interaction," by T.-J. Tzong, S. Gupta and J. Penzien - August 1981 (PB82 142 118)A04
- UCB/EERC-81/12 "Studies on Effects of Infills in Seismic Resistant R/C Construction," by S. Brokken and V.V. Bertero - September 1981 (PB82 166 190)A09
- UCB/EERC-81/13 "Linear Models to Predict the Nonlinear Seismic Behavior of a One-Story Steel Frame," by H. Valdimarsson, A.H. Shah and H.D. McNiven - September 1981 (PB82 138 793)A07
- UCB/EERC-81/14 "TLUSH: A Computer Program for the Three-Dimensional Dynamic Analysis of Earth Dams," by T. Kagawa, L.H. Mejia, H.B. Seed and J. Lysmer - September 1981 (PB82 139 940)A06
- UCB/EERC-81/15 "Three Dimensional Dynamic Response Analysis of Earth Dams," by L.H. Mejia and H.B. Seed - September 1981 (PB82 137 274)A12
- UCB/EERC-81/16 "Experimental Study of Lead and Elastomeric Dampers for Base Isolation Systems," by J.M. Kelly and S.B. Hodder - October 1981 (PB82 166 182)A05
- UCB/EERC-81/17 "The Influence of Base Isolation on the Seismic Response of Light Secondary Equipment," by J.M. Kelly - April 1981 (PB82 255 266)A04
- UCB/EERC-81/18 "Studies on Evaluation of Shaking Table Response Analysis Procedures," by J. Marcial Blondet - November 1981 (PB82 197 278)A10
- UCB/EERC-81/19 "DELIGHT.STRUCT: A Computer-Aided Design Environment for Structural Engineering," by R.J. Balling, K.S. Pister and E. Polak - December 1981 (PB82 218 496)A07
- UCB/EERC-81/20 "Optimal Design of Seismic-Resistant Planar Steel Frames," by R.J. Balling, V. Ciampi, K.S. Pister and E. Polak - December 1981 (PB82 220 179)A07
- UCB/EERC-82/01 "Dynamic Behavior of Ground for Seismic Analysis of Lifeline Systems," by T. Sato and A. Der Kiureghian - January 1982 (PB82 218 926)A05
- UCB/EERC-82/02 "Shaking Table Tests of a Tubular Steel Frame Model," by Y. Ghanaat and R. W. Clough - January 1982 (PB82 220 161)A07
- UCB/EERC-82/03 "Behavior of a Piping System under Seismic Excitation: Experimental Investigations of a Spatial Piping System supported by Mechanical Shock Arrestors and Steel Energy Absorbing Devices under Seismic Excitation," by S. Schneider, H.-M. Lee and W. G. Godden - May 1982 (PB83 172 544)A09
- UCB/EERC-82/04 "New Approaches for the Dynamic Analysis of Large Structural Systems," by E. L. Wilson - June 1982 (PB83 148 080)A05
- UCB/EERC-82/05 "Model Study of Effects of Damage on the Vibration Properties of Steel Offshore Platforms," by F. Shahrivar and J. G. Bouwkamp - June 1982 (PB83 148 742)A10
- UCB/EERC-82/06 "States of the Art and Practice in the Optimum Seismic Design and Analytical Response Prediction of R/C Frame-Wall Structures," by A. E. Aktan and V. V. Bertero - July 1982 (PB83 147 736)A05
- UCB/EERC-82/07 "Further Study of the Earthquake Response of a Broad Cylindrical Liquid-Storage Tank Model," by G. C. Manos and R. W. Clough - July 1982 (PB83 147 744)A11
- UCB/EERC-82/08 "An Evaluation of the Design and Analytical Seismic Response of a Seven Story Reinforced Concrete Frame - Wall Structure," by F. A. Charney and V. V. Bertero - July 1982 (PB83 157 628)A09
- UCB/EERC-82/09 "Fluid-Structure Interactions: Added Mass Computations for Incompressible Fluid," by J. S.-H. Kuo - August 1982 (PB83 156 281)A07
- UCB/EERC-82/10 "Joint-Opening Nonlinear Mechanism: Interface Smeared Crack Model," by J. S.-H. Kuo - August 1982 (PB83 149 195)A05
- UCB/EERC-82/11 "Dynamic Response Analysis of Techi Dam," by R. W. Clough, R. M. Stephen and J. S.-H. Kuo - August 1982 (PB83 147 496)A06
- UCB/EERC-82/12 "Prediction of the Seismic Responses of R/C Frame-Coupled Wall Structures," by A. E. Aktan, V. V. Bertero and M. Piazza - August 1982 (PB83 149 203)A09
- UCB/EERC-82/13 "Preliminary Report on the SMART 1 Strong Motion Array in Taiwan," by B. A. Bolt, C. H. Loh, J. Penzien, Y. B. Tsai and Y. T. Yeh - August 1982 (PB83 159 400)A10
- UCB/EERC-82/14 "Shaking-Table Studies of an Eccentrically X-Braced Steel Structure," by M. S. Yang - September 1982 (PB83 260 778)A12
- UCB/EERC-82/15 "The Performance of Stairways in Earthquakes," by C. Roha, J. W. Axley and V. V. Bertero - September 1982 (PB83 157 693)A07
- UCB/EERC-82/16 "The Behavior of Submerged Multiple Bodies in Earthquakes," by W.-G. Liao - Sept. 1982 (PB83 158 709)A07
- UCB/EERC-82/17 "Effects of Concrete Types and Loading Conditions on Local Bond-Slip Relationships," by A. D. Cowell, E. P. Popov and V. V. Bertero - September 1982 (PB83 153 577)A04

- UCB/EERC-82/18 "Mechanical Behavior of Shear Wall Vertical Boundary Members: An Experimental Investigation," by M. T. Wagner and V. V. Bertero - October 1982 (PB83 159 764)A05
- UCB/EERC-82/19 "Experimental Studies of Multi-support Seismic Loading on Piping Systems," by J. M. Kelly and A. D. Cowell - November 1982
- UCB/EERC-82/20 "Generalized Plastic Hinge Concepts for 3D Beam-Column Elements," by P. F.-S. Chen and G. H. Powell - November 1982 (PB83 247 981)A13
- UCB/EERC-82/21 "ANSR-III: General Purpose Computer Program for Nonlinear Structural Analysis," by C. V. Oughourlian and G. H. Powell - November 1982 (PB83 251 330)A12
- UCB/EERC-82/22 "Solution Strategies for Statically Loaded Nonlinear Structures," by J. W. Simons and G. H. Powell - November 1982 (PB83 197 970)A06
- UCB/EERC-82/23 "Analytical Model of Deformed Bar Anchorages under Generalized Excitations," by V. Ciampi, R. Eligehausen, V. V. Bertero and E. P. Popov - November 1982 (PB83 169 532)A06
- UCB/EERC-82/24 "A Mathematical Model for the Response of Masonry Walls to Dynamic Excitations," by H. Sucuoğlu, Y. Mengi and H. D. McNiven - November 1982 (PB83 169 011)A07
- UCB/EERC-82/25 "Earthquake Response Considerations of Broad Liquid Storage Tanks," by F. J. Cambra - November 1982 (PB83 251 215)A09
- UCB/EERC-82/26 "Computational Models for Cyclic Plasticity, Rate Dependence and Creep," by B. Mosaddad and G. H. Powell - November 1982 (PB83 245 829)A08
- UCB/EERC-82/27 "Inelastic Analysis of Piping and Tubular Structures," by M. Mahasuverachai and G. H. Powell - November 1982 (PB83 249 987)A07
- UCB/EERC-83/01 "The Economic Feasibility of Seismic Rehabilitation of Buildings by Base Isolation," by J. M. Kelly - January 1983 (PB83 197 988)A05
- UCB/EERC-83/02 "Seismic Moment Connections for Moment-Resisting Steel Frames," by E. P. Popov - January 1983 (PB83 195 412)A04
- UCB/EERC-83/03 "Design of Links and Beam-to-Column Connections for Eccentrically Braced Steel Frames," by E. P. Popov and J. O. Malley - January 1983 (PB83 194 811)A04
- UCB/EERC-83/04 "Numerical Techniques for the Evaluation of Soil-Structure Interaction Effects in the Time Domain," by E. Bayo and E. L. Wilson - February 1983 (PB83 245 605)A09
- UCB/EERC-83/05 "A Transducer for Measuring the Internal Forces in the Columns of a Frame-Wall Reinforced Concrete Structure," by R. Sause and V. V. Bertero - May 1983 (PB84 119 494)A06
- UCB/EERC-83/06 "Dynamic Interactions between Floating Ice and Offshore Structures," by P. Croteau - May 1983 (PB84 119 486)A16
- UCB/EERC-83/07 "Dynamic Analysis of Multiply Tuned and Arbitrarily Supported Secondary Systems," by T. Igusa and A. Der Kiureghian - June 1983 (PB84 118 272)A11
- UCB/EERC-83/08 "A Laboratory Study of Submerged Multi-body Systems in Earthquakes," by G. R. Ansari - June 1983 (PB83 261 842)A17
- UCB/EERC-83/09 "Effects of Transient Foundation Uplift on Earthquake Response of Structures," by C.-S. Yim and A. K. Chopra - June 1983 (PB83 261 396)A07
- UCB/EERC-83/10 "Optimal Design of Friction-Braced Frames under Seismic Loading," by M. A. Austin and K. S. Pister - June 1983 (PB84 119 288)A06
- UCB/EERC-83/11 "Shaking Table Study of Single-Story Masonry Houses: Dynamic Performance under Three Component Seismic Input and Recommendations," by G. C. Manos, R. W. Clough and R. L. Mayes - June 1983
- UCB/EERC-83/12 "Experimental Error Propagation in Pseudodynamic Testing," by P. B. Shing and S. A. Mahin - June 1983 (PB84 119 270)A09
- UCB/EERC-83/13 "Experimental and Analytical Predictions of the Mechanical Characteristics of a 1/5-scale Model of a 7-story R/C Frame-Wall Building Structure," by A. E. Aktan, V. V. Bertero, A. A. Chowdhury and T. Nagashima - August 1983 (PB84 119 213)A07
- UCB/EERC-83/14 "Shaking Table Tests of Large-Panel Precast Concrete Building System Assemblages," by M. G. Oliva and R. W. Clough - August 1983
- UCB/EERC-83/15 "Seismic Behavior of Active Beam Links in Eccentrically Braced Frames," by K. D. Hjelmstad and E. P. Popov - July 1983 (PB84 119 676)A09
- UCB/EERC-83/16 "System Identification of Structures with Joint Rotation," by J. S. Dimsdale and H. D. McNiven - July 1983
- UCB/EERC-83/17 "Construction of Inelastic Response Spectra for Single-Degree-of-Freedom Systems," by S. Mahin and J. Lin - July 1983

- UCB/EERC-83/18 "Interactive Computer Analysis Methods for Predicting the Inelastic Cyclic Behaviour of Structural Sections," by S. Kaba and S. Mahin - July 1983 (PB84 192 012) A06
- UCB/EERC-83/19 "Effects of Bond Deterioration on Hysteretic Behavior of Reinforced Concrete Joints," by F.C. Filippou, E.P. Popov and V.V. Bertero - August 1983 (PB84 192 020) A10
- UCB/EERC-83/20 "Analytical and Experimental Correlation of Large-Panel Precast Building System Performance," by M.G. Oliva, R.W. Clough, M. Velkov, P. Gavrilovic and J. Petrovski - November 1983
- UCB/EERC-83/21 "Mechanical Characteristics of Materials Used in a 1/5 Scale Model of a 7-Story Reinforced Concrete Test Structure," by V.V. Bertero, A.E. Aktan, H.G. Harris and A.A. Chowdhury - September 1983 (PB84 193 697) A05
- UCB/EERC-83/22 "Hybrid Modelling of Soil-Structure Interaction in Layered Media," by T.-J. Tzong and J. Penzien - October 1983 (PB84 192 178) A08
- UCB/EERC-83/23 "Local Bond Stress-Slip Relationships of Deformed Bars under Generalized Excitations," by R. Eligehausen, E.P. Popov and V.V. Bertero - October 1983 (PB84 192 848) A09
- UCB/EERC-83/24 "Design Considerations for Shear Links in Eccentrically Braced Frames," by J.O. Malley and E.P. Popov - November 1983 (PB84 192 186) A07
- UCB/EERC-84/01 "Pseudodynamic Test Method for Seismic Performance Evaluation: Theory and Implementation," by P.-S. E. Shing and S. A. Mahin - January 1984 (PB84 190 644) A08
- UCB/EERC-84/02 "Dynamic Response Behavior of Xiang Hong Dian Dam," by R.W. Clough, K.-T. Chang, H.-Q. Chen, R.M. Stephen, G.-L. Wang, and Y. Ghanaat - April 1984
- UCB/EERC-84/03 "Refined Modelling of Reinforced Concrete Columns for Seismic Analysis," by S.A. Kaba and S.A. Mahin - April, 1984
- UCB/EERC-84/04 "A New Floor Response Spectrum Method for Seismic Analysis of Multiply Supported Secondary Systems," by A. Asfura and A. Der Kiureghian - June 1984
- UCB/EERC-84/05 "Earthquake Simulation Tests and Associated Studies of a 1/5th-scale Model of a 7-Story R/C Frame-Wall Test Structure," by V.V. Bertero, A.E. Aktan, F.A. Charney and R. Sause - June 1984
- UCB/EERC-84/06 "R/C Structural Walls: Seismic Design for Shear," by A.E. Aktan and V.V. Bertero
- UCB/EERC-84/07 "Behavior of Interior and Exterior Flat-Plate Connections subjected to Inelastic Load Reversals," by H.L. Zee and J.P. Moehle
- UCB/EERC-84/08 "Experimental Study of the Seismic Behavior of a two-story Flat-Plate Structure," by J.W. Diebold and J.P. Moehle
- UCB/EERC-84/09 "Phenomenological Modeling of Steel Braces under Cyclic Loading," by K. Ikeda, S.A. Mahin and S.N. Dermitzakis - May 1984
- UCB/EERC-84/10 "Earthquake Analysis and Response of Concrete Gravity Dams," by G. Fenves and A.K. Chopra - August 1984
- UCB/EERC-84/11 "EAGD-84: A Computer Program for Earthquake Analysis of Concrete Gravity Dams," by G. Fenves and A.K. Chopra - August 1984
- UCB/EERC-84/12 "A Refined Physical Theory Model for Predicting the Seismic Behavior of Braced Steel Frames," by K. Ikeda and S.A. Mahin - July 1984
- UCB/EERC-84/13 "Earthquake Engineering Research at Berkeley - 1984" - August 1984
- UCB/EERC-84/14 "Moduli and Damping Factors for Dynamic Analyses of Cohesionless Soils," by H.B. Seed, R.T. Wong, I.M. Idriss and K. Tokimatsu - September 1984
- UCB/EERC-84/15 "The Influence of SPT Procedures in Soil Liquefaction Resistance Evaluations," by H. B. Seed, K. Tokimatsu, L. F. Harder and R. M. Chung - October 1984
- UCB/EERC-84/16 "Simplified Procedures for the Evaluation of Settlements in Sands Due to Earthquake Shaking," by K. Tokimatsu and H. B. Seed - October 1984
- UCB/EERC-84/17 "Evaluation and Improvement of Energy Absorption Characteristics of Bridges under Seismic Conditions," by R. A. Imbsen and J. Penzien - November 1984
- UCB/EERC-84/18 "Structure-Foundation Interactions under Dynamic Loads," by W. D. Liu and J. Penzien - November 1984
- UCB/EERC-84/19 "Seismic Modelling of Deep Foundations," by C.-H. Chen and J. Penzien - November 1984
- UCB/EERC-84/20 "Dynamic Response Behavior of Quan Shui Dam," by R. W. Clough, K.-T. Chang, H.-Q. Chen, R. M. Stephen, Y. Ghanaat and J.-H. Qi - November 1984

- UCB/EERC-85/01 "Simplified Methods of Analysis for Earthquake Resistant Design of Buildings," by E.F. Cruz and A.K. Chopra - February 1985
- UCB/EERC-85/02 "Estimation of Seismic Wave Coherency and Rupture Velocity using the SMART 1 Strong-Motion Array Recordings," by N.A. Abrahamson - March 1985
- UCB/EERC-85/03 "Dynamic Properties of a Thirty Story Condominium Tower Building," by R.M. Stephen, E.L. Wilson and N. Stander - April 1985
- UCB/EERC-85/04 "Development of Substructuring Techniques for On-Line Computer Controlled Seismic Performance Testing," by S. Dermitzakis and S. Mahin - May 1985
- UCB/EERC-85/05 "A Simple Model for Reinforcing Bar Anchorages under Cyclic Excitations," by F.C. Filippou - March 1985
- UCB/EERC-85/06 "Rocking Behavior of Wood-Framed Gypsum Panels under Dynamic Load," by M.G. Oliva - June 1985
- UCB/EERC-85/07 "Earthquake Analysis and Response of Concrete Arch Dams," by K.-L. Fok and A.K. Chopra - June 1985

